ISSN 0911-5730
UVSOR-21
March 1994

UVSOR
ACTIVITY REPORT
1993

Ultraviolet Synchrotron Orbital Radiation Facility
Institute for Molecular Science

CONTENTS

RESEARCH ACTIVITIES

APPENDIX

Preface

It was in 1983 that the storage ring of IMS emitted the SR light for the first time. We celebrated the 10th anniversary of UVSOR on December 3 of 1993. I would like to express my sincere thanks to all the participants in this ceremony. During the past 10 years the number of users continues to grow with no sign of saturating . The numbers of proposals/users during FY92 are 159/840. The number of proposals grows by 7.5 % in FY93.

The improvement of the stability and life time of the SR light was attained by introducing the harmonic cavity and thinning out the bunches. Another impressive achievement was the successful experiment of Free Electron Laser in an ultraviolet region on July 5 of 1993. The oscillation of FEL in 295-305 nm region has passed the record of France and now approaching the world record of Russia.

BL5B, which had been used for the calibration of instruments by the National Institute for Fusion Science, was moved to IMS from FY93, and this beam line is used for general experiments as well. UVSOR provides 9 beam lines (BL1B, BL2B1, BL3A1, BL3A2, BL5B, BL6A1, BL7A, BL7B, and BL8A) for general users, and 9 beam lines (BL1A, BL2A, BL2B2, BL3B, BL4A, BL4B, BL6A2, BL6B, and BL8B2) for in-house groups.

I am much pleased to meet in this memorial year that two research staffs, Profs. Makoto Watanabe and Kosuke Shobatake, who had contributed to the construction of beam lines of UVSOR, were promoted to the Tohoku University and Nagoya University, respectively. I am also pleased to mention that Dr. Shin-ichi Kimura was appointed as a Research Associate of UVSOR Facility.

I would like to express my thanks to all the UVSOR staff for their incredible efforts for maintaining the machines and responding users and visitors as well as for devoting themselves to the research. I would appreciate the kind cooperation of all the users.

February 1994

Kyuya Yakushi
Director of UVSOR

LIGHT SOURCE & BEAMLINES

Double RF System for Suppression of Longitudinal Coupled Bunch Instability on the UVSOR Storage Ring

Kazuhiro TAMURA[1], Toshio KASUGA*[1], Makoto TOBIYAMA*[1],
Hiroyuki HAMA[2], Toshio KINOSHITA[2] and Goro ISOYAMA[2]

[1] *Department of Materials Science, Faculty of Science, Hiroshima University, Higashi-Hiroshima 724*

[2] *UVSOR Facility, Institute for Molecular Science, Myodaiji, Okazaki 444*

A higher harmonic RF system whose frequency is the third harmonic of the main RF frequency has been installed on the UVSOR storage ring in order to suppress longitudinal coupled bunch instability with a double RF system. The RF acceleration field with the double RF system is shown in Fig. 1, where the voltage of the third harmonic field is maintained at one third of that of the main RF field. Since the synchrotron oscillation frequency is proportional to the square root of the slope of the RF field and the bunch length is inversely proportional to the synchrotron oscillation frequency, we can control the bunch length by varying the phase of the third harmonic field relative to the main field. Two extreme cases are shown in Figs. 1 (a) and (b). In the (b) mode, the slope of the combined field is twice as much as that of the main RF field alone so that the bunch length is expected to decrease to 70 % of the normal value. In the (a) mode, slopes of the respective field components cancel out, so that not only the bunch length becomes longer but also the frequency spread of the synchrotron oscillation increases due to the non-linearity of the RF field at the electron bunch. The frequency spread leads to Landau damping against the coherent oscillation of electron bunches due to the longitudinal instability.

First, we measured the synchrotron oscillation frequency, the frequency spread and the bunch length in single bunch operation at an electron energy of 600 MeV, in order to see whether the double RF system worked as expected. The main RF system was operated in the same conditions as usual; the frequency is 90.115 MHz, the peak

RF voltage is 47 kV and the tuning angle is around -30 degrees. The resonant frequency of the harmonic cavity ω_{res} was set to be lower than the driving frequency ω. The tuning angle of the cavity Φ defined as

$$\tan\Phi = -\frac{2Q_0}{1+\beta}\left(\frac{\omega-\omega_{res}}{\omega_{res}}\right) \qquad (1)$$

was set at -60 degrees in order to avoid Robinson instability, where Q_0 is the unloaded Q factor, β the coupling coefficient. The bunch length and the synchrotron oscillation frequency were measured in the (a) and (b) modes as a function of the RF voltage of the harmonic cavity. The measured values agreed well with theoretical predictions for the double RF system. Next, we carried out experiments in multi-bunch operation to suppress longitudinal coupled bunch instability. The peak RF voltage in the harmonic cavity was set at 15.6 kV, which is one third of the voltage in the main cavity, and the phase was adjusted to operate the system in the (a) mode. When the beam current was low, the instability was completely suppressed with the double RF system. As the beam current increased, however, it became difficult to keep the phase of the harmonic field due to the beam-induced RF field in the harmonic cavity, and the instability appeared again. Meanwhile, it turned out that the instability could be suppressed even at the higher beam current if the tuning angle of the harmonic cavity was set at a positive value. This result indicates that the strong instability excited by the fundamental resonance of the harmonic cavity can be suppressed by Landau damping with the double RF system. Since the beam induced field in the harmonic cavity at the negative tuning angle is in the same phase as the RF field in the (a) mode, this operation mode works even at a very high beam current.

The double RF system is routinely used for user experiments in multi-bunch operation to suppress longitudinal coupled bunch instability. Another advantage of this system is that the beam lifetime becomes longer because the bunch is 2 ~ 3 times longer. The lifetime at the beam current of 200 mA increases from 240 min to 350 min. The maximum beam current in multi-bunch operation had been limited by the

instability to approximately 500 mA. With the double RF system, it could be increased to more than 1 A.

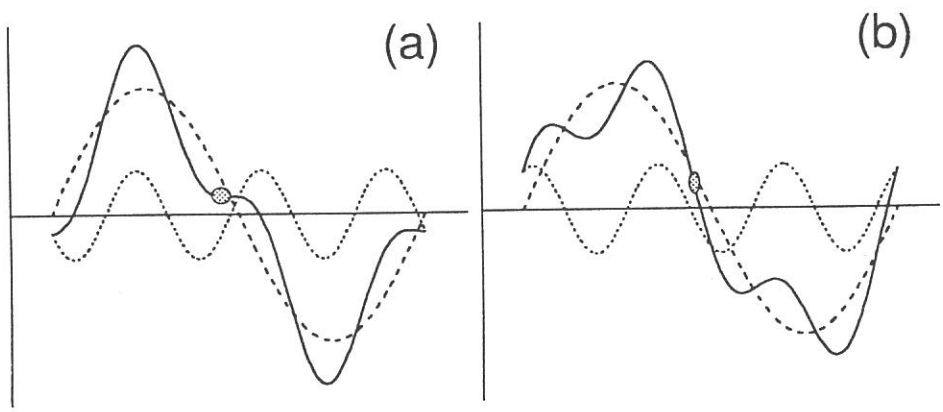

Figure 1. RF field in the double RF system. The peak voltage of the third harmonic field (dotted line) is one third of the main RF field (broken line). The solid line is the combined field. In the (a) mode, the phase of the higher harmonic field is adjusted such that the slope of the combined field becomes zero at the bunch position. In the (b) mode, the slope becomes higher and the bunch length is reduced.

Lasing of a Free Electron Laser in Ultraviolet Region on the UVSOR Storage Ring

Hiroyuki Hama, J. Yamazaki and G. Isoyama
UVSOR Facility, Institute for Molecular Science, Myodaiji, Okazaki 444

We have been carrying out free electron laser (FEL) experiments on the UVSOR storage ring. The first lasing was obtained at wavelengths around 460 nm in Spring, 1992 [1]. Since then, we have been preparing for experiments in the ultraviolet (UV) region. Because the FEL gain and the reflectivity of mirrors used for the optical cavity are anticipated to decrease as the wavelength becomes shorter, we have developed a gain-enhancement technique using a higher harmonic RF cavity (HCV) [2].

The FEL gain is directly proportional to peak density of electrons n_{peak} which is inversely proportional to the bunch length. The bunch length of the UVSOR storage ring can be controlled with a double RF system, which was recently commissioned. When the phase of the RF field in the HCV to that of the main cavity (MCV) is adjusted to make the slope of the RF field steeper, the bunch is shortened and the peak current becomes higher. In this operation mode, the gain is increased independently of the other parameters. For experiments in the UV region, we have kept the electron energy at 500 MeV. We measured the bunch length σ_l with a streak camera at a very low current of less than 0.1 mA. As shown in Fig. 1, the minimum σ_l was 57 ps when the rf voltage in the HCV was set at the maximum value and the phase of the third harmonic field was optimized. On the other hand, regular value of σ_l with the MCV alone is 100 ps. The bunch length with the HCV remains much shorter than that in the regular operation even at higher beam currents. It can be concluded that the gain with the HCV is increased to be approximately 1.7 times higher over the whole range of the wavelength and the beam current.

At first, we chose the wavelength around 340 nm for experiments in the UV

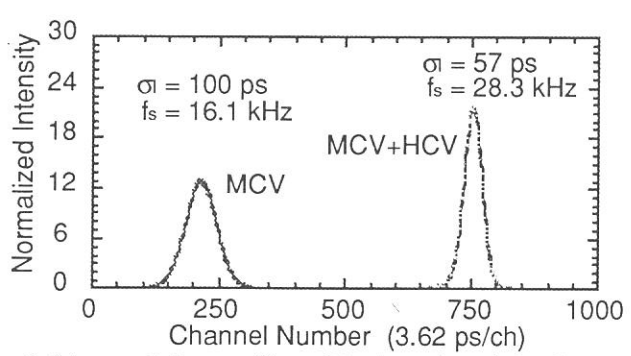

Fig. 1 Measured time profiles of the beam bunch for the normal operation (left) and the operation with the HCV (right).

region. The coating materials of mirrors for 340 nm were same as those used in the visible region. However, it turned out that the mirror degradation was much more serious than in the visible region. The reflectivity of mirrors for 340 nm decreased very much in the longer wavelength side, while that of the mirrors for 490 nm decreased appreciably in the shorter wavelength side. We have not identified exactly the origin of the mirror degradation at present. However, it seems that an absorption band appeared on the region from 340 to 440 nm by irradiation with higher harmonic radiation from the optical klystron. Based on this experience we decided to choose the wavelength at 300 nm for the experiment, where the mirror degradation is less serious. We obtained the first lasing in the UV region at 303 nm on July 5, 1993 with the initial beam current of 22 mA/bunch. The laser wavelength could be varied from 310 nm to 290 nm by changing the undulator gap. As the dose increased, the relative peak intensities at longer wavelengths decreased due to the mirror degradation. The mirror degradation was still serious in the wavelength region above 300 nm. Lasing at 293 nm, where the mirror degradation was less significant, continued until the beam current decayed down to 8.6 mA/bunch. The round-trip reflectivity of mirrors was measured after the lasing experiment to be 99.4 %. The estimated threshold current from the gain and the mirror reflectivity is approximately 9 mA/bunch, which agrees very well with the experimental value.

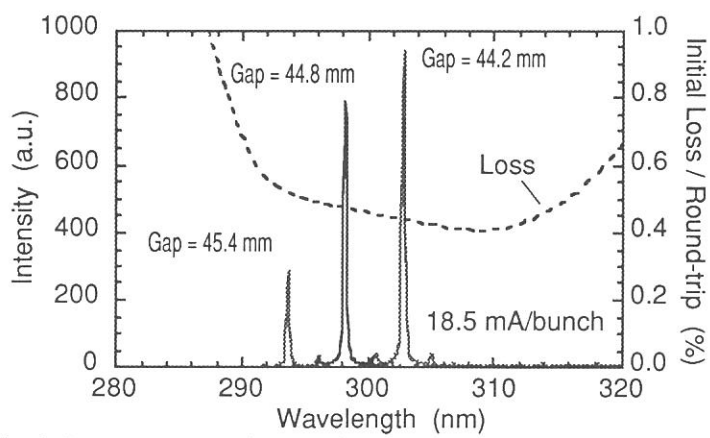

Fig. 2 Laser spectra at the wavelength around 300 nm measured by a monochrometor for various undulator gaps. The initial round-trip loss is also indicated by the dashed line.

We have also conducted experiments to derive the effective gain at the visible region around 500 nm with the gain enhacement technique. The effective gain can be deduced from the time dependent variation of the laser intensity as $G = (I_2 / I_1)^{\frac{1}{n}}$, where I_1 is the intensity at certain time and I_2 is that after n round-trips. Therefore we derived the effective gain as a function of time from the measured shape of the macropulse. In order to secure enough time for beam cooling by radiation damping, lasing was controlled by the gain-switching (G-switching) with a repetition rate of 1

Hz, in which the RF frequency was shifted by 200 Hz to stop lasing. The macropulse was measured with a biplanar photodiode. Time spectra of the laser power were taken by a digital oscilloscope and the data were transferred to a personal computer. Figure 3 shows the experimental value of gain at 490 nm as a function of the beam current, which was derived from the beginning of macropulses in the G-switching mode. The experimental gain is in good agreement with the calculated gain curve with the HCV. It was confirmed that the gain was enhanced as expected by the reduction of the bunch length using the HCV.

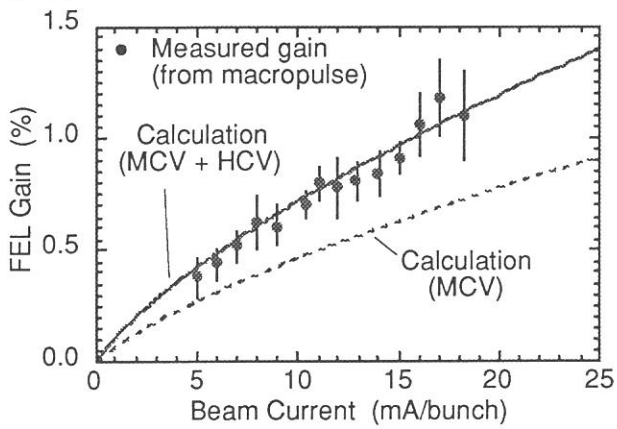

Fig. 3 Beam current dependence of the measured gain derived from the macropulse (solid circle) and the calculated one (solid line). The calculated gain for the normal operation with MCV only is also shown by the dashed line.

The further study including the bunch length measurement during the laser oscillation is in progress.

References

[1] S. Takano, H. Hama and G. Isoyama, Nucl. Instr. and Meth. A331 (1993) 20.

[2] K. Tamura, T. Kasuga, T. Tobiyama, H. Hama, T. Kinoshita and G. Isoyama, submitted to Jpn. J. Appl. Phys.

Improvement of Open Beam Lines

Masao Kamada, Atsunari Hiraya, Shin-ichiro Tanaka, Kusuo Sakai, Osamu Matsudo, Toshio Kinoshita, Jun-ichiro Yamazaki, Eiken Nakamura, and Makoto Watanabe*

UVSOR Facility, Institute for Molecular Science, Myodaiji, Okazaki 444
*Research Institute for Scientific Measurements, Tohoku University, Sendai 980

In 1993, we have carried out improvement of several beam lines opened for outside users as follows.

(1) **BL1B**: In April the device exchanging three gratings for 1-m Seya-Namioka type monochromator was suddenly broken. This is due to the fatigue of supporting springs, and so we repaired it by replacing with new springs. Moreover, when we fixed this trouble, we also replaced the G1 and G3 gratings with new ones, which have 2400 and 600 grooves/mm, respectively. The typical photon flux is now about $1x10^{10}$ photons/s/100mA at 280 nm with 0.1-0.1 mm slits.

(2) **BL2B1**: In March the M0 mirror in the premirror chamber was replaced with new one, since the old one has been used for 7 years. The intensity around 500 eV became ten times intense more than the previous one, but there is still a deep dip around 280 eV, which is due to the C K absorption of contaminated carbon on the mirrors and grating in the Grasshopper monochromator.

(3) **BL3A2**: In October the grating G1 of 2400 grooves/mm was replaced by new one. Then, the available maximum photon energy from the 2.2 m Constant Deviation Grazing Incidence Monochromator was extended up to 125 eV. In December the electronic circuit driving the monochromator was shut down. We doubted the virus coming from outside, but the reason of this trouble was the loosening of the contact of the cable between the linear encoder to ADC.

(4) **BL6A1**: In recent years, the Martin-Pupplet

interferrometer lost the accuracy so often that the users had to measure several times to get reproducibility of the spectra. This is because the thread of a driving gear of a movable mirror has been consumed. Can you imagine how many the mirror in the interferrometer has moved for 8 years ? We guess it is more than 100,000 motions. Thus, the driving mechanism of the interferrogram was replaced with newly constructed one in June. The present performance of the interferrometer is the same as that obtained in 8 years before.

(5) **BL7A**: The motion of the crystals in the double crystal monochromator follows the L-shaped bases moving along the linear guides. This allows us to get monochromatized lights in fixed direction. However, the previous linear guides were so short that the L-shaped bases were tilted slightly at low Bragg angle. In October the linear guides were replaced with new sound and long guides.

(6) **BL7B**: In December the device exchanging three gratings in 1-m Seya-Namioka type monochromator was repaired, since the extraordinary sound happened several times last autumn. This is due to the lack of lubricating powder MoS_2 in the translating and rotating part of the device exchanging and rotating gratings. We also replaced grating G2 and G3 with new ones and got the considerable increase in intensity around 100 nm. The driving mechanism of 1-m Seya-Namioka at BL 7B is not the same as that at BL 1B, but the fact that the driving mechanisms of BL 1B and BL 7B were shut down at almost the same time indicates that it is the good time to consider the renewal of the mechanism of 10-years-old monochromators.

The authors would like to express their sincere thanks to Mrs. N. Mizutani, K. Suzui, and T. Horigome of the machine shop of IMS for their supports and kind advice.

Construction of 15-m Constant-Deviation Grazing Incidence Monochromator with Laminar-type Gratings at BL8B1

Atsunari HIRAYA, Eiken NAKAMURA, Masami HASUMOTO, Toshio KINOSITA, Kusuo SAKAI, Eiji ISHIGURO*, and Makoto WATANABE**

Institute for Molecular Science, Myodaiji, Okazaki 444
**Department of Applied Physics, Osaka City University, Sumiyoshi-ku, Osaka 558*
***Research Institute for Scientific Measurements, Tohoku University, Sendai 980*

A 15-m constant-deviation grazing incidence monochromator was constructed at beamline 8B1. The principle of the monochromator is essentially the same with the monochromator at BL3A2, that is the sum of incident angle and diffraction angle is kept constant (constant deviation) and both entrance and exit slit are fixed (constant length). This monochromator was designed to cover the photon energy 31-620 eV (40.5 - 2 nm) by changing three laminar-type gratings. All gratings are original grating fabricated on synthetic quarts and coated with Au. Parameters of gratings are listed below.

	radius	groove density	lower limit	resolution*	duty factor+	depth	Au-coating
G1	15m	1080/mm	368 eV	92 meV	40%	15 nm	20 nm
G2	15m	540/mm	184 eV	46 meV	35%	20 nm	30 nm
G3	7.5m	360/mm	31 eV	8 meV	40%	20 nm	30 nm

*at lower energy limit, with 10μm slit, +pattern width / groove width

Other parameters of the monochromator and its optical elements are listed below.

acceptance angle	vertical: 1.5mrad, horizontal: 10mrad
M0 (horizontal focus)	spherical mirror: r=86.8m, incidence angle=87.5°
M1 (vertical focus)	bent elliptic mirror: incidence angle 88.5°, L1=6717mm, L2=1680mm, demagnification 1/4
M2	plane mirror
M3	toroidal mirror: $r_{vert.}$= 35655mm, $r_{hor.}$ = 86.5mm
Spot size at sample	horizontal: 2.0mm, vertical: 0.7mm

Fig. 1. shows the side view of the monochromator including premirror chamber (M1) and postmirror (M3) chamber. Total electron yield spectrum of TiO_2 obtained with using 1080 *l*/mm (G1) grating is shown in Fig. 2. Monochromatized photons were observed from 360 eV up to about 1 keV. After the final adjustment, this beamline will be used for absorption and total electron yield measurements on gases and solids, as well as fluorescence and (fragment) ion measurements on molecules.

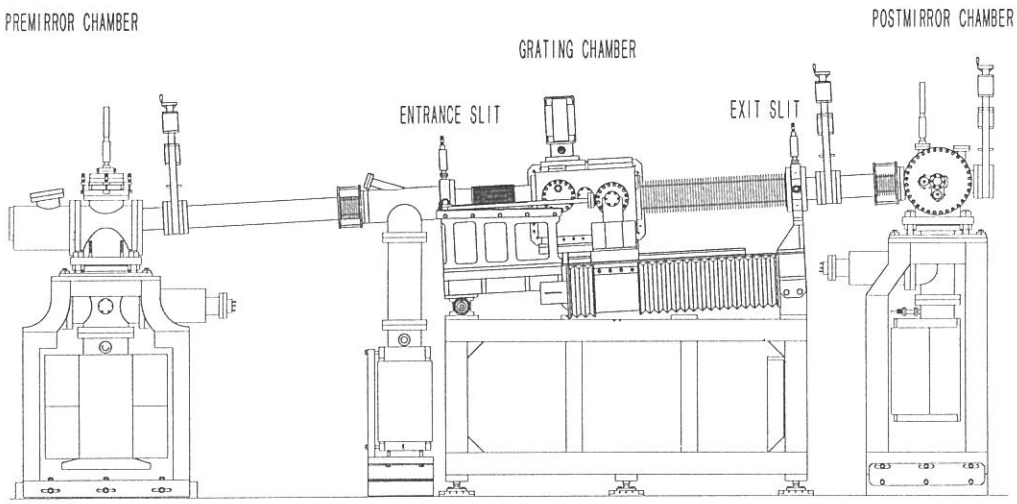

Figure 1. Side view of the monochromator including the premirror and postmirror chambers.

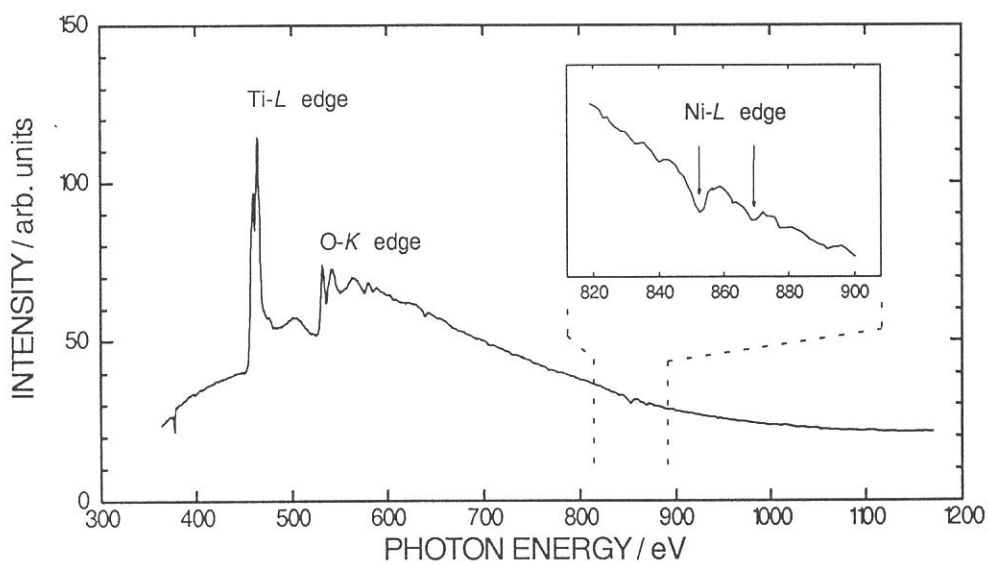

Figure 2. Electron yield spectrum of TiO_2 obtained with 1080 *l*/mm grating (G1).

Development of an Intense Source of Metal-Cluster Anions

Minoru KANNO[†] and Koichiro MITSUKE[§†]

The Graduate University for Advanced Studies,[†] and Institute for Molecular Science,[§]
Myodaiji, Okazaki 444

Study of photodetachment spectroscopy of metal cluster anions is very useful to obtain valuable information on the ground and electronically excited states of neutral clusters. We are constructing a source of metal cluster anions using plasma sputtering. This source is a cluster-ion version of the "BLAKE V" ion source which has been developed by Mori *et al.*[1] to generate intense beam of heavy-mass negative metal ions such as Au^- and Cu^- at National Laboratory for High Energy Physics (KEK) in cooperation with a research group of Tsukuba University.

A photographic view and a schematic diagram of the apparatus are shown in Figs. 1 and 2, respectively. Negative ions are produced at the surface of the sample metal which is placed in a Xe plasma confined by a multicusp magnetic field. The sputtered atomic ions are decelerated by collisions with flowing He gas, and then cluster ions condensed out of the quenched vapor. Atomic and cluster ions extracted from the source are mass-separated by a magnetic mass spectrometer and allowed to intersect at 90° with the dispersed light from a 1 m Seya-Namioka monochromator. The extraction voltage is set to 10 - 20 kV. In the first stage, we are planning to measure threshold photoelectron spectra of size-selected metal cluster anions.

1) Y.Mori, Rev. Sci. Instrum., **63**, 2357 (1992).

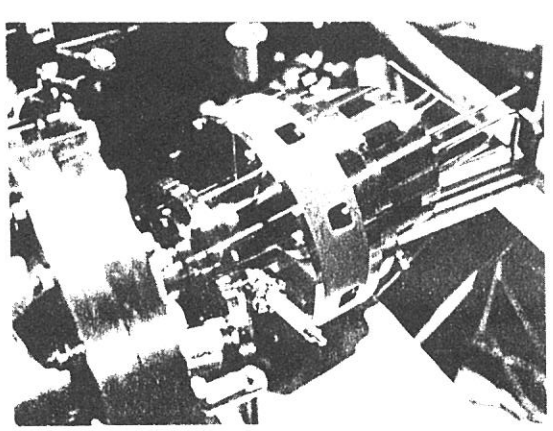

Figure 1. Photographic view of a source of metal-cluster anions.

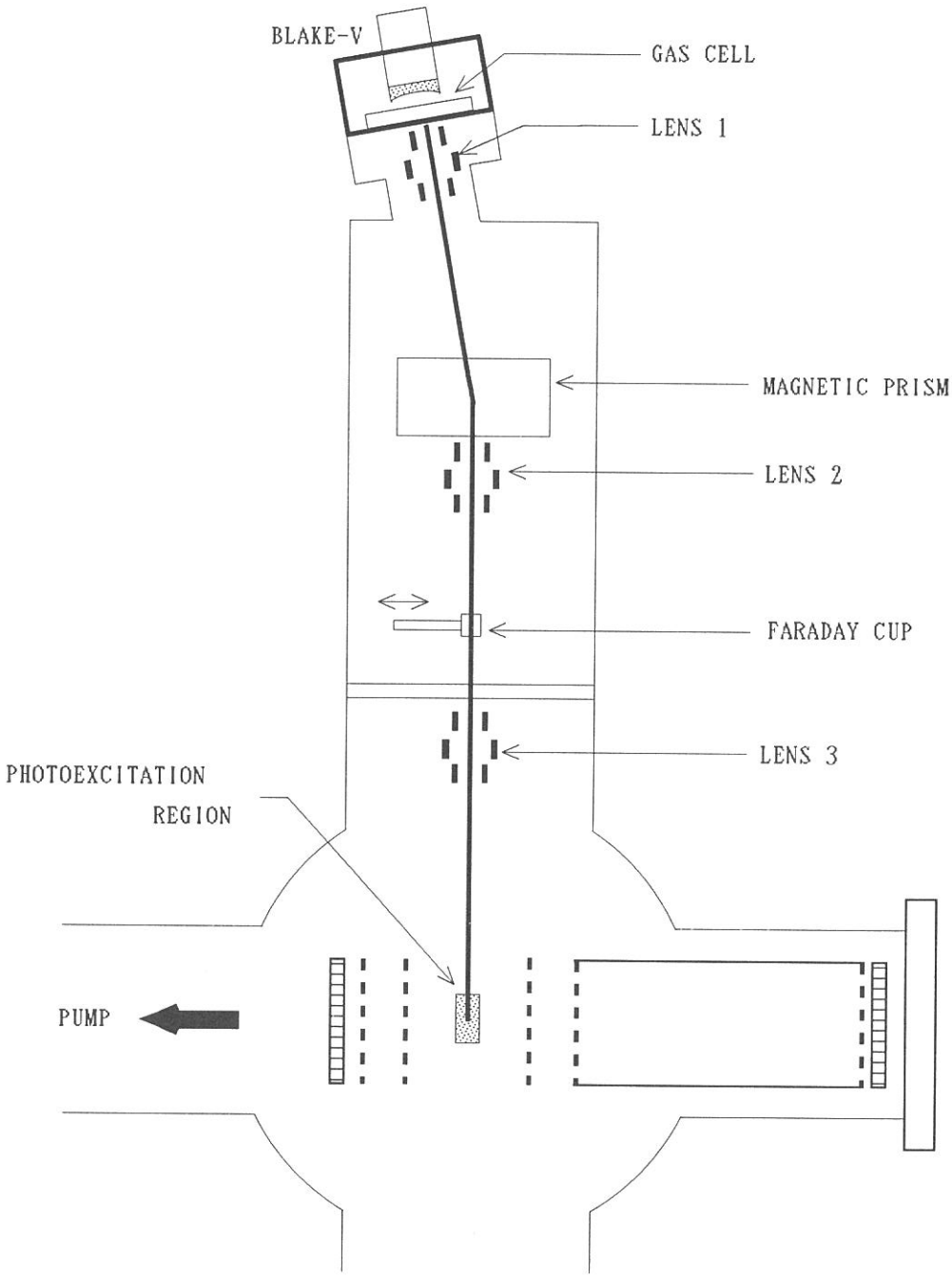

Figure 2. Schematic diagram of the apparatus for photodetachment spectroscopy of metal-cluster anions.

DEVELOPMENT OF HIGH INTENSITY CLUSTER BEAM SOURCE USING A CRYOPUMPING SYSTEM FOR PHOTOIONIZATION AND PHOTODISSOCIATION STUDIES

Hiroaki YOSHIDA and Koichiro MITSUKE

Department of Vacuum UV Photoscience, Institute for Molecular Science, Myodaiji, Okazaki 444

Photoionization and photodissociation studies of atomic or molecular clusters are very important to bridge the gap between atoms or molecules and solids. A great deal of efforts have been made to determine the geometrical structure and ionization potential of clusters. However, dynamical behaviors of clusters excited above their lowest ionization potential are hardly elucidated yet. In such an energy region, superexcitation and decay such as autoionization, neutral dissociation, and ion–pair formation are important in competition with direct ionization. We have been studying the ion–pair formation via molecular superexcited states by a positive ion–negative ion coincidence spectroscopy.[1,2] In order to apply this methodology to investigation of superexcited states of clusters, we have developed a supersonic cluster beam source using a cryopumping system.

A schematic diagram of the apparatus is shown in Fig.1. This type of beam source was originally developed by Hirayama et al. for electron energy loss spectroscopy of rare–gas clusters.[3] The three–stage cryogenic differential pumping system consists of inner and outer cylinders and two stainless steel pipes blazed around each cylinder. The system is mounted on a beam source chamber. A sample gas is expanded into the first stage from a conical nozzle of 100–μm diameter at room temperature (Laser technics, Inc.). A molecular beam is introduced through a conical skimmer with an entrance hole of 380–μm diameter (Beam Dynamics, Inc.) into the second stage and collimated by two slits of 2–mm diameter. The inner and outer cylinders are cooled by cold He and N_2 gases, respectively, flowing through the blazed pipes. The temperature of the wall of the inner cylinder is kept at about 30K. We are now examining the performance of the apparatus.

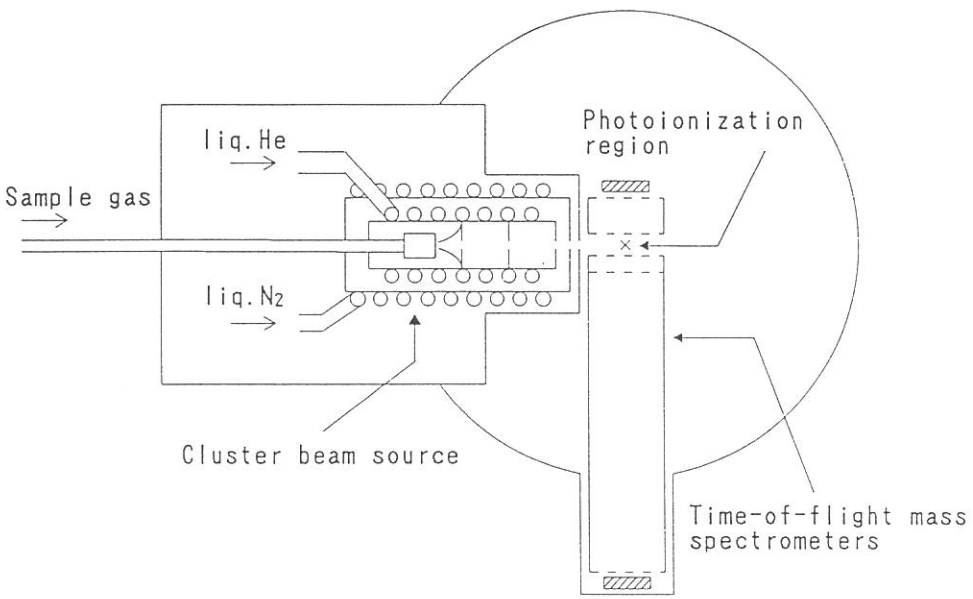

Fig.1 Schematic diagram of the supersonic cluster beam source using a three-stage cryogenic differential pumping system.

References

1) K.Mitsuke, H.Yoshida, and H.Hattori, Z.Phys.D **27**, 267(1993).

2) H.Yoshida and K.Mitsuke, J.Chem.Phys., submitted.

3) T.Hirayama, A.Kanehira, and I.Arakawa, Rev.Sci.Instrum. **64**, 962(1993).

Construction and performance of an apparatus for photoelectron spectroscopy and electron-ion coincidence measurement

Hideo Hattori and Koichiro Mitsuke

Department of Vacuum UV Photoscience, Institute for Molecular Science, Myodaiji, Okazaki 444

Ionization is a major phenomenon for photoexcited molecules in the VUV region. Photoionization cross section curves frequently show characteristic features, associated with a variety of ionization mechanisms.

In attempt to study the ionization mechanism in detail, we have constructed a versatile photoionization spectrometer at the beamline BL3B, as shown in Figure 1. We can make the experiments of photoionization mass spectrometry, photoelectron spectroscopy, constant-ionic-state spectroscopy, and photoelectron-photoion coincidence spectroscopy. This apparatus consists of an electron energy analyzer and a time-of-flight mass spectrometer. The energy analyzer is a 160° spherical electrostatic deflection type. The mean radius of the electron orbit is 54.7 mm. The mass spectrometer containing four grids and a drift tube of 50-cm length, is designed to satisfy space focusing conditions.[1] Measurements and data acquisition are controlled by the CAMAC and NIM system. The molecular beam of a sample gas is expanded into the ionization region from a nozzle of 50-μm diameter, and intersects perpendicularly with a VUV photon beam dispersed by a 3-m normal incidence monochromator. Produced ions are pushed away into the drift tube by a 1kV pulsed electric field and mass-analyzed. On the other hand, ejected electrons are focused onto the entrance slit of the energy analyzer and deflected electrostatically to a different region in space for different kinetic energies. The resolution of the analyzer is estimated to be about 50 meV with photoexcitation at 600 Å.

Figures 2 and 3 show photoelectron spectra of O_2 taken at 584 Å and 885-890 Å, respectively. In Figure 3, a long series of peaks can be seen on the lower energy side of the ionization limit for O_2^+ ($\tilde{X}^2\Pi_g$). The corresponding vibrationally excited states exist in the region of a so-called Franck-Condon gap, and are considered to result from autoionization of Rydberg states converging to upper ionic states. The spectrum at 885 Å shows an irregularly strong intensity of the $v'=5$ component. This may be ascribed to a

large overlap of vibrational wave functions between $O_2^+(\tilde{X}^2\Pi_g, v'=5)$ and the $(3s\sigma_g\,^3\Pi_u, v'=7)$ Rydberg state converging to $O_2^+(\tilde{A}^2\Pi_u)$.

1) W.C.Wiley and I.H.McLaren, Rev. Sci. Instrum. **26**, 1150 (1955).

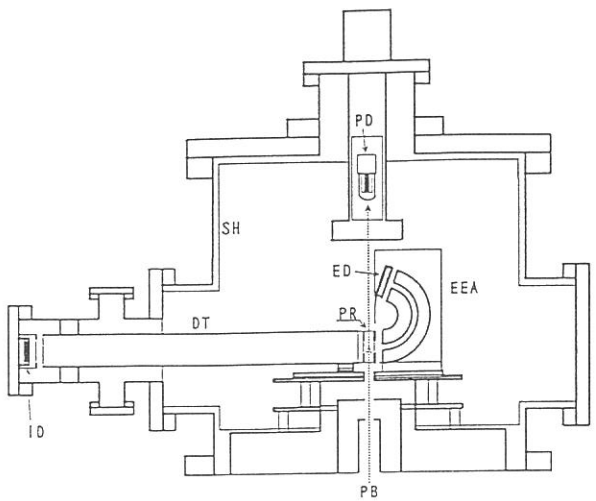

Figure 1. Schematic diagram of the photoionization spectrometer. PB: monochromatized photon beam, PR: photoionization region, DT: drift tube for ions, EEA: electron energy analyzer, ID: ion detector, ED: electron detector, PD: photon detector, SH: μ-metal shield. The molecular beam is introduced into PR perpendicularly to both PB and the symmetric axis of DT.

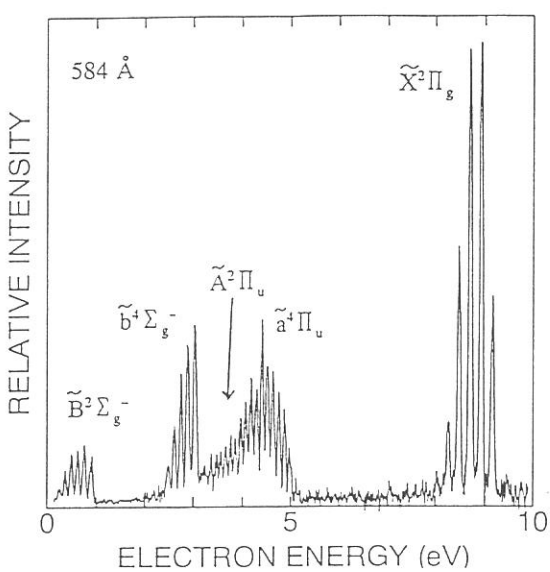

Figure 2. Photoelectron spectrum of O_2 taken with a excitation wavelength of 584 Å.

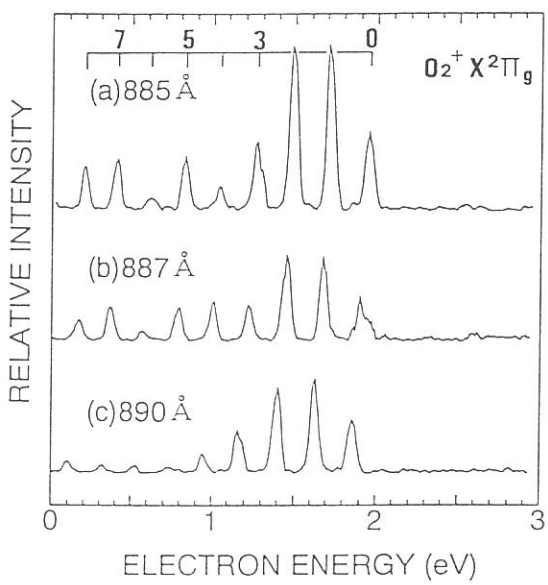

Figure 3. Photoelectron spectra of O_2 taken with excitation wavelengths of (a)885 Å, (b)887 Å and (c)890 Å. The observed band results from a transition to the $\tilde{X}$ ionic state.

CONSTRUCTION OF DEPOSITION SYSTEM IN BEAM LINE BL-4A AND EPITAXIAL GROWTH OF ZnTe BY SYNCHROTRON RADIATION

Mitsuhiro NISHIO, Toshihiro OGATA*, Makoto IKEJIRI* and Gheyas Syed IRFAN*

Institute for Molecular Science, Myodaiji, Okazaki 444, Japan

*Department of Electronic Engineering, Faculty of Science and Engineering, Saga University, Honjo-1, Saga 840, Japan

Low temperature growth is one of the key factors for growing ZnTe of high quality. We have already demonstrated by the experiment in the BL-8A that synchrotron radiation (SR) provides a powerful light source for a novel low-temperature growth technique of ZnTe. In order to investigate systematically the growth of ZnTe, we have constructed the deposition system connected to the analysis chamber in the BL-4A, as shown schematically in fig. 1. Here, the differential pumping system has been designed carefully in order to make sure that the growth experiment can be carried out at a pressure of 10^{-4} Torr without contaminating in the analysis chamber by source gases. Three apertures, each having an inner diameter 8 mm, were used. The length of the aperture near the growth chamber was prepared as long as 350 mm to reduce the conductance and its alignment could be done easily by using the X-Y stages, as shown in the figure.

In this experiment, diethylzinc and diethyltelluride were employed as source materials. Hydrogen was used as a carrier gas. The substrate was (100) oriented GaAs. The growth was carried out at room temperature by two different methods. One is the growth by the repetition of the cycle which is composed of the formation of adsorbed layer of the reactants followed by the irradiation of SR to the resulting layer. Another is the growth in a continuous gas flow in order to investigate the possibility of rapid epitaxial growth. In both cases, the film, having a relatively smooth and featureless surface morphology, was deposited on the substrate. The film was identified as ZnTe epitaxial layer by XPS, X-ray diffraction and RHEED techniques. Furthermore, it should be emphasized that no signals with regard to carbon and oxygen can be detected in the film by XPS and photoluminescence techniques. Figure 2 shows the relationship between the growth thickness and growth cycle in

the former procedure. The growth rate can be estimated to be 6 Å/growth cycle, indicating that the growth thickness can be controlled on an atomic scale by this method. In the latter procedure, on the other hand, the growth rate is as high as around 0.1Å/mAmin even when the total pressure and partial pressures of diethylzinc and diethyltelluride were kept at 5×10^{-5}, 3×10^{-6} and 2×10^{-6} Torr, respectively (fig. 3). We have also carried out the growth experiment using the sapphire window. However, it has been found that no growth happens in this case, indicating that the photons corresponding to wavelengths below 1500Å is effective for the growth of ZnTe.

The authors would like to thank to Dr. Hiraya of UVSOR facility for his helpful discussion with the design of differential pumping system.

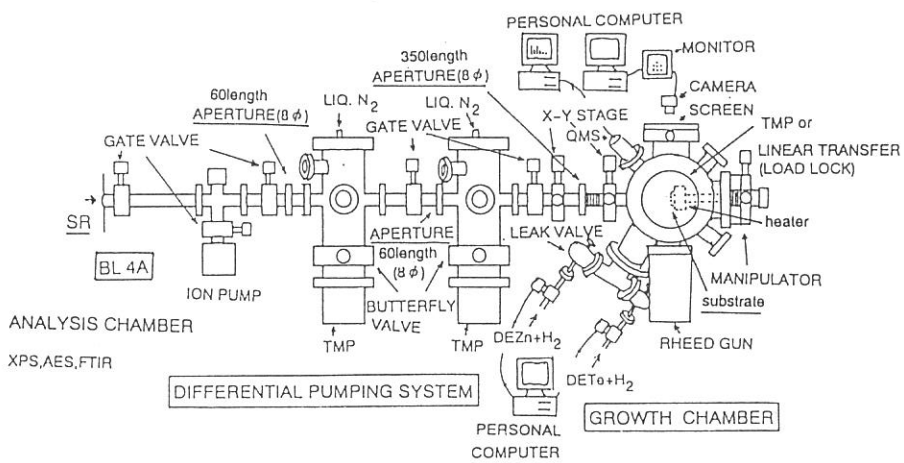

Fig.1. Schematical experimental apparatus.

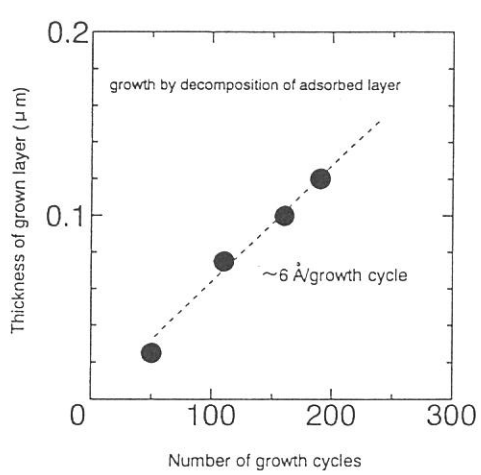

Fig.2. The thickness of the film versus the number of growth cycles.

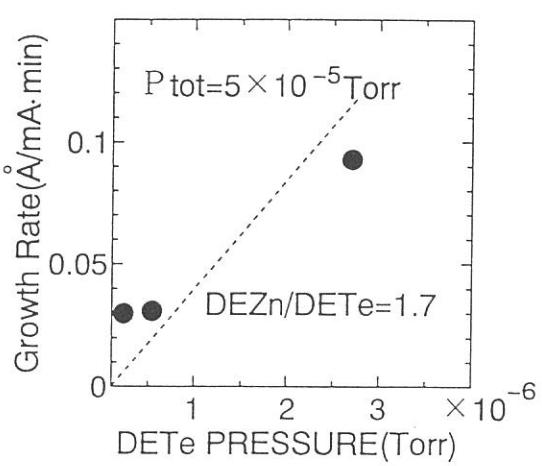

Fig.3. The growth rate of the film versus the partial pressure of diethyltelluride.

Construction of Infrared Reflection Absorption Spectroscopy for Study of Surface Photochemical Reactions Induced by Synchrotron Radiation

Mitsuru NAGASONO, Akitaka YOSHIGOE, Kazuhiko MASE, and Tsuneo URISU

Department of Vacuum UV Photoscience, Institute for Molecular Science, Myodaiji, Okazaki 444

Recently, surface photochemical reactions induced by synchrotron radiation (SR) have been applied to semiconductor processes such as atomic layer epitaxial growth and atomic layer etching. The reactions have different characters from thermal or plasma ones, but the detailed mechanism is scarcely explored.

The aim of the present study is to measure the change of the adsorbed species and/or the adsorption states under reactions induced by SR using infrared reflection absorption spectroscopy (IRAS), and to clarify the reaction mechanisms. Advantage of IRAS is high resolution as compared with electron energy loss spectroscopy, and feasibility to measure under presence of gas in a reaction chamber, i.e., *in situ*. This paper describes construction of IRAS for study of reactions induced by SR.

Fig. 1 shows the apparatus attached with an IRAS system. The apparatus consists of four ultra high vacuum chambers, i.e., an etching, an epitaxial growth, a sample storage, and an airlock chamber. The IRAS system is composed of a Fourier transform infrared spectrometer (FTIR: JEOL JIR-7000), three mirror systems and a mercury cadmium telluride (MCT) detector, and can measure the reactions in the etching and the epitaxial chamber. Optical paths are purged with dry air without CO_2. For measurements in the etching chamber, a collimated parallel infrared beam that is interfered by the FTIR is focused on the sample at an incident angle of 85° by an off-axis paraboloidal mirror M2 (diameter, D = 50mm, effective focal length, F = 320mm, diverting angle, α = 65°) through a ZnSe window. A reflected beam is collimated again by a mirror M5 (D = 50mm, F = 320, α = 65°), and is focused on the MCT detector by mirror M6 (D = 50mm, F = 45mm, α = 90°). For measurements in the epitaxial growth chamber, the IR beam is focused at incident angle of 82.5° by a mirror M4 (D = 50mm, F = 320, α = 90°) through a ZnSe window. The reflected beam is collimated by a mirror M7 (D = 50mm, F = 320, α = 90°), and is focused on the MCT detector by

mirror M8 (D = 50mm, F = 45mm, $\alpha = 90^{\circ}$). The signals from the MCT detector are amplified, and give IR spectra after fast FT calculation.

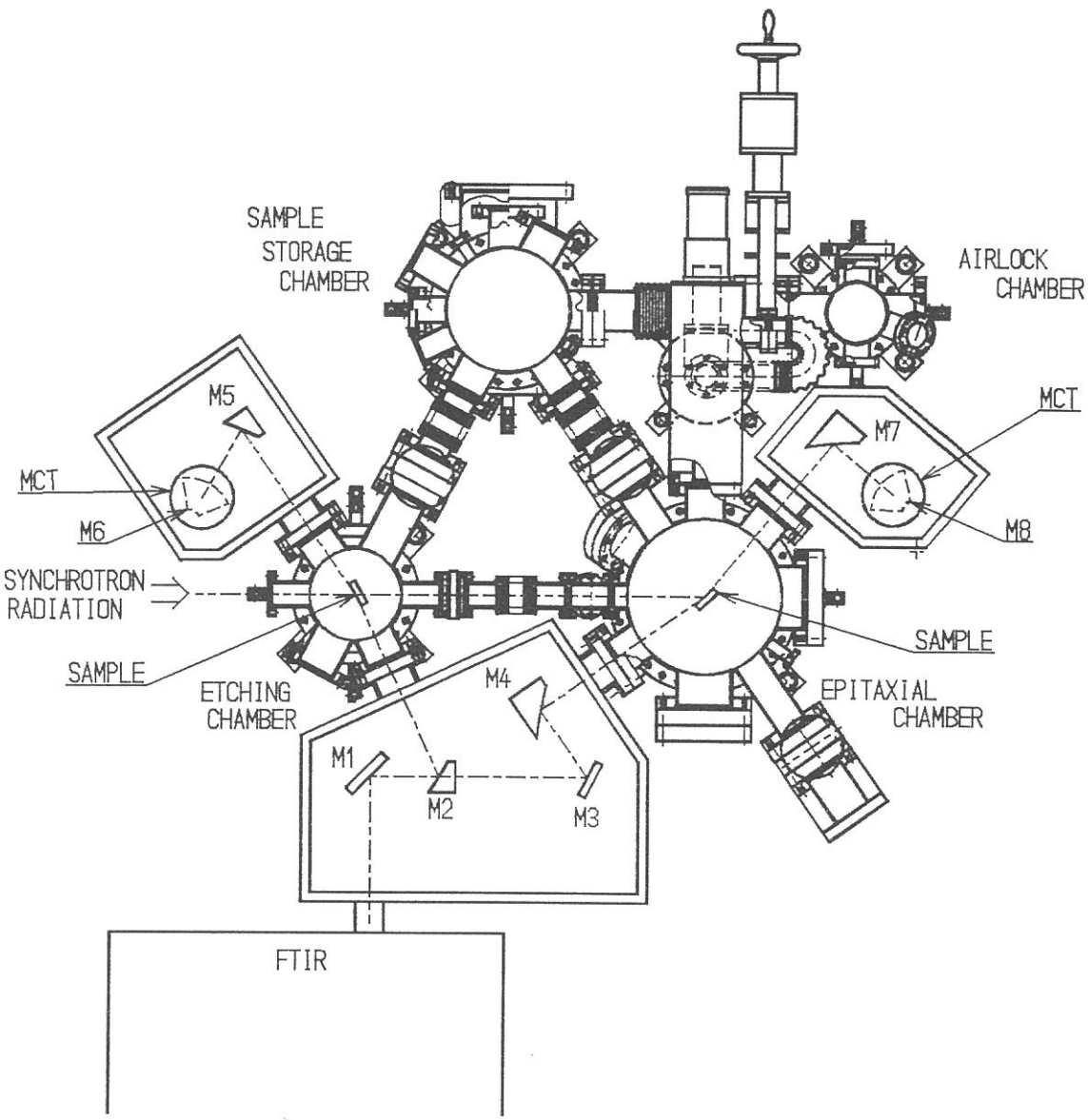

Fig. 1 IRAS system for study of SR excited surface photochemical reactions. For measurements in the etching chamber, IR beam passes through M1, M2, Sample, M5, and M6. For measurements in the epitaxial growth chamber, IR beam passes through M1, M3, M4, Sample, M7, and M8.

RESEARCH ACTIVITIES

Dissociative Double Ionization Following Valence and Si:2*p* Core Level Photoexcitation of $SiCl_4$ in the Range 38 - 133 eV

Bong Hyun Boo,[a] Seung Min Park,[b] and Inosuke Koyano,[c]

[a]*Department of Chemistry, Chungnam National University, Taejon 305-764 and Center for Molecular Science, 373-1 Kusung-dong Yusung-gu, Taejon 305-701, Korea*
[b]*Department of Chemistry, Kyung Hee University, Seoul 130-701, Korea*
[c]*Department of Material Science, Himeji Institute of Technology, 1479-1 Kanaji, Kamigohri, Hyogo 678-12, Japan*

The photoionization of $SiCl_4$ has been investigated in the valence and Si:2*p* inner shell region using time-of-flight mass spectrometry and synchrotron radiation in the range 38 - 133 eV. Branching ratios are reported for all charged species arising from the dissociative photoionization processes. Various monocations such as Cl^+, $SiCl_n^+$ (n=0-4) are observed together with doubly charged cations such as Si^{2+}, Cl^{2+} and $SiCl^{2+}$. A photoion-photoion coincidence (PIPICO) technique has been employed to investigate a variety of dissociation processes *via* Coulomb explosion and to interpret the dissociation mechanisms.

The total PIPICO efficiency curve has two sharp peaks and one broad peak near the Si:2*p* photoexcitation/photoionization threshold, as shown in Fig. 1. The first peak starts to rise at 103.0 eV and then reaches a maximum at 105.0 eV. This onset corresponds to the threshold for the dissociative double ionization following the Si:2*p* core photoexcitation. As shown in Fig. 2, processes 1 and 2 account for almost all the PIPICO intensities in the Si:2*p* core excitation region.

$$SiCl_4^{2+} \rightarrow Cl^+ + Si^+ + n.p. \qquad (1)$$

$$SiCl_4^{2+} \rightarrow Cl^+ + SiCl^+ + n.p. \qquad (2)$$

where n.p. denotes neutral fragments.

The obvious rise from 103.0 eV in $I_{\text{tot-PIPICO}}/I_{\text{tot-photon}}$ is due to photoexcitation of the Si:2*p* electron to the σ^* (a_1) orbital. This interpretation is based on the assignments of Si:2*p* absorption spectra of molecular SiF_4.[1] Friedrich *et al* proposed that experimental position of the peak due to the photoexcitation of Si:$2p_{3/2}$ to σ^* (a_1) is 106.13 ± 0.2 eV.[1] This value is in good agreement with the maximum in the total PIPICO efficiency curve.

The second sharp peak in Fig. 1 corresponds to the photoexcitation of Si:2*p* to σ^* (t_2), 4s, 3d, 4d, 5s and etc. converging to the Si:2*p* photoionization threshold.

The broad and strong peak above the threshold seen in the total PIPICO efficiency curve may be due to the backscattering of the excited electron by the Cl ligands, which gives rise to shape resonances above the threshold.[1] Fig. 2 account for the dissociation behaviors of doubly charged precursor ions in the Si:2*p* region as outlined below in Scheme 1.

Scheme 1.

$SiCl_4 + h\nu \rightarrow SiCl_4^*$ (Si:2*p* excitation to antibonding or Rydberg orbitals)
$SiCl_4^* \rightarrow SiCl_4^{2+} + 2e$
$SiCl_4^{2+} \rightarrow Cl^+ + SiCl_n^+$ (n=0-3) + n.p.

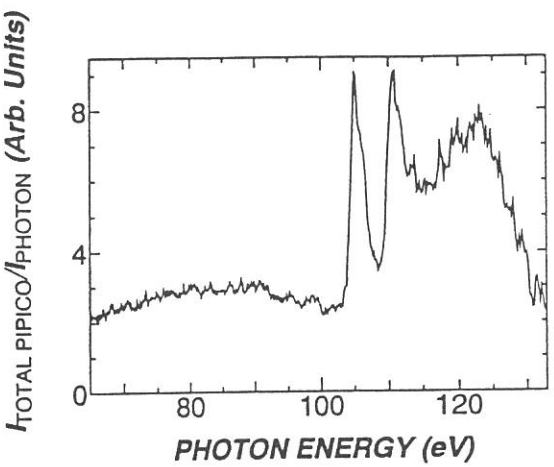

Figure 1. Total photo-ion-photoion coincidence efficiency curve of $SiCl_4$ in the range 65 - 133 eV.

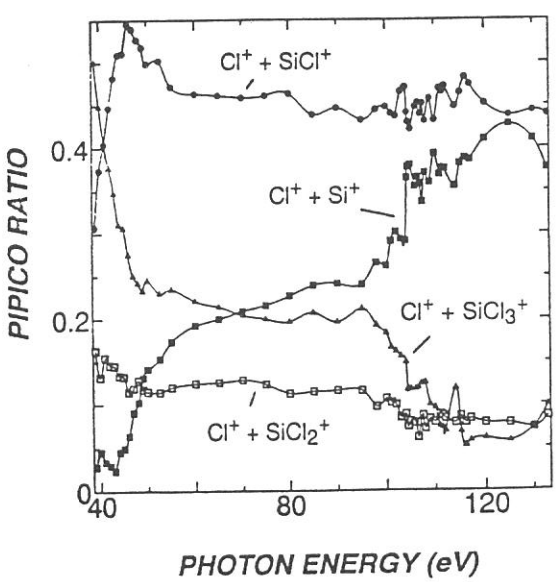

Figure 2. Ratios of integrated intensities of $Cl^+ - SiCl_n^+$ (n=0-3) ion pairs in PIPICO spectrum to total double photoionization ($I_{PIPICO}/I_{tot\text{-}PIPICO}$) in $SiCl_4$ as a function of photon energy.

References

1. H, Friedrich, B. Pittel, P. Rabe, W. H. E. Schwarz, and B. Sonntag, *J. Phys. B: Atom. Molec. Phys.* **13**, 25 (1980).

ABSORPTION AND EMISSION SPECTRUM OF CS_2 MOLECULE

P.Meenakshi Raja Rao and B.N.Raja Sekhar

Spectroscopy Division

BARC,Trombay,Bombay

INDIA.

and

M.Kouno,K.Tabayashi,K.Shobatake and M.Watanabe

Institute of Molecular Science

Myodaiji,Okazaki 444,

JAPAN.

Absorption and emission spectrum spectra of CS_2 molecule have been recorded in the wavelength region of 105-300 nm using continunm radiation from 600 Mev synchrotron radiation source (UVSOR), at the Institute of Molecular Science,Okazaki,Japan. The spectra were recorded at room temperature using a 10.9 cm gas cell with CS_2 vapour at 30 m.torr.A one meter Seya-Namioka monoch romator was used as a premonochromator.Several band heads due to CS_2 could be identified in the absorption spectrum.The fluorescence spectrum could arise due to CS_2 molecule as well as photofragmentated species of CS_2.The spectrum in the region 160-180 nm is of interest because of lack of information. Emission spectrum as shown in fig.I has got more features than the absorption spectrum. These may correspond to the photofragmented species of CS_2 . A detailed analysis of the spectrum which will enable the identification of the emitters and the characterisation of the states involved in the transitions is under progress.

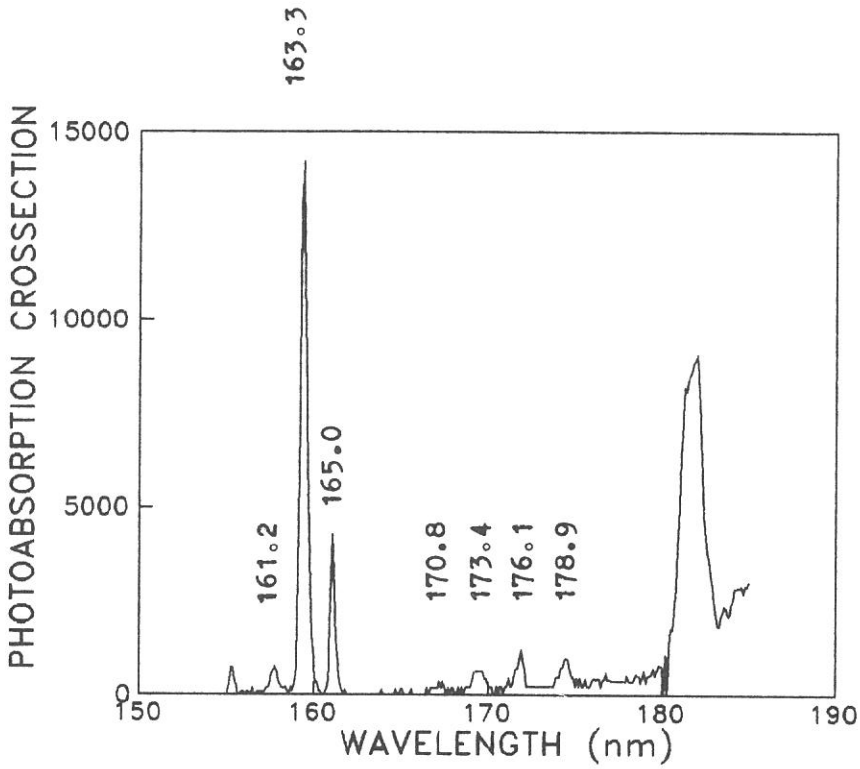
163.3
PHOTOABSORPTION CROSSECTION
15000
10000
5000
0
161.2
165.0
170.8
173.4
176.1
178.9
150
160
170
180
190
WAVELENGTH (nm)

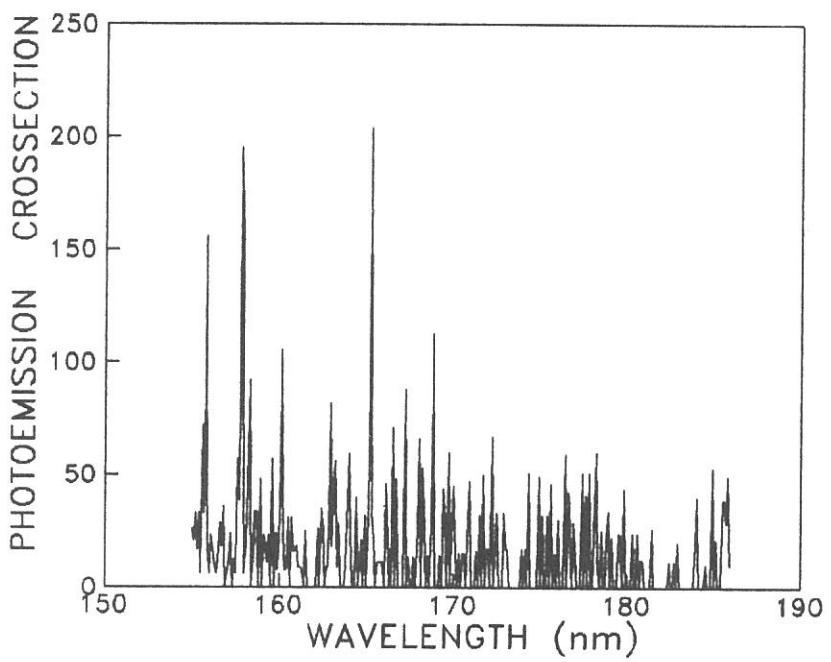
PHOTOEMISSION CROSSECTION
250
200
150
100
50
0
150
160
170
180
190
WAVELENGTH (nm)

Sulfur and Silicon K-Edges X-Ray Absorption Spectroscopy Studies of CdS Microcrystallites in Silicate Glasses

L. C. Liu[1], P. K. Tseng[1], G. T. Lin[1], W. F. Pong[2], A. Yoshida[3], A. Hiraya[4], Y. Takata[4], and N. Kosugi[4]

(1) Dept. of Phys., Natl. Taiwan U., Taipei, Taiwan, (2) Dept. of Phys., Tamkang U., Tamsui, Taiwan, (3) Dept. of Elec. Eng., Toyohashi U., Toyohashi, Japan, (4) Institute for Molecular Science, Myodaiji, Okazaki, Japan.

We have measured the x-ray absorption spectra of sulfur and silicon K-edges for the CdS microcrystallites precipitated in silicate glasses. The samples were measured using total electron yield mode using the beamline 1A, and the data were taken using a double-crystal InSb (111) monochromator (2d = 7.481 A).

Our silicate glasses containing ~1 wt% dissolved-CdS have been prepared by melting and fast quenching. We then heat treated these quenched glasses which contain no CdS microcrystallites (CdS in glass, no MCG) under five different conditions (600C, 16hr; 640C,1hr; 640C,2hr; 640C,4hr; 700C,16hr) to obtain CdS microcrystallites in glasses (CdS MCG). A CdS powder (99.99 %) sample and a CdS thin-film grown on the Corning 7059 glass surfaces were also prepared as referential samples. Fig. 1 shows the sulfur K-edge spectra of these eight samples. Comparing with three near edge absorption peaks of the standard CdS powder spectrum, the central peak of CdS film on glass shifted ~1 eV toward low energy direction. All the CdS MCG and CdS in glass (no MCG) spectra show a weak single peak near the standard central peak. Fig. 2 shows the silicon K-edge spectra of CdS in silicate glass (no MCG) and CdS MCG (700C,16hr). Detailed studies and data analyses are in progress.

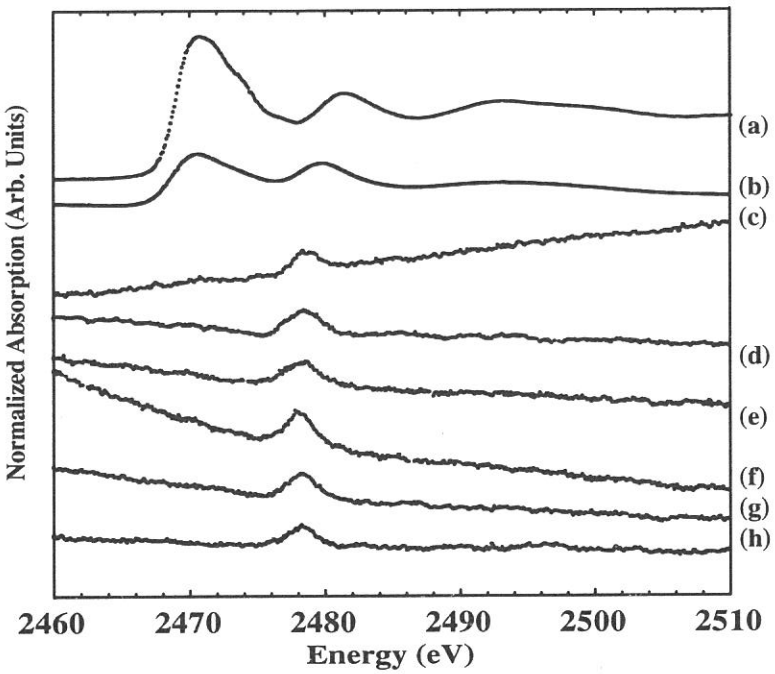

Figure 1: The sulfur K-edge spectra of (a) CdS power, (b) CdS film on glass, and CdS microcrystallites in glasses under various heat treating conditions [(c) 700C,16hr; (d) 640C,4hr; (e) 640C,2hr; (f) 640C,1hr; (g) 600C,16hr; (h) as quenched glass].

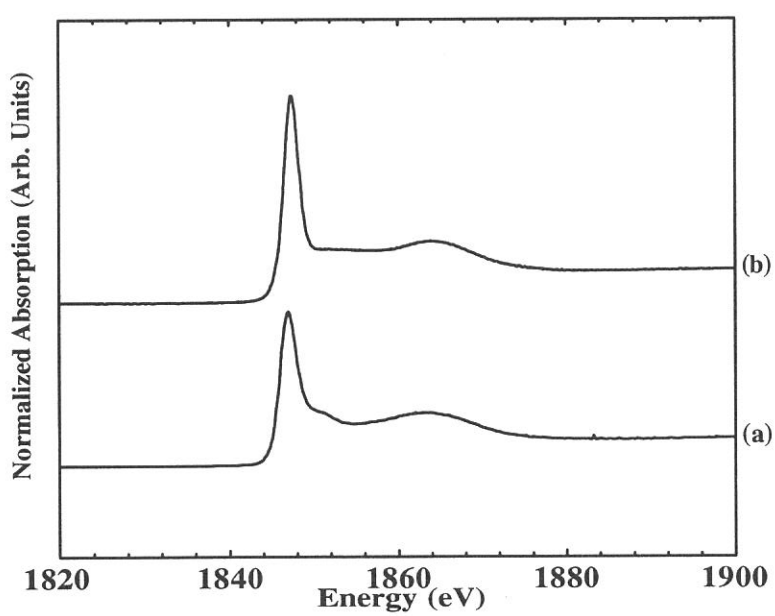

Figure 2: The silicon K-edge spectra of (a) CdS dissolved in glass and (b) CdS microcrystallites over grown in glass.

Si *K*-EDGE X-RAY ABSORPTION SPECTROSCOPY STUDIES OF Co SILICIDES

W. F. Pong,[1] Y. K. Chang,[1] P.K. Tseng,[2] S. H. Ko,[3] A. Hiraya,[4] M. Watanabe.[4]

(1) Dept. of Phys. Tamkang U., Tamsui, Taiwan, (2) Dept. of Phys. Natl. Taiwan U., Taipei, Taiwan, (3) Dept. of Materials Eng., Rensselaer Polytechnic Institute, Troy, New York, (4) Institute for Molecular Science, Okazaki, Japan.

Cobalt disilicide is one of the several transition metal silicides which have been considered for application as contact and interconnect metallization in the *very large scale integrated* (VLSI) circuits. Thin $CoSi_2$ films can be formed by rapid thermal annealing (RTA) of Co films sputtered on a single-crystal Si(100) substrate. The kinetic of the formation of $CoSi_2$ from $CoSi/Co_2Si$ was followed by the reaction with the silicon, and the growth of CoSi and Co_2Si were created by the thin films of cobalt on silicon with RTA.

We have measured the *x*-ray absorption spectra of Si *K*-edge for the Co silicides at room temperature using the beamline 1A. The samples were measured using total electron yield mode with an electron multiplier under a base pressure of less than $1x10^{-7}$ torr, and the data was collected using a double-crystal InSb (111) monochromator. Fig. 1 shows the white line regions of the absorption spectra from thin films Si(100), Si/Co(<100 Å), Si/CoSi(600 Å)/Co_2Si(1500 Å), and $CoSi_2$(2560 Å). Preliminarily, the spectra has a first peak (labelled I) for all samples and a second prominent peak (labelled II) only for Si/CoSi(600 Å)/Co_2Si(1500 Å) and $CoSi_2$(2560 Å), which are believed to be attributed to the empty Si p states and hybridization of the Co d states with the Si p states, respectively.

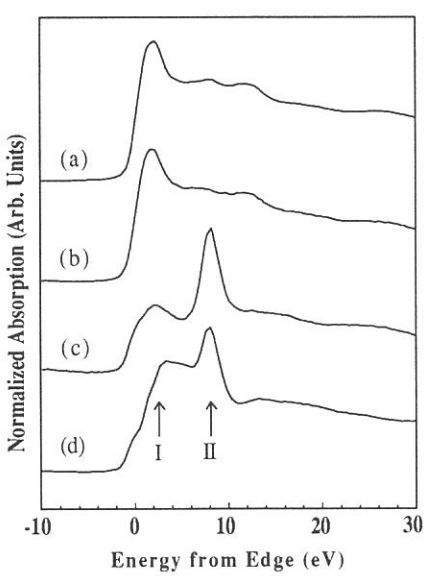

Fig. 1 Normalized Si *K*-edge absorption spectra for thin films (a) Si(100), (b) Si/Co(<100 Å), (c) Si/CoSi(600 Å)/Co_2Si(1500 Å), and (d) Si/$CoSi_2$(2560 Å). The zero energy corresponds to 1839.3 eV.

MO-SI MULTILAYER AS SOFT X-RAY MIRRORS FOR THE WAVELENGTHS AROUND 20 NM REGION.

D. Kim, and H.W. Lee
Physics Department,

J. J. Lee, and J. H. Je
Department of Materials Science & Engineering,
Pohang University of Science and Technology,
Pohang, Kyungbuk 790-600, Korea

M. Sakurai, Department of Physics, Kobe University, Kobe 657, Japan

M. Watanabe, Institute for Molecular Science, Okazaki 444, Japan.

Molybdenum-silicon multilayer soft x-ray mirrors have been fabricated using a magnetron sputtering system. Their structures have been characterized by x-ray diffraction (XRD) and reflectivities at normal incidence have been measured by using monochromatized synchrotron radiation in the 18- 24 nm region. A normal incidence reflectivity as high as 40% at 20.8 nm was achieved.

In Fig. 1, the small-angle x-ray diffraction data obtained from a sample (the sample number: m930111) is shown. The dynamic range is approximately five orders of magnitude. The number of Bragg peaks observed (10 peaks) and their narrow widths indicate that the sample has a relatively well-defined multilayer structure. The estimate yields d = 11.01 nm. The decrement of the effective real part of the index of refraction of the multilayer structure can also be evaluated, which can then be used to estimate γ, the ratio of the thickness of the Mo layer to the multilayer period: $\gamma = (\delta - \delta_{Mo}) / (\delta_{Mo} - \delta_{Si})$. δ_{Mo} and δ_{Si} are the decrements of the effective real part of the index of refraction of Mo and Si, respectively. The estimated γ for this sample is 0.21

Figure 2 shows the variation of the reflectivity of s-polarized soft x-ray lights measured from the sample of m930109. Figure 3 is the wavelength-scan of the reflectivity from 18 to 24 nm at the incidence angle of 2.5°. The solid line is the calculation using the parameters found in XRD with the assumption of abrupt and smooth interfaces. Dots are the measured reflectivity. The calculation and the measurement were done with the s-

polarized incident light. The calculation uses the characteristic matrix algorithm that was originally developed by Abeles

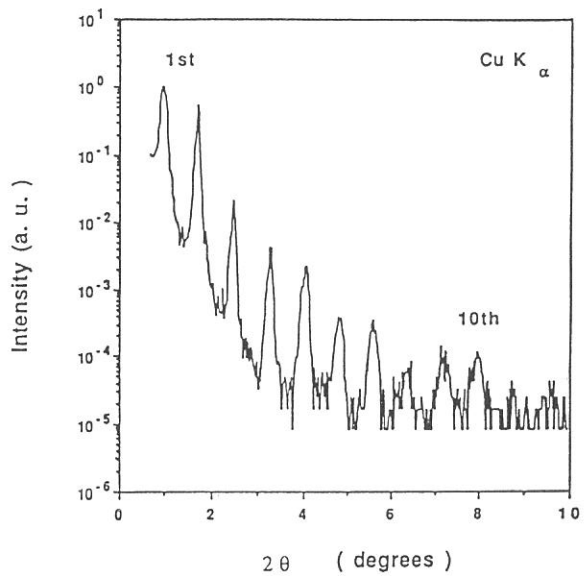

Figure 1 X-ray diffraction data with Cu K_{α} characteristic x-ray (0.154 nm)

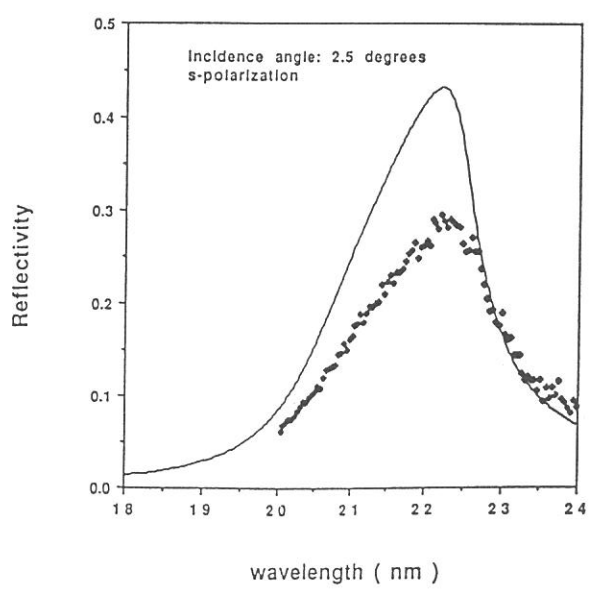

Figure 2 Reflectivity at the incidence angle of 2.5° from 18 to 24 nm

Photoemission Studies of Na Adsorption on Ge(111)-c(2×8) Surface

Jeongwon KIM, Sehun KIM, Jaemyung SEO[a], and Masao KAMADA[b]

Department of Chemistry and Center for Molecular Science, Korea Advanced Institute of Science and Technology, Taejon 305-701, Korea
[a] *Department of Physics, Jeonbuk National University, Jeonju 560-756, Korea*
[b] *UVSOR, Institute for Molecular Science, Myodaiji, Okazaki 444, Japan*

Metal/semiconductor interface has been one of great interest related to Schottky barrier formation and oxidation enhancements. As a special case, Si(111) and Ge(111) show (3×1) ordered structure when alkali metal is adsorbed and the substrate is annealed. One of the surprising properties for this surface is passivation to oxidation contrary to the common trend that alkali metals on semiconductor enhance the oxidation due to charge transfer to substrate. In this work, the absolute coverage of the alkali metal and bonding nature between alkali metal and substrate were investigated by applying the core-level and angle-resolved photoemission spectroscopy (ARPES).

The experiments were conducted at BL6A2 covering the photon energy 10 eV to 130 eV by a plane grating monochromator. The UHV chamber (base pressure of 2×10^{-10} Torr) was equpped with a LEED optics, AES, and hemispherical analyser for angle resolved photoemission. During the photoemission the overall energy resolution was 0.15~0.2 eV. Ge(111) wafer was cleaned by repeated cycles of Ar^+ sputtering and annealing, so to observe the c(2×8) LEED pattern. The (3×1) reconstruction was achieved by deposition of Na through the thermal dispenser cell and susequent annealing at about 400°C for 10 seconds.

During the Na evaporation, the actual coverage was determined by the change of secondary electronb cutoff in photoemission spectrum. In Fig.1 shown the change of the work function *vs.* Na evaporation time. The structural transformation to (3×1) was done around 1/3 of saturated Na ($\Delta\phi = -0.85 \sim -1.0$ eV) and the (1×1) appeared at slightly below half the saturation coverage.

In Fig. 2 and 3, ARPES spectra using $h\nu = 21.1$ eV photon are shown for Na/Ge(111)-3×1 surface as a function of polar angle. In both directions $\overline{\Gamma}$ - $\overline{K}$ $[1\bar{1}0]$ and $\overline{\Gamma}$ - $\overline{M}$ $[\bar{1}\bar{1}2]$ of (1×1) surface Brillouin zone, surface states S_1 and S_2 can be seen at $E_b = 0.35$~0.8 eV and 1.0~1.4 eV respectively. They are Na-induced surface states similar to the adatom and rest-atom surface states of the clean Ge(111)-c(2×8).

In Fig. 4 is shown the deconvoluted core-level spectra with superposition of bulk and surface emission in binding energy scale referred to bulk Ge $3d_{5/2}$. In the bottom curve of the Fig. 4, well known surface core-level components

are at 0.25 eV and 0.71 eV lower binding energy relative to bulk. On the center spectrum of (3×1), two surface components are located at 0.22 eV and 0.59 eV, which are shifted to higher binding energy. It is oppsite direction from what is assumed by electronegativity difference between Na and Ge atom. In simple charge transfer model, it represents a predominant character of covalent bonding in this surface. Comparing the upper spectrum of clear (1×1) surface, the intensity of Na 2p of (3×1) is about 1/3 ML.

The true structure of (3×1) surface is not known at this stage and further studies are necessary. However, the study of bonding nature and coverage-detemination in this report can be a contribution to solve the properties of the (3×1) reconstructed surface.

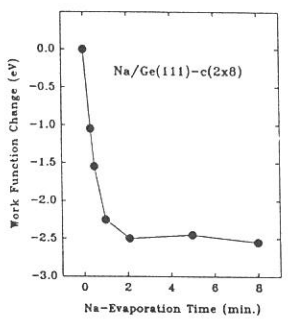

Fig. 1

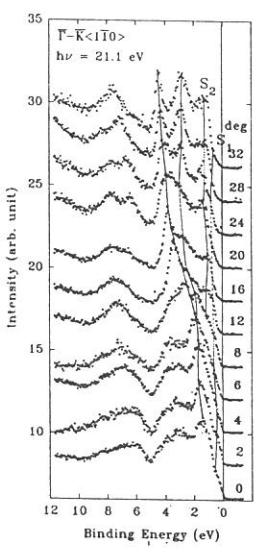

Fig. 2

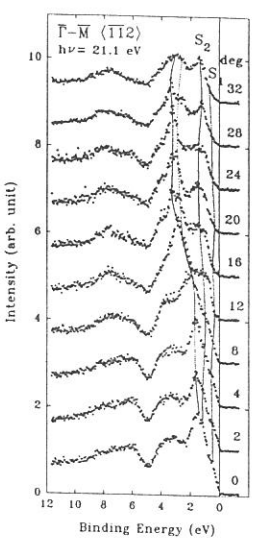

Fig. 3

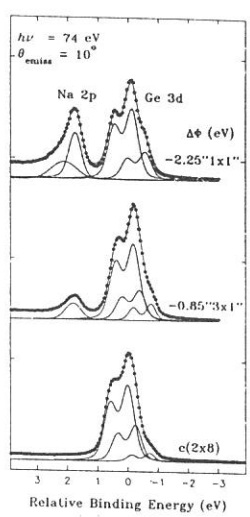

Fig. 4

Effect of Quenching Processes on Fluorescence Decay Curves of Barium Fluoride Excited by VUV Synchrotron Radiation

M.A.Terekhin[1], A.N.Vasil'ev[2],M.Kamada[3], S.Ohara[3], E.Nakamura[3], S.Kubota[4]

[1]*RRC 'Kurchatov Institute', Moscow 123182, Russia*
[2]*Physics Department, Moscow State University, Moscow 117234 Russia*
[3]*Institute for Molecular Science, Myodaiji, Okazaki 444 Japan*
[4]*Rikkyo University, Nishi-Ikebukuro 3 Tokyo 171 Japan*

The mechanism of the fast UV luminescence of some ionic crystals as a radiative transitions between valence and upper core bands was introduced at the first time for BaF_2 about ten years ago.[1] It was shown recently that the nanosecond decay kinetics of the most crystals with this type of luminescence was nonexponential[2,3] and depend on the excitation energy in XUV region.[2,4] We assume nonexponential decay due to at least two mechanisms of quenching depending on the excitation manner: the surface losses and the quenching due to the interaction of the core hole with the closely spaced electronic excitations.

Luminescence measurements were performed using BL3A2 beamline, equipped with a constant-deviation grazing-incidence type monochromator covering the VUV energy range from 12 to 100 eV.

In order to investigate the role of different types of quenching we have studied the decay curves of the BaF_2 (220 nm emission band) excited by photons with different energies (from 22 to 90 eV; Fig. 1, 2a) and at different angles of incidence (from 12° to 87°; Fig. 2b). All curves are normalised and shifted at their maximum. The kinetics is nonexponential for all energies. The deviation from the single exponential law increases with energy above 30 eV. In this energy region the BaF_2 absorption coefficient decreases[5] from $5 \cdot 10^5$ (for 30 eV) to $1.5 \cdot 10^5$ cm^{-1} (for 90 eV). These curves demonstrate the role of the quenching due to the increase of the mean number of secondary excitations. For excitation energies below 30 eV only the primary electron can interact with the core hole. This type of quenching should not be very intensive. Fig. 2b demonstrates the angle dependence of the quenching due to decrease of the penetration depth. Figure 3 presents the stationary fluorescence excitation spectrum and the quenching function $Q(t) = -\ln(I(t)/I_0(t))$ (at t=3 ns after the response maximum) calculated from the decay curves for different energies. The excitation spectrum is normalised by the sodium salycilate excitation efficiency. The dips in the excitation spectrum $\eta(h\nu)$ are strongly correlated with the peaks of $Q(t)$ in accord with the relation $\eta(h\nu) = \tau^{-1} \int \exp(-Q(t)-t/\tau)\, dt$, where τ is the radiation time. In order to compare these spectra with optical functions we present the absorption spectrum from the paper of Tarrio *et al.*[5]

The present investigations demonstrate pure role of two different mechanisms of the luminescence quenching (the surface quenching and the energy transfer to the excitations produced by the same photon). The role of these mechanisms seems to be general for most of fast luminescent crystals, and further study of these effects will allow to construct the detailed models of the quenching processes in ionic crystals.

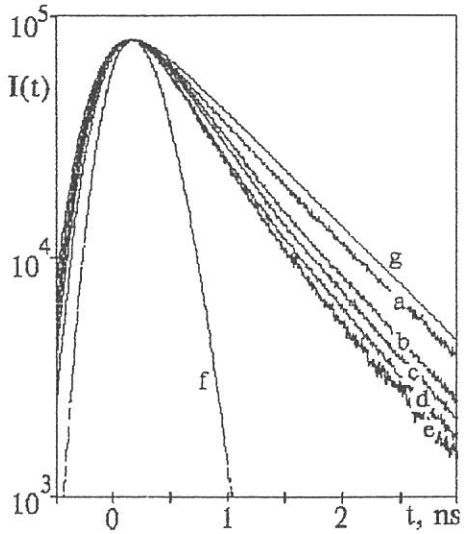

Fig.1 BaF_2 fluorescence decay curves for different excitation energies: (a) - 30 eV; (b) - 40 eV; (c) - 52 eV; (d) - 70 eV; (e) - 90 eV; (f) - excitation profile; (g) - $I_0(t)$, i.e. the single exponential decay curve (τ=0.92 ns) convoluted with the excitation profile. The radiation time τ is determined by fitting the asymptotic behavior of the slowest decay curve (a).

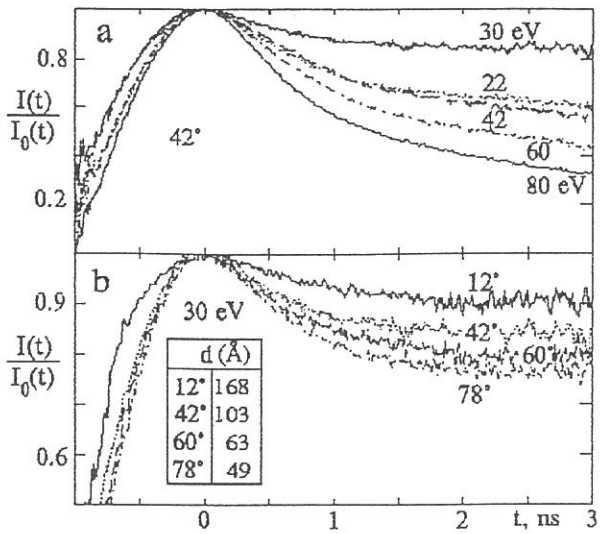

Fig.2 The ratio $I(t)/I_0(t) = \exp(-Q(t))$ for BaF_2 at different excitation energies: (a) - 30 eV, 22 eV, 42 eV, 60 eV, 80 eV; 42°, and different incidence angles: (b) - 30 eV; 12°, 42°, 60°, and 78°. The values of the penetration depth d are presented in the figure. $I_0(t)$ is the convolution shown in Fig. 1, curve g.

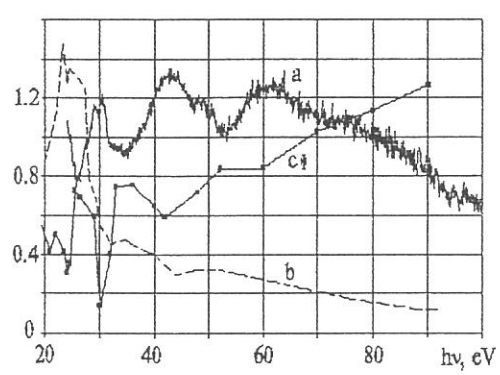

Fig. 3 (a) - BaF_2 stationary fluorescence excitation spectrum relative to sodium salycilate (arb. un.); (b) - BaF_2 absorption coefficient ($\times 1 \cdot 10^{-6}$ cm^{-1})[5]; (c) - quenching function $Q(t)$ at t=3 ns after the maximum of the curve.

References

1) Yu.M.Aleksandrov, V.N.Makhov, P.A.Rodny, T.I.Syreishchikova, M.N.Yakimenko, Sov. Phys. Solid. State 26 1734 (1984). 2) S.Kubota, M.MacDonald, I.Munro, J.Lumin. 48&49 589 (1991). 3) I.A.Kamenskikh, M.A.MacDonald, I.H.Munro, V.V.Mikhailin, M.A.Terekhin, Rev.Sci.Instrum. 63 1447 (1992). 4) I.A.Kamenskikh, M.A.MacDonald, I.H.Munro, V.N.Makhov, V.V.Mikhailin, M.A.Terekhin, Preprint of Daresbury Laboratory DL/SCI/P882E, 1993. 5) C.Tarrio, D.E.Husk, S.E.Schnatterly, J. Opt. Soc. Am. B 8, 1588 (1991).

DISSOCIATION DYNAMICS OF CH_4^+ CORE ION IN THE $^2A_1$ STATE

Kenji FURUYA,[a),b)] Katsumi KIMURA,[a),c)] Yasuhiro SAKAI[d),e)], Toshinobu TAKAYANAGI[d)], and Nobuaki YONEKURA[b)]

[a)]Institute for Molecular Science, Okazaki 444

[b)]Department of Molecular Science and Technology, Kyushu University, Kasuga, Fukuoka 816

[c)]Department of Materials Science, Japan Advanced Institute of Science and Technology, Tatsunokuchi, Ishikawa 923-12

[d)]Department of Physics, Sophia University, Chiyoda-ku, Tokyo 102

[e)]Department of Physics, Toho University, Funabashi, Chiba 274

Threshold-photoelectron photoion coincidence (TPEPICO) spectra of CH_4 have been observed with synchrotron radiation at the excitation to the $^2A_1$ ($v_1 = 0$ - 3) ionic states as well as to the $4pt_2$ Rydberg ($v_1 = 0$ - 4) states. In all the TPEPICO spectra observed, the CH_3^+ band shape is almost rectangular, this fact indicating that the translational and internal energy distributions of CH_3^+ are very narrow. The total kinetic energy releases (KERs) have been estimated from the CH_3^+ band shape. As a result, it has been found that the CH_3^+ species is in an electronically excited state.[1] From the narrow distributions of the total KERs and the similarity in the TPEPICO CH_3^+ band shapes between the spectra at the $^2A_1$ ionic state and the $4pt_2$ Rydberg state excitations, it has been found that the Rydberg electron is just a spectator and the dissociation of the core ion plays an important role in the dissociation through the $4pt_2$ Rydberg state. Similar results have also been obtained for CH_2^+ and CH^+ productions.

Figure 1 shows H^+ bands observed in the TPEPICO spectra. The H^+ fragment has been observed only at the $^2A_1$ state excitation, showing a band with a long tail in the slower flight time region. The total average KERs and the decay rates have been estimated from band shape simulation, and they are summarized in Table I. From these results, it has been found that a dissociation limit of the H^+ ion exists just below the $^2A_1$ ionic state. In contrary to the case of the CH_3^+ production, the H^+ production mechanism at the $^2A_1$ ionic state excitation is essentially different from that of H* production at the $4pt_2$ Rydberg state excitation.

1. Y. Sakai, K. Furuya, T. Takayanagi, and K. Kimura, *Ann. Rev. (IMS)*, p.94 (1992).

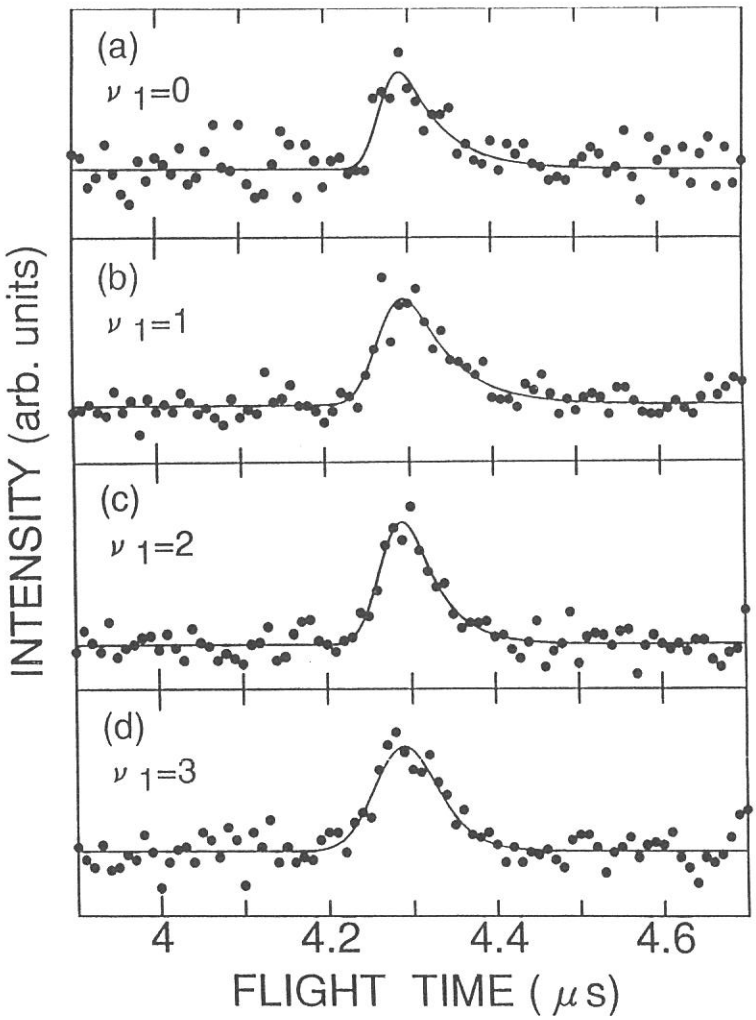

Fig. 1 H^+ band shapes in CH_4 TPEPICO spectra observed in the $^2A_1$ state region (dots). The simulated spectra are indicated by solid lines.

TABLE I. FWHMs, average KERs, and decay rates estimated from the H^+ band shapes in TPEPICO spectra of CH_4

ν_1	FWHM(ns)	average KER (meV)	decay rate (μs^{-1})
0	38	40	19
1	53	78	19
2	50	70	26
3	74	150	34

OBSERVATION OF DOUBLY-EXCITED RYDBERG STATES OF N_2O BY POSITIVE ION-NEGATIVE ION COINCIDENCE SPECTROSCOPY

Hiroaki YOSHIDA and Koichiro MITSUKE

Department of Vacuum UV Photoscience, Institute for Molecular Science, Myodaiji, Okazaki 444

Ion-pair formation processes of N_2O are studied in detail using synchrotron radiation to observe superexcited states N_2O^{**} lying in the 24-34eV excitation energy range. Positive ion-negative ion coincidence (PINICO) spectroscopy makes it possible to distinguish dissociation into three bodies,

$$N_2O + h\nu \rightarrow N_2O^{**} \rightarrow O^- + N^+ + N, \quad (1)$$

from dissociation into two bodies,

$$N_2O + h\nu \rightarrow N_2O^{**} \rightarrow O^- + N_2^+. \quad (2)$$

Figure 1 shows the photodissociation efficiency curves for the two processes at 24-34eV. The efficiency curve for process (2) rapidly falls with the increase of the energy, while that for process (1) makes a maximum at about 27.6eV and then gradually fades out with showing some peak structures. Sum of the efficiencies for processes (1) and (2), which is considered to be proportional to a total O^- yield, accords well with the previous result.[1] This suggests that the detection efficiency of the ion pair is nearly the same for processes (1) and (2). It is, thus, concluded that the three-body dissociation is dominant in the ion-pair formation from N_2O above 25.3eV.

Several resonancelike peaks are observed in the efficiency curves in Fig.1. Peaks appearing in the two curves are numbered from 1 to 15. The positions of the ionic states with multiple electron being excited (multiple electron transitions: MET) obtained from PES data[2] are also indicated. It is highly likely that most of the peaks are ascribed to transitions to superexcited states with double-electron excitation, judging from the electronic configurations of METs II $[(2\pi)^{-2}(3\pi)^1\ ^2\Pi]$ and III $[(1\pi)^{-1}(2\pi)^{-1}(8\sigma)^1\ ^2\Sigma]$,[3] which exist in this particular energy region. There are a number of doubly-excited Rydberg states in which an electron is promoted to an unfilled valence orbital and another electron to a Rydberg orbital. Excitation energy E_R for the Rydberg state is related to the vertical ionization potential E_I for the corresponding doubly-excited ionic state by the Rydberg

formula

$$E_R = E_I - R/(n-\delta)^2 , \qquad (3)$$

where R and n are the Rydberg constant and the principal quantum number, respectively. Comparing E_R obtained using eq.(3) with the peak energies in Fig.1, we will make tentative assignments of Peaks 1–15. Analysis of the shape of coincidence signals show that the three–body dissociation O^-+N^++N results from a transition to a superexcited state with $^1\Sigma^+$ symmetry. With this symmetry restriction, possible configurations of the involved Rydberg states converging to MET II are $(2\pi)^{-2}(3\pi)^1(np\pi)^1\ ^1\Sigma^+$ and $(2\pi)^{-2}(3\pi)^1(nd\pi)^1\ ^1\Sigma^+$. As shown in Fig.2, the positions of Peaks 5–8 are in fair agreement with those expected from E_R values for several doubly–excited Rydberg states.

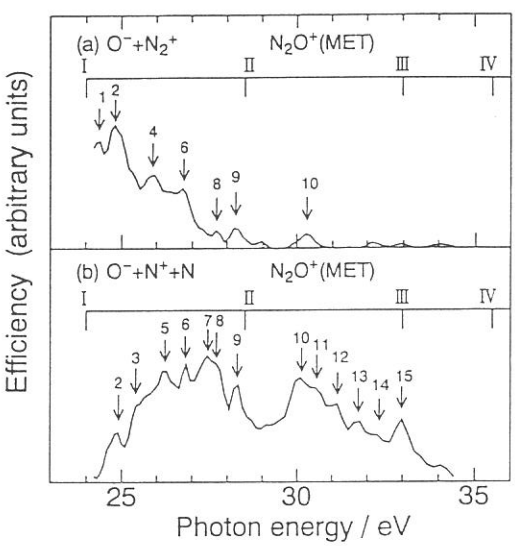

Fig.1 Photodissociation efficiency curves for the ion–pair formation from N_2O as a function of the photon energy. (a) the two–body dissociation $N_2O+h\nu\rightarrow O^-+N_2^+$ and (b) the three–body dissociation $N_2O+h\nu\rightarrow O^-+N^++N$.

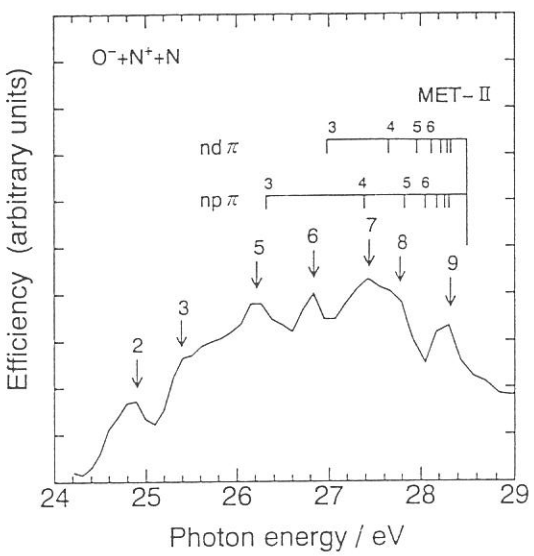

Fig.2 Photodissociation efficiency curve for the three–body dissociation $N_2O+h\nu\rightarrow O^-+N^++N$ in the photon energy of 24–29eV.

References

1) K.Mitsuke, S.Suzuki, T.Imamura, and I.Koyano, J.Chem.Phys. **92**, 6556(1990).

2) C.E.Brion and K.H.Tan, Chem.Phys. **34**, 141(1978).

3) H.Nakatsuji, Chem.Phys. **75**, 425(1983).

Fragmentation of short-lived CO_2^+ in van der Waals molecules

Masatoshi UKAI and Yoshihiko HATANO
Department of Chemistry, Tokyo Institute of Technology, Tokyo 152

Hiroaki YOSHIDA and Koichiro MITSUKE
Institute for Molecular Science, Myodaiji, Okazaki 444

Photoionization and following ionic fragmentation of a molecule in a framework of van der Waals (vdW) complex gives the opportunity to study ion-molecule reaction as a "half-process". This framework of vdW-complex enables to examine the reactions involving short-lived species,[1] which is difficult in a "full" collision experiment. We show ionic fragmentation of CO_2^+ in a vdW complex.

A vdW complex of CO_2 is produced by a skimmed expansion of a pure CO_2 or Ar/CO_2 (1:1 ratio) mixture gas (0.4 or 1 atm. back pressure) through 100 $\mu m\phi$-aperture. CO_2 in a vdW complex is ionized by the absorption of synchrotron radiation of the wavelength λ from a 1m Seya-Namioka monochromator at BL-2B2. In a "full-process", since excited ions are attenuated before a collision due to optical relaxation for CO_2^+(A and B states)[2] and the predissociation for CO_2^+(C and satellites),[3] the ground-state ion is only possible as a projectile of full-collision. The aim of this work is to make a "half-collision" experiment of these short-lived species with CO_2. Following "intramolecular" charge-transfer reactions of $CO_2^+ + CO_2$ is examined by a mass-spectrometric analysis of product ions using a quadrupole mass filter,

$$CO_2^+(\tilde{A},\ \tilde{B},\ \tilde{C},\ \text{or satellite})\cdot CO_2 \rightarrow (CO_2)_2^+,\ (CO_2\cdot CO)^+,\ (CO_2\cdot O)^+,\ \text{or } (CO_2\cdot O_2)^+.$$

Photoionization efficiencies (PIE's) for these ions were measured as a function of λ for $30<\lambda<95$ nm, which are shown in Fig.1 together with the PIE for CO_2^+.

The PIE of CO_2^+ clearly shows autoionization structures due to Rydberg states converging onto $\tilde{A}$, $\tilde{B}$, and $\tilde{C}$ ions. However, most of these structures are diminished for complex ions. Dehmer[4] observed the same trend with higher resolution in λ.

The PIE's for $(CO_2O)^+$, $(CO_2CO)^+$, and $(CO_2O_2)^+$ show different λ-dependence from those for CO_2^+ and $(CO_2)_2^+$ parent ions. It is probable that the dissociative ions are originated from highly excited predissociating ions, such as CO_2^+ ($\tilde{C}$ or satellites). However, λ-dependence of the present PIE's is not similar to those for O^+, CO^+, or O_2^+ in dissociative photoionization of free CO_2. Also the PIE's increase very weakly above the $CO_2^+(\tilde{C})$ ionization threshold, which makes

a contrast to the steep onset structures in the PIE's for O^+, CO^+, or O_2^+. It is expected that ionization onto satellites of CO_2 in a framework of vdW complex mainly yields these dissociative ions.

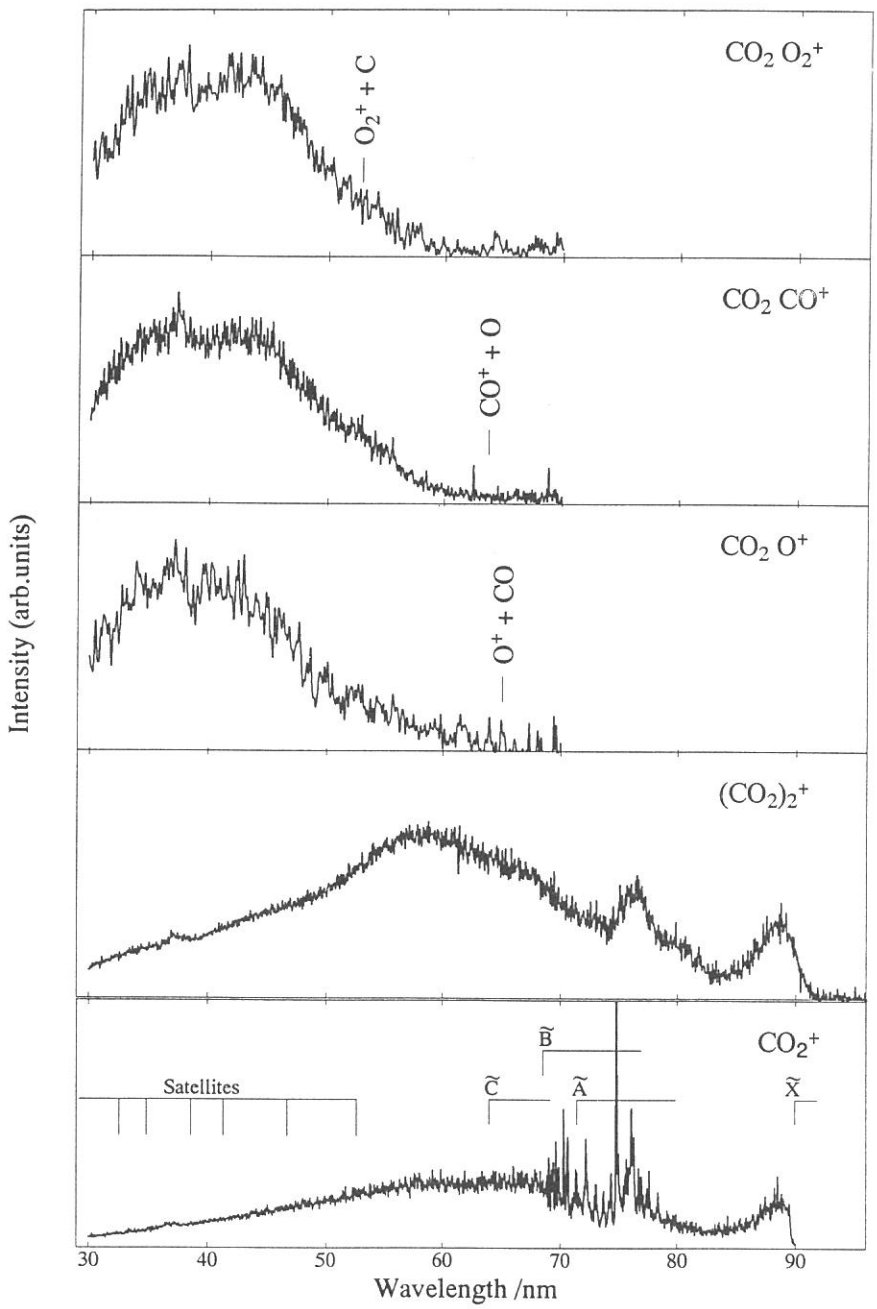

Fig.1
PIE curves for CO_2^+, $(CO_2)_2^+$ $(CO_2O)^+$, $(CO_2CO)^+$, and $(CO_2O_2)^+$

[1]M.Ukai et al., *Chem.Phys.Lett.* 167,334(1990); [2]M.Ukai et al., *J.Chem. Phys.* 97,2835(1992); [3]J.H.D.Eland & J.Berkowitz, *J.Chem.Phys.* 67,2782 (1977); [4]P.M.Dehmer *J.Chem.Phys.* 83,24(1985).

SITE-SPECIFIC FRAGMENTATION FOLLOWING Si:2*p* CORE-LEVEL PHOTOEXCITATION OF $F_3SiCH_2Si(CH_3)_3$ IN THE VAPOR PHASE

Shin-ichi NAGAOKA, Joji OHSHITA,[a] Mitsuo ISHIKAWA,[a]
Keiko TAKANO,[b] Umpei NAGASHIMA,[b] Takae TAKEUCHI,[c]
and Inosuke KOYANO[d]

Department of Chemistry, Faculty of Science, Ehime University, Matsuyama 790
[a]Department of Applied Chemistry, Faculty of Engineering, Hiroshima University, Higashi-Hiroshima 724
[b]Department of Information Sciences, Faculty of Science, Ochanomizu University, Otsuka, Bunkyo-ku, Tokyo 112
[c]Department of Chemistry, Faculty of Science, Nara Women's University, Kitauoya Nishimachi, Nara 630
[d]Department of Material Science, Faculty of Science, Himeji Institute of Technology, 1479-1 Kanaji, Kamigohri, Hyogo 678-12

In recent years, relaxation processes following core excitation in molecules have been a topic of much interest. We have investigated site-specific fragmentation following photoexcitation of (trifluorosilyl)(trimethylsilyl)methane ($F_3SiCH_2Si(CH_3)_3$, FSMSM) in the range of Si:2*p* excitation by means of the photoelectron-photoion and photoion-photoion coincidence methods (PEPICO and PIPICO methods, respectively).

The experiments were performed using a time-of-flight spectrometer with variable path length, coupled to a constant-deviation grazing incidence monochromator installed on the BL3A2 beam line of the UVSOR synchrotron radiation facility in Okazaki.[1]

The total photoionizaion efficiency curve of FSMSM has one broad peak near the 2*p* core-ionization threshold of the silicon atom. The site-specific fragmentation following the Si:2*p* core-level photoexcitation of FSMSM can be seen by means of the PIPICO technique. Figure 1 shows plots of the ratios of the

integrated intensities of the various ion pairs in the PIPICO spectrum to the total double-photoionization ($I_{PIPICO}/I_{tot\text{-}PIPICO}$) as a function of photon energy. It is seen that there are two thresholds for $I_{PIPICO}/I_{tot\text{-}PIPICO}$ (104.5 and 107 eV).

It is concluded that the relative yields of H^+-SiF^+ and CH_n^+-SiF_3^+ (n = 1-3) ion pairs are enhanced around 104.5 eV, and those of CH_3^+-$F_3SiCH_2Si(CH_3)_2^+$ and H^+-$SiCH_3^+$ are enhanced around 107 eV. The former and latter thresholds are likely to correspond to the Si:2p core-level photoexcitation at the Si atom bonded to three F atoms and at Si bonded to three methyl groups, respectively. The fragmentation occurs selectively around the Si atom where the photoexcitation takes place.

1. T. Masuoka, T. Horigome, and I. Koyano, Rev. Sci. Instr. 60, 2179 (1989); E. Ishiguro, M. Suzui, J. Yamazaki, E. Nakamura, K. Sakai, O. Matsudo, N. Mizutani, K. Fukui, and M. Watanabe, Rev. Sci. Instr. 60, 2105 (1989). T. Masuoka and S. Nagaoka, Trends Chem. Phys., in press.

Fig. 1 $I_{PIPICO}/I_{tot\text{-}PIPICO}$ in FSMSM as a function of photon energy. $(P\text{-}CH_3)^+$ refers to $F_3SiCH_2Si(CH_3)_2^+$.

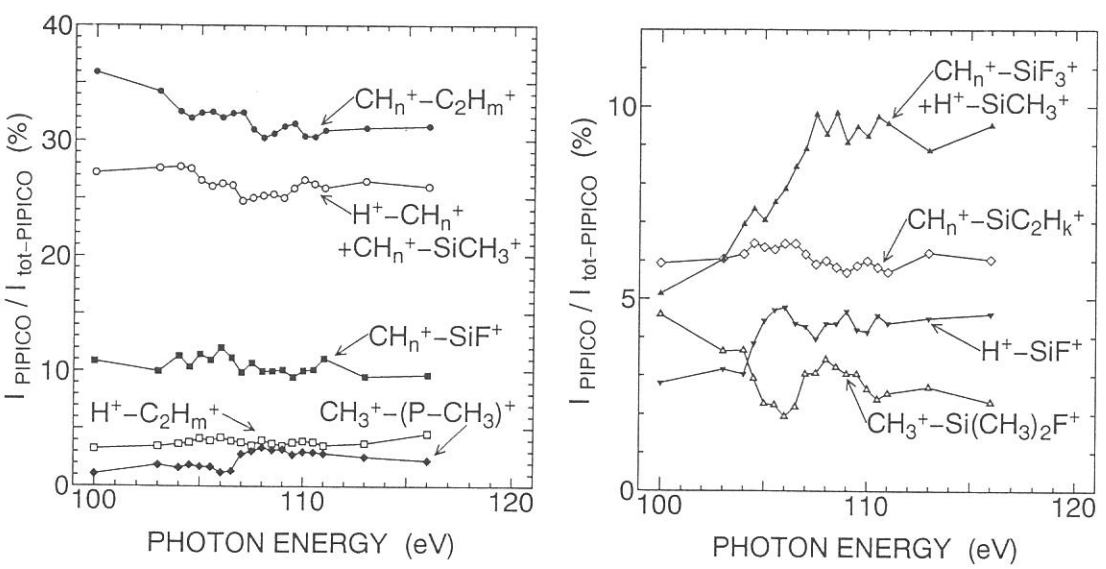

Dissociation Dynamics of NF_3 Studied Using PEPICO and PIPICO Technique in the Vacuum Ultraviolet

Shinzo Suzuki,[a] Eiken Nakamura,[b] and Inosuke Koyano[c]

[a]Department of Chemistry, Tokyo Metropolitan University, Tokyo 192-03, JAPAN
[b]UVSOR, Institute for Molecular Science, Myodaiji, Okazaki 444
[c]Department of material Science, Himeji Institute of Technology, 1479-1, Kanaji, Kamigohri, Hyogo 678-12

Dissociative single and double photoioniozation processes of NF_3 have been studied by use of photoelectron-photoion coincidence (PEPICO) and photoion-photoion coincidence (PIPICO) technique in the photon energy range of 32-130 eV.

The branching ratios of product ions and PIPICO ratios were measured as a function of the incident photon energy. Figure 1 shows that the threshold for the formation of F^+ is located around 32 eV and that the N^+ formation has a maximum at about 40 eV, then decreasing as the incident photon energy increases. Figure 2 shows that a metastable molecular dication NF^{++} is observed in the photon energy range $h\nu$ < 40 eV. The threshold is lower than the value (43.8 eV) determined using electron impact ionization mass spectrometry.[1]

There are two possible photoexcitation processes responsible for the formation of doubly ionized NF_3 via normal Auger process, in the photon energy range 40-50 eV.

$$(F_{2s}\ 2e)^{-1} \text{ --> } NF_3^{++}(V_j^{-1}V_k^{-1}) + e \text{ --> } NF^{++} + 2F + e \quad (1)$$

$$(F_{2s}\ 3a_1)^{-1} \text{ --> } NF_3^{++}(V_j^{-1}V_k^{-1}) + e \text{ --> } NF^{++} + 2F + e \quad (2)$$

The ionization thresholds for $(F_{2s}\ 2e)^{-1}$ and $(F_{2s}\ 3a_1)^{-1}$ have been estimated as 39.62 eV and 43.06 eV, respectively by XPS study [2]. Then, the energy threshold for the NF^{++} formation observed here below 40 eV, may indicate that the process (1) is

responsible for the NF^{++} formation near the threshold.

REFERENCES

[1] S.E.Rogers, P.J.Miller, and S.R.Leone, Chem.Phys.Lett., 166, 137(1990).
[2] Data from R.N.S.Sodhi and C.E.Brion, J.Elec.Spectro. Rel.Phen., 34, 373(1984).

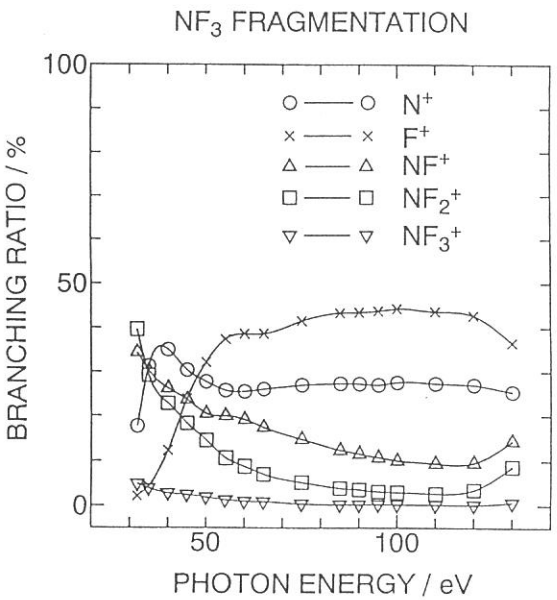

Figure 1. The branching ratios of the product ions for single and double ionization of NF_3 (major product ions)

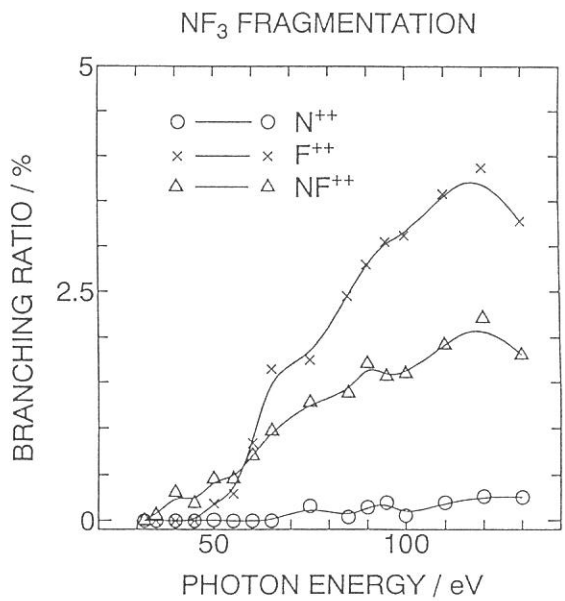

Figure 2. The branching ratios of the product ions for single and double ionization of NF_3 (minor product ions)

Single-, Double-, and Triple-Photoionization Cross Sections of Carbon Monoxide (CO) and Ionic Fragmentation of CO^+, CO^{2+}, and CO^{3+}

Toshio Masuoka

Department of Applied Physics, Faculty of Engineering,
Osaka City University, Sugimoto 3, Sumiyoshi-ku, Osaka 558

Eiken Nakamura

UVSOR, Institute for Molecular Science, Myodaiji, Okazaki 444

Single-, double-, and triple-photoionization processes of carbon monoxide (CO) have been studied in the photon-energy region of 37-100 eV by use of time-of-flight mass spectrometry and a photoion-photoion-coincidence method together with synchrotron radiation.[1] The single-, double-, and triple-photoionization cross sections of CO are determined by a newly developed method.[2] The results are shown in Fig. 1 as a function of photon energy. The total cross section is from Ref. 3. It is emphasized that the double photoionization cross section shown in Fig. 1 includes both the dissociative and nondissociative processes of the precursor CO^{2+}. As for the ratio of σ^{2+}/σ^{+}, Lablanquie et al.[4] reported the value of about 0.25 at 80 eV from their photoionization data measured with synchrotron radiation. Becker et al.[5] have estimated the ratio in the region of 50-120 eV from their photoelectron spectra. If 10 % uncertainty is assumed at 90 eV in the present data, excellent agreement can be found among the three sets of data.

The threshold for molecular double photoionization was found to be 41.3 ± 0.2 eV. The threshold for the dissociative triple photoionization was observed at 82 ± 2 eV, which is in close agreement with 81 ± 2 eV reported by Lablanquie et al.[4] The cross section for triple photoionization is also in good agreement with that reported by Lablanquie et al.[4]

Ion branching ratios and the partial cross sections for the individual ions respectively produced from the precursors CO^+ and CO^{2+} are determined separately at excitation energies where the molecular and dissociative single- and double-photoionization processes compete. The ion branching rations for the CO^{2+} precursor separately determined from those for CO^+ are shown in Fig. 2. The $C^+ + O^+$ ion-pair formation is dominant because of Coulomb repulsion between two positive holes. However, the metastable CO^{2+} ion is also observed due to the presence of attractive chemical forces at smaller internuclear distances. The charge-localized dissociation of CO^{2+} forming C^{2+} and O^{2+} becomes appreciable at higher excitation energies, where two electrons in the atomic orbitals of carbon or oxygen are ejected.

Only the $C^+ + O^+$ ion pair is produced in double photoionization in the 38.4-41.3-eV region, which is below the appearance potential of the molecular CO^{2+} ion. Lablanquie et al.[4] proposed an indirect process that highly excited CO^{**} states (Rydberg states converging to the CO^{2+} states) autoionize to the ionization continuum of the lowest dissociative $^3\Sigma^-$ state of CO^{2+} at large internuclear distances. Just above the threshold of CO^{2+}, the ion branching ratio for CO^{2+} increases sharply. In this energy region, the $1^1\Sigma^+$, $1^3\Pi$, $1^1\Pi$, $1^3\Sigma^+$, and $2^1\Sigma^+$ states of CO^{2+} exist[6] and predissociation of these states via the $1^3\Sigma^-$ state is expected to be slow.[7] Because these CO^{2+} states produce the molecular CO^{2+}, a peak is formed in the ion branching ratio for CO^{2+} around 45 eV.

References

1) T. Masuoka and E. Nakamura, Phys. Rev. A **46**, 4379 (1993).
2) T. Masuoka and H. Doi, Phys. Rev. A **44**, 278 (1993).
3) J. A. R. Samson and J. L. Gardener, J. Electron Spectrosc. Relat. Phenom. **8**, 35 (1976); J. A. R. Samson and G. N. Haddad (unpublished).
4) P. Lablanquie, J. Delwiche, M. J. Hubin-Franskin, I. Nenner, P. Morin, K. Ito, J. H. D. Eland, J. M. Robbe, G. Gandara, J. Fournier, and P. G. Fournier, Phys. Rev. A **40**, 5673 (1989).
5) U. Becker, O. Hemmers, B. Langer, A. Menzel, R. Wehlitz, and W. B. Peatman, Phys. Rev. A **45**, R1295 (1992).
6) M. Larsson, B. J. Olsson, and P. Sigray, Chem. Phys. **139**, 457 (1989).
7) L. H. Andersen, J. H. Posthumus, O. Vahtras, H. Ågren, N. Elander, A. Nunez, A. Scrinzi, M. Natiello, and M. Larsson, Phys. Rev. Lett. **71**, 1812 (1993).

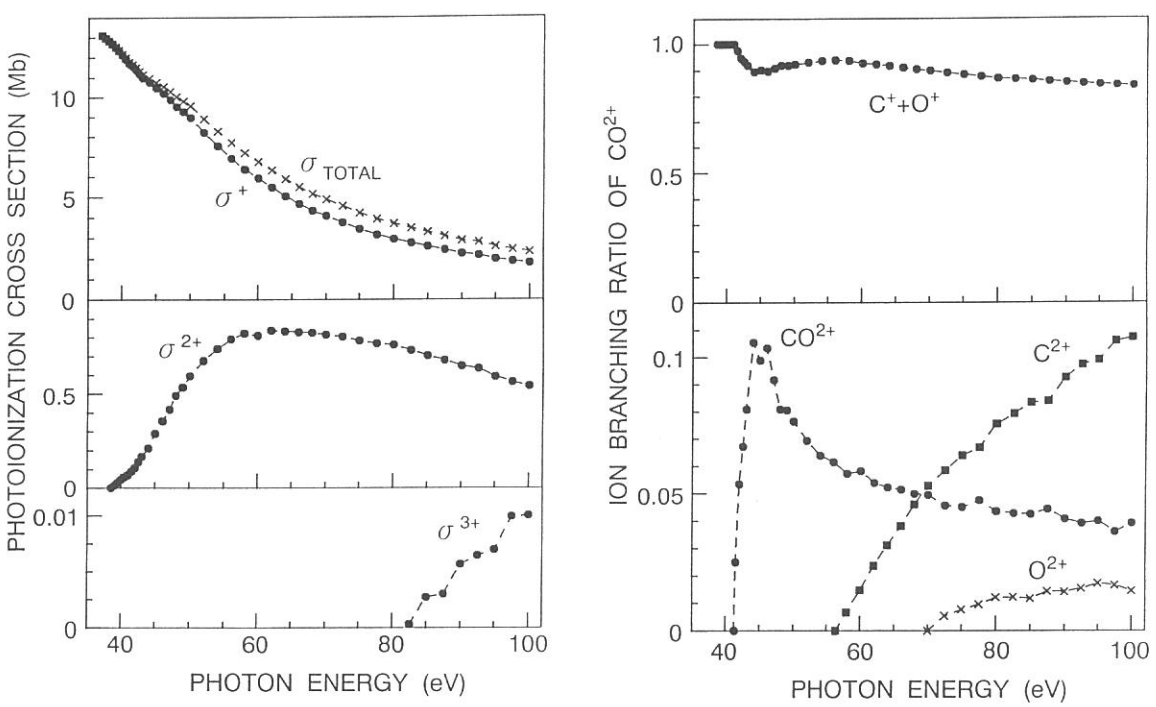

FIG. 1 Cross sections for single, double, and triple photoionization of CO. The total cross section is from Ref. 3.

FIG. 2 Ion branching ratios of double photoionization of CO. For details, see Ref. 1.

Kinetic-Energy Release in the Dissociation of CO^{2+}

Toshio MASUOKA

Department of Applied Physics, Faculty of Engineering, Osaka City University, Sugimoto 3, Sumiyoshi-ku, Osaka 558

Kinetic-energy release distributions of the fragment ions (C^+ and O^+) produced in dissociative double photoionization of carbon monoxide have been determined by analyzing photoion-photoion coincidence (PIPICO) spectra measured in the region $h\nu$=39-100 eV by use of a time-of-flight mass spectrometer and synchrotron radiation. At low excitation energies (39-46.5 eV), low kinetic-energy components were observed, which cannot be explained by a simple framework whereby a doubly charged molecular ion is directly produced upon single photon absorption which then dissociates into two ionic fragments. The majority of the ion pairs are produced through indirect processes, in which highly excited CO^{**} and CO^{**} (double Rydberg) converging to the CO^{2+} electronic states autoionize before and after dissociation.

The KERDs of the C^++O^+ ion pair obtained at various energies between 39 and 45 eV are shown in Fig. 1. The results in the region of 39-41 eV is due to indirect processes, i.e., autoionization of highly excited CO^{**} and CO^{**} states into the underlying ionization continuum of the $1^3\Sigma^-$ state of CO^{2+}, with emission of low kinetic-energy electrons.

Among several theoretical calculations of the potential-energy curves for the low-lying electronic states of CO^{2+}, the one reported by Larsson et al.[1] is referred in the discussion of the present results. The energy scale of the calculated potential-energy curves was calibrated by assuming that the v=0 level of the $1^1\Sigma^+$ state corresponds to the CO^{2+} threshold at 41.3 eV.[2] According to the potential-energy curves of CO^{2+}, the direct dissociative double ionization is energetically possible above 41.4 eV and only the first dissociation limit (35.98 eV) of CO^{2+} is included in the dissociation below 46.5 eV.

In the simple model whereby a doubly charged molecular ion (AB^{2+}) is produced directly from absorption of single photon; AB^{2+} then dissociates into A^+ and B^+ and the KER is given by the energy difference between the internal energy of the precursor dication and the various dissociation limits of AB^{2+}, the KERs should be in the region of 5.4-6.0 eV at 42 eV, 5.4-7.0 eV at 43 eV, and 5.4-9.0 eV at 45 eV. The KERDs shown in Fig. 1 extend to the lower energy side because of emission of low kinetic-energy electrons, i.e., the majority of the C^++O^+ ion pairs are produced via autoionization in the region of 41.4-46.5 eV. The complexity of the excitation and dissociation pathways for the C^++O^+ ion-pair formation is schematically summarized in Fig. 2. For simplicity, the number of photoelectrons ejected is not complete in the figure. It is obvious from the figure that the excitation energy is shared not only by the fragment ions but also by various kinds of photoelectrons (E_1-E_5). These complex excitation and dissociation pathways contribute to the formation of the ion pairs having lower kinetic energies via autoionization. Lablanquie et al.[3] reported the KERDs in the C^++O^+ dissociation of CO^{2+}. However, they did not recognize the importance of autoionization processes mentioned above in the discussion of their results. Instead, they used the simple model. The results cannot be explained by such a simple model, as is obvious from Fig. 2.

References

1) M. Larsson, B. J. Olsson, and P. Sigray, Chem. Phys. **139**, 457 (1989).
2) T. Masuoka and E. Nakamura, Phys. Rev. A **48**, 4379 (1993).
3) P. Lablanquie et al. Phys. Rev. A **40**, 5673 (1989).

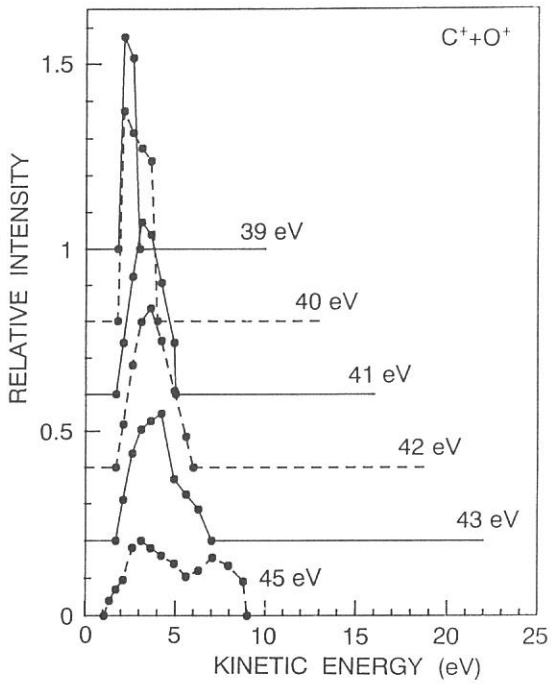

FIG. 1 Kinetic-energy release distribution in the $C^+ + O^+$ channel of CO^{2+} at excitation energies of 39-45 eV.

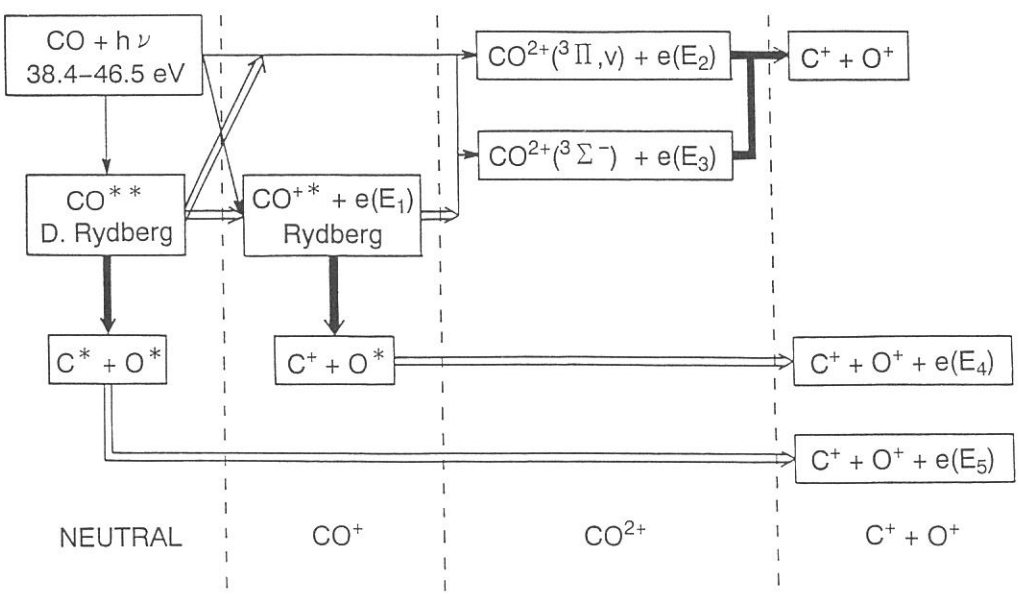

FIG. 2 Excitation and dissociation pathways for the C^+ and O^+ ion-pair formation. D. Rydberg represents the double Rydberg states converging to the electronic states of CO^{2+}. For simplicity, the number of photoelectrons is not complete. → direct transition, ⟹ electronic and resonant autoionization, ➡ dissociation.

Observation of Anisotropic Angular Distribution of Ionic Fragments in the Dissociation of CO^{2+}

Toshio MASUOKA

Department of Applied Physics, Faculty of Engineering, Osaka City University, Sugimoto 3, Sumiyoshi-ku, Osaka 558

Angular distributions of fragment ions (C^++O^+) produced in dissociative double photoionization of carbon monoxide have been studied in the photon energy region 39-100 eV by use of a photoion-photoion coincidence (PIPICO) technique and a source of synchrotron radiation.

The spectral profiles of PIPICO peaks are determined by the kinetic-energy distribution and the angular distribution of the fragment ions, both with respect to the spectrometer axis, and other experimental conditions such as the electric field across the ionization region, the size and the degree of polarization of the photon beam and so on. In order to obtain the angular distribution of fragment ions, the kinetic-energy distribution was determined first by analyzing the PIPICO spectra measured at the so-called "pseudomagic angle," which is equal to about 55° under the assumed condition that the degree of polarization of the light p=0.9 (Ref. 1).

The anisotropic β parameter was obtained by the following three steps. (1) Spectral profiles at an angle θ (0° and 90°) were calculated for a set of various kinetic energies of the fragment ions with an arbitrarily fixed β parameter. (2) The spectral profile of the PIPICO peak at the angle θ was calculated, based on the kinetic-energy distribution already determined and the profiles calculated in step 1. (3) By treating the β value as a running parameter, its most probable value was determined as the one for which the sum of squares of the residuals between the observed and calculated profiles was minimized.

The observed β parameter is shown in Fig. 1 as a function of excitation energy. Above 80 eV, the β parameter obtained at 0° does not agree with that obtained at 90°. The reason for this is not clear at present. One possibility is that the least-squares fit using only one common β parameter for every KER component is not a proper way in the simulation. The β parameters measured at the two angles do not agree one another also at 43 eV probably because of bad quality of the PIPICO spectra. The background of the PIPICO spectra is wavy due to random coincidences of ion produced in single ionization. This wavy background is superposed on the PIPICO spectra and deforms the PIPICO spectra. In Fig. 1, the mean value of the β parameters measured at the two angles is 0.685 at 39 eV, 0.2 ± 0.1 in the region 40-47.5 eV except for the one at 43 eV, about 0.4 in the region 50-60 eV, and gradually decrease above 60 eV.

The ratio of the parallel transition (Σ-Σ) to the perpendicular one (Σ-Π) is shown in Fig. 2, which is given by $(1+\beta)/(2-\beta)$.

The observation of anisotropy in double photoionization from the valence orbitals of CO will be discussed in relation to the symmetry consideration involved in the transition.

Reference

1) T. Masuoka, I. Koyano, and N. Saito, Phys. Rev. A 44, 4309 (1991).

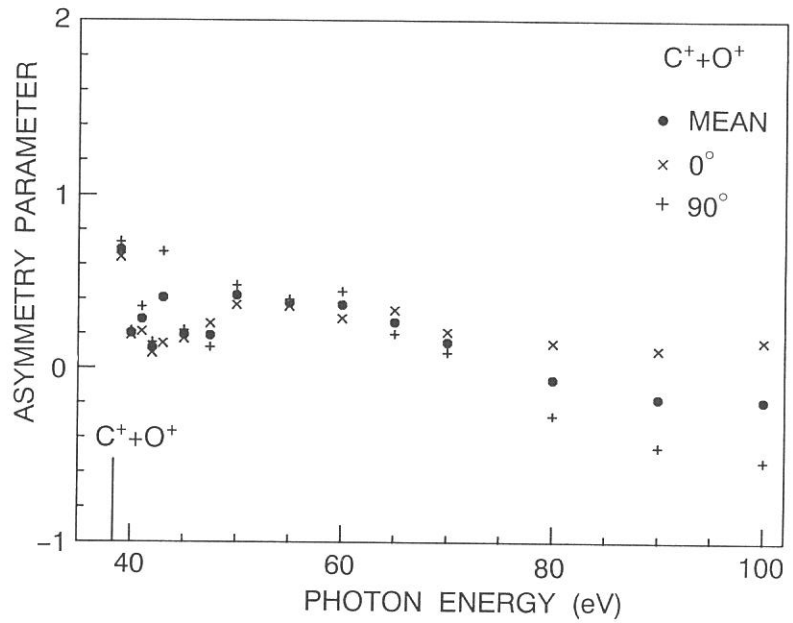

FIG. 1 Asymmetry parameter β for the $C^+ + O^+$ dissociation channel of CO^{2+} measured at $\theta = 0°$ (×) and 90° (+).

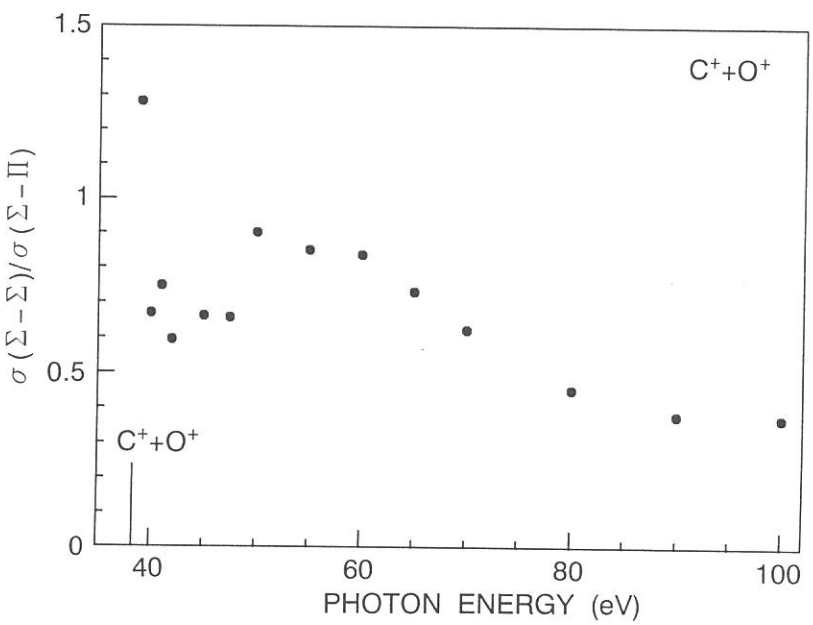

FIG. 2 Ratio of the cross sections $\sigma(\Sigma\text{-}\Sigma)/\sigma(\Sigma\text{-}\Pi)$ for the $C^+ + O^+$ channel of CO^{2+} as a function of excitation energy.

Kinetic-Energy Release in the Dissociation of NO^{2+}

Toshio MASUOKA

Department of Applied Physics, Faculty of Engineering, Osaka City University, Sugimoto 3, Sumiyoshi-ku, Osaka 558

Kinetic-energy release distributions (KERDs) of the fragment ions (N^+ and O^+) produced in dissociative double photoionization of nitric oxide have been determined by analyzing photoion-photoion coincidence (PIPICO) spectra measured in the region 42-100 eV by use of a time-of-flight mass spectrometer and synchrotron radiation. The PIPICO spectra were measured at an angle of about 55° with respect to polarization vector where the second-order Legendre polynomial is close to zero, thus minimizing any effects of anisotropic angular distribution of fragment ions.

In the simple framework whereby a doubly charged molecular ion (AB^{2+}) is produced directly from absorption of a single photon and then AB^{2+} dissociates into A^+ and B^+, the kinetic-energy release (KER), K(E), is given by

$$K(E) = AB^{2+}(^M\Lambda, v) - [A^+(^M L) + B^+(^M L) + D_o],$$

where $AB^{2+}(^M\Lambda, v)$ is the internal energy of the precursor, $A^+(^M L)$ and $B^+(^M L)$ are the internal energies of the two ionic fragments, all measured from the respective neutral ground states, and D_o is the dissociation energy of the neutral. The values in the bracket correspond to the various dissociation limits of AB^{2+}. In almost all studies of the KERs so far reported, this simple model was assumed explicitly or implicitly. However, as reported by Becker et al.[1] for CO, dissociative double photoionization is not that simple. Autoionization of valence-excited CO^{**} states in the molecule and after dissociation plays an important role, particularly at low excitation energies.

Typical examples of KERDs of the $N^+ + O^+$ ion pair obtained at several excitation energies between 42 and 100 eV are shown in Fig. 1. As the excitation energy increases, the KERD becomes wider and wider, extending up to about 21.5 eV at a photon energy of 100 eV. However, the increase of the KER is not as much as the increase in the excitation energy. This means that the high-lying electronic states of NO^{2+} result in N^{**} and/or O^{**} with higher levels of excitation and with larger KER than those resulting from the low-lying states. In other words, the potential-energy curves of the high-lying states are steeper and more repulsive than those of the low-lying states. Qualitatively, this is a natural consequence of increased Coulomb repulsion because the shielding of positive core charges weakens when two inner-valence electrons are ejected.

At the lowest excitation energy of 42 eV, the KERD extends from about 1.9 to 7.3 eV. The first dissociation limit of NO^{2+} is at 34.66 eV and the NO^{2+} ion partially dissociates above 41.0 ± 0.5 eV.[2] If the simple model mentioned above is applicable, the KER should be in the range 6.3-7.3 eV. An obvious implication of the KERD at 42 eV is that only a small fraction of the ion pairs $N^+ + O^+$ is produced via direct dissociative double photoionization. The majority of the ion pairs are produced through indirect routes, in which highly excited NO^{**} and NO^{**} (double Rydberg) converging to the NO^{2+} electronic states (the dissociation limits of which are higher than the lowest limit), (i) autoionize to the higher vibrational levels of the $X\ ^2\Sigma^+$ state of NO^{2+} and to the underlying ionization continuum of the $A^2\Pi$ state and (ii) autoionize after dissociation (i.e., relaxation in the

excited atom). These two processes, (i) indirect double ionization followed by dissociation and (ii) direct dissociation of the molecular ion with subsequent relaxation in the excited atom, have been clearly differentiated in CO by photoelectron spectroscopy.[1]

The average, minimum, and maximum KERs are shown in Fig. 2 as a function of excitation energy. The maximum KER increases linearly up to 46 eV as a function of excitation energy. This means that, in the excitation-energy region 41-46 eV, some components exist which dissociate to the lowest dissociation limit.

References

1) U. Becker, O. Hemmers, B. Langer, A. Menzel, and R. Wehlitz, Phys. Rev. A **45**, R1295 (1992).
2) T. Masuoka, Phys. Rev. A **48**, 1955 (1993).

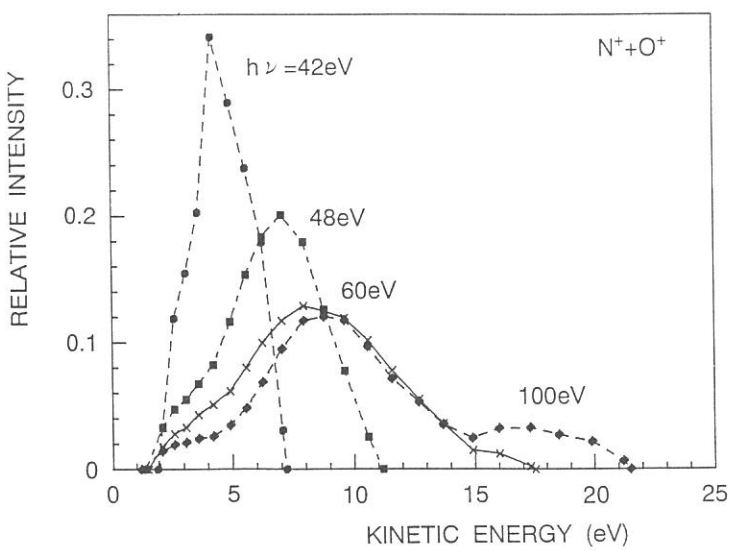

FIG. 1 Kinetic-energy release distribution in the $N^+ + O^+$ channel of NO^{2+}.

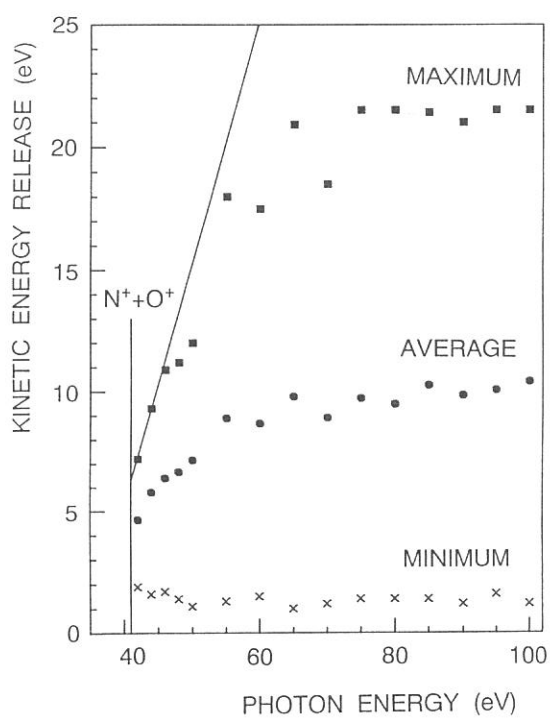

FIG. 2 Average-, minimum-, and maximum-kinetic energy releases in the dissociation of NO^{2+} as a function of excitation energy.

DISSOCIATIVE SINGLE AND DOUBLE PHOTOIONIZATION OF CO_2

Toshio MASUOKA

Department of Applied Physics, Faculty of Engineering, Osaka City University, Sugimoto 3, Sumiyoshi-ku, Osaka 558, Japan

Youngmin CHUNG

Pohang Accelerator Laboratory, P.O.Box 125, Pohang, Kyungbuk 790-600, South Korea

In order to study dissociative single and double photoionization of CO_2, time-of-flight (TOF) mass and photoion-photoion-coincidence (PIPICO) spectra were measured in the region 37-100 eV by the use of a constant-deviation grazing incidence monochromator together with synchrotron radiation. Aluminum and beryllium optical filters were used to eliminate higher-order radiation. The drift tube of the TOF mass spectrometer was 20 cm long and the TOF mass and PIPICO spectra were measured at an angle of about 55° with respect to the polarization vector where the second-order Legendre polynomial is close to zero, thus minimizing any effects of anisotropic angular distribution of fragment ions.

The TOF mass spectrometer was operated in two modes for the measurement of TOF mass spectra. In mode A, the photoelectron signal detected by a channel electron multiplier was fed into the start input of a time-to-amplitude converter (TAC). The storage ring was operated in a multi-bunch mode. In this mode of operation of the TOF mass spectrometer, the relative ion yields in single and double photoionization are affected by the different kinetic energies of individual photoelectrons and by the different numbers of photoelectrons in the two processes. At $h\nu$=60 eV, for example, the kinetic energy of a photoelectron ejected from CO_2 (forming the ground state of CO_2^+) is about 46 eV, whereas that of a photoelectron (forming the ground state of CO_2^{2+}) is about 22 eV. These more energetic photoelectrons produces by single photoionization are more easily discriminated in the TOF mass spectrometer than those produced by double photoionization, resulting in an underestimation of the number of ions produced in single photoionization. Furthermore, the different numbers of ejected electrons in single and double photoionization causes an overestimation of the number of the ions produced in double photoionization because the probability of forming one output pulse in the electron detector is higher for two electrons hitting simultaneously than that for one electron.

In mode B, the rf frequency (90.115 MHz) of the storage ring was used as the start signal of the TAC by reducing it to 1/32 through a frequency demultiplier. The storage ring was operated in a single-bunch mode, which was essential to obtain meaningful TOF mass spectra. In mode B, it is believed that the observed mass spectra are free from the discrimination effects mentioned above because the ratio of the partial cross sections Ar^{2+}/Ar^+ measured in the region from the double-photoionization threshold to 100 eV was in good agreement with previous reports.[1] The collection efficiencies of energetic fragment ions in the TOF mass spectrometer were calculated with a computer program. The results show that the collection efficiency for the O^++CO^+ ion pair having 8.5-eV kinetic energy is 90 % and that with 20-eV kinetic energy is 84 %. This discrimination effect against energetic ions is not corrected in the present study.

The ion branching ratios measured in both modes are shown in Fig. 1 and compared with those reported by Hitchcock, Brion, and Van der Wiel[2] who

used the (e, e+ion) technique. The present results obtained in mode B are in good agreement (within about 10 % discrepancy) with those reported by Hitchcock et al. for all types of ions except for O^+, for which a slightly large discrepancy (about 15-20 %) exist. This is because if the ion detection efficiency is high, the heavier ion (O^+) in the $C^+ + O^+$ dissociation channel of CO_2^{2+} is not counted due to the characteristic of the TAC. Since the ion detection efficiency in the present experiment is quite low (a few percent), the C^+ and O^+ ions produced as a pair from CO_2^{2+} are detected with an almost equal weight in the present experiment, thus giving the more accurate ion branching ratios than those reported by Hitchcock et al.

The threshold for the molecular doubly-charged-ion (CO_2^{2+}) was found to be 37.6 ± 0.3 eV. The thresholds for the $CO^+ + O^+$ and $C^+ + O^+$ channels of CO_2^{2+} are at 39.2 ± 0.3 and 47.0 ± 0.3 eV, respectively. The $O^+ + O^+$ channel of CO_2^{2+} cannot be observed by the PIPICO method by the use of a microchannel plate ion detector with a single anode. This channel was examined by the photoelectron-photoion-photoion triple coincidence (PEPIPICO) technique. The results show that this channel exists with a threshold between 50 and 70 eV.

References

1) D.M.P.Holland, K.Codling, J.B.West, and G.V.Marr, J.Phys.B **12**, 2465 (1979).
2) A.P.Hitchcock, C.E.Brion, and M.J.Van der Wiel, Chem.Phys. **45**, 461 (1980).

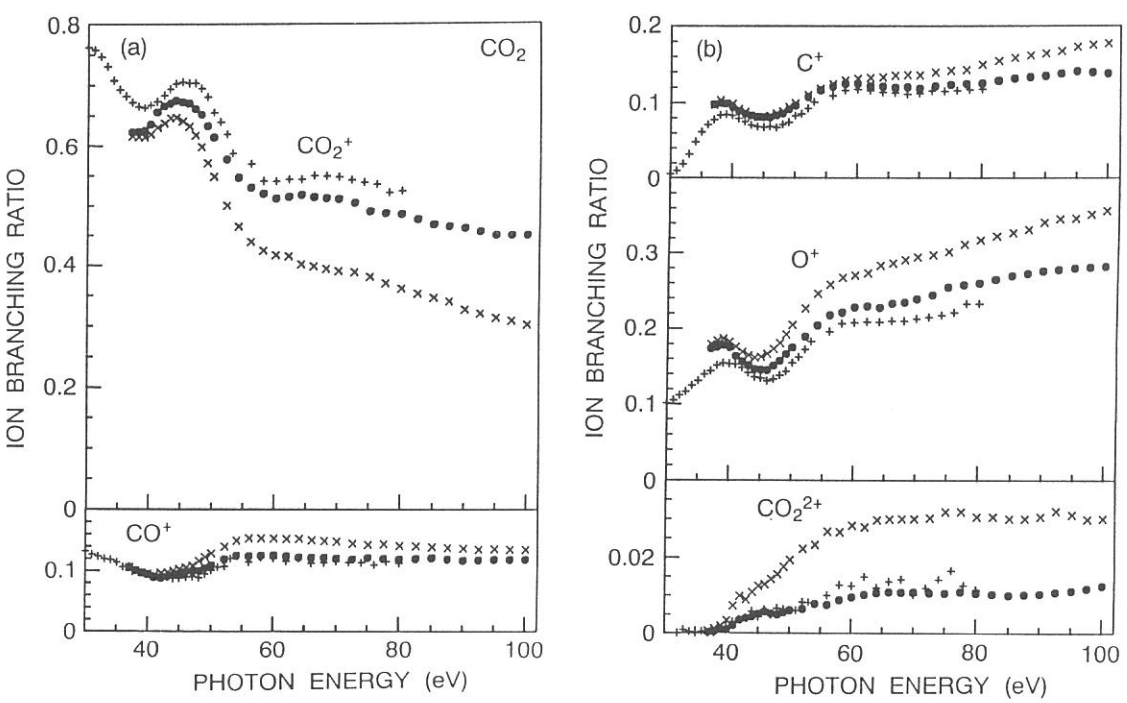

FIG. 1 Apparent ion branching ratios for CO_2 directly obtained from the TOF mass spectra as a function of photon energy. × (mode A) and ● (mode B), present data; + from Hitchcock et al. (ref. 2).

Absorption Spectrum of C_{60} in the Gas Phase: Formation and Recombination of Electron-Hole Pair

Hisato Yasumatsu*, Tamotsu Kondow*, Hiroshi Kitagawa, Kiyohiko Tabayashi, and Kosuke Shobatake

* *Department of Chemistry, University of Tokyo, Hongo, Bunkyo-ku, Tokyo 113, Japan*
Institute for Molecular Science, Myodaiji, Okazaki 444, Japan

The absorption spectrum of gaseous C_{60} at temperatures of 830-870 K was measured in the energy range of 3.5 - 11.4 eV. The peaks at 7.9 and 9.2 eV, and a dip at 8.5 eV were assigned as Feshbach resonance with superexcited states. The photoionization quantum yield was explained in terms of formation and recombination of an electron-hole pair.

A sample of C_{60} was synthesized in a "Fullerene Factory" by discharging a graphite rod in He atmosphere, and purified by liquid chromatography.[1] The absorption spectrum of C_{60} vapor was measured on an experimental apparatus[2] constructed on the Beamline BL2A of UVSOR. The C_{60} sample in a windowless absorption cell was resistively heated to temperatures of 830-870 K in a vacuum chamber pumped down to 1 x 10^{-6} Torr so that the vapor pressure of C_{60} is kept at 5-10 mTorr. The light from the 1 m Seya-Namioka monochromator goes through the high temperature cell and the transparent light intensity is monitored by a sodium salicilate convertor followed by a photomultiplier (Hamamatsu Model R585). Figure 1 shows a typical absorption spectrum of the C_{60} vapor whose vapor pressure is known.[3] The uncertainty in the absolute absorption cross section is estimated to be about 25 %, most of which is due to the uncertainty of temperature reading.

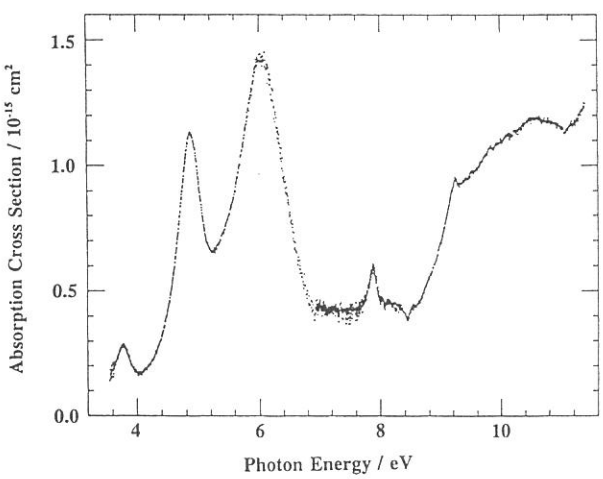

Figure 1. Absorption spectrum of C_{60} in the gas phase in the temperature range 830-870 K. The ordinate represents absolute absorption cross section whose uncertainty is estimated as 25 %.

In the low energy range three broad bands peaked at 3.8, 4.9, and 6.0 eV are observed; the maxima positions of which agree with those observed in hexane solution[4] and in Ar matrix[5] within ± 0.1 eV. The absorption cross section for the band at 3.8 eV is determined as (0.29 ± 0.07) x 10^{-15} cm^2 which is comparable with (0.422 ± 0.073) x 10^{-15} cm^2 measured by Brady

and Beiting[5] at 870 K.

Two distinct bands peaked at 7.9 and 9.2 eV and a dip at 8.5 eV appear in the energy range higher than the ionization energy, 7.61 eV.[6] Therefore it is highly likely that these peaks and dips arise from Feshbach resonances involving superexcited states which originate from core-excited Rydberg states of C_{60}. The energy level of a Rydberg state measured from the ground state is expressed as

$$E_n = -\frac{R}{\epsilon^2(n-\delta)^2} + IP$$

where R is the Rydberg constant in vacuum, ε the relative dielectric constant of C_{60}, n the principal quantum number, δ a quantum defect, and IP the ionization energy of C_{60}. The minimum principal number, n is n = 3. The second and third ionization energies are 8,89 and 10.82-11.59 eV,[7] respectively. The band peaks at 7.9 and 9.2 eV are assignable to the Rydberg states for n = 3 converging to the second and third ionization enegies, respectively.

The two additional bands discernible in the higher energy side of 7.9 eV peak are assigned as the vibrational progression of the totally symmetric mode a_g. Since the photoionization efficiency curve has been obtained, the relative quantum yield for photoionization has been determined by dividing the photoionization efficiency by the absorption cross section and it is found to increase with energy above the ionization energy. The quantum yield for photoionization curve was fitted to a theoretical curve, assuming that it is the sum of three photoionization efficiency yields, ϕ_i's (i = 1, 2, and 3), each of which is derived by a photoelectron-hole recombination model[8] as expressed by

$$\phi_i = A_i \exp\left(-\frac{B_i}{\Delta E_i^{3/2}}\right)$$

where A_i and B_i are the parameters related to a diffusion constant and screening length, respectively, and ΔE_i is approximately given by the photon energy, E, minus the photoinonization energy, IP_i. Although not shown, the overall photoionization quantum yield curve can be fitted well to the theoretical curve except the lower energy region. Therefore it is concluded that photoionization is retarded by efficient electron-hole recombination.

The present results will be published in a forthcoming paper.[9]

[1] M. Nagata, N. Mizutani, S. Bandow, Y. Maruyama, H. Kitagawa, and T. Mitani, Annual Review 1992 of Inst. for Molecular Science, **1992**, 141.
[2] H. Yasumatsu, T. Kondow, K. Suzuki, K. Tabayashi, and K. Shobatake, J. Phys. Chem. **98**,(1994) (in press).
[3] J. Abrefah, et al. Appl. Phys. Lett., **60**, 1313 (1992).
[4] See for example, S. Leach et al., Chem. Phys., **160**, 451 (1992).
[5] Z. Gasyna, et al., Chem. Phys. Lett. **183** , 283 (1991).
[6] B. B. Brady and E. J. Beiting, J. Chem. Phys., **97**, 3855 (1992).
[7] D. L. Lichtenberger, et al., Mat. Res. Soc. Sym. Proc., **206**, 673 (1991).
[8] E. W. Schlag and R. D. Levine, J. Phys. Chem., **96**, 10608 (1992).
[9] To be submitted to J. Chem. Phys.

Polarized Fluorescence of CN($B^2\Sigma^+$-$X^2\Sigma^+$) Observed in Photodissociation of ICN in the 56500 - 95200 cm^{-1} Region

Kazuhiro Kanda, Shunji Katsumata,
Takashi Nagata[1], Tamotsu Kondow[2], Kiyohiko Tabayashi[3],
Atsunari Hiraya[4] and Kosuke Shobatake[4]

Department of Fundamental Science, College of Science and Engineering, Iwaki Meisei University, Iwaki 970
[1] Department of Chemistry, College of Arts and Sciences, The University of Tokyo, Komaba, Meguro-ku 153
[2] Department of Chemistry, School of Science, The University of Tokyo, Hongo, Bunkyo-ku 113
[3] Department of Chemistry, Faculty of Science, Hiroshima University, Higashihiroshima 724
[4] Institute for Molecular Science, Myodaiji, Okazaki 444

The subsequent CN($B^2\Sigma^+$-$X^2\Sigma^+$) emission formed in photodissociative excitation of ICN was observed in the exciting wavenumber region of 56500-95200 cm^{-1} (105-180 nm). The polarization of photofragment emission provides information on the symmetry of the relevant electronic state and the time scale of the dissociation. The assignments for the absorption bands of ICN were reexamined by using of the synchrotron radiation dispersed by a 1-m monochrometer at the BL2A line of UVSOR as a polarized light source.

Figure 1 shows the observed polarization anisotropy (R) as a function of the excitation wavenumber along with the fluorescence excitation spectrum in the 66700-80000 cm^{-1} region. The R-$\tilde{\nu}$ curve shows a sharp minimum at the center of the intense emission peak located at 71337 cm^{-1}. This implies that a perpendicular-type transition is responsible for the absorption band at 71337 cm^{-1}. This feature is in remarkable contrast to that the corresponding peak in BrCN are obviously the parallel-type transition [1]. This band is ascribable to the $2\pi\rightarrow 3p\sigma$ Rydberg transition.

Felps et al. have assigned the diffuse bands appearing around ~68500 and ~72500 cm^{-1} to the $2\pi\rightarrow 6\sigma$ intravalence transition [2]. These band systems can be regarded as the transition by the promotion of the 2π electron, because they are situated at the spectral interval corresponding to the spin-orbit splitting of $ICN^+(2\pi^{-1})$. The R value for these bands is observed to be ~0.1, which is close to the theoretical limit. This implies that these bands arise from the parallel-type transition and that the lifetime of the relevant upper electronic state is short compared with the rotational period of ICN molecule. Therefore, these

bands are assignable to the intravalence transition from 2π orbital to the π-character orbital. This transition tentatively termed as the $2\pi \rightarrow 4\pi$ transition.

The 75120 cm^{-1} band does not show its transition type clearly in the R-$\tilde{\nu}$ curve, because of neighboring 75313 cm^{-1} peak, which is attributed to the $2\nu_3$ progression of the $2\pi \rightarrow 3p\sigma(^1\Pi)$. The 75563 cm^{-1} peak corresponding to the ν_1 excitation reveals a hump in the R-$\tilde{\nu}$ curve at the band maximum. Therefore, this band system is associated with a parallel-type transition. From the assignment of the corresponding peak in BrCN [1], this band is ascribable to the $1\pi \rightarrow 3\pi$ intravalence transition. Thus, every principal bands in the absorption spectrum of ICN below the first ionization potential have been assigned to the Rydberg series, converging to first or second ionization potentials or the intravalence transitions on the basis of the polarization measurement.

[1] K. Kanda, S. Katsumata, T. Kondow, K. Kuchitsu, A. Hiraya and K. Shobatake, Chem. Phys. 175 (1993) 399.

[2] W. S. Felps, K. Rupnik and S. P. McGlynn, J. Phys. Chem. 95 (1991) 639.

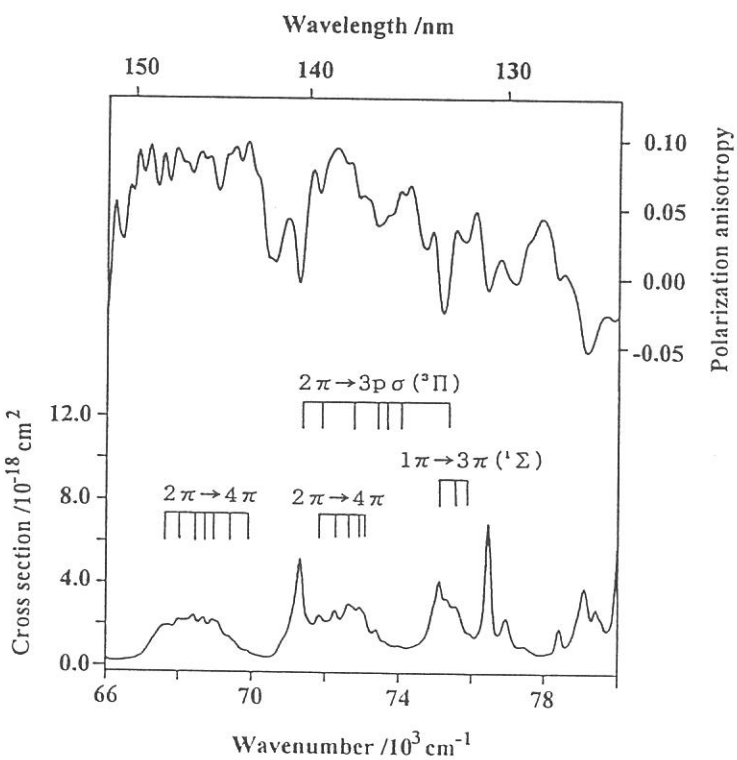

Figure 1 Fluorescence excitation and polarization spectra of ICN

Fluorescence Excitation Spectra and Quantum Yield in Vacuum Ultraviolet Photodissociation of CF_3CN

Dock-Chil Che,* Toshio Kasai,* Hiroshi Ohoyama,* Keiji Kuwata,* Mitsuhiko Kono, Kiyohiko Tabayashi, and Kosuke Shobatake

**Department of Chemistry, Faculty of Science, Osaka University, Toyonaka, Osaka 560, Japan, Department of Functional Molecular Science, The Graduate University for Advanced Studies, and Institute for Molecular Science, Modaiji, Okazaki 444, Japan*

The fluorescence excitation spectra of CN(A, B $\rightarrow$ X) and $CF_3(2A'_1 \rightarrow 1A''_2)$ and the quantum yield for the CN(B) radical formation are measured in the photodissociation of CF_3CN in 105 - 35 nm.

Based on the similarity in the behaviors in forming electronically excited fragments, $CN^*(B)$ and $CN^*(A)$, in collision-induced dissociative excitation processes: $Ar^*(^3P_{0,3}) + CF_3CN \rightarrow CF_3^*(2A'_1) + CN(X) + Ar$ (1), $CF_3 + CN^*(B) + Ar$ (2), $CF_3 + CN^*(A) + Ar$ (3), the existence of a common excited state of CF_3CN^* leading to the formation of $CN^*(B)$ and $CN^*(A)$ radicals has been proposed.[1] In order to obtain more information on dissociative excitation process, another excitation process, i.e. photoexcitation has been employed, and in the present project the following processes have been studied:

$$CF_3CN + h\nu \rightarrow CN^*(B^2\Sigma^+) + CF_3 \quad (4)$$

$$CN^*(A^2\Pi_i) + CF_3 \quad (5)$$

$$CF_3^*(1A'_1) + CN(X) \quad (6)$$

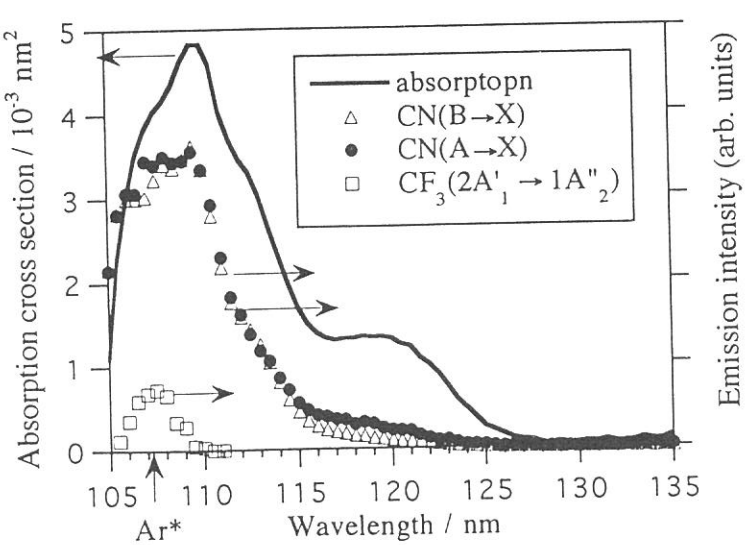

Figure 1. The absorption spectrum of CF_3CN and fluorescence excitation spectra of CN(B X), CN(A X), and $CF_3(2A'_1\ 1A''_2)$. The emission intensities are in arbitrary units.

Experiments have been carried out on a gas phase photochemistry apparatus constructed on the Beam-line BL2A of UVSOR. Figure 1 shows the absorption spectrum (solid line) of CF_3CN along with the fluorescence excitation spectra for CN(B→X) (△), CN(A→X) (●), and CF_3 $(2A'_1 \rightarrow 1A''_2)$ (□) in the exciting light wavelength region of 105 - 135 nm. The wavelength resolution was set at 0.30 nm and the pressure of the CF_3CN vapor was 30 mTorr. For

isolating the $CF_3(2A'_1 \rightarrow 1A''_2)$ emission a band pass filter (SWPF 300) centered at 300 nm was used. A low-path filter (HOYA O-58) with 580 nm cut-off wavelength was employed. Since the CN(A→X) emission intensity is very low compared with that of CN(B→X), the excitation spectrum for CN(B→X) formation was observed without a filter. The quantum yield for $CN^*(B)$ formation has been determined by comparing the fluorescence intensity to that of H_2O under the same experimental conditions.[2] The arrow in Figure 1 is the excitation energy of $Ar^*(^3P_2)$ state.

We find that the spectral profiles for florescence excitation process for both CN(B→X) and CN(A→X) resemble with each other and this fact indicates the existence of a common excited state leading to the excited CN^* fragments, $CN^*(B)$ and $CN^*(A)$ via the 3s Rydberg state of CF_3 for both state.

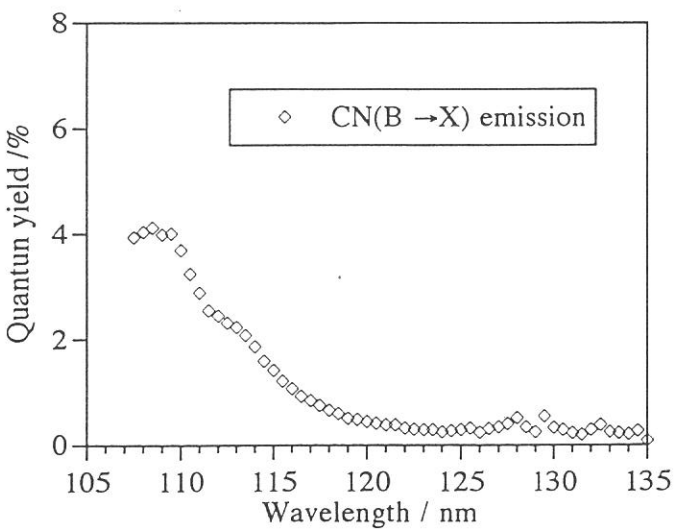

Figure 2. The quantum yield for $CN^*(B)$ radical formation plotted vs. exciting light wavelength in photodissociative excitation of CF_3CN.

In Figure 2 is plotted the quantum yield for $CN^*(B)$ formation against exciting light wavelength. It is interesting to note that the quantum yield profile for photodissociative excitation process, $CF_3CN + h\nu \rightarrow CF_3 + CN^*(B)$ (3), is similar to that for CD_3CN.[2] The maximum values for both compounds are about 4.0 % at around λ_{exc} = 110 nm.

Fluorescence polarization anisotropy has been measured for the process (4).[3] It would suffice to mention that a strong pressure dependence has been observed for $CN^*(B)$ radical formation, whereas for the photodissociative excitation processes of CH_3CN, CD_3CN, and ClCN such strong pressure dependence has never been observed.[3] Since the dipole moments for these molecules are comparable, the different behaviors in the pressure dependence in fluorescence polarization anisotropy might be due to lower rotational energy for $CN^*(B)$ fragments from CF_3CN than those for CD_3CN, CH_3CN, and ClCN.

[1] D-C. Che, T. Kasai, H. Ohoyama, K. Ohashi, T. Fukawa, and K. Kuwata, *J. Phys. Chem.*, **95,** 8159 (1991).

[2] K. Shobatake, A. Hiraya, K. Tabayashi, and T. Ibuki, *Vacuum Ultraviolet Photoionization and Photoemission of Molecules and Clusters*, Ed. by C. Y. Ng (World Scientific Publishing Co., Singapore, 1991), pp. 503.

[3] K. Kono and K. Shobatake (unpublished results).

Fluorescence Excitation Spectra of CN(A,B→X) and of CF_3 ($2A'_1 \rightarrow 1A''_2$) and Quantum Yield for the CN(B) Radical Formation in Vacuum Ultraviolet Photodissociation of CF_3CN

Dock-Chil CHE, Toshio KASAI, Hiroshi OHOYAMA, Keiji KUWATA,
Mitsuhiko KONO,† Kiyohiko TABAYASHI,† and Kosuke SHOBATAKE†

Department of Chemistry, Faculty Of Science, Osaka University, Toyonaka, Osaka 560
†Department of Functional Molecular Science, The Graduate University for Advanced Studies, and Institute for Molecular Science, Myodaiji, Okazaki 444

Based on the similarity observed in the orientational dependences, the existence of a common excited state of CF_3CN which leads to the CN(A) and CN(B) radical formations was proposed in the CF_3CN + Ar(^{3}P) reaction.[1] To fill out the lack of data on the fluorescence excitation spectra and the quantum yield for the CF_3CN molecule, photodissociation of CF_3CN was carried out in 105-135 nm. The wavelength resolution of the exciting light was set as 3.0 Å for improving the S/N ratio. The quantum yield of the CN(B) radical formation was determined by comparative measurement of the OH(A→X) emission of water under the given experimental conditions.[2]

Figure1 shows the absorption spectrum of CF_3CN and the fluorescence excitation spectra of the product radicals by VUV-light excitation. The maximum energy available from Ar* is shown by the arrow. The locations of the main two peaks of the absorption spectrum were found to coincide with those in the literature where the peaks were assigned as the $7a_1 \rightarrow 3s$ and/or $2e \rightarrow 3s$ Rydberg transitions.[3] The fluorescence excitation spectra of CN(B→X) and CN(A→X) are shown by Δ and O, respectively.

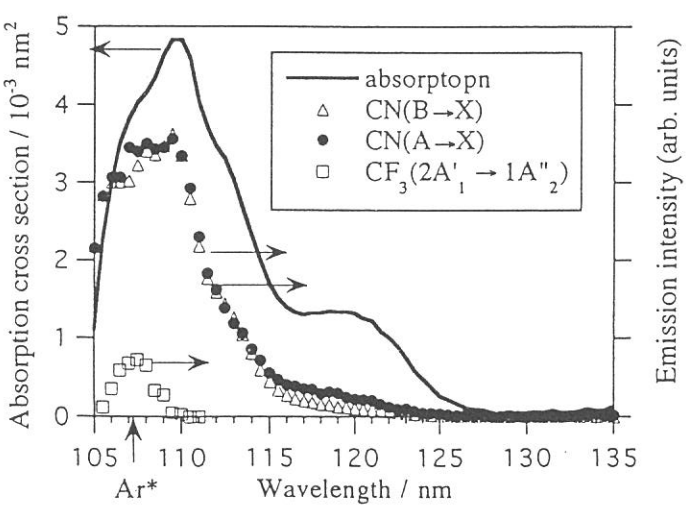

Fig. 1. The absorption spectrum of CF_3CN and the fluorescence excitation spectra of CN(B→X), CN(A→X), and $CF_3(2A'_1 \rightarrow 1A''_2)$. The emission intensity, the vertical axis on the right is arbitrary on each spectrum. The arrow of Ar* shows the wavelength corresponds to the maximum energy available in the CF_3CN + Ar(^{3}P) reaction.

A weak excitation emission isolated by the 300 nm band-pass filter is shown by □. The threshold at ~100 nm(equivalent to 11.3 eV) corresponds to the sum of the dissociation energy of CF_3-CN and the energy gap for the $2A'_1 \rightarrow 1A''_2$ transition of CF_3. Thus the $CF_3(2A'_1)$ radical is expected to be the emitter.[4] The corrected emission intensity of $CF_3(2A'_1)$ is about two orders of magnitude smaller than that of CN(B). The excitation energy dependence of the emissions of CN(B→X) and CN(A→X) turned out to be almost the same, suggesting some common excited state of CF_3CN prior to dissociation.

Figure 2 shows the quantum yield for the CN(B) radical formation.[2] The maximum value is about 4 % at 108 nm near the largest peak of the absorption in Fig. 1. It appears that the quantum yield for the CN (B) formation increases in parallel to the excess internal energy of CF_3CN in the excited state as the excitation wavelength becomes shorter. The small quantum yield for the CN(B) radical formation seems to reflect a close resemblance to the small branching ratio for the CN(B) formation in the $CF_3CN + Ar(^3P)$ reaction.[1] The similarity in the fluorescence excitation spectra for both states of the CN radical in photodissociation also accords with the orientational dependence for the CN(B) and for the CN(A) radical formation in the $CF_3CN + Ar(^3P)$ reaction. Those agreements between the two methods of excitation strongly suggest that the 3s Rydberg state of the molecule plays a common role as a precursor leading to dissociation.

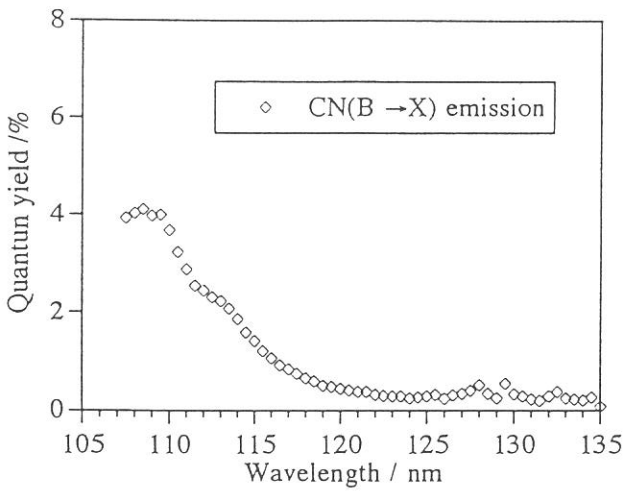

Fig. 2. The quantum yield for the CN(B) radical formation in the photodissociation of CF_3CN.

References

1) D-C. Che, Doctoral thesis, Osaka University (1993); D-C. Che, T. Kasai, H. Ohoyama, K. Kuwata, *J. Phys. Chem.*, (1994) in press.

2) L.C. Lee, L. Oren, E. Phillips, D. L. Judge, *J. Phys. B*, **11**, 47 (1978); L. C. Lee, *J. Chem. Phys.*, **72**, 4334 (1980).

3) M. N. R. Ashfold, J. P. Simons, *J. Chem. Soc., Faraday Trans. 2*, **74**, 1263, (1978).

4) N. Washida, M. Suto, S. Nagase, U. Nagashima, K. Morokuma, *J. Chem. Phys.*, **78**, 1025 (1983).

Photodissociation dynamics of HNCO studied by photofragment fluorescence polarization measurements

Yoshihisa Matsushita, Yasumasa Hikosaka, Mitsuhiko Kono*, Kosuke Shobatake*, and Takumi Hikida

Department of Chemistry, Tokyo Institute of Technology, Ohokayma, Meguro 152

**Institute for Molecular Science, Myodaiji, Okazaki 444*

It has been known that measurements of photofragment anisotropy give detailed information on the dynamics of the photoejection process,[1] and the relation between the lifetime of excited molecule and the degree of fragment polarization has been established for triatomic molecules.[2] In order to develop the theory for four-atomic molecules, we have measured fluorescence polarization of NH ($c^1\Pi$) radical formed by photodissociative excitation of NH_3 as shown in figure 1. In this investigation, photodissociative processes of gaseous HNCO were studied in the wavelength region 105-130 nm by photofragment fluorescence polarization measurements.

It has been known that photolysis of HNCO forms NH radicals in various electronic states. Using UVSOR as a light source, we have reported photodissociative excitation spectra of NH ($c^1\Pi$, $A^3\Pi$) radicals and quantum yields for formation of the radicals in the wavelength region of 107-180 nm.[3] In this study, fluorescence polarization of NH ($c^1\Pi$, $A^3\Pi$) radicals were measured under near collision-free conditions. An absorption and fluorescence measurement apparatus constructed in the beamline BL2A was used. The monochromated VUV light as a polarized light source was introduced to a gas cell filled with HNCO from 20 to 50 mTorr. The NH ($c^1\Pi \rightarrow a^1\Delta$) and ($A^3\Pi \rightarrow X\,^3\Sigma^-$) fluorescence parallel and perpendicular to the vector of the incident light were observed with equipped plate polarizers. The degrees of polarization for the fluorescence ware measured using a photoelastic modulator at several reference wavelengths.

The intensities of parallel and perpendicular components of the NH($c^1\Pi \rightarrow a^1\Delta$) and ($A^3\Pi \rightarrow X\,^3\Sigma^-$) fluorescence are shown in figure 2 (a) and (b), respectively. In contrast to the case of NH_3, no significant difference was found between the spectral shapes of the parallel and perpendicular components for both the NH($c^1\Pi \rightarrow a^1\Delta$) and ($A^3\Pi \rightarrow X\,^3\Sigma^-$) fluorescence. Moreover the degrees of polarization obtained by the measurements using photoelastic

modulator were equal to zero at all reference wavelengths within the observational errors. As our result, the polarization anisotropy for both the NH($c^1\Pi \rightarrow a^1\Delta$) and ($A^3\Pi \rightarrow X\ ^3\Sigma^-$) fluorescence was not observed in the photodissociative excitation process of HNCO.

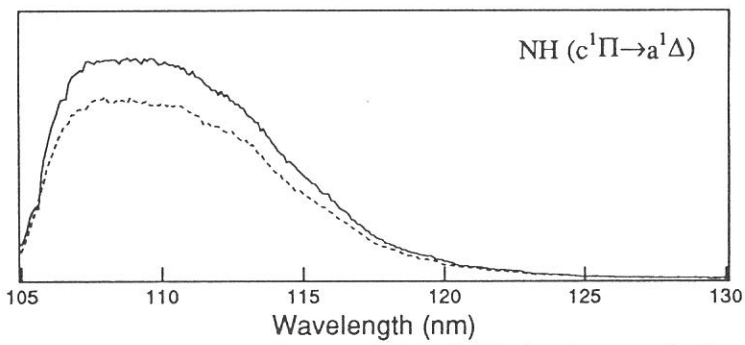

Figure 1 Observed fluorescence polarized parallel (solid line) and perpendicular (dashed line) to the polarization vector of the incident light in the photolysis of NH_3.

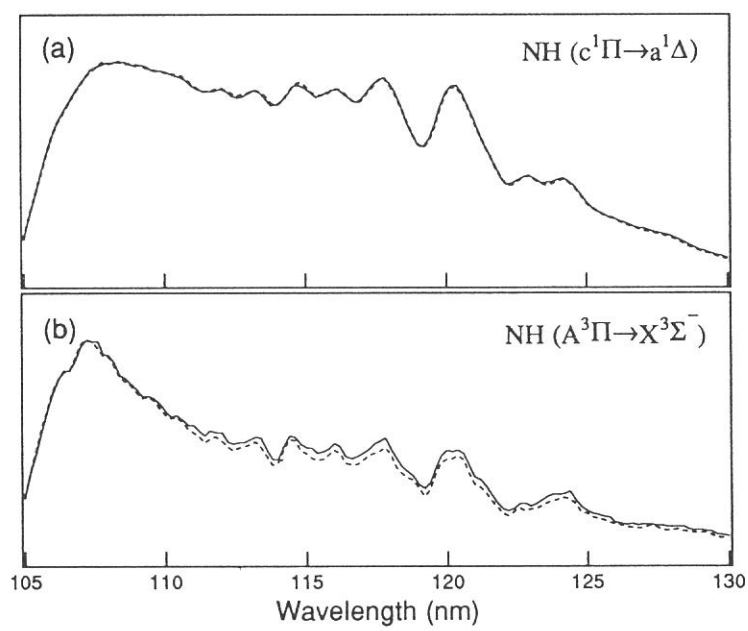

Figure 2 Observed fluorescence polarized parallel (solid line) and perpendicular (dashed line) to the polarization vector of the incident light in the photolysis of HNCO.

(1) C. H. Greene, and R. N. Zare, *Ann. Rev. Phys. Chem.*, **33** (1982) 119.

(2) T. Nagata, T. Kondow, K. Kuchitsu, G. W. Loge, and R. N. Zare, *Mol. Phys.* , **50** (1983) 49.

(3) K. Uno, T. Hikida, A. Hiraya, K. Shobatake, *Chem. Phys. Lett.*, **166** (1990) 475.

Symmetry Assignments of the Rydberg States in CH_3CN and CD_3CN Studied by the Measurements of $CN(B\rightarrow X)$ Fluorescence Polarization Anisotropy

Mitsuhiko KONO and Kosuke SHOBATAKE

Department of Functional Molecular Science, The Graduate University for Advanced Studies, and Institute for Molecular Science, Myodaiji, Okazaki 444, Japan

The polarization anisotropy for the $CN(B^2\Sigma^+\rightarrow X^2\Sigma^+)$ fluorescence arising from photodissociative excitation of CH_3CN and CD_3CN was measured as a function of excitation wavelength from 105 to 145 nm. From the results of these polarization anisotropy measurements we have determined the orientations of Rydberg p-orbitals in a series of Rydberg bands. The experiment was performed at the Beamline BL2A of UVSOR. The details of experimental set up are described in a previous paper.[1)]

Fragment fluorescence excitation spectra for $CN(B\rightarrow X)$ emission and its polarization anisotropy spectra in CH_3CN and CD_3CN are shown in Figure 1 and 2. The wavelength resolutions of exciting light for the polarization and the photoemission cross section were set at 0.50 nm and 0.10 nm, respectively. The assignments for the present work are indicated in Figure 1 and 2. Nuth and Glicker have assigned the photoabsorption bands of CH_3CN observed in the region from 94 to 140 nm as the Rydberg transitions conversing to the 2e and $7a_1$ ionization energies.[2)] Fridh has reported that most of the CH_3CN and CD_3CN bands measured by means of electron impact energy loss spectrometry are assigned as the Rydberg transitions.[3)] They have assigned that, of npR Rydberg states, the energy levels of the π (e) symmetric orbitals are higher than those of the σ (a_1) orbitals. Our polarization anisotropy results contradict the previous assignments.[2,3)] A series of the $2e \rightarrow np(\pi$: e)R Rydberg absorption bands have transition moments with A_1 symmetry parallel to the molecular C_3 axis. A series of the $2e \rightarrow np(\sigma$: a_1)R Rydberg absorption bands have transition moments with E symmetry perpendicular to the molecular C_3 axis. The transition dipole of $CN(B\rightarrow X)$ emission is parallel to C_∞ axis of CN radical. Hence, the polarization anisotropy increases for $2e \rightarrow np(\pi)$R bands and decreases for $2e \rightarrow np(\sigma)$R bands. If π and σ notations are interchanged the previous assignments[2,3)] are consistent with our polarization results. The band origins of Rydberg transitions in the energy region of present work are summarized in Table 1. From the present work we find that the $np(\sigma)$R states are higher in energy than the $np(\pi)$R states.

Table 1. Rydberg band position (± 0.05 nm)

band	CH_3CN	CD_3CN
$2e\rightarrow 3p(\pi)R$	129.24 nm	128.85 nm
$2e\rightarrow 3p(\sigma)R$	127.62 nm	128.05 nm
$2e\rightarrow 4p(\pi)R$	113.26 nm	113.04 nm
$2e\rightarrow 4p(\sigma)R$	112.41 nm	112.13 nm

References

[1)]K. Kanda, S. Katsumata, T. Nagata, Y. Ozaki, T. Kondow, K. Kuchitsu, A. Hiraya, and K. Shobatake, *Chem. Phys.* **175**, 399 (1993)

[2)]J. A. Nuth and S. Glicker, *J. Quant. Spectrosc. Radiat. Transfer* **28**, 223 (1981)

[3)]C. Fridh, *J. Chem. Soc. Faraday Trans. II* **74**, 2193 (1978)

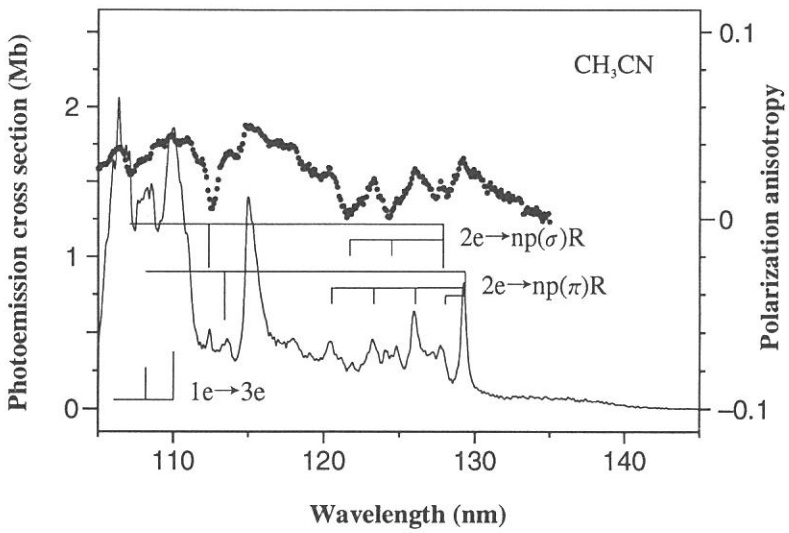

Figure 1. Polarization anisotropy (dots) and fluorescence excitation (curve) spectra for CN($B \rightarrow X$) observed in photodissociative excitation of CH_3CN.

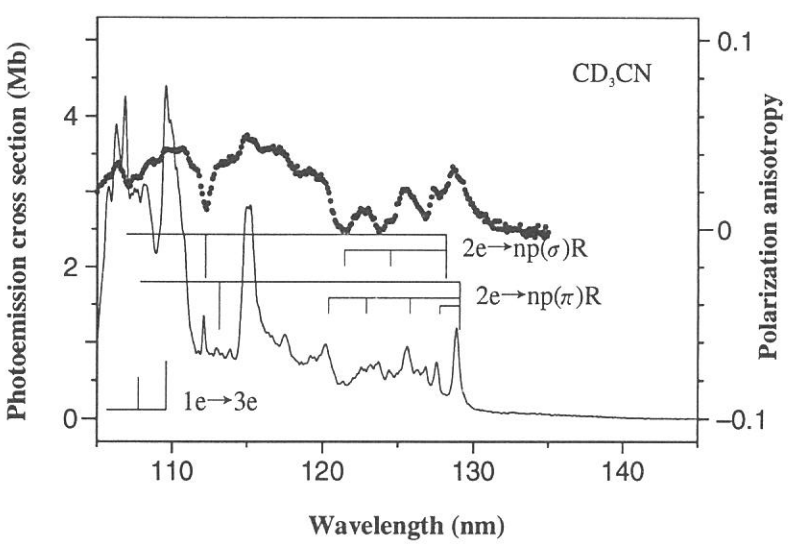

Figure 2. Polarization anisotropy (dots) and fluorescence excitation (curve) spectra for CN($B \rightarrow X$) observed in photodissociative excitation of CD_3CN.

High Quantum Yields for Photodissociative Excitation Process in and Nonradiative Photoabsorption Bands of XeF_2

Mitsuhiko KONO and Kosuke SHOBATAKE
Department of Functional Molecular Science, The Graduate University for Advanced Studies, and Institute for Molecular Science, Myodaiji, Okazaki 444, Japan

Photodissociative excitation processes of XeF_2 for $XeF_2 + h\nu \rightarrow XeF^*(B, C \text{ and } D) + F$ are studied by absorption and fluorescence spectroscopies in the vacuum UV region of 105-165 nm. The quantum yields and polarization anisotropy are measured along with the dispersed fluorescence spectra for emissions from XeF(*B, C* and *D*) excimers formed from XeF_2 excited by linearly polarized, monochromated synchrotron radiation on an apparatus at the Beamline BL2A of UVSOR. The absorption and the fluorescence excitation spectra are measured to determine the quantum yield for the XeF^* excimer formation from XeF_2 as are shown in Figure 1. The latter has been determined by comparing the fluorescence intensity to that of $OH(A \rightarrow X)$ formed from photodissociative excitation of H_2O.[1)]

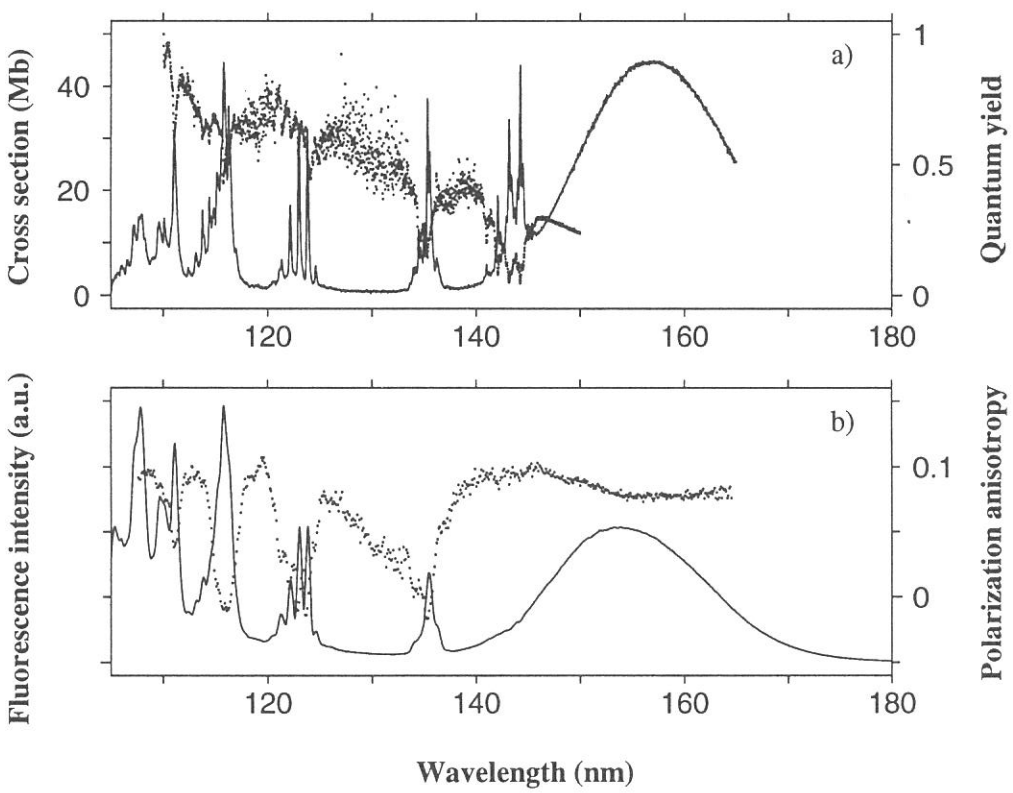

Figure 1. a) Absorption spectrum and quantum yield for XeF^* formation in dissociative excitation of XeF_2. b) Polarization anisotropy for total fluorescence and fluorescence excitation spectrum.

Figure 1a shows the absorption spectrum (solid line) of XeF_2 along with the quantum yield for total emission (dots) in the excitation wavelength (λ_{exc}) region 105-165 nm at a resolution of 0.10 nm. Most of the bands have been assigned by Nielsen and Schwartz.[2] However some of the assignments are questioned in light of the results of fluorescence polarization anisotropy measured[3] for XeF^* formed at 193 nm and that in the wavelength region 110-165 nm shown in Figure 1b which also illustrates the fluorescence excitation spectrum obtained by monitoring the total emission at a resolution of 0.5 nm for the excitation light. It is noted that the quantum yield for XeF^* excimer formation is found to be very high, especially at 110 nm it reaches a unity. In qualitative agreement with the previous work[4], the quantum yield for the broad absorption band has been found as 0.23 at 150 nm.

Another interesting phenomenon was observed in a series of $\pi_{u\ 3/2} \rightarrow$ 6sR bands around λ_{exc} = 143 nm. Figure 2 illustrates the absorption spectrum of XeF_2 and XeF^* fluorescence excitation spectra in the expanded region from λ_{exc} = 140 to 146 nm observed at a resolution of 0.10 nm. Note that no strong peaks are found in the excitation spectrum in spite of intense absorption bands. In contrast even fluorescence dips are observed at 143.18 nm and 144.26 nm whereas weak positive bands are observed at 141.02 and 142.11 nm. It seems that the bands which are positive at higher energies tend to become negative as the exciting light energy decreases. A similar phenomenon has been observed for I_2.[5]

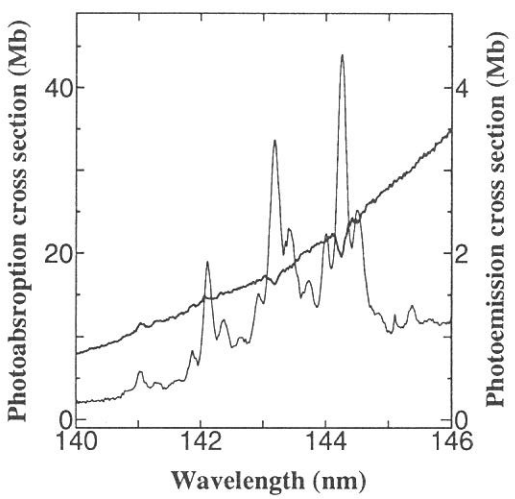

Figure 2. Photoabsorption cross section of XeF_2 and total emission cross section measured for XeF^* formed vs. excitation wavelength.

The dispersed fluorescence spectra for nascent XeF^* formed are briefly described in following: 1) with increasing the excitation energy the relative intensity for the $XeF(D \rightarrow X)$ emission ($\lambda_{obs} \approx$ 260 nm) increases. 2) The $XeF(B \rightarrow X)$ band ($\lambda_{obs} \approx$ 350 nm) is found to be strong at every exciting energy measured but the vibrational distribution is strongly dependent on its excitation energy. 3) The $XeF(C \rightarrow A)$ band ($\lambda_{obs} \approx$ 460 nm) is weak.

References

[1] L. C. Lee, *J. Chem. Phys.* **72**, 4334 (1980)

[2] U. Nielsen and W.H.E. Schwarz, *Chem. Phys.* **13**, 195 (1976)

[3] a) G. W. Loge and J. R. Wiesenfeld, *Chem. Phys. Lett.* **78**, 32 (1981); b) G. W. Loge, J. R. Wiesenfeld, *J. Chem. Phys.* **75**, 2795 (1981)

[4] G. Black, et al. *J. Chem. Phys.* **75**, 4840 (1981)

[5] A. Hiraya, K. Shobatake, R. J. Donovan, and A. Hopkirk, *J. Chem. Phys.* **88**, 52 (1988)

Photoemission study of the adsorption process of alkali metals on NbC(100)

K. Ozawa, T. Anazawa, S. Tokumitsu, E. Miyazaki and K. Edamoto
Deptartment of Chemistry, Tokyo Institute of Technology,
Ookayama, Meguro-ku, Tokyo 152

S. Tanaka
UVSOR, Institute for Molecular Science, Myodaiji, Okazaki 444

1. Introduction

Transition metal nitrides and carbides (TMNC's) are of considerable interest because of an interesting combination of physical properties such as an ultrahigh hardness, a high melting point, metallic conductivity, etc. From a practical point of view, they have been used as catalysts, electron emitters, coating materials, etc.; thus their surface properties are of particular interest. Alkali metal adsorption on metal surface has been subject of intensive studies because of the importance also in the preparation of an effective electron emitter and catalyst. Thus the study of alkali metal adsorption on TMNC surface is much motivated. In this work, the adsorption processes of Na and K on a NbC(100) are studied with core-level photoemission spectroscopy using synchrotron radiation.

2. Experimental

The PES measurements were conducted on BL2B1 of the UVSOR, Institute for Molecular Science, using a Grasshopper monochromator and a cylindrical mirror analyzer of a double-pass type. The clean NbC(100) surface was prepared in a vacuum chamber by flashing to about 1800 K. Na and K were evaporated from resistively heated dispenser (SAES getters) sources which were carefully degassed.

3. Results and discussion

Fig. 1 shows the work function change ($\Delta\phi$) of the NbC(100) surface as a function of Na and K deposit times. The $\Delta\phi$ is deduced from the secondary electron threshold in the photoemission spectra. The work function decreases rapidly in the initial stage and then becomes plateau which shows very similar value for the polycrystalline metal, for both adsorption. The $\Delta\phi$ curves shown in fig. 1 is very similar to those for previously published metal - alkali metal systems, which imply large dipole moment formation in the initial stage and subsequent metallic layer formation.

Fig. 2 shows the change in the spectrum as a function of K coverage. The K 3p and 3s emissions are developed with the increase of K coverage. The spectral change is saturated at 1ML and splitting of peaks due to the multilayer

formation are not found, indicating that the adsorption is saturated when the single layer is formed. This is in contrast to the case for the NbC(100)-Na system where the multilayer formation is found. For more than 0.5 ML, subbands appear in the higher binding energy side of the main lines, which are due to the excitation of K layer plasmon. This result also implies that the adsorption layer is transformed to the metallic layer at > 0.5 L.

Binding energies of K core-level emissions are nearly independent on the K coverage (fig. 2). This indicates that the chemical environment of K atom is independent on the coverage. This is in contrast to the case for the many metal - alkali metal systems where ionic adsorption layers are formed in the initial stage, which results in the large coverage dependence of core-level emission energies. It is concluded from figs. 1 and 2 that the alkali metal adsorption on the NbC(100) surface proceeds via the Ishida model which does not include the oonization of alkali metal.

The surface-induced component of C 1s emission is much affected by K adsorption while the Nb core-level emissions are uniformly suppressed. The surface shift is only observed for C core-level, which is compatible with the electronic structure deduced from the relaxation model for the TMNC (100) surface.

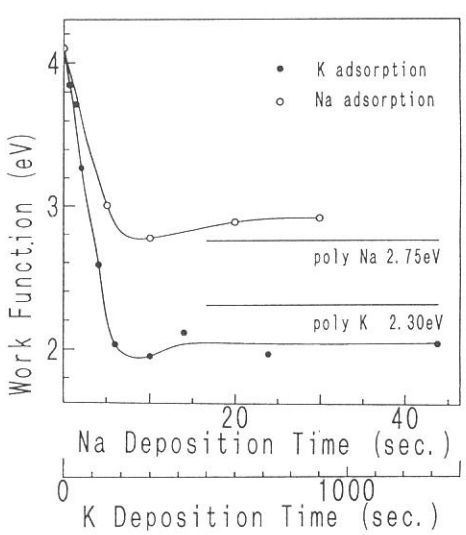

Fig. 1.

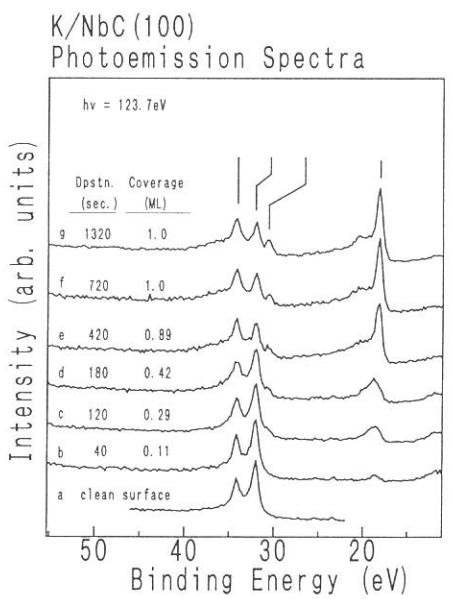

Fig. 2.

Formation of the Quasi-Two Dimensional Alkali Halide on the Si(100) surface

Shin-ichiro TANAKA and Masao KAMADA

Co-adsorption of K and Cl on the Si(100) surface was investigated with photoelectron and XANES (X-ray Absorption Near Edge Structure) spectroscopy. Experiments were performed by using the grasshopper monochromator and a double-pass CMA at BL2B1 of UVSOR. The Si(100) surface were firstly covered with a monolayer of K and subsequently exposed to Cl [Si(100)/K/Cl]. The Si(100)/Cl/K system was also prepared in a similar way. The valence-band photoelectron spectra of these systems were very similar to that of the KCl film evaporated on gold, indicating that K and Cl atoms are ionic on both surfaces (Fig.1). This is consistent with the results obtained from XANES spectra around the K-$L_{2,3}$ edge. Both surfaces showed the diffused (2x1) LEED pattern. It is considered that quasi-two dimensional KCl surfaces are produced in these systems. However, the Si-2p photoelectron spectra showed that the bonding configuration in the Si(100)/K/Cl system is different from that in the Si(100)/Cl/K system. (Fig. 2) The spectrum for Si(100)/K/Cl is similar to that for Si(100)/Cl and the spectrum for the Si(100)/Cl/K is similar to that for the Si(100)/Cl.

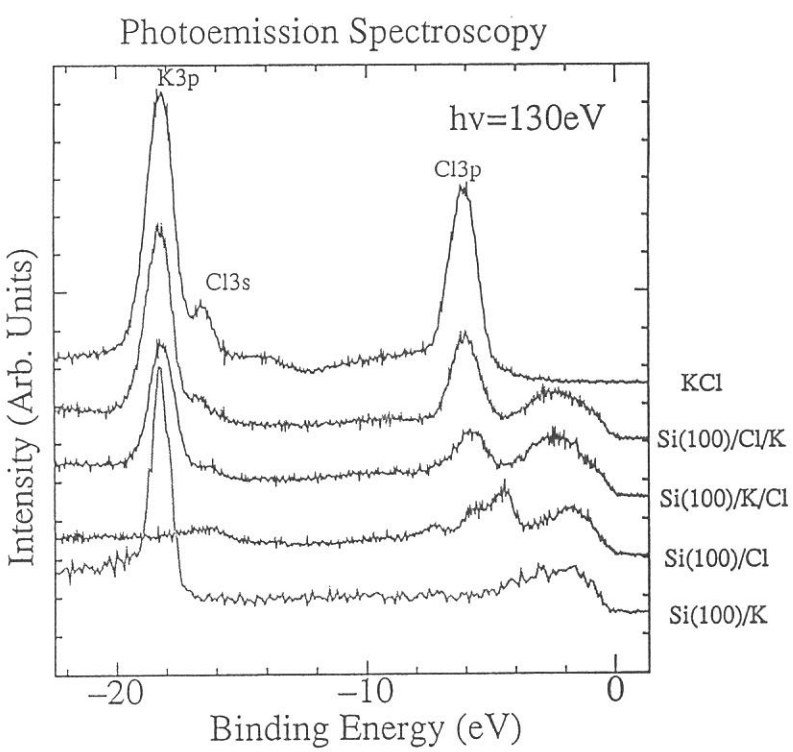

Figure 1

Photoelectron spectra of the Si(100) surfaces covered with a monolayer of K atoms [Si(100)/K], the Si(100) surface with a monolayer of Cl [Si(100)/Cl], the Si(100)/K surface after an exposure to Cl [Si(100)/K/Cl], the Si(100)/Cl surface after a deposition of K [Si(100)/Cl/K], and the KCl film evaporated on the gold substrate. The energy scale of the spectrum of KCl film were shifted by +0.6 eV. The sample preparation and the measurements were made at room temparature. Photon energy was about 128eV, and the kinetic energy corresponding to the valence band maximum was 123.5 eV.

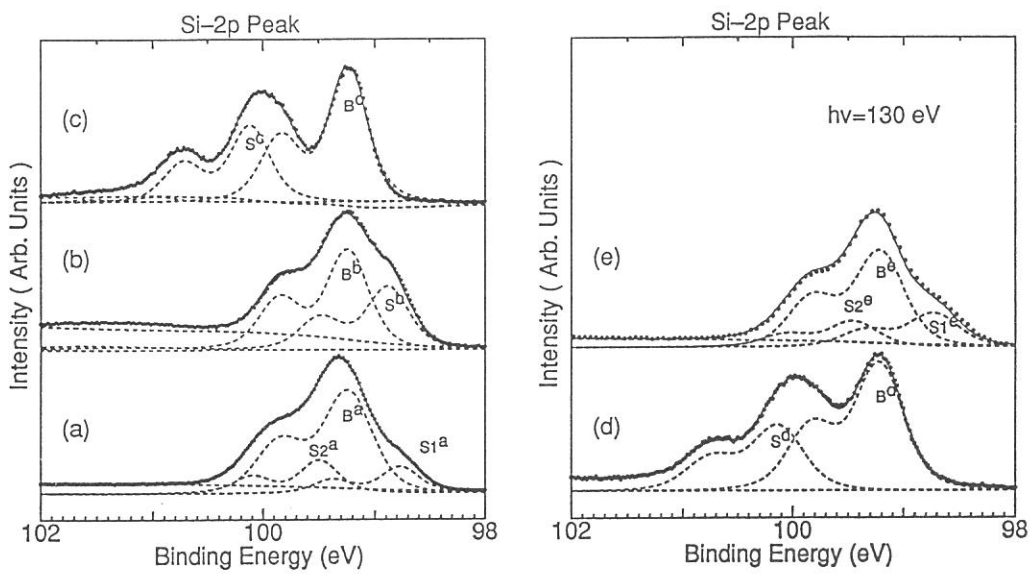

Figure 2

Photoelectron spectra of the Si-2p level for the Si(100) surfaces: (a)clean Si(100)(2x1), (b) Si(100)/K, (c)Si(100)/Cl, (d)Si(100)/K/Cl. (e)Si(100)/Cl/K. Dots are experimental data, lines are least square fits, and dotted lines are backgrounds. Each component has two peaks due to the spin-orbit splitting. "S" indicates the surface peak, and "B" indicates the bulk peak.

Infrared Reflection Absorption Spectroscopy (IRAS) using Buried Metal Layer (BML) Substrate -Application for surface photo-chemical reaction-

A.Yoshigoe[a], M.Nagasono[b], K.Mase[a,b], and T.Urisu[a,b]

[a] *The Graduate University for Advanced Studies, Institute for Molecular Science, Myodaiji, Okazaki 444, Japan*

[b] *Institute for Molecular Science, Myodaiji, Okazaki 444, Japan*

Synchrotron Radiation(SR) induced surface photo-chemical reaction, such as etching and chemical vapor deposition(CVD), is one of the most interesting field in not only technology but also in science.[1] Characteristic phenomena, such as material selectivity, have been found in the photo-chemical reaction induced by vacuum ultraviolet (VUV). To understand the reaction mechanism, in-situ measurements of adsorbed spieces are important. Infrared reflection absorption spectroscopy (IRAS) is a powerful technique with high resolution (< 1 cm^{-1}), high sensitivity, little destruction, and little pressure restriction. However, IRAS is known to be effective only for metal substrates , which has negligibly small phase shift for p-polarized beam. But, it is difficult to apply IRAS for semicondustor or insulator surfaces, which are important materials in the SR induced semiconductor processes. To overcome this disadvantage, the method of buried metal layer (BML) substrate has been proposed by several groups.[2,3,4] The experimental quantitative evaluation of the advantageous characteristics of BML substrate has not yet been studied. Since the BML is an artificial structure, the quantitative measurement of the enhancement is important to evaluate the usefullness of this technique. In the present paper, characteristics of the BML have been demonstrated by caluculations and experiments using Langmuir-Blogett films.

Figure 1 shows the angular dependence of IRAS of Ba stearate LB films deposited by 5 layers on the SiO_2 BML substrate. The Si(100) wafer with 20-nm-Al layer buried by 15-nm-SiO_2 thin films was used as the BML substrate. The peaks at 2957.7, 2917.3, 2872.4, 2850.0, 1542.8, and 1446.2 cm^{-1} are assigned to antisymmetric CH_3 streching, antisymmetric CH_2 streching, symmetric CH_3 streching, symmetric CH_2 streching, antisymmetric COO^- streching, and symmetric COO^- streching, respectively. The intensity of each peak increases with increasing angle of incidence. This result agrees with the theoretical prediction.[2] This result shows that BML substrate is similar to the buried metal in the optical property, and that the BML method is useful for observing adsorbates on surfaces of semiconductor or insulator.

Figure 2 shows the calculated intensity curve and the experimental values of IRAS using BML substrate. Calculation was made by using the multilayer reflection equation.[2] In the calculation, the complex reflective index (n - ik) values at 1446.2 cm^{-1}, n_1=1.00, k_2=0.00 for air, n_2=1.148, k_2=0.198 for LB films, n_3=1.11, k_3=0.00 for SiO_2 buffer layer, and n_4=13.0, k_4=47.0 for Al were used. LB film thickness was assumed to be 25 Å for one monolayer. The n_2 and k_2 values between calculated and experimental agree with the reported refractive index values with stearate compounds or stearic acid. Therefore it is conclued that our fabricated BML structure is complete as a substrate of IRAS. We will apply this method to monitor synchrotron radiation induced surface photo-chemical reactions.

References

1.T.Urisu,J Takahashi,Y,Utsumi and H Akazawa, Appl Organo Chem.5,229(1991)

2.V.M.Bermudez,J.Vac.Sci.Technol.10,152(1992)

3.V.M.Bermudez and S.M.Prokes,Sur.Sci.248,201(1991)

4.S.J.Finke and G.L.Schrader,Spectrochem.Acta Part A,91(1990)

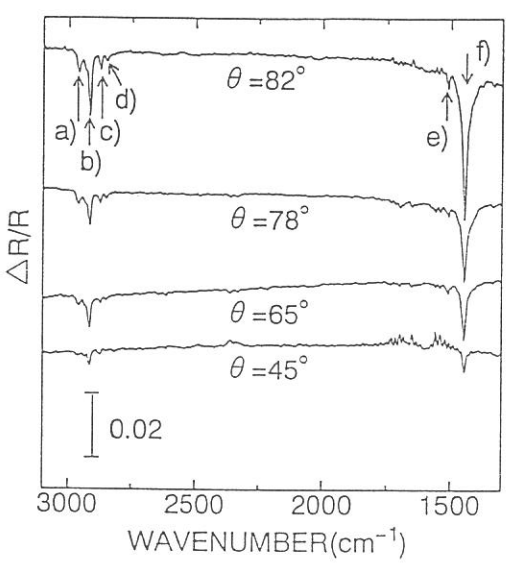

Figure 1 Angular dependence of IRAS for Ba stearate LB films deposited by 5 layers on the SiO_2 BML substrate. Vertical line is $\Delta R/R = (R_0 - R)/R$, where R and R_0 are reflectivity with and without LB films, respectively.

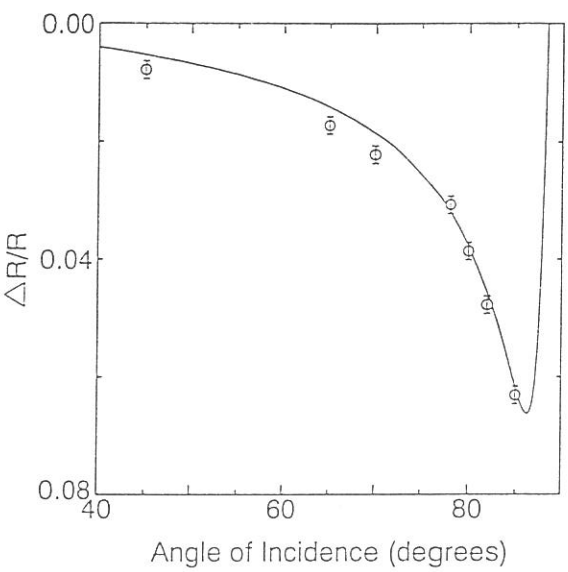

Figure 2 Intensity curve caluculated for the symmetric COO^- peak at 1446.2 cm^{-1} of 5 monolayer Ba stearate LB films on BML substrate by p-polarized beam. The open circle are experimental data for p-polarized beam.

SYNCHROTRON RADIATION EXCITED ETCHING OF SILICON SURFACE STUDIED BY VELOCITY DISTRIBUTION MEASUREMENTS OF DESORBED SPECIES (II)

Haruhiko OHASHI and Kosuke SHOBATAKE

Institute for Molecular Science, Myodaiji, Okazaki 444, Japan

Synchrotron radiation excited etching of Si(100) surface with XeF_2 is studied by measuring the velocity distributions of the desorbed neutral species using a time-of-flight (TOF) technique and an electron bombardment ionization mass spectrometer detector(EBIMS). A new reaction chamber is set up to the beam line BL4B and was constructed to lower the residual gas background due to the desorbed species. Focused synchrotron radiation from a bending magnet was shone on the Si(100) sample in XeF_2 environment. In the present study very reactive etchant XeF_2 gas was used to avoid the etchant gas pressure to exceed 1.0×10^{-4} Torr in the reaction chamber and yet to supply enough F atoms to the surface. The schematics of the apparatus is shown in Figure 1. The angle between the incident light beam and the

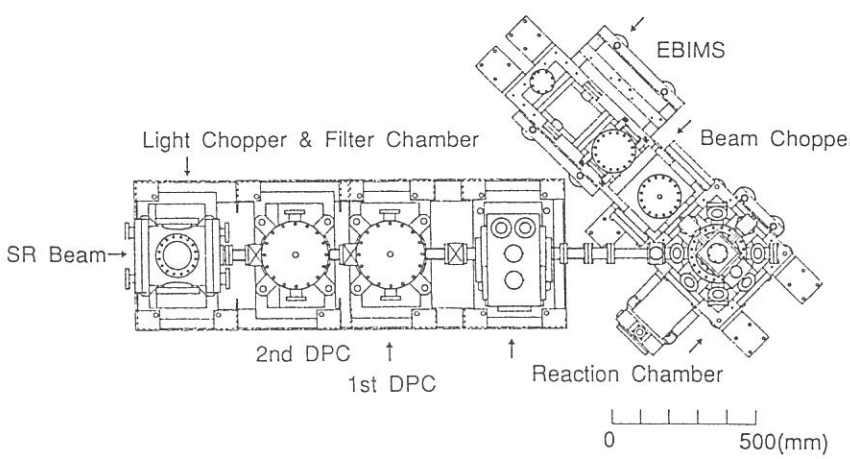

Figure 1. The schematic top view of the apparatus.

velocity vector of desorbing product detected is 135 degrees. The flight length from the correlation chopper to the ionizer, L, was 31 cm.

Figure 2 shows the TOF spectra observed at mass m/e = 85(SiF^+) with the SR on and off. The conspicuous difference between the two distributions is that with the SR on a fast moving species appears as a shoulder in addition to the slow species. The shoulder band for the fast moving species in the TOF spectrum with SR on can be fitted by a shifted Maxwell Boltzmann (SMB) distribution as follows.

$$F(t) \propto \left(\frac{v}{\alpha}\right)^4 \exp\left[-\left(\frac{v-u}{\alpha}\right)^2\right]$$

where α is the most probable velocity $\alpha = \{2RT/M\}^{1/2}$ and t is the neutral flight time given by $t = L/v$. In the upper figure in Figure 2 the dotted and the dashed curves are the calculated SMB distributions, respectively and the solid curve is the sum of them. The average velocities for the fast and slow components with SR on are 870 and 340 m/s, respectively, and that with SR off is 320 m/s. The intensity level measured when SR is irradiated is more than that when SR is off. The intensity level for only the slow component with SR on is as high as that with SR off. A fast peak was not at all observed even when Si is irradiated with undulator light (35.8 eV) and nor when un-irradiated[1]. From a series of measurements under different experimental conditions it has been found that the substrate temperature goes up as much as about 200 ℃ depending upon the irradiation time and the stored current level. The peak for the fast moving species was not always observed even when Si was irradiated with focused white SR, but was observed only after some twenty minutes of irradiation. It seems that the appearance of the fast peak depends upon the irradiation time and SR intensity as well as substrate temperature. Although the mechanism for formation of the fast moving species is not well understood at the moment, it is distinctly observed only when SR is shone upon Si.

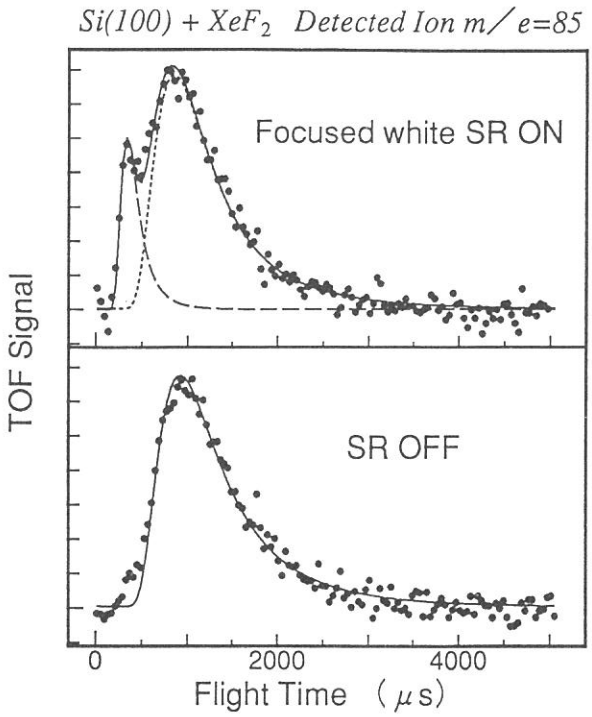

Figure 2. TOF spectra of desorbed species detected at mass m/e = 85 (SiF^+) with focused SR beam on and off. The curve corresponds to the calculated SMB distribution.

Reference

1) H. Ohashi, K. Tabayashi and K. Shobatake, UVSOR Activity Report (1992) 122.

Dynamics of Photon-Stimulated Desorption of Excited-State K Atoms from KCl and KBr

Sayumi Hirose and Masao Kamada
Institute for Molecular Science, Myodaiji, Okazaki 444

Photon-stimulated desorption (PSD) of constituent ions and atoms from solids has aroused considerable interest, because of its close relation to fundamental interaction between incident beams and solid surfaces, and also because of its applicability to microfabrication. There are most desorption studies of ions and ground-state atoms from alkali halides, while several works are reported about the PSD of excited atoms.[1] The purpose of present study is to improve our understanding of the PSD mechanism, especially the dynamics of excited-state alkali desorption, by measuring the time response of excited-state alkali desorption.

The experiment was carried out with synchrotron radiation pulses under a single-bunch operation at a undulator beam line 3A1. An excitation source was used by the undulator radiation through a 1300-Å-thick aluminum filter. Time response of excited-state alkali desorption was investigated by using a time-correlated single photon counting method at room temperature. The interval of successive SR pulses was 178 ns and the full-width at half-maximum of incident photon pulse including the detector system was 480 ps. Single crystals of KCl and KBr were cleaved with a knife edge in sample chamber, of which base pressure was about 2×10^{-7} Pa.

Figure 1 shows the time response of excited-state K desorption from KCl and KBr. These time responses are composed of fast and slow components. The fast component is in the time scale of nano-second and the slow component is between 178 ns and 3 ms. The slowest limit was determined by using the mechanical chopper. Therefore, this result indicates the two PSD mechanisms of excited-state alkali atoms.

The time response of ground-state alkali atoms has been reported to be in the scale of μs to ms by Kanzaki *et al.*[2] and Loubriel *et al.*[3] They proposed that the desorption process of ground-state alkali atoms is related to the diffusion of F or V_K centers and the surface reaction of F centers and alkali ions. The slow component of excited-state alkali desorption is seemed to be in the time scale of ground-state alkali desorption. However, the substance dependence and the temperature dependence of the desorption

yield are clearly different between excited-state and ground-state alkali atoms.[4] Therefore, we propose here that the slow desorption of excited-state alkali atoms may be due to the thermal instability of surface defects, which are different from those concerning the ground-state alkali desorption.

On the other hand, the fast component of excited-state alkali desorption is in the time scale of nano-second. On the basis of the substance dependence,[5] it becomes evident that the substance having a larger Rabin-Klick parameter shows a larger efficiency of the fast desorption. This result indicates that the lattice instability due to the electronic excitation in the surface layers may play an important role on the fast PSD of excited-state alkali atoms. We propose that excited-state alkali atoms may be produced by way of the precursor state (for example, off-center distorted STE, F-H pair, and F center), which is produced instantly by electronic transition in the surface layers with photon irradiation, and they decay with emitting optical fluorescence, which is observed as an atomic line. The solid curves in Fig. 1 are the decay curves analyzed with the model mentioned above. It should be noticed that there is good agreement between the analyzing curves and the observed decay curves. This result supports the present fast desorption model for excited-state alkali atoms.

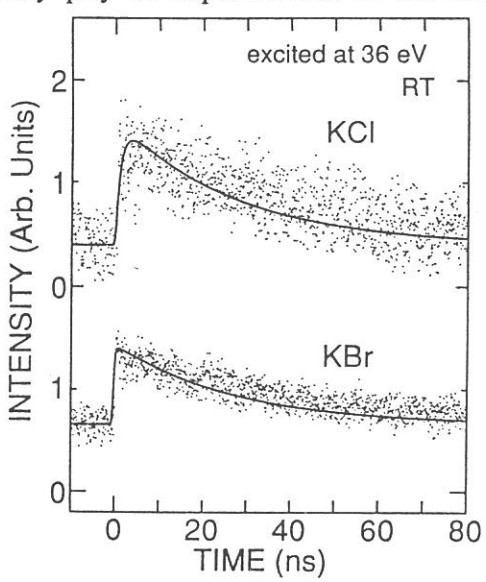

Fig. 1. Time response of excited-state K desorption from KCl and KBr excited with undulator radiation of 36 eV. Solid curves are the analyzing curves.

References

1) Desorption Induced by Electronic Transitions (DIET IV), edited by G. Betz and P. Varga (Springer, Berlin, 1990).
2) H. Kanzaki and T. Mori, Phys. Rev. B 29, 3573 (1984).
3) G. M. Loubriel, T. A. Green, N. H. Tolk and R. F. Haglund, Jr., J. Vac. Sci. Technol. B 5, 1514 (1987).
4) S. Hirose and M. Kamada, J. Phy. Soc. Jpn., 60, 4376, (1991).
5) S. Hirose and M. Kamada, Phys. Rev. B 48, 17641 (1993).

PHOTON STIMULATED DESORPTION OF METASTABLES FROM THE SURFACE OF RARE GAS SOLIDS.

D. E. Weibel, T. Nagai, I. Arakawa, M. Kanno[A], K. Mitsuke[B], and M. Sakurai[C]

Dep. Phys. Gakushuin Univ., Grad. Univ. Advanced Studies[A], Inst. Molec. Sci.[B],
Dep. Phys. Kobe Univ.[C]

The excitation of rare gas solids by electrons or photons leads to the desorption of ions, ground state, excited atoms (including metastables), etc. Two models of the desorption process have been proposed to describe the desorption of excited neutral species[1]: Cavity-Ejection (CE) in which the excited atom at the surface is ejected by a repulsive potential around it caused by negative electron affinity of the matrix and Excimer-Dissociation (ED) in which the conversion of the electronic excitation energy into the kinetic one occurs after an electronic transition to an antibonding state.

We have investigated the kinetic energy of the metastables desorbed by excitonic excitation by photon from the surface of Ne and Ar alloy to get an insight into the mechanism of the desorption induced by electronic transitions (DIET). We have also obtained some preliminary results of the angular distribution of the Ne metastables from the surface of pure Ne. The experiments were carried out at the beam line BL5B in UVSOR, Institute for Molecular Science. Details of the experimental system and procedure have been previously described[2].

Figure 1 shows a typical time-of-flight spectrum of the desorbed particles from the solid surface of Ne/Ar alloy with 12 % of Ne. The two metastable signals are assigned to Ar* (CE) at TOF ≅ 250 μsec, and a mixture of Ne*(CE) and Ar* (ED) at TOF ≅ 95 μsec. Photon signal is chosen as the origin of the flight time.

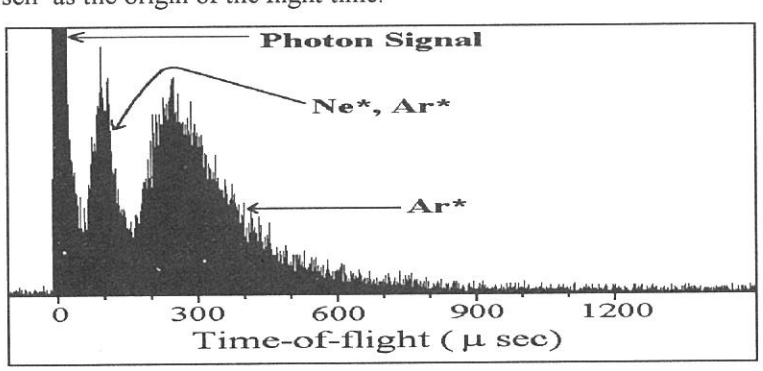

Fig. 1. TOF spectrum of metastables desorbed from an Ne/Ar alloy (12 % of Ne, λ_{scan}: 50-110 nm).

When we used a detector which quantum efficiency for Ar* was almost null, Ne*(CE) signal desorbed by first (S1, λ = 72.2 nm) and second (S', λ = 65.3 nm) order surface

excitation was only observed (See Fig. 2). The fact that the Ne* signal disappeared at the excitation of bulk excitons (B1, λ = 70.5 nm; B2, λ = 61.2 nm) of Ne suggests that there is an efficient mechanism of energy transfer from Ne bulk excitons to Ar matrix. Figure 3 shows the effect of this mechanism in the enhancement of Ar* yields desorbed from an Ne/Ar alloy (12% of Ne) with respect to pure Ar. In this case a detector with high quantum efficiency for Ar* was used.

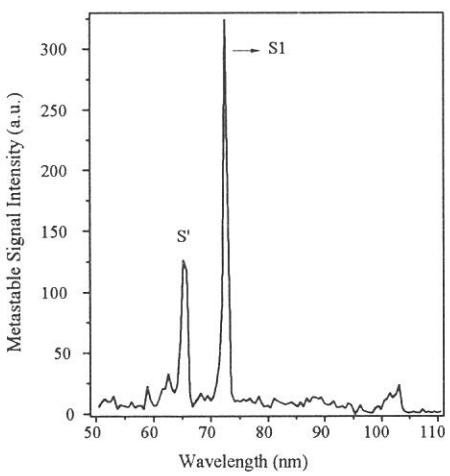

Fig. 2. Dependence of the total metastable signal on λ for an Ne/Ar alloy with 28.7% of Ne. This spectrum was obtained using a detector with quantum efficiency for Ar*≈0.

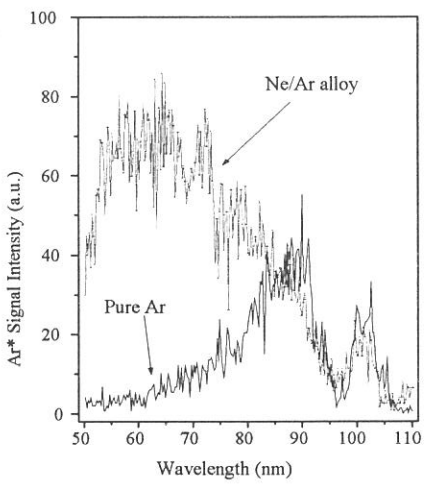

Fig. 2. Dependence of the Ar* signals on λ for pure solid Ar and an Ne/Ar alloy (12 % of Ne). Results obtained by a detector with high quantum efficiency for Ar*.

At the excitation energy of Ar excitons ($\lambda \geq 85$ nm), the signal ratio Ar*(ED)/Ar*(CE) increased as the amount of Ne increase from 0 to 73% (results not shown). These results show that the diffusion of Ar exciton from bulk to surface is blocked by Ne and the formation of the excimer (probably (NeAr)* heteronuclear one) is enhanced.

Preliminary results of PSD angular distributions of Ne* from pure solid Ne were obtained. In these experiments we used a position-sensitive, single-event counting device that includes two microchannel plates mounted in front of a (2-dimensional) position sensing resistive anode recorder. Kinetic energy and angular distribution can be simultaneously obtained with this detector. Each metastable (CE, ED) has a very characteristic angular distribution which is in agreement with the previous ESD (Electron Stimulated Desorption) studies[3], and support the proposed two desorption mechanisms.

REFERENCES

1) F. Coletti, J.M. Debener and G. Zimmerer, J. Physique Lett. **45**, L-467 (1984).
2) M. Sakurai, T. Hirayama, and I. Arakawa, Hosyakou **5**, 13 (1992) (in Japanese); M. Sakurai, T. Hirayama, and I. Arakawa, Vacuum **41**, 217 (1990).
3) D.E. Weibel, T. Hirayama, and I. Arakawa, Surf. Sci. 283, 204 (1993).

Photoemission Study of $Sr_{1+x}La_{1-x}FeO_4$

Takahisa OMATA, Kazushige UEDA, Hideo HOSONO,
Takafumi MIYAZAKI*, Naoyuki UEDA* and Hiroshi KAWAZOE*

Research Laboratory of Engineering Materials, Tokyo Institute of Technology, Midori-ku, Yokohama 227
**Institute for Molecular Science, Myodaiji, Okazaki 444*

Electrical insulator of 3d transition metallic compounds are usually classified in to Mott-Hubbard type or charge-transfer type. It has been clarified recently that the oxides of Cu and Ni are described as charge-transfer insulators. La_2CuO_4 is known as a typical charge-transfer insulator, and its hole-doped system shows a insulator to metal transition upon the doping. Photoemission studies of the hole-doped cuprates has been intensively carried out and revealed that the introduced positive holes occupy newly formed in-gap states, which mainly consist of O 2p character.

$SrLaFeO_4$, isostructure with La_2CuO_4, dose not show a insulator to metal transition upon the hole doping.[1] In this report, electronic structure of hole-doped $Sr_{1+x}La_{1-x}FeO_4$ ($0 \leq x \leq 0.3$) was studied by ultraviolet photoemission spectroscopy. It will be concluded that the valence band structure in this system did not change and Fermi level was settled above $\sim$1.2eV of the valence band maximum upon the doping.

The samples sintered were prepared at 1500°C for 48h in O_2 flow. Photoemission measurements were performed at the beam line BL8B2. The surfaces of the samples were scraped with a diamond file just before measurements to avoid the surface contamination under a vacuum of $4 \times 10^{-9} \sim 1 \times 10^{-8}$ Torr.

Figures 1 and 2 show photoemission spectra in the valence band region for the excitation photon energies of 28 and 40eV, respectively. The spectra of bulk and non-doped sample showed charging effects, which were detected as a uniform shift of the whole spectrum to higher binding energies ($\sim$1.5eV) and as a spectral broadening. Since no charging effect was observed in the spectra of the doped samples, we concentrated on results of the doped samples. Strong features centered at $\sim$6eV and $\sim$10eV were seen in the valence band photoemission spectra. No significant change was detected in the spectra of the samples with the different doping level. It must be noted that the valence

band maximum of each spectrum was settled at ~1.2eV of binding energy. This suggests that the Fermi level do not shift upon the doping and the rigid band model cannot apply to this system.

The emission cross section of O 2p steeply increases toward lower photon energies, while that of Fe 3d emission becomes more dominant for higher excitation photon energies ($h\nu \gtrsim 40$eV).[2] Therefore, the band, which consists mainly of Fe 3d character, is enhanced in the spectra with excitation photon energy of 40eV (Fig. 2), if such a band exists in the valence band region. But the line shape has unchanged for both excitation photon energies in contrast with such different photon energy dependence of Fe 3d and O 2p. This suggests that the valence bands in this system are composed of well mixed Fe 3d and O 2p states. This is consistent with the results of Fe 3p - 3d resonant photoemission measurements[3].

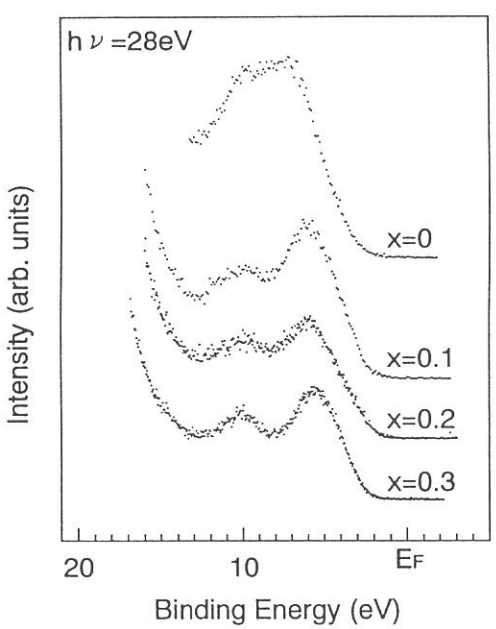

Fig. 1. UPS spectra of $Sr_{1+x}La_{1-x}FeO_4$ with excitation photon energy of 28eV.

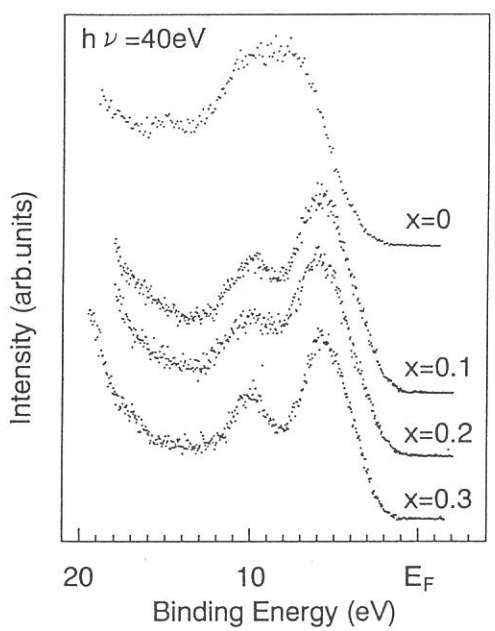

Fig. 2. UPS spectra of $Sr_{1+x}La_{1-x}FeO_4$ with excitation photon energy of 40eV.

1) T.Omata, K.Ueda, H.Hosono, M.Katada, N.Ueda and H.Kawazoe, Phys. Rev. B, in press.

2) J.J.Yeh and I.Lindau, At. Data Nucl. Data Tables 32, 1(1985).

3) T.Omata, K.Ueda, H.Hosono, T.Miyazaki, S.Hasegawa, N.Ueda and H.Kawazoe, Phys. Rev. B, in press.

Resonant Photoemission Studies of Mn 3d States in $Cd_{0.67}Mn_{0.33}Te$ and $Cd_{0.65}Mn_{0.35}Se$

H. Sato, N. Happo, M. Tamura, M. Taniguchi,
M. Kamada[1] and S. Ohara[2]

Department of Materials Science, Faculty of Science, Hiroshima University,
Kagamiyama 1-3, Higashi-Hiroshima 724, Japan
[1]Institute for Molecular Science, Myodaiji, Okazaki 444, Japan
[2]Department of Physics, Nagoya Institute of Technology, Showa-ku
Gokisho, Nagoya 466, Japan

Mn-substituted II-VI diluted magnetic semiconductors have attracted a great deal of interest. The replacement of the group II-cation with Mn yields novel magneto-optical phenomena[1]. These effects are derived from a hybridization of the Mn 3d states in the high spin configuration with the sp-band states of the host crystals. Resonant photoemission spectroscopy is a powerful technique for investigating a measure of the Mn 3d partial density of states (DOS). In this report, we present the results for $Cd_{0.67}Mn_{0.33}Te$ and $Cd_{0.65}Mn_{0.35}Se$.

The resonant photoemission experiments in the Mn 3p-3d excitation region were carried out on BL-6A2 of UVSOR equipped with a plane grating monochromator. Clean surfaces of samples were prepared by cleavage under ultrahigh vacuum below 5×10^{-10} Torr in the preparation chamber. Then, the sample was *in situ* transferred into the analysis chamber with base pressure of 4×10^{-10} Torr. All measurements were performed at room temperature. Bulk crystals of $Cd_{0.67}Mn_{0.33}Te$ and $Cd_{0.65}Mn_{0.35}Se$ were grown through a Bridgman method. We verified the samples forming homogeneous crystal phase by x-ray diffraction measurement. The Mn concentration was determined by electron-probe micro-analysis.

Figure 1 shows the Mn 3d partial DOS's of $Cd_{0.67}Mn_{0.33}Te$ and $Cd_{0.65}Mn_{0.35}Se$ obtained by subtracting the spectrum measured at $h\nu$=47.5 eV (antiresonance) from that taken at $h\nu$=50.0 eV (on-resonance), after the normalization of spectral intensities to the monochromator output by use of photoelectron yield from Au film. Binding energy is referred to the valence-band maximum, which was determined by a linear extrapolation of the leading edge. In addition, contribution from inelastic secondary electrons has been removed. The Mn 3d partial DOS's exhibit a characteristic feature consisting of three structures; a main peak at 3.5 eV, valence bands in 0-2.5 eV, and a broad satellite in 5-9 eV. It should be noticed that the intensity of the valence bands relative to that of the main peak increases on going from Te to Se, whereas the relative intensity of the satellite decreases.

On the basis of the configuration interaction (CI) theory using $MnTe_4$ cluster, the spectral shape of the Mn 3d partial DOS depends on Δ and $(pd\sigma)$, where they denote the ligand-to-3d charge-transfer energy and the p-d transfer integral, respectively. With increasing Δ or $(pd\sigma)$, the relative

intensity of the valence-bands increases while that of the satellite decreases. Δ and $(pd\sigma)$ for $Cd_{1-x}Mn_xTe$ ($Cd_{1-x}Mn_xSe$) obtained from the d-d optical absorption spectra are 2.0 (2.5) and 1.1 (1.2), respectively[2]. Thus, the difference of the Mn 3d partial DOS features between $Cd_{0.67}Mn_{0.33}Te$ and $Cd_{0.65}Mn_{0.35}Se$ can be well explained within the framework of the CI theory. Measurements on the Mn 3d partial DOS of $Cd_{1-x}Mn_xS$ are now in progress.

[1] *Dilute Magnetic Semiconductors*, Vol. 25 of Semiconductors and Semimetals, edited by J. K. Furdyna and J. Kossut (Academic, New York,1988).

[2] T. Mizokawa and A. Fujimori, Phys. Rev. B, in press. The previous analysis were performed using d^5 and $d^6\underline{L}$ configurations as the ground states [M. Taniguchi *et al.*, Solid State Commun. **62**, 431(1987).], while the present analysis includes further $d^7\underline{L}^2$ configurations.

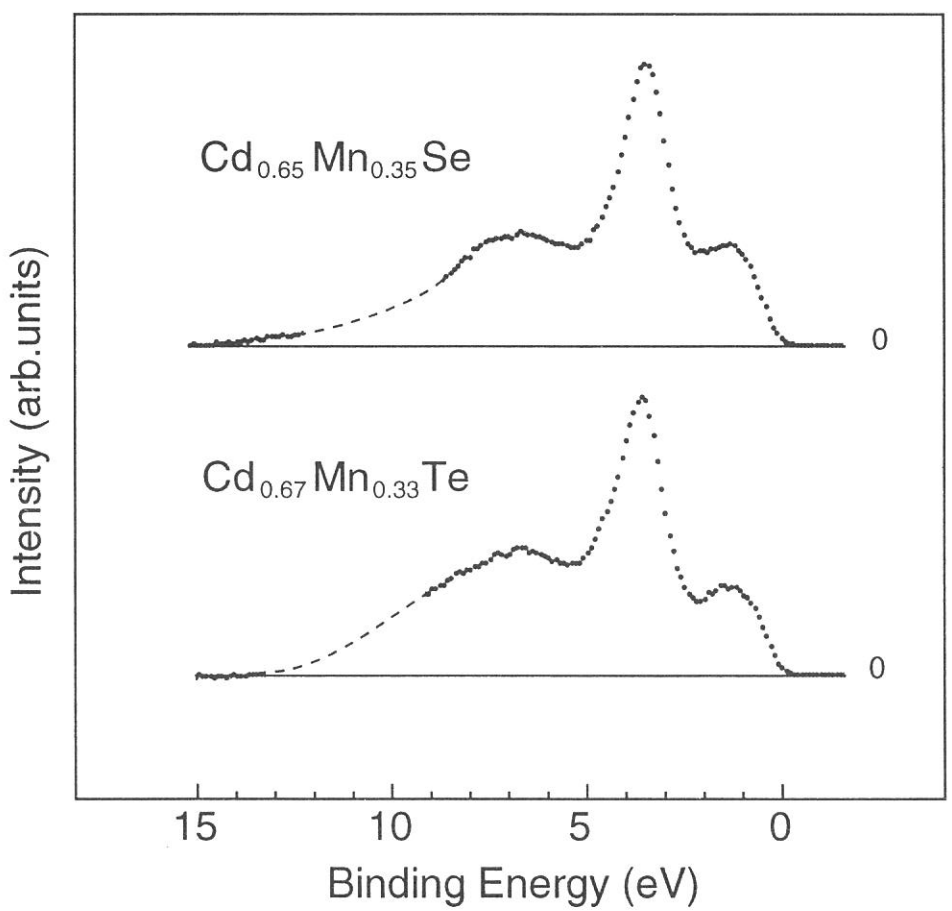

Fig.1 Mn 3d partial DOS in $Cd_{0.67}Mn_{0.33}Te$ and $Cd_{0.65}Mn_{0.35}Se$ obtained from the photoemission spectra measured at antiresonance and just on resonance.

Resonant Photoemission Study of an Al-Pd-Mn Icosahedral Phase

M. MORI, T. MIYAZAKI[‡], S. HASEGAWA[‡], T. ISHIMASA[†], T. HAYASI and S. MATSUO

Department of Natural Science Informatics, School of Informatics and Sciences, Nagoya University, Nagoya 464-01

[†]Department of Nuclear Engineering, School of Engineering, Nagoya University, Nagoya 464-01

[‡]Institute for Molecular Science, Myodaiji, Okazaki 444

Since the discovery of an icosahedral phase (i-phase) in Al-Mn alloys by Shechtman *et al.* [1], there have been reported a large number of studies about the electronic properties of icosahedral materials in spite of remaining the arrangement of the atoms in an i-phase unclear. By intuition the pseudogap structure can be interpreted in terms of the nearly-free-electron-like energy gap inferred from the strong diffraction spots, which may be related to the stability of the i-phase. Friedel pointed out the possibility that the pseudogap structure can be enhanced by a crossing effect of 3d state with the nearly-free-electron-like state, and the stability would be augmented in an i-phase system containing transition metals by the crossing effect at about E_F which enhances the energy gap of the Brillouin zone. Recently a pseudogap-like anomaly in the DOS structure near E_F was directly confirmed with the photoemission study of an Al-Cu-Fe i-phase by Mori *et al.* [2]. The CIS spectra, being a kind of photoemission study, at the binding energy region between 0 – 2 eV show a resonant characteristic near the 3p-electron excitation of Fe atom in the Al-Cu-Fe i-phase.

The purpose is to observe the resonant photoemission study to search the Mn 3d emission and discuss about the role of the Mn 3d states on the stability of the i-phase. The sample – an Al-Pd-Mn i-phase quasicrystal – was an ingot prepared by the same method in ref. [3]. It was confirmed that the specimen used with this study consists of only *a usually-reported F-type i-phase* but does not contain the other phases. Photoemission studies were performed with an angle-resolved spectrometer on beamline BL-8B2. All measurements were carried out at room temperature. The clean surface of the specimen was obtained by scraping with a diamond file in a vacuum of $2 - 4 \times 10^{-8}$ Pa. Immediately after this process, the sample was transferred to the UPS experimental chamber and measured in a vacuum of $0.5 - 2 \times 10^{-8}$ Pa. A spectral dependence of incident radiation was determined from a photoelectric yield spectrum of gold.

The line shape of overall observed spectrum is like a single large peak on a plateau cut off at E_F shown in Fig. 1. The large peak observed at 4.3 eV below E_F seems to originate mainly from 4d state of Pd atoms. We could not find out the clear peak of Mn 3d states in spite of this sample contained of 10 at.% Mn. We have tried about the resonant photoemission of the Mn 3d emission in the Al-Pd-Mn i-phase. A poor change in the EDC of the Al-Pd-Mn i-phase could be observed for the incident photon energy near the 3p-excitation threshold energy of 47 eV for Mn shown in Fig. 1. But the energy position of Mn 3d band may nevertheless be estimated by using such a resonant

photoemission study. The CIS spectra were measured at room temperature as shown in Figure 2. The CIS spectra A, B, C and D do not show a remarkable resonance effect. But a weak resonant phenomena is observed in the spectrum E at the energy region of the Mn 3p-3d core excitation. Only the electron state near E_F can be assigned to be the states hybridized with the Mn 3d orbitals which contains appreciable amounts of Mn 3d electrons. As the result, the Mn 3d band seems to be located near E_F. The CIS intensity depends on the incident photon energy severely and the resonance effect at the Mn core excitation energy is little. One reason of such a weak resonance effect is because the sample has a considerable amount of Pd atoms having more electrons. The other may be that Mn core excitation energy is widely distributed from site to site. The binding energy at maximum of Mn 3d DOS seems to be at E_F.

[1] Shechtman D., Blech I., Gratias D. and Cahn J. W., 1984, *Phys. Rev. Lett.*, **53**, 1951

[2] Mori M., Matsuo S., Ishimasa T., Matsuura T., Kamiya K., Inokuchi H. and Matsukawa T., 1991, *J. Phys.: Condens. Matter*, **3**, 767 *ibid.*, 1992, *J. Phys.: Condens. Matter*, **4**, L157

[3] Ishimasa T. and Mori M., 1992, *Phil. Mag.*, **B18**, L175

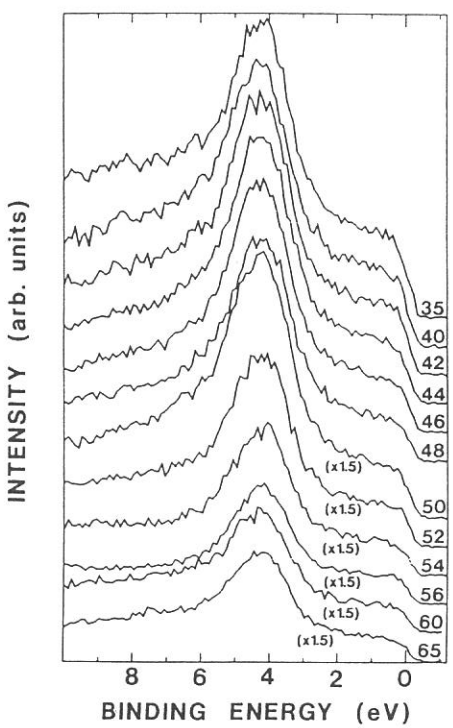

Fig. 1. Photoemission spectra of Al-Pd-Mn i-phase measured at room temperature for several incident photon energies, the values of which are shown in eV on each spectrum. Intensity of the spectrum is scaled up by 1.5 for the incident photon energy above 50 eV.

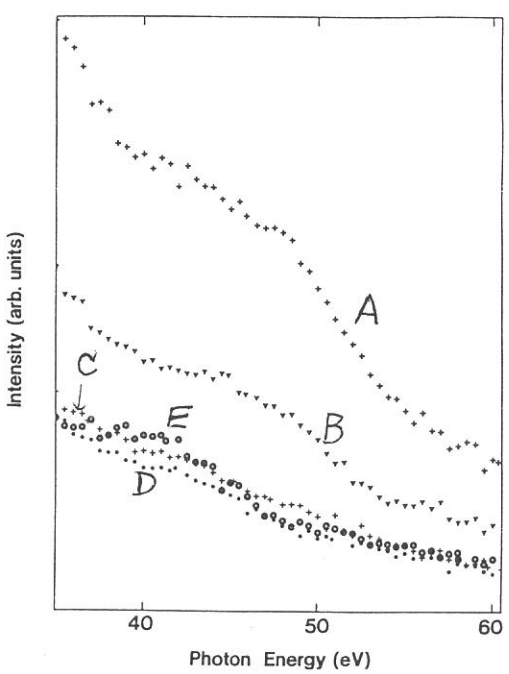

Fig. 2. CIS spectra of Al-Pd-Mn i-phase at room temperature for several binding energies. A, B, C, D and E corresponds to the spectrum at the binding energies 4.1 eV, 3.1 eV, 2.1 eV, 1.1 eV and 0.1 eV, respectively.

Large Anisotropy of Electronic Structure due to BiO Superstructure in $Bi_2Sr_2CaCu_2O_8$ Studied by Angle-Resolved Photoemission

T. Yokoya and T. Takahashi
Department of Physics, Tohoku University, Sendai 980

1. Introduction

It is well known that Bi-system oxide superconductors such as $Bi_2Sr_2CaCu_2O_8$ (Bi2212) have an incommensurate superstructure in the BiO plane in the crystal. Although a several angle-resolved photoemission studies on Bi2212 have been performed so far, a possible effect of the BiO superstructure has been overlooked. The electronic structure along the two directions, *a*- and *b*-axes, in the crystal structure (ΓX and ΓY directions in the Brillouin zone, respectively) has been regarded as the same, although the BiO superstructure runs along only the b-axis. We report a careful angle-resolved photoemission spectroscopy to study the difference in the electronic structure due to the BiO superstructure in Bi2212 superconductor.

2. Experimental

A Bi2212 single crystal of 5x5x0.2 mm^3 was prepared by a floating-zone method. Its sigle-crystalinity was checked by x-ray diffraction and the resistivity measurement showed that it becomes superconductive at 85 K.

Photoemission measurement was performed with an angle-resolved photo-

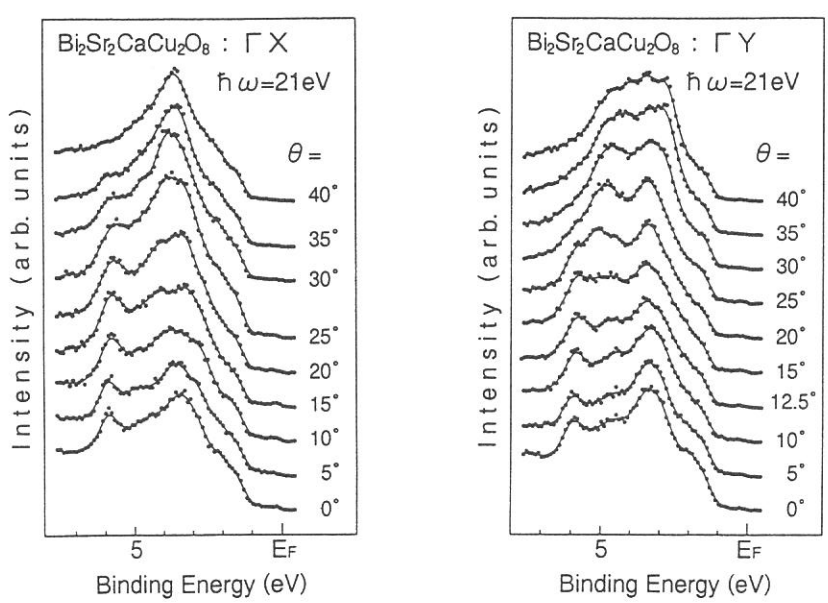

Figure 1 Angle-resolved photoemission spectra of $Bi_2Sr_2CaCu_2O_8$ measured along the *a*- and *b*-axes in the crystal (ΓX and ΓY directions in the Brillouin zone, respectively).

electron spectrometer at BL8B2. Its energy and angular resolutions were about 0.2 eV and 2°, respectively. A clean surface of the crystal for measurement was obtained by *in-situ* cleaving. The Fermi level of the sample was referenced to that of a gold film deposited on the sample.

3. Results and discussion

Figure 1 shows angle-resolved photoemission spectra of Bi2212 single crystal measured along the two high symmetry directions, ΓX (*a*-axis) and ΓY (*b*-axis) in the crystal. We find that a substantial difference arises when we go to higher polar angles while the spectra look similar in the low polar angle region. Figure 2 shows the spectra in the vicinity of the Fermi level. We find in the ΓX direction that a dispersive band approaches the Fermi level with the polar angles and finally crosses it around 15°, while in the ΓY direction along which the incommensurate BiO superstructure runs, we cannot observe such a remarkable change of the spectrum with the angle. The observed insensitivity of the spectrum against the polar angle in the ΓY direction would be due to the band-folding caused by the BiO superstructure. Thus, a remarkable difference is recognized between the two directions. This indicates that the effect due to the BiO superstructure should be properly considered when we discuss the electronic structure of the Bi-system superconductors.

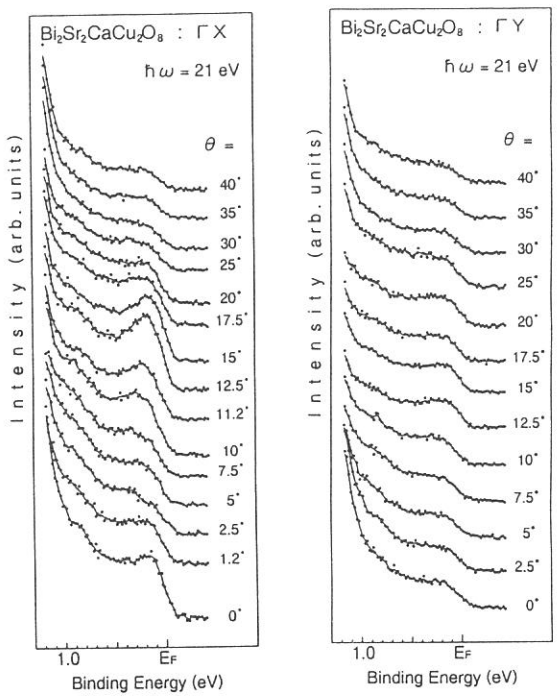

Figure 2 Angle-resolved photoemission spectra of Bi2Sr2CaCu2O8 in the vicinity of the Fermi level measured along the *a*- and *b*-axes in the crystal (ΓX and ΓY directions in the Brillouin zone, respectively).

Acknowledgment - We thank T. Mochiku and K. Kadowaki, National Research Institute for Metals, for supplying a high quality Bi2212 single crystal.

Electron Transfer in Metallofullerene Observed by Ultraviolet Photoelectron spectra [1]

Shojun HINO, Kentaro IWASAKI, Hiroaki TAKAHASHI,

Department of Image Science, Chiba University, Inage-ku, Chiba 263 Japan

Koichi KIKUCHI and Yohji ACHIBA

Faculty of Science, Tokyo Metropolitan University, Hachioji Tokyo 192-03 Japan.

There have been a controversy [2-5] whether metal atoms in so-called metallofullerene are actually inside the carbon cage or not. An ESR measurement on LaC_x [2] indicates - 3 oxidation state of the carbon cage and an XPS result of LaC_x [3] indicates + 3 oxidation state of the La atom. They suggest that the metal atom is inside the cage. However, EXAFS studies [4,5] show different coordination numbers of the metal atom, which could be a counter evidence of an encapsulation of the metal atom. The investigation of the electronic structure gives a clew of the actual position of the metal atom in the metallofullerene molecules.

Ultraviolet photoelectron spectra (UPS) of metallofullerene, LaC_{82} are shown in Fig.1. The intensity of the spectral bands, particularly the first and second bands, change upon varying the incident photon energy as have been observed in the spectra of other fullerenes. This means that metallofullerene acts as the other empty fullerenes.

The spectra resemble those of empty fullerene ,C_{82}. Figure 2 shows the UPS of LaC_{82} and C_{82}. However, a comparison of the UPS reveals a formation of new electronic states in LaC_{82} in the vicinity of the Fermi level (E_F) as is shown in an insert of Fig.2. The new states locates at 0.9 and 1.6 eV below the E_F with the intensity ratio of 1 : 2. Their origin is the transfer of three electrons from La to C_{82} to form the electronic structure of $La^{+3}C_{82}^{-3}$. Present result combined with theoretical calculations on the position of the La atom in the molecule asserts an encapsulation of the La atom inside the carbon cage. As the second lowest unoccupied molecular orbital of C_{82} is half filled, LaC_{82} is expected to behave as a metal. LaC_{82} is, however, found to be semiconductive, since there is a clear gap between its UPS onset and the E_F. This indicates the existence of a molecular aggregation to stabilize the total electronic energy of solid LaC_{82}.

References
1. S. Hino *et al.* Phys Rev. Letters, in press.
2. R. D. Johnson *et al.*, Nature **355**, 239 (1992).
3. J. H. Weaver *et al.*, Chem. Phys. Letters **190**, 460 (1992).
4. L. Soderholm *et al.*, J. Phys. Chem. **96**, 7153 (1992).
5. Y. Tomioka et al., C60 Symposium, Hachioji, August 1993.

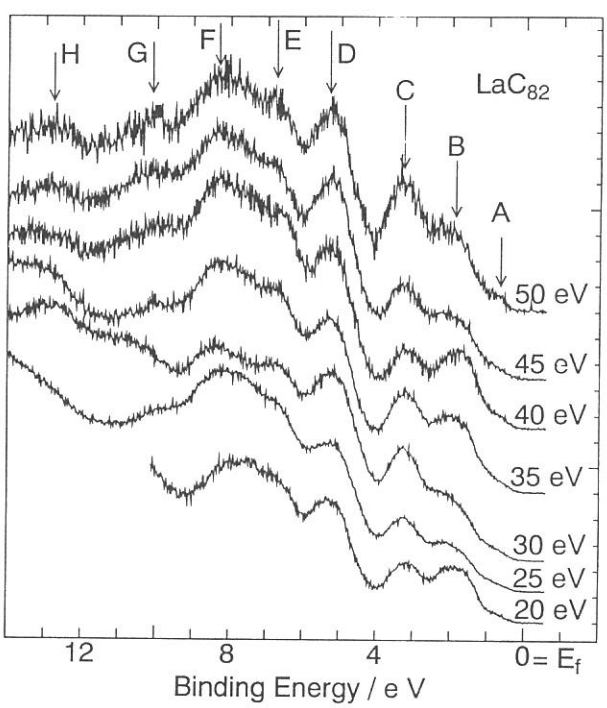

Fig. 1 Photon energy dependence of metallofullerene, LaC_{82}.

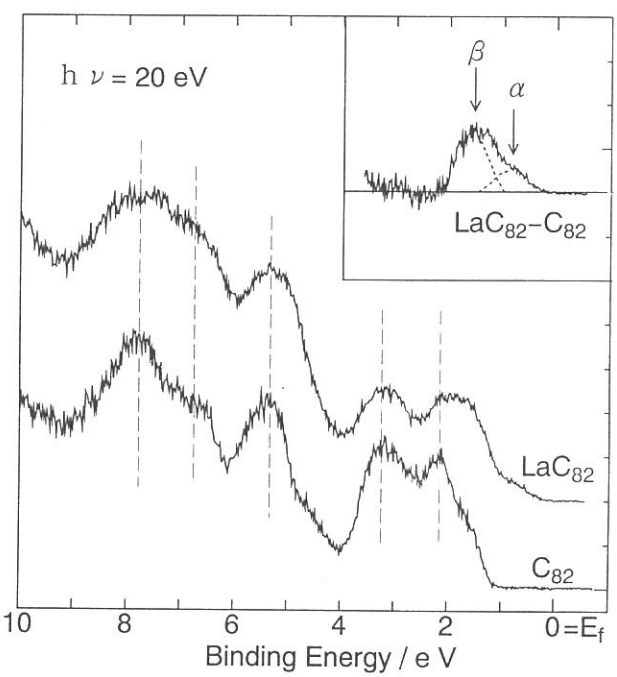

Fig. 2 Comparison of the UPS of LaC_{82} and empty fullerene, C_{82}.

Photoemission Study on the Electronic Structure of Porphyrins

H. Ishii, S. Narioka, D. Yamamoto, M. Sei, Y. Ouchi, K. Seki, T. Miyazaki[a)],
S. Hasegawa[a)], Y. Harima[b)], and K. Yamashita[b)]
Department of Chemistry, Faculty of Science, Nagoya University, Furo-cho, Chikusa-ku, Nagoya 464-01
a) *Institute for Molecular Science, Okazaki 444*
b)*Department of Environmental Science, Faculty of Integrated Arts and Sciences, Hiroshima University, Kagamiyama, Higashihiroshima 724*

Porphyrin has been the subject of considerable interest because of their unique properties as organic semiconductors. Recently the conductive property of 5, 10, 15, 20-tetraphenylporphyrin was found to change between n-type and p-type by substituting four phenyl groups and central metal [1]. But the mechanism of the change of conductive type is not well understood. In this study, we investigated the electronic strucure of three porphyrins 5, 10, 15, 20-zinctetraphenylporphyrin (ZnTPP,p-type), 5, 10, 15, 20-tetraphenyl porphyrin (H_2TPP,p-type), 5, 10, 15, 20-tetra(4-pyridyl)porphyrin (H_2T(4-Py)P, n-type) by ultraviolet photoelectron spectroscopy (UPS). Their molecular structures are shown in figure 1. The change of the electronic structure by air-dosing was also discussed.

UPS spectra were measured with angle-resolving UPS system at the beamline 8B2 of UVSOR with plane-grating monochromator. The substrate was vacuum evaporated Ag film on molybdenum plate. Porphyrin thin films (28nm thick) were prepared by vacuum deposition on the substrate. The incident angle of photon ($h\nu$=40 eV) was 50° and electrons were detected in normal emission.

In figure 2, the spectra of ZnTPP, H_2TPP, and H_2T(4-Py)P prepared and measured under ultrahigh vacuum are shown on binding energy scale relative to vacuum level. These spectra can be explained by superposition of the density of states (DOS) of porphine and the substituents [2].

In the case of inorganic semiconductors, p-type (n-type) semiconductor has its Fermi level below (above) the midgap. In order to investigate whether the same relation holds in the case of porphyrin, we discuss the energy separation between HOMO and Fermi level. In figure 3, the spectra in the HOMO region of fig.2 are shown on binding energy scale relative to the Fermi level of Ag substrate in figure 3. The energy position and lineshape of the HOMOs of the three porphyrins are similar. The energy difference among the HOMOs were within 0.2 eV. Since the HOMOs of the porphyrins are assigned to π orbital which is distributed over the macrocycle, this results indicates that the change of substituent does not significantly affect the electronic structure of the macrocycle.

Figure 4 shows the spectra of porphyrin films exposed to air (1 atm, 1 hr) before UPS measurement. Air exposure treatment did not change the lineshape of the spectra, but caused shift of HOMO peaks to the Fermi level. The binding energy of HOMO increases in the order of ZnTPP, H_2TPP, H_2T(4-Py)P. The conductive types of the porphyrins

have been estimated to be strong p-type, weak p-type, n-type for ZnTPP, H_2TPP and H_2T(4-Py)P, respectively [1]. This is consistent with the order of the HOMO's binding energy if the position of the Fermi level in the band gap is determined by the same mechanism as in inorganic semiconductors. These results suggest that oxygen molecules mixed in films serve as acceptor which leads to the shift of the Fermi level and that the conductive character is dependent on the sensitivity of each compound to air.

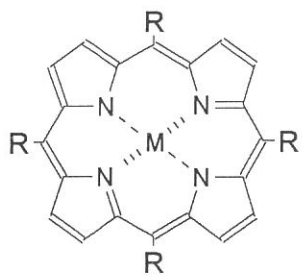

Figure 1. Molecular structure of porphyrins.
ZnTPP: M=Zn and R=C_6H_5
H_2TPP: M=H_2 and R=C_6H_5
H_2T(4-Py)P: M=H_2 and R=C_5H_5N

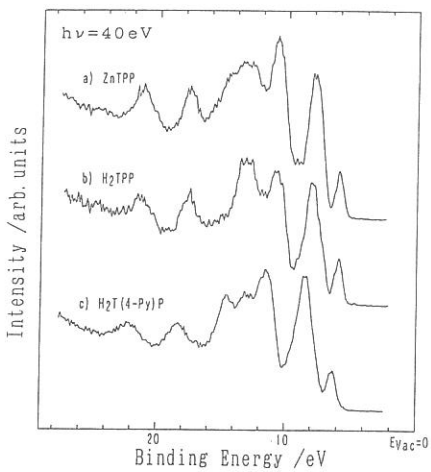

Figure 2. Ups spectra of porphyrins.
a) ZnTPP, b)H_2TPP, c)H_2T(4-Py)P

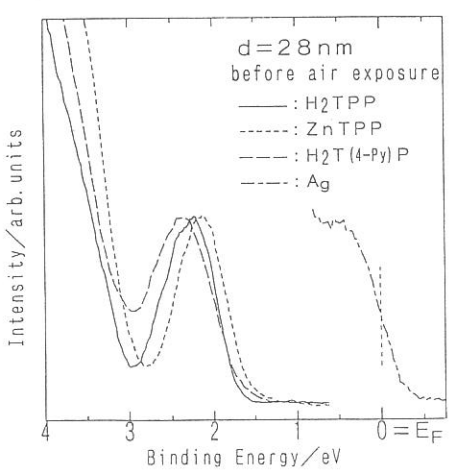

Figure 3. UPS spectra of porphyrins without air exposure in the threshold region.

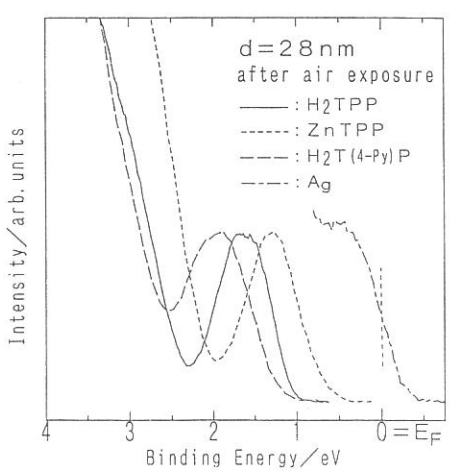

Figure 4. UPS spectra of porphyrins after air exposure in the threshold region.

References

[1] K.Yamashita, Y.Harima, and T.Matsubayashi, *J. Phys. Chem.*, 93, 5311 (1989).

[2] S.Narioka,M.Sei,H.Ishii,S.Hasegawa,Y.Ouchi,T.Ohta, and K.Seki.,
the proceedings of the 3rd IUMRS international conference on advanced materials, 1993, Tokyo.

Intermolecular energy-band dispersion in oriented thin films of bis(1,2,5-thiadiazolo)-*p*-quinobis(1,3-dithiole) (BTQBT) by angle-resolved photoemission

Shinji Hasegawa, Takehiko Mori, Kenichi Imaeda, Shoji Tanaka, Yoshiro Yamashita, Hiroo Inokuchi, Hitoshi Fujimoto[a], Kazuhiko Seki[b], Nobuo Ueno[c]

Institute for Molecular Science [a]Department of Environmental Science, Kumamoto University [b]Department of Chemistry, Nagoya University [c]Department of Materials Science, Chiba University

The energy-band dispersion relation, $E = E(k)$, is a fundamental basis for understanding the basic properties of solids. Angle-resolved ultraviolet photoemission spectroscopy (ARUPS) using synchrotron radiation is a powerful technique for directly measuring the valence band dispersion, and is well established for inorganic solids [1]. For organic solids, however, a few experiments have been reported during the past 10 years [2, 3]. Recently, we succeeded in preparing well oriented thin films of BTQBT by vacuum evaporation on cleaved HOPG graphite, and observed the energy-band dispersion of π-bands for the highest (HOMO) and next highest(NHOMO) bands. This is the first observation of intermolecular dispersion in a single-component organic molecular crystal. The results demonstrate that the BTQBT molecules have a strong intermolecular interaction.

The ARUPS measurements were carried out at BL8B2 of Ultraviolet synchrotron orbital radiation facility (UVSOR) in the Institute for Molecular Science. BTQBT was purified and carefully evaporated on HOPG substrate in vacuum of $\simeq 10^{-10}$ Torr. The film thickness was $\simeq 30$ Å. The incident photon energy ($h\nu$) dependence was measured at an electron take-off angle $\theta = 0°$ and a photon incidence angle of $\alpha = 50°$. The photon energy was changed in the region from $h\nu = 12$ to 60 eV.

As shown in Fig. 1, the BTQBT molecules in a single crystal form a two-dimensional network by the short S$\cdots$S contact of 3.26Å. The network sheets are stacked with a small spacing of 3.45Å to form molecular columns. In the thin films, the network sheets were deduced to lie parallel to the HOPG surface by the take-off angle dependence of photoelectron spectra [4].

Figure 2 shows an example of the $h\nu$ dependence of photoelectron spectra for the oriented thin films of BTQBT. The HOMO band and NHOMO band are well separated from other valence bands. For the HOMO band, the continuous change of peak position with $h\nu$ is clearly seen. The total energy shift in the peak position is about 0.5 eV. Although it is only $\simeq 0.1$ eV for the NHOMO band, we can still see that the peak shifts in the opposite direction to the HOMO band.

The energy-band dispersion for the HOMO band is determined by a least-squares fit of the experimental results supposing that it can be expressed by a simple tight-binding model. In Fig. 3, the results are shown in the reduced zone scheme. The filled circles are the experimental results, and the solid line at the HOMO band represents the best fit dispersion curve by a least-squares fit. We could estimate the inner potential for final states $V_0 = -12.5$ eV, the lattice spacing normal to the film surface $a_\perp = 3.4$Å and, the transfer integral for the HOMO band $t_{\mathrm{HOMO}} = 0.092$ eV.

References

[1] F. J. Himpsel, Adv. Phys., **32**, 1 (1983).

[2] K. Seki, U. O. Karlsson, R. Engelhardt and E. E. Koch, Chem. Phys. Lett., **103**, 343 (1984). N. Ueno, W. Gaedeke, E. E. Koch, R. Engelhardt, R. Dudde, L. Laxhuber and H. Moehwald, J. Mol. Electron, **1**, 19 (1985).

[3] D. Schmeißer, W. Jaegermann, Ch. Pettenkofer, H. Wachtel, A. Jimenez-Gonzales, J. U. von Schütz, H. C. Wolf, P. Erk, H. Meixner and S. Hünig, Solid State Commun., **81**, 827 (1992).

[4] S. Hasegawa, S. Tanaka, Y. Yamashita, H. Inokuchi, H. Fujimoto, K. Kamiya, K. Seki and N. Ueno, Phys. Rev. B, **48**, 2596 (1993).

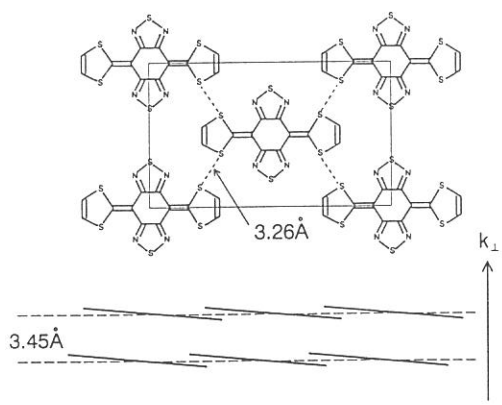

Fig. 1 BTQBT molecules in single crystal. In the present experiment, the energy-band dispersion was observed along $k_\perp$.

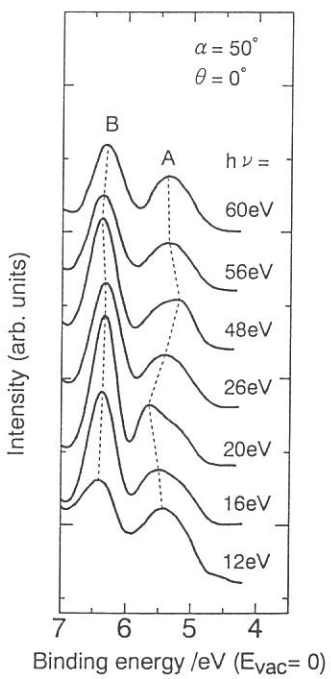

Fig. 2 Photon energy dependence of photoelectron spectra at normal emission for BTQBT thin films.

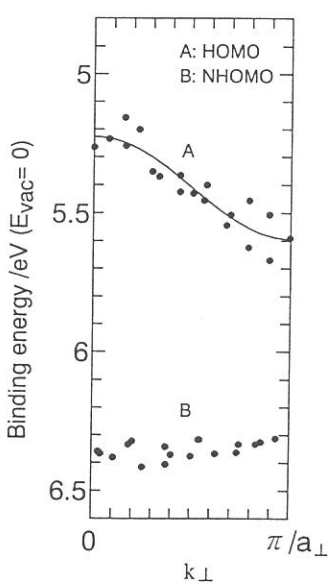

Fig. 3 Intermolecular energy-band dispersion for BTQBT thin films in the reduced zone scheme, where $a_\perp$ is 3.4Å.

Quantitative Analysis of Photoelectron Angular Distribution from Thin Films of Copper Phthalocyanine on MoS_2 surfaces: Determination of Molecular Orientation

Koji KAMIYA, Masahiro MOMOSE, Nobuo UENO
Faculty of Engineering, Chiba University, Yayoi-cho, Inage-ku, Chiba 263

Shinji HASEGAWA and Hiroo INOKUCHI
Institute for Molecular Science, Okazaki 444

Kazuhiko SEKI
Faculty of Science, Nagoya University, Chikusa-ku, Nagoya 464

The angular distribution of photoelectrons from thin films of organic crystals involves information on the molecular orientation in the film as well as on the wave functions of valence electron. Therefore, the quantitative analysis of the photoelectron angular distribution from a valence state gives a detailed information on the molecular orientation in ultrathin films of functional organic molecule. An advantage of the angle-resolved ultraviolet photoelectron spectroscopy (ARUPS) in determining the molecular orientation is that it introduces less radiation damages into the organic films in comparison with other surface sensitive techniques which use electron beams. However, the quantitative analysis of the angular distribution from thin films of large organic molecules is usually difficult, and no one has performed the quantitative analysis after a challenging work by Permien *et al.* [1], which was reanalyzed by Richardson [2], on thin films of lead phthalocyanine. Recently, we have found that the angular distributions calculated with the independent atomic center approximation combined with molecular orbital calculation (IAC/MO) agree excellently with observed ones for thin films of BTQBT [3] and metal-free phthalocyanine (H_2Pc) [4] on MoS_2 surfaces.

In the present study, we measured angular dependence of photoelectrons from HOMO orbital of Cu-phthalocyanine (CuPc) thin films deposited on MoS_2 surface, and determined the molecular orientation by the quanitative analysis of the observed angular distributions using IAC/MO method. For the calculation of the photoelectron angular distribution we used the wave function of HOMO orbital of H_2Pc [4] for the HOMO state of CuPc. The molecular azimuthal angle ϕ_s, which used in the calculation of ϕ_s dependence of the photoelectron intensity, is shown in Fig. 1.

The experiments were performed at beam line BL8B2. The incident photon energy (hv) was 40 eV and the incident angle of photons (α) was 0°(normal incidence). In the present measurements, the momentum vector of photoelectrons and the electric vector of incident photons were on the same plane perpendicular to the sample surface. The experimental azimuthal angle ϕ was the angle between the electric vector and $[11\bar{2}0]$ direction of MoS_2 surface which was determined by LEED measurements before CuPc deposition.

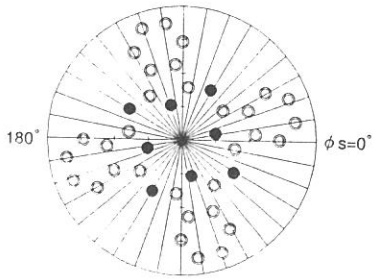

Fig. 1 Molecular azimuthal angle ϕ_s. CuPc structure is shown by carbon (○) and nitrogen (●) atoms.

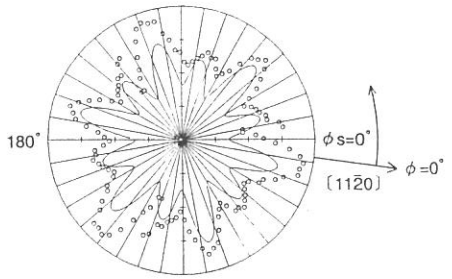

Fig. 2 Comparison between the observed (o) and calculated (–) ϕ dependencies of ARUPS intensity of the HOMO band of thin films (6A) of CuPc on MoS_2. The origin of the experimental azimuthal angle ϕ is at [11$\bar{2}$0] direction of MoS_2 surface. ϕ_s is the molecular azimuthal angle (see Fig. 1) used in the calculation. The calculated results are for flat-lie orientation of CuPc and after averaging the effects of the three-directional molecular orientation.

The ϕ dependence of the HOMO-band intensity at the take-off-angle θ=36°is shown in Fig.2. The measurements were performed for ϕ=15–135° due to the limitation of azimuthal rotation of the sample manipulator. In the figure, the observed results are plotted for ϕ=15–375° assuming the relation expected for thin films deposited on MoS_2 surface, $\phi=\phi+120°=\phi+240°$ [5], since MoS_2 surface structure shows 6-hold symmetry around the surface normal. The calculated ϕ_s dependence for flat-lie molecular orientation was compared with observed results by changing azimuthal CuPc orientation on MoS_2. The best agreement between the observed and calculated results was obtained as compared in Fig. 2. The molecular orientation thus determined is shown in Fig.3. The present results show excellent agreement with those proposed by Hara *et al.* from RHEED experiments [5].

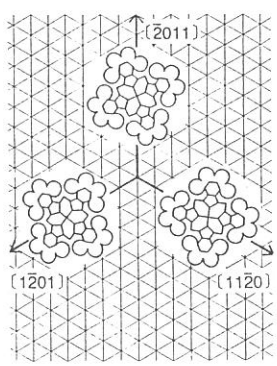

Fig. 3 Orientation of CuPc on MoS_2 surface determined by the present work. Three directional orientation is shown schematically.

From the above results, it is concluded that (i) IAC-MO method is useful in simulating the photoelectron angular distribution, and (ii) CuPc molecules orient with the molecular plane parallel to the substrate surface and with azimuthal orientation shown in Fig. 3.

References

[1] T. Permien, R. Engelhardt, C. A. Feldmann and E. E. Koch, Chem. Phys. Lett. **98** 527 (1983).
[2] N. V. Richardson, Chem. Phys. Lett. **102** 390 (1983).
[3] S. Hasegawa, S. Tanaka, Y. Yamashita, H. Inokuchi, H. Fujimoto, K. Kamiya, K. Seki and N. Ueno, Phys. Rev. B**48** 2596 (1993).
[4] N. Ueno, K. Suzuki, S Hasegawa, K. Kamiya, K. Seki and H. Inokuchi, J. Chem. Phys. 99 7169 (1993).
[5] M. Hara, H. Sasabe, A. Yamada and A. F. Garito, Jpn. J. Appl. Phys. **28** L306 (1989).

ORIENTATION OF ORGANIC MOLECULE ON LITHIUM THIN FILM SURFACE

Masaya KAWASE, Yoshiharu UCHIMOTO*, Shunsuke NAKANISHI and Hiroshi ITOH

Faculty of Education, Kagawa University, Saiwai-cho, Takamatsu 760
**Faculty of Engineering, Kyoto University, Yoshida, Sakyou-ku, Kyoto 606*

All solid type lithium batteries have been attracting much attentions as a new type secondary batteries. In studies on an exploitation of all solid type lithium batteries, a reaction between lithium electrode surface and polymer electrolyte is one of the most important subject. IR spectroscopy and XPS studies suggested that ether polymer electrolyte reacted lithium, resulted in forming C-O-Li bond on lithium surface. An orientation of the products, however, which remarkably influences a batteries' function, is not clear, yet. We studied this subject, the orientation of the reaction products, by using UPS and report our results here.

The UP spectra were measured at BL-8B2 in UVSOR under following conditions; exciting photon energy 40 to 50 eV, $\alpha = 50^{o}$, $\theta = 0^{o}$ at room temperature. Li was evaporated on Mo substrate, thereafter, reacted with chemically synthesized $C_{16}H_{33}O\text{-}C_2H_4\text{-}OC_{16}H_{33}$, which was evaporated into the pre-chamber of BL-8B2.

Generally, ether polymer is employed as a solid electrolyte in all solid type lithium batteries. In this study, reaction of Li thin film with $C_{16}H_{33}O\text{-}C_2H_4\text{-}OC_{16}H_{33}$ was employed as model reaction on Li electrode surface in all solid type lithium batteries. $C_{16}H_{33}O$-Li and ethene was formed as reaction products (Eq. 1).

$$C_{16}H_{33}O\text{-}C_2H_4\text{-}OC_{16}H_{33} + Li \rightarrow 2C_{16}H_{33}O\text{-}Li + CH_2{=}CH_2 \quad \text{(Eq. 1)}$$

Figure 1 shows the UP spectra of $C_{16}H_{33}O$-Li on Mo. Peak 1 did not shift by the exciting photon energy, while peak 2 showed the exciting photon energy dependence in the range from 40 to 50 eV. Moreover, a signal intensity ratio of peak 2 to peak 1 also clearly showed the exciting photon energy dependence in this energy range. These results suggest that the reaction product, $C_{16}H_{33}O$-Li, is oriented on Li electrode as illustrated in

Fig.2. The angle (θ) dependent UP spectra must be measured in order to obtain the more details on the orientation of the reaction products on Li electrode. We will also investigated about this point to clarify the cause of deterioration of lithium batteries and to improve them.

The results obtained here are present an important information for the exploitation of the novel type secondary lithium batteries.

We thank Dr. Kamada (UVSOR), Dr. Hasegawa (IMS) and Prof. Seki (Nagoya Univ.), for their help in promoting this study.

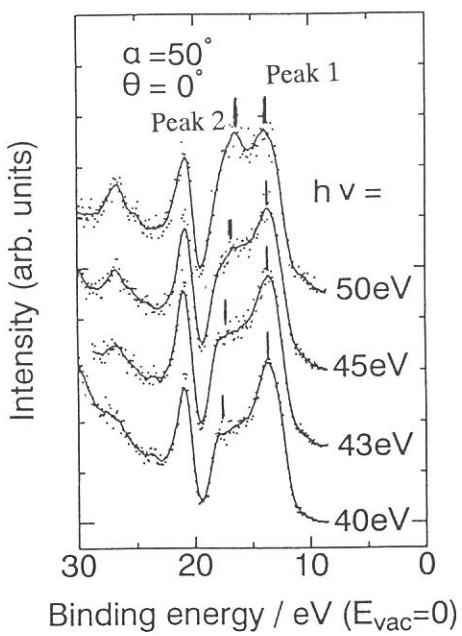

Fig. 1 Exciting photon energy dependent UP spectra of $C_{16}H_{33}O$-Li on Mo

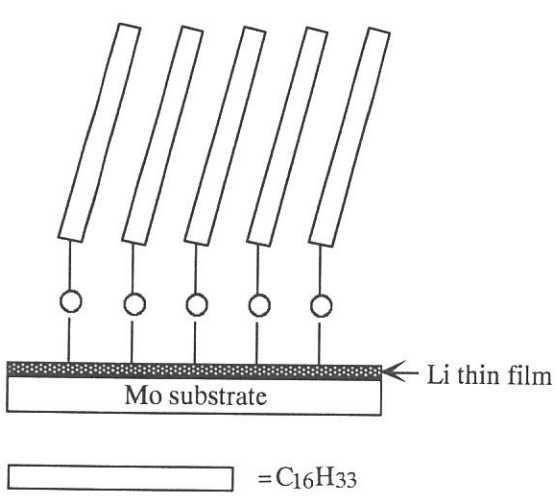

Fig. 2 Schematic model of the orientation of reaction products on Li film

FAR INFRARED ABSORPTION OF ICE UNDER PRESSURE

M. KOBAYASHI, D. TAZAWA, T. NANBA* and M. KAMADA†

Faculty of Engineering Science, Osaka University, Toyonaka, Osaka 560
*Department of Science, Kobe University, Rokkodai, Kobe 657
† Institute for Molecular Science, Myodaiji, Okazaki 444

Recently we observed far infrared absorption spectra of ice VII and VIII for the first time by using a diamond anvil cell and the synchrotron radiation [1]. Large spectral change with respect to the lattice mode was elucidated by means of the far infrared absorption. Such change could not been observed in Raman spectra [2]. There appears an intense absorption designated as band A for ice VII in wavenumbers between 80 and 160 cm^{-1} which correspond to a transparent region for ice VIII as shown in Fig. 1 of ref. [1]. Since ice VII takes a proton disordered structure, light absorption due to acoustic phonon modes becomes allowed. Theoretical prediction by Whalley and Bertie says that the absorption coefficient α should be proportional to ν^2 multiplying the density of states for phonon $D(\nu)$ [3]. In the low frequency limit, since D is proportional to ν^2, α is expected to be proportional to ν^4. In Fig. 1 we plot the absorption spectrum at the low energy side of band A in ice VII on logarithmic scales. The least square fitting by a straight line gives a relation; $\alpha \propto \nu^{4.7}$. The deviation of the index from 4 could be attributed to an increased index of the phonon density of states than 2.

Kolesnikov et al. reported inelastic incoherent neutron scattering (IINS) spectra for D_2O ice VIII at 25 K and ambient pressure [4]. They found three peaks at 117, 160 and 206 cm^{-1} corresponding to peaks in the density of states for phonon in the translational region. The peak of our B band in D_2O ice VIII is found to locate at 165 cm^{-1} when extraporated to zero pressure and 25 K. Therefore the band B corresponds to the 160 cm^{-1} peak in IINS spectrum which was attributed to the optic mode [4]. The peak of A band in D_2O ice VII is found to locate at 105 cm^{-1} when extraporated to zero pressure and 25 K. This is very near to the first peak in IINS spectrum which was interpreted as the peak of density of states in the acoustic branch [4]. This confirms the validity of our interpretation regarding the origin of band B in ice VII.

Figure 2 shows far infrared absorption spectrum of liquid H_2O (solid line) at room temperature at 0.3 GPa and one obtained at 100 K and 0.3 GPa (broken line). It should be noted that the spectrum taken at 100 K shows an increased absorption than that of liquid H_2O. Usually, liquid H_2O transforms

to ice I_h phase with decreasing temperature at 0.3 GPa. The spatial fluctuation with respect to the molecular orientations decreases in I_h compared with liquid phase. Therefore, I_h should show a weaker far infrared absorption than the liquid. The experimental result, however, contradicts this description as long as we assign I_h phase to the broken line in Fig. 2. One possible solution for this is that super cooled water transformed directly into an amorphous phase without passing I_h phase and the broken line is identified to an absorption spectrum of the amorphous ice. Kanno et al. reported [5] that the homogeneous nucleation temperature T_H of H_2O reaches -92 ℃ at 0.2 GPa. On the other hand, the glass transition temperature Tg of H_2O is known to be -138 ℃ at ambient pressure [6]. If T_H becomes lower than T_g by some reasons in our experimental conditons, the phase transition from liquid to amorphous phase might occur.

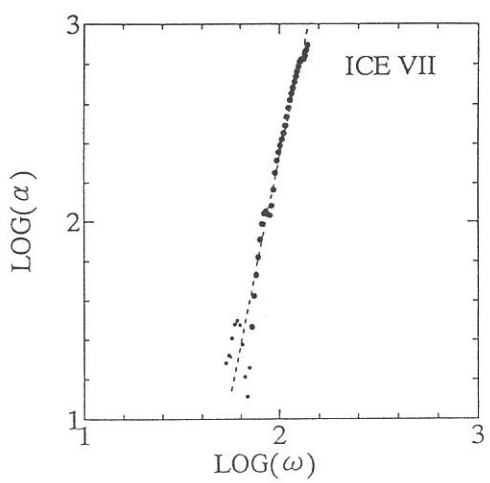

Fig.1 Far-infrared absorption spectra of band A in D_2O ice Ⅶ at 4.3 GPa and 270 K on logarithmic scales.

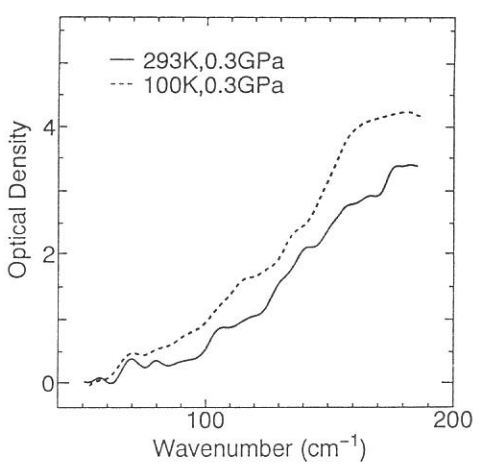

Fig.2 Far infrared absorption spectrum of liquid H_2O (solid line) and one at 100 K (dotted) at 0.3 GPa.

REFERENCES

[1]M.Kobayashi, T.Nakai, T.Nanba and M.Kamada, UVSOR Activity Rep. (1992) 150.

[2]P.T.T.Wong and E.Whalley, J. Chem. Phys. 64 (1976) 2359.

[3]E.Whalley and J.E.Bertie, J. Chem. Phys. 46 (1967) 1264.

[4]A.I.Kolesnikov et al., Phys. Lett. A168 (1992) 308.

[5]H.Kanno, R.J.Speedy and C.A.Angel, Science 189 (1975) 880.

[6]M.Sugisaki, H.Suga and S.Seki, Bull. Chem. Soc. Jpn. 41 (1968) 2591.

Far Infrared Absorption of SmTe Single Crystal

Takao NANBA,Shin-ichi KIMURA[1],Yong Seung KWON[2]
and
Takashi SUZUKI[3]

Department of Physics, Kobe University, Kobe 657
1 UVSOR Facility, Institute for Molecular Science, Okazaki 444
2 Department of Physics, Sung Kyun Kwan University, Suwon, Korea
3 Department of Physics, Tohoku University, Sendai 980

Transmission and reflection spectrum of single crystalline SmTe in the far infrared region were measured at 10, 80 and 300 K. SmTe has been known to be insulator at normal pressure and to show gradually metallic properties with pressure. According to the electric resistivity measurement of SmTe, the electric resistivity decreases gradually with pressure and at pressure of 4 GPa the magnitude becomes smaller by the magnitude of 4 order of that at normal pressure. The magnitude is comparable with that of normal metals. In SmTe, that is, a metal-insulator (M-I) transition occurs gradually with pressure in contrast with SmS. Our final interest is to make clear the origin of such M-I transition by the observation of the change of the optical spectrum with pressure. The present purpose of the experiment is to observe the far infrared spectrum of SmTe at normnal pressure.

The obtained reflection (a) and transmission (b) spectra of SmTe at the temperatures of 300, 80 and 10 K are shown in the figure. The reststrahlen band which is peculiar to insulating materials was observed clearly.

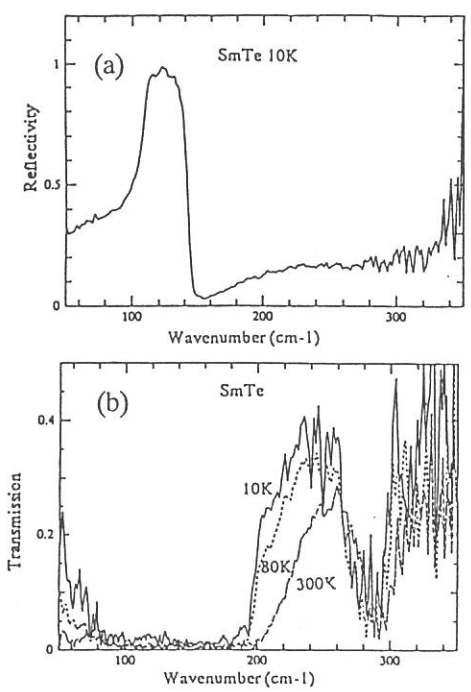

Figure
The reflection (a) and transmission (b) spectra of SmTe single crystal at 300, 80,10 K. The spectral resolution was 1 cm^{-1}.

FAR-INFRARED AND MILLIMETER WAVE SPECTRA OF ALKALI CUPROUS HALIDES

Teruyoshi AWANO, Takao NANBA*
Department of Applied Physics, Tohoku Gakuin University, Tagajo 985
*Department of Physics, Kobe University, Kobe 657

Alkali cuprous halides consist of alkali halides and cuprous halides. Ionic bond between alkali and halogen atom and covalent bond between copper and halogen atom coexist in these crystals[1]. It is interesting to investigate optical phonon structure in these crystals. Some of these crystals show superionic conductivity. We have studied far-infrared and millimeter wave spectra of silver and copper ion conductors[2]. In this study, three intermediate compounds of Rb-Cu-X system, $Rb_4Cu_{16}Cl_{13}I_7$(σ = 0.34 Scm^{-1} at 300 K), $Rb_3Cu_7Cl_{10}$ ($\sigma = 3\times10^{-3}$ Scm^{-1} at 300 K) and $Rb_9Cu_{16}Cl_{25}$ ($\sigma = 10^{-6}$ Scm^{-1} at 300 K) were investigated.

Fig. 1 shows reflectivity spectra of these crystals at 300 K. Low energy tail below 30 cm^{-1} increased in proportion to their ionic conductivity. This is due to Drude like behavior of copper ions as discussed about $Rb_4Cu_{16}Cl_{13}I_7$ in ref. 2. The damping is so large in $Rb_3Cu_7Cl_{10}$ that the ionic plasmon model is hardly appropriate.

Fig. 2 shows conductivity spectra at 15 K. Main peaks were observed at 33, 44, 68, 80, 97, 110 and 124 cm^{-1} in $Rb_4Cu_{16}Cl_{13}I_7$ and 32, 73, 108, 126 and 165 cm^{-1} in $Rb_3Cu_7Cl_{10}$ and 34, 51, 73 94, 104 and 123 cm^{-1} in $Rb_9Cu_{16}Cl_{25}$. The bands around 30 cm^{-1} are due to attempt mode of a cuprous ion in a cage of tetrahedron of halogen ions. The bands around 120 cm^{-1} are due to breathing mode of them. These phonon structures are shifted toward high frequency according to the difference of mass of conduction ion from silver ion conductors.

1) R.W.G.Wyckoff, *Crystal structures* (Interscience Publishers, New York, 1968) vol.4, p.457.
2) T. Awano, T. Nanba and M. Ikezawa, Solid State Ionics, **53-56** (1992)1269.

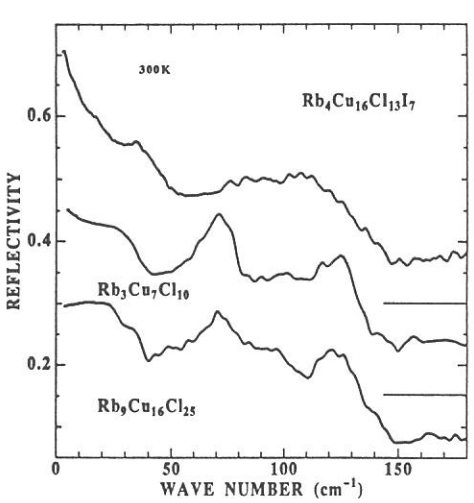

Fig. 1 Reflectivity Spectra of Alkali Cuprous Halides

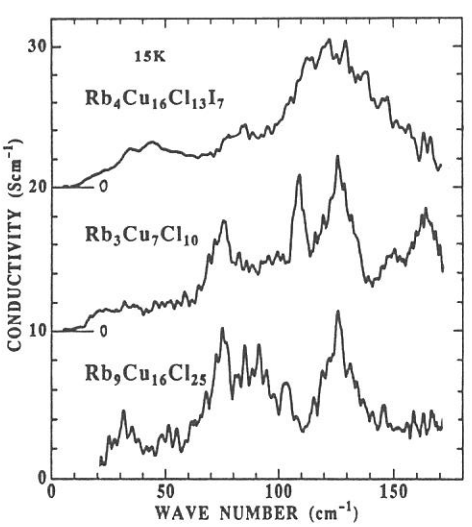

Fig. 2 Conductivity Spectra of Alkali Cuprous Halides

Far infrared reflectivity spectra for $La_{1-x}Sr_xMnO_3$

T. Katsufuji, Y. Okimoto, T. Arima, and Y. Tokura
Dept. of Phys, Univ. of Tokyo

Since the discovery of high-T_c cuprate superconductors, transition metal oxides have been attracting considerable interest as strongly correlated electron systems. Among these oxides, $La_{1-x}Sr_xMnO_3$ system is characterized by the ferromagnetic property in the metallic state [1] (known as a "double exchange" system [2]). To understand the electronic origin, not only magnetic measurements but also investigation of the electronic state with strong Coulomb correlation is needed. Optical measurement over a wide range of energy scale is very informative for this purpose. In this study, as one part of optical studies of this system, far infrared reflectivity spectra were measured by using BL6A1 of UVSOR with varying Sr (doping) concentration x and temperature.

Samples investigated in this study are melt grown crystals by the floating-zone method. Fig.1 shows the temperature dependence of the resistivity for these samples. Samples for $x = 0$ ($LaMnO_3$) and $x = 0.05$ show the insulating behavior of a typical activation type. The magnitude of the resistivity decreases with doping concentration x, and the resistivity for $x \geq 0.1$ samples has quite anomalous temperature dependence. According to the magnetization measurements of these samples, those for $x \geq 0.1$ show ferromagnetism at low temperature, and the Curie temperature of each sample is shown by arrows in Fig.1. The anomaly in the temperature dependence of the resistivity well coincides with the Curie temperature, indicating that the magnetic property and the conduction property are closely correlated in this system.

Fig.2 shows the reflectivity spectra below $300cm^{-1}$ at room temperature. The value of reflectivity increases over the whole energy region investigated here with x, which indicates increase of Drude part. Such x-dependent reflectivity spectra are related to the conduction property of this system; i.e., it becomes conductive with doping. Fig.3 (a) and (b) show the temperature dependence of reflectivity spectra for $x = 0.15$ and $x = 0.20$, respectively. As can be seen, there is quite a large difference in the temeprature dependence of the reflectivity spectra between these two samples. For $x = 0.15$, the value of reflectivity largely increases between 250K and 220K, and keeps on increasing down to 190K. Below this temperature, however, the reflectiviy rather decreases with temperature. On the contrary, the value of reflectivity for $x = 0.2$ monotonously increases with decreasing temperature. Such a temperature dependence of the reflectivity for each sample is qualitatively consistent with that of the resistivity as shown in Fig.1.

In order to make quantitative discussion, the supplemented reflectivity measurements in the energy scale sufficiently above the far infrared region as well as the Kramers-Kronig analysis of the data is required. Such an investigation is now under way.

References

[1] G. H. Jonker and J. van Santen, Physica **16**, 337 (1950).

[2] C. Zener, Phys. Rev. **82**, 403 (1951).

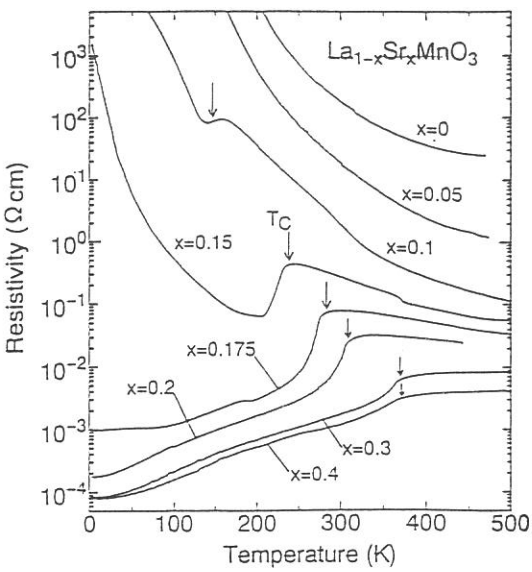

Fig.1 Temperature dependence of resistivity for $La_{1-x}Sr_xMnO_3$.

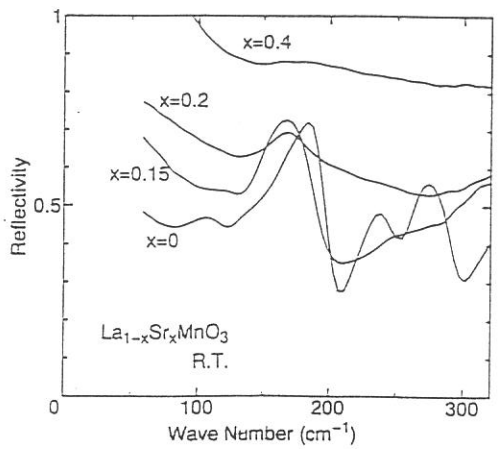

Fig.2 Doping dependence of reflectivity spectra for $La_{1-x}Sr_xMnO_3$at room temperature.

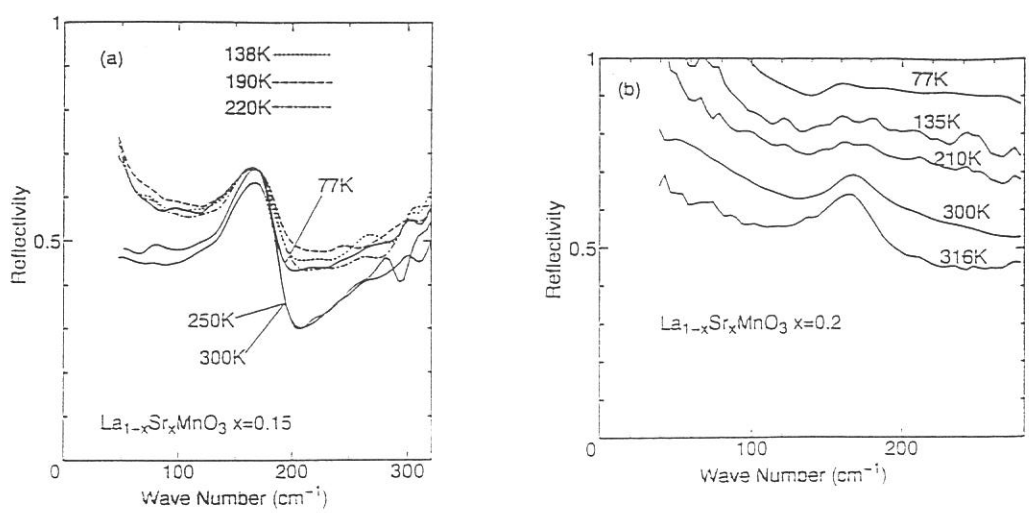

Fig.3 Temperature dependence of reflectivity spectra for (a) $x = 0.15$ and (b) $x = 0.20$.

VACUUM ULTRAVIOLET ABSORPTION SPECTRA OF POLYETHYLENE TEREPHTHALATE FILMS

Isuke OUCHI, Ikuo NAKAI, Masao Kamada* and Shin-ichiro TANAKA*

Department of Physics, Faculty of General Education, Tottori University
Koyama, Tottori 680
* Institute for Molecular Science, Myodaiji, Okazaki 444

In the previous reports[1, 2], we described preliminary results on the core electron absorption spectra of thin films of polyethylene terephthalate (PET) and polyethylene 2,6-naphthalate (PEN) by transmission mode; namely, we utilized so-called Grasshopper monochromator equipped at the BL2B1 of UVSOR facilities and measured the intensity of transmitted light through a sample in the range between 270 and 640 eV. The thickness of the samples was about 0.7 to 0.4 μm. The samples were held between a pair of copper frames and the incident angle was either normal or 25° to the film plane. Attempts to assign absorption peaks were made utilizing the published data of various carbons and carbonaceous compounds including polymers. Summary of the results is shown in the table below. However, data on the polarization were somewhat obscure, partially because some samples were possibly splitted during irradiation and also because only one oblique angle was attempted except normal incidence.

Therefore, this time, the absorption spectra by means of the total electron yield method was tried; the advantage of this method was an ease in realizing various oblique angles of incidence because of the sample holding method, while the charging up on samples was afraid. In actuality, the sample films were pasted by use of two-sided carbon adhesive tapes on a molibdenum disk, which was mounted on the holder rotatable around a vertical axis along the film plane. No bias voltage was applied on the sample.

Table I

	Assignment and polarization						
Sample	peak	sh.	peak	sh.	sh.	br.peak	br.peak
PET undrawn	285.7eV	287.8eV	289.2eV		293.5eV	297.2eV	305 eV
PET x3.5 (obliq.)	285.4		289.3		293.5	296.6	303.5
PET biax.drawn	285.6		289.1		293.5		304.7
PEN undrawn	285.8		289.3	291.4	293.6		ca.303.7
PEN x3.5 Y	285.5		289.5		294.3		
PEN x3.5(obliq.)	285.7		289.4		ca.293.5		ca.305
PEN biax.drawn	285.5	287.7	290.5		293.3		
Average	285.6	287.8	289.3	291.4	293.5	296.9	304.5
Polarization	(z)		(z)		(x,y)	(x,y)	(x,y)
Assignment	1s->π^*		1s->π^*		1s->σ^*	1s->σ^*	1s->σ^*
	C = C	C − O	C = O C − H		C − C	C − C	C − C

An example of the spectra of biaxially drawn PET film 0.7μm thick is shown in Fig. 1; namely, such spectra taken at 90°(normal incidence), 45° and 30° by means of the total electron yield method were superposed so as the absorption intensities at just below K-edge and at the plateau above 360 eV become equal for the three samples. The absorption peaks at 285.6 and also at 289.3eV increased for more tilted geometry, conforming to the fact that the molecular plane including a benzene ring is parallel to the film plane. These changes in absorption intensity were not found for the undrawn films in which the state is amorphous and the orientation is almost isotropic. The change in the absorption intensity in the region assigned to σ^* seemed somewhat different for each component; also, some difference was seen between PET and PEN, which was not so clear in the transmission mode measurements. The distribution of the direction of C-H orbitals should be responsible to the change in this range; since the energy difference between the uppermost and the lowest unoccupied π orbitals is about 4.6 eV according to the PPP calculation[3], there would not be π^* contribution in the range above 293 eV. For the oxygen core electron absorption, the main peak existed at near 537 eV. A peak at 529 eV was sensitive to the incident angle and film orientation and was conceived as originated from O 1s to π^*.

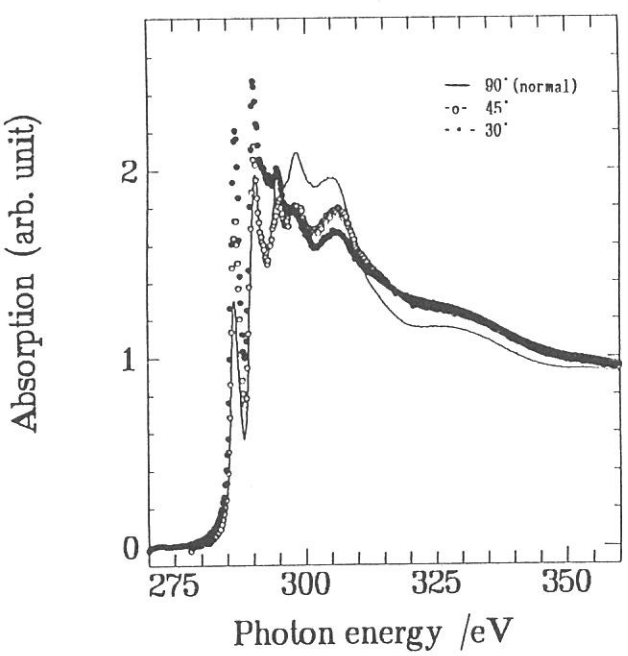

Fig. 1. Absorption spectra of a biaxially oriented PET film 0.7μm thick in the range between 270 and 360 eV.

1) I. Ouchi, I. Nakai, M. Kamada, S. Tanaka & T. Hagiwara: UVSOR Activ. Rep. (1992) 88.
2) I. Ouchi, I. Nakai, M. Kamada & S. Tanaka: Rep. Progr. Polym. Phys. Jpn. 36 (1993) 413.
3) I. Ouchi: Polym. J. 15 (1983) 225.

O K-edge XAS Study of $Sr_{1+x}La_{1-x}FeO_4$

Takahisa OMATA, Kazushige UEDA, Hideo HOSONO,
Naoyuki UEDA* and Hiroshi KAWAZOE*

Research Laboratory of Engineering Materials, Tokyo Institute of Technology, Midori-ku, Yokohama 227
**Institute for Molecular Science, Myodaiji, Okazaki 444*

$SrLaFeO_4$, isostructure with La_2CuO_4, dose not show a insulator to metal transition upon the hole doping.[1] In this report, electronic structure of hole-doped $Sr_{1+x}La_{1-x}FeO_4$ was studied by O K-edge X-ray absorption spectroscopy, and it will be concluded that the new hole states were formed around the original conduction band edge upon the doping.

The samples sintered were prepared at 1500°C for 48h in O_2 flow. O K-edge X-ray absorption measurements were performed by total photoelectron yield mode at the beam line BL2B1. The surfaces of the samples were scraped with a diamond file just before measurements to avoid the surface contamination under a vacuum of 1×10^{-9} Torr.

Fig. 1 shows the obtained O K-edge XAS spectra of $Sr_{1+x}La_{1-x}FeO_4$ ($0 \leq x \leq 0.3$). Since the energy resolution in this study was several electron volts, the spectra were broader than the reported XAS and EELS data on $(La,Sr)CuO_4$ and $(La,Sr)NiO_4$.

Before discussing the effects of the doping on the spectra, we analyze the spectrum of non-doped $SrLaFeO_4$ (x=0). Four broad features were observed in the spectrum of the non-doped $SrLaFeO_4$, marked by vertical arrows in the figure. The broad features at ~2eV and ~4eV are attributed to O 2p part of the bands, to which Fe 3d states (upper Hubbard band) also are contributing heavily. The bands are split by octahedral crystal field into t_{2g} and e_g bands. The strong feature centered around 7eV is attributed to O 2p part of the bands mainly constructed from La 5d and Sr 4d orbitals. The broad feature around 12eV may be attributed to O 2p part of the bands mixing with Fe 4s states.

Upon the doping, it is observed that the ~7eV feature for x=0 shifted toward higher energy region with increasing the doping level. This is probably caused by the energy differences between La 5d and Sr 4d orbitals.

The most remarkable change in the O K-edge XAS spectra upon the doping was an increase in the peak intensity at 2eV on going from x=0 to 0.3. The increase suggests that the new hole states, to which O 2p contributes considerably, are formed upon the doping around the conduction band edge. We also measured Fe K-edge XAS spectra on these samples.[2] The results suggested that the unoccupied Fe 3d density of states also increased upon the doping. Thus it is concluded that new hole states composed of O 2p and Fe 3d characters were formed around the original conduction band edge.

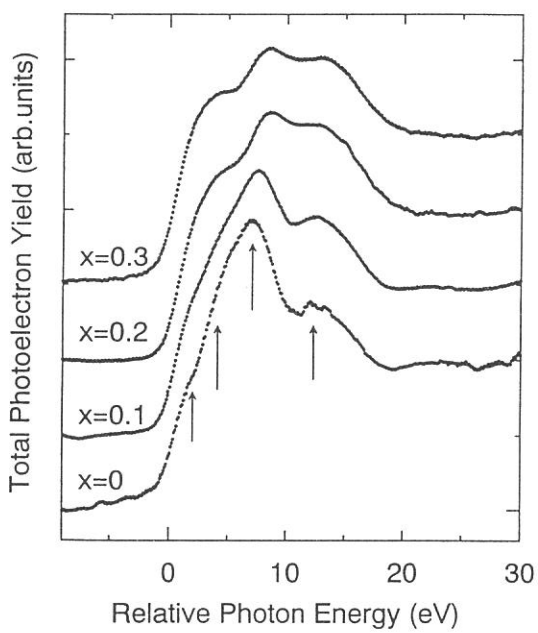

Fig. 1. O K-edge XAS spectra of $Sr_{1+x}La_{1-x}FeO_4$.

1) T.Omata, K.Ueda, H.Hosono, M.Katada, N.Ueda and H.Kawazoe, Phys. Rev. B, in press.

2) T.Omata, K.Ueda, H.Hosono, T.Miyazaki, S.Hasegawa, N.Ueda and H.Kawazoe, Phys. Rev. B, in press.

Fe $L_{2,3}$-edge XAS Study of $Sr_{1+x}La_{1-x}FeO_4$

Takahisa OMATA, Hiroshi MIZOGUCHI, Hideo HOSONO,
Naoyuki UEDA* and Hiroshi KAWAZOE*

Research Laboratory of Engineering Materials, Tokyo
Institute of Technology, Midori-ku, Yokohama 227
*Institute for Molecular Science, Myodaiji, Okazaki 444

Electrical insulator of 3d transition metallic compounds are usually classified into Mott-Hubbard type or charge-transfer type based on their electronic structure. This categorization seems to be important in order to consider changes in the electronic structure upon the carrier doping. Fe-oxides are considered to be intermediate compounds between Mott-Hubbard and charge-transfer insulators. Abbate et al. measured Fe $L_{2,3}$-edge and O K-edge X-ray absorption spectra (XAS) of $La_{1-x}Sr_xFeO_3$ with perovskite structure, suggesting that $LaFeO_3$ was of charge-transfer type insulator and new hole states mainly composed of O 2p character were formed upon the Sr doping.[1)]

We studied Fe K-edge and O K-edge XAS spectra of hole-doped $Sr_{1+x}La_{1-x}FeO_4$ with K_2NiF_4 structure, which is regarded as an intermediate compound between Mott-Hubbard and charge-transfer insulators. It is concluded that the new hole state had not only O 2p character but also Fe 3d character. In this report, unoccupied electronic states of hole-doped $Sr_{1+x}La_{1-x}FeO_4$ ($0 \leq x \leq 0.3$) was examined by Fe $L_{2,3}$-edge XAS and the unoccupied Fe 3d states increased upon the hole doping.

Sintered samples were prepared at 1500°C for 48h in an O_2 flow. Fe $L_{2,3}$-edge XAS measurements were performed by total photoelectron yield mode at the beam line BL7A, where incident photons were monochromatized with a double crystal monochromator using β-alumina ($NaAl_{11}O_{17}$, 2d=22.53Å) crystals. The energy resolution of this system was considered to be ~1.2eV in the photon energy region relevant to the present experiment. The surfaces of the samples were scraped with a diamond file just before measurements to avoid the surface contamination.

Fig. 1 shows Fe $L_{2,3}$-edge XAS spectra of $Sr_{1+x}La_{1-x}FeO_4$ ($0 \leq x \leq 0.3$). Since the energy resolution in this measurements was lower than the measurements performed by Abbate et al., the spectra obtained in this study were broader than the reported

data on $La_{1-x}Sr_xFeO_3$[1]. The weak shoulder at ~2eV and strong peak at ~4eV in the spectrum of the non-doped sample are seen (marked by vertical arrows in the figure). These two peaks attributed to Fe 3d states with t_{2g} and e_g symmetry split due to octahedral crystal field. Upon doping, the intensity of the peak centered at ~4eV corresponding to e_g symmetry increased and the shoulder at ~2eV corresponding to t_{2g} level became unclear. It is considered that these changes in the spectra are caused by the increase in the unoccupied Fe 3d states, mainly that of e_g symmetry, upon the doping. The results obtained here appear to be consistent with those obtained by Fe K-edge (Fe 1s 3d transition) XAS spectroscopy. In conclusion, we found that the new hole states formed upon the doping are composed of both Fe 3d and O 2p characters.

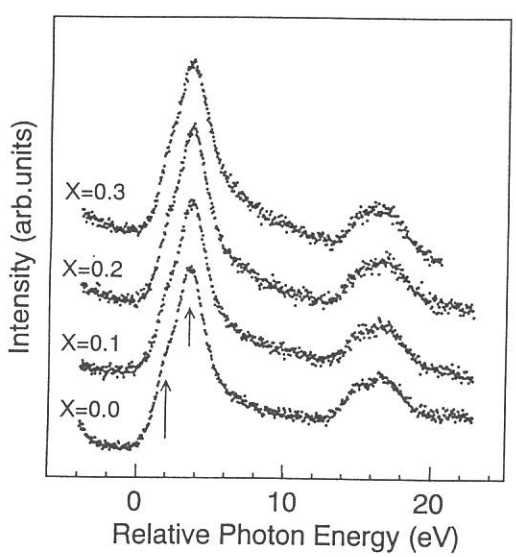

Fig. 1. Fe $L_{2,3}$-edge XAS spectra of $Sr_{1+x}La_{1-x}FeO_4$.

1) M.Abbate, F.M.F.de Groot, J.C.Fuggle, A.Fujimori, O.Strebel, F.Lopez, M.Domke, G.Kaindl, G.A.Sawatzky, M.Takano, Y.Takeda, H.Eisaki and S.Uchida, Phys. Rev. B 46, 4511(1992).
2) T.Omata, K.Ueda, H.Hosono, T.Miyazaki, S.Hasegawa, N.Ueda and H.Kawazoe, Phys. Rev. B, in press.

POLARIZED XANES STUDIES ON FLUORINATED POLYETHYLENE AND ITS MODEL COMPOUNDS

Kouhei NAGAYAMA, Ryuichi MITSUMOTO, Tohru ARAKI, Hisao ISHII, Yukio OUCHI, and Kazuhiko SEKI

Department of Chemistry, Nagoya University, Chikusa-ku, Nagoya 464

Fluorinated polyethylene and its model compounds are of great interest lately for their applications to the aligning-layers for various organic-functional molecules.[1] However, the mechanisms responsible for the alignment in relation to the mechanical rubbing process are hardly understood. In this study, we have performed a series of experiments with use of X-ray absorption near edge structure (XANES) spectroscopy in order to determine (1) the initial alignment of the fluorinated polyethylene and its model compounds and (2) the possible structure change of the polymers subjected to the mechanical rubbing process.

Samples used were tetrafluoroethylene oligomer (TFO, n≈85) and perfluorotetracosane (PFT, $C_{24}F_{50}$). F K-edge XANES spectra were measured at the beam line 1A of UVSOR at IMS. The spectra were taken for evaporated films (1000Å) in total current mode.

Figure 1 shows a typical F K-edge XANES spectrum of PFT. The first peak A was assigned as σ^* (C-F).[2] In order to determine the molecular orientation of PFT, the incident-angle-dependences of the peak(A) intensity are taken as shown in Figure 2 with theoretical fit, where we have assumed the helicoidal structure of PFT and the polarization factor of the incident beam P=1. From this analysis, we conclude that PFT chains are oriented normal to the surface.

After applying the mechanical rubbing on the evaporated PFT films, we have conducted the similar experiment to see the possible structural change of PFT. In Figure 3, the incident-angle-dependence of the peak(A) intensity are shown with theoretical fit. The definitions of the rubbing direction and the incident angle are illustrated in the inset. As is clear from the figure, the inclination of PFT chains induced by the mechanical rubbing is about 5° from the surface normal. On the contrary to the case of TFO[3], PFT film hardly changes its structure by the rubbing process. This is probably due to the fact that PFT has higher crystallinity than TFO.

References

1)J. C. Wittmann and P. Smith; Nature **352** (1991) 414

2)T. Ohta, K. Seki, T. Yokoyama, I. Morisada, and K. Edamatsu; Physica Scripta **41** (1990) 150.

3)K. Nagayama et al., to be published.

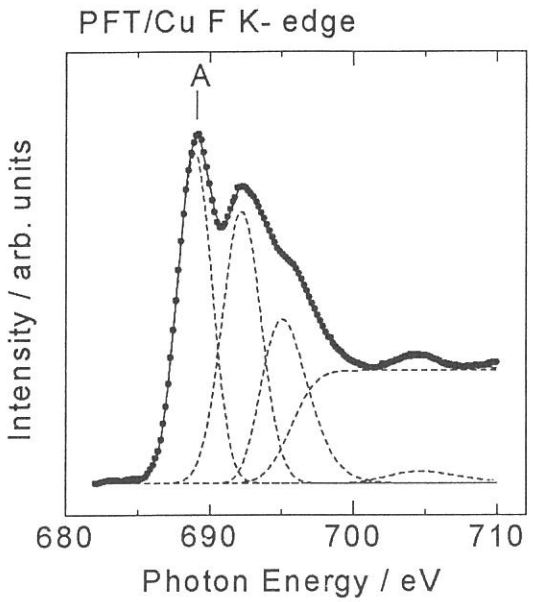

Figure 1 F K-edge XANES spectrum of PFT(filled circles,solid line) and theoretical fit (dashed line). The first peak(A) is assigned as σ^* (C-F).[2)]

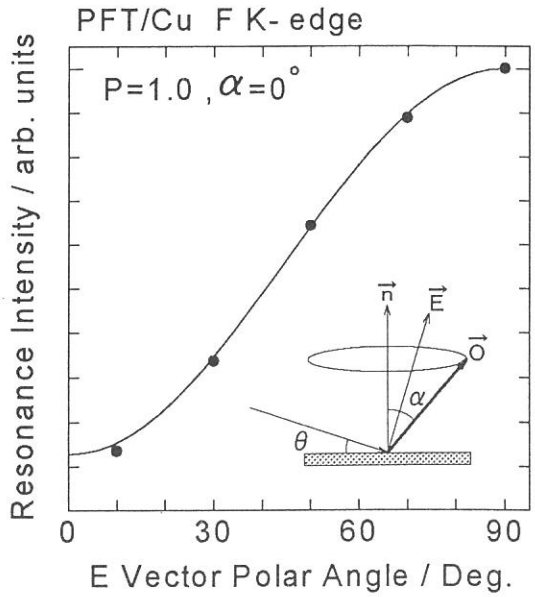

Figure 2 Incident angle dependence of the peak(A) intensity of the PFT film. The definition of the angle is illustrated in the inset. We have assumed the polarization factor P=1 and the helical structure of PFT.

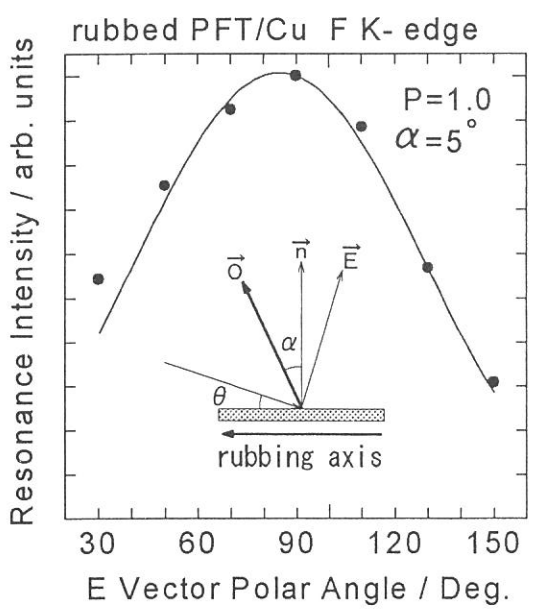

Figure 3 Incident angle dependence of the peak(A) intensity of the rubbed PFT film. The definition of the angle is illustrated in the inset.

Mg K-edge XAFS Study of Alkali-Metal Ion Loaded on MgO Catalysts

Sadao Hasegawa*, Hirofumi Aritani*, Kentaro Nakamura*, Yusuke Yoshinaga*,
and Tsunehiro Tanaka**

*Department of Chemistry, Tokyo Gakugei University, Koganei, Tokyo 184
**Division of Molecular Engineering, Kyoto University, Kyoto 606

1. Introduction

In our previous report[1], Na-doped Al_2O_3 catalyst has been exhibited a basic property. It was determined on the basis of Na K-edge XANES of sodium halides that the ionicity of Na-O bonds in that catalyst relates to the energy position of the prominent peak, which is consistent with the catalytic behavior[2]. And also, we reported previously that manganese ions interacting with sodium ions on MgO surface are present Mn^{4+} ions under an ambient condition and are converted as Mn^{2+} ions by evacuation at 773K. In this process, the Na ions on the surface play a role in electron donation though Na-O bonds[3].

It was reported that Na-evaporated MgO has super-basic sites[4]. In this report, we researched that alkali-metal ion loaded on MgO catalysts from Mg K-edge XAFS studies. We discuss the correlation of the electronic structure of the alkali-metal ion loaded on MgO with the generation of new basic sites.

2. Experimental

Magnesium oxide was prepared by evacuation of magnesium hydroxide at 873K for 3h. Alkali-metal loaded samples were prepared by impregnating magnesium oxide with the ethanol solution of $LiNO_3$, NaOEt and KNO_3, respectively (Content of alkali-metal is 2.2mmol/g) . All the catalysts were followed by drying and calcining in air at 873K for 3h. Catalytic behavior was examined by 1-butene isomerization at 323K.

The Mg K-edge absorption spectra of the catalysts were measured at BL-7A soft X-ray beam line with UVSOR facilities, when used a beryl two-crystal monochrometer.

3. Results and Discussion

Fig.1 shows the Mg K-edge XANES pattern over alkali-metal ion loaded on MgO. At 1310.1eV, a sharp absorption due to 1s-3p transition were observed. From these profiles of Mg K-edge XANES, the intensity of the Mg K-edge absorption at 1310.1eV is relatively increased with the alkali-metal ion loading, and the ratio of the intensity of broad bands at 1316.0 eV and 1318.0 eV were varied from bulk MgO. Further, in the case of Li ion-loaded MgO, the shape of X-ray absorption were similar to that of MgO at relatively higher-loading (content is 7.8mmol/g). This change was not observed over Na/MgO or K/MgO.

During the 1-butene isomerization on Na/MgO and K/MgO, the value of *cis*/*trans* isomers of produced 2-butene was increased by alkali-metal loading. The sample of Li/MgO exhibited no reactivity for 1-butene isomerization. In the study of X-ray diffraction, the samples of alkali-metal loaded on MgO only possessed the diffraction pattern due to bulk MgO, except Li/MgO. This sample has a structure which was determined to the mixture of bulk MgO and lithium hydroxide monohydrate. It is quite different from Na or K ion loaded-MgO, and no basic site was observed.

In the results of k^3-weighted Mg K-edge EXAFS (Fig.2), the radial distance were obtained at about 0.25nm over MgO and alkali-metal ion loaded on MgO. This distance is attributed to a bond length between Mg^{2+} and O^{2-} over bulk MgO. This distance corresponds with the spacing of MgO(100) plane by X-ray diffraction. On the other hand, 0.18nm of radial distance was obtained

over MgO. This distance agrees very closely with the radial distance of $Mg(OH)_2$, that was mainly observed over this sample. Therefore, the distance observed by MgO may correspond with that of remained magnesium hydroxide. In the case of alkali-metal ion loaded on MgO, the distances around 0.18nm were shortened from the result of EXAFS. Therefore, we discuss that new active sites are formed on MgO surface by alkali-metal ion which combine with hydroxyl group and/or O^{2-} as anion. Thus, alkali-metal ion linked to surface oxygen ion such as $Mg\text{-}O\text{-}Na^{+}$ activates surface oxygen ion in the case of Na or K ion loaded-MgO. Consequently, the dispersion of electric charge between Mg^{2+} and O^{2-} causes an increase of ionicity. Now, in the result of XANES pattern, the energy positions were not shift but change the relative intensities at 1310eV and others of absorption peaks by each alkali-metal ion loading. Therefore, the effect of alkali-metal loading is rather an increase of ionicity on MgO surface than the generation of partial basic sites attributed to surface OH group. From these results, activated surface oxygen ion, which was induced by alkali-metal ion, acts as basic sites.

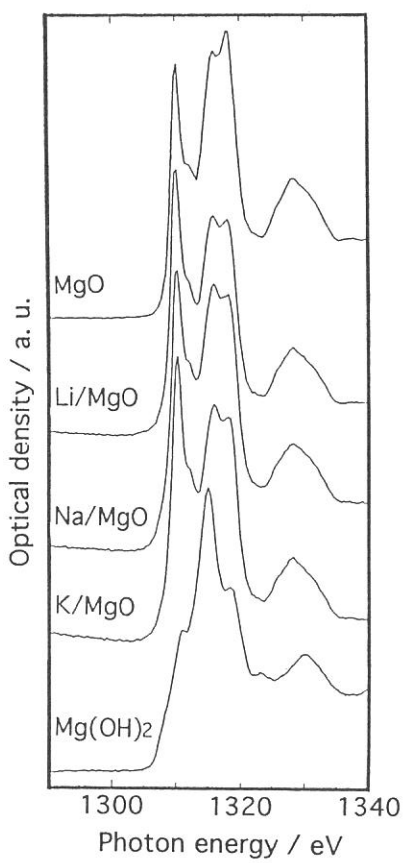

Fig. 1 Mg K-edge XANES of alkali-metal loaded on MgO

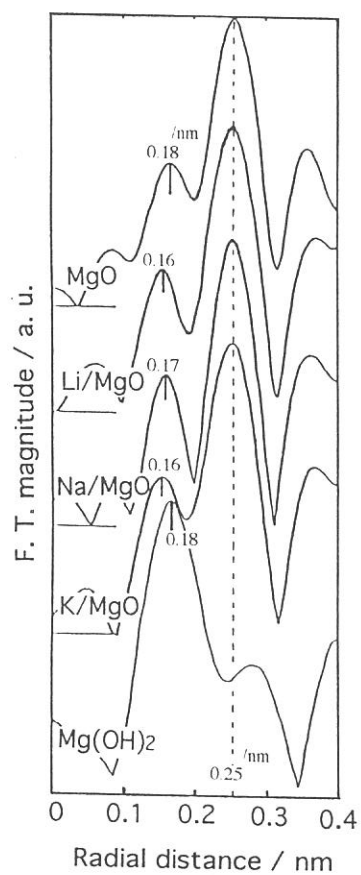

Fig. 2 F. T. of k^3-weighted EXAFS of alkali-metal loaded on MgO

References

1. N.Yoshihara, T.Kitagawa, I.Ihara, S.Hasegawa, T.Hasegawa, Bull. Chem. Soc. Jpn., 65 (1992) 1185.
2. S.Hasegawa, M.Morooka, H.Aritani, H.Yoshida, T.Tanaka, Jpn. J. Appl .Phys., Suppl.32-2 (1993) 508.
3. H.Suzuka, S.Hasegawa, T.Tanaka, G.Zhang, H.Hattori, Surf. Sci., 221 (1989) L769.
4. J.Kijenski, S.Marinowski, J. Inst. Catal. Hokkaido Univ., 28 (1980) 97.

Polarized Ni–$L_{2,3}$, P–K and S–K Absorption Spectra in $NiPS_3$

N.Kozuka, S.Nakai, K.Odagawa, K.Noguchi, T.Yokohama

Faculty of Engineering, Utsunomiya University, Utsunomiya 321

$NiPS_3$ is a 3d transition–metal compound related to the $CdCl_2$ structure. The crystal is constructed of a stack of sandwich layers each of which is weakly bonded by van der Waals forces. The magnetic and electric property indicates that this material shows antiferromagnetic property at low temperature, the Nèel temperature is 155K, and the Ni ion is present in high spin state at room temperature. We measured polarized Ni–$L_{2,3}$, P–K and S–K absorption spectra in $NiPS_3$ single crystal. The crystal–field–strength parameter 10Dq was estimated from the experimental multiplet structure by comparing the calculated spectrum.

Measurements have been performed by using synchrotron radiation at the BL–7A line of the Ultraviolet Synchrotron Radiation Facility (UV–SOR), Institute for Molecular Science. We have used a double crystal monochromator, and applied Beryl(1010) to the crystal for measurement of Ni–L absorption, and InSb(111) for P–K and S–K absorption. Absorption spectra were measured by using an electron multiplier by means of photoelectric yield from single crystal surfaces. The sample was cleaved in a vacuum by pealing off with Scotch tape along the sample surface (ab plane). The polarization dependency was measured by changing the incident angle to the sample surface from normal ($\theta = 0^\circ$) to grazing incidence ($\theta = 80^\circ$).

Ni 2p absorption spectra (XAS) of $NiPS_3$ were shown in Fig.1. The solid curve ($\theta = 0^\circ$) was taken for the polarization of electric field parallel to the ab plane(E//ab), and the dotted curve ($\theta = 80^\circ$) was taken for nearly parallel to the c–axis(E//c). These spectra were normalized at the top of the first peak. The first peak which appeared about 852.5eV corresponds to the $2p_{3/2}$ absorption peak, and the second one which appeared about 870eV corresponds to the $2p_{1/2}$ absorption peak. The peak shift is not clear at present. The structure appeared about 857eV shows a weak polarization dependency. The $L_{2,3}$ XAS spectra are interpreted in terms of multiplet structure which results from the interaction between a 2p hole and 3d electrons of metal ions [1].

We have estimated the strength of the crystal field of $MnPS_3$ and $FePS_3$ to be about 0.6eV by comparing with the theoretical spectra which calculated for these dihalides by de Groot et al.[2] In the case of $NiPS_3$, there is no data which corresponds to our experimental spectra. Then we compared with the another spectra of Ni dihalides calculated by van der Laan et al.[3] in which hybridization effect with ligand orbital was taken in account. The spectrum of NiI_2 is similar to our spectrum. In this calculation, the strength of covalency hybridization V value is 1.5eV and 10Dq value is 1.5eV. However, from the optical measurements, P.A.Joy et al. reported that all three materials ($MnPS_3$, $FePS_3$

and $NiPS_3$) indicate nearly same value of $10Dq$.[4] Recently, Kotani et al[5] calculated the spectra of Ni dihalides with cluster model in order to explain the X-ray photoemission spectra and XAS spectra using a same parameter. From the good agreement between the spectrum of $NiPS_3$ and that of $NiBr_2$, calculated by Kotani, we can estimate the crystal field strength and the covalency hybridization value V to be 0.6eV and 2eV, respectively.

P-K XAS spectra of $NiPS_3$ was shown in Fig.2(a). And S-K XAS spectra of $NiPS_3$ was shown in Fig.2(b). The solid curve represent the E//ab spectrum, and the dotted one represent the E//c spectrum. The intensity of the spectra were normalized at the first peak. Both spectra show the polarization dependency at the absorption edge. Especially the S-K XAS spectra show the dominant change. The interpretation of these polarization dependency is now in progress.

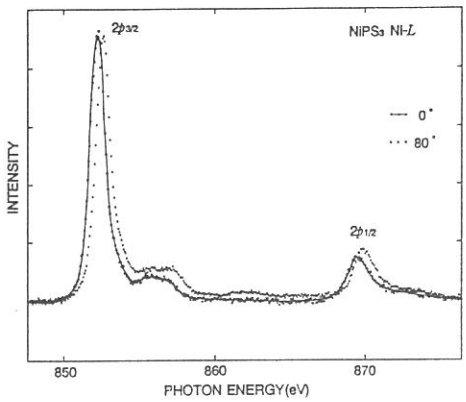

Fig.1. Ni-$L_{2,3}$ XAS spectra

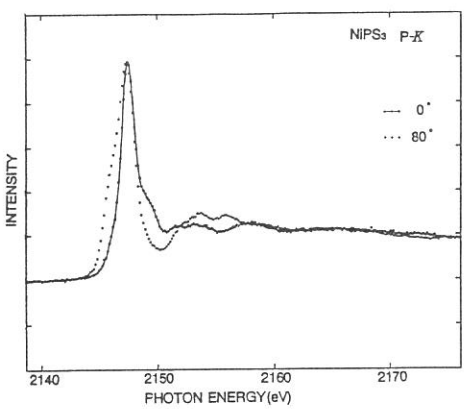

Fig.2.(a) P-K XAS spectra

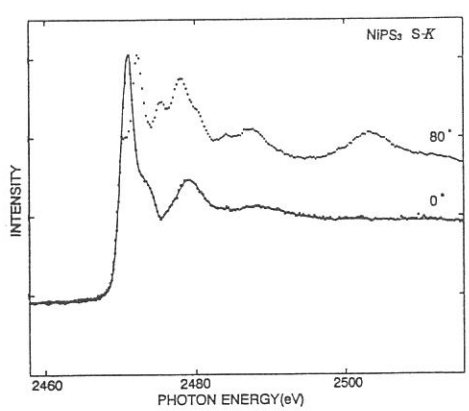

Fig.2.(b) S-K XAS spectra

References

1) S.Nakai et al., J.Phys. Soc. Jpn. 54(1985)4034
2) F.M.F.de Groot et al., Phys. Rev. B42(1990)5459
3) G.van der Laan et al., Phys.Rev. B33(1986)4253
4) P.A.Joy et al., Phys. Rev. B46(1992)5134
5) A.Kotani et al., in "Recent Advances in Magnetism of Transition Metal Compounds" (World Scientific 1992)

Study on Electronic States of Amorphous Semiconductors by Soft X-ray Core-Absorption Spectroscopy

S. Hosokawa, I. Ono, Y. Hari, T. Mihara, H. Sato, M. Taniguchi, A. Hiraya[A], M. Watanabe[A,*] and N. Kosugi[A]

Department of Materials Science, Faculty of Science, Hiroshima University, Kagamiyama 1-3, Higashi-Hiroshima, 724

[A] Institute for Molecular Science, Myodaiji, Okazaki, 444

We have already obtained the unoccupied density of states (DOS) of amorphous (a-) $GeSe_2$ by means of inverse-photoemission spectroscopy (IPES) in our laboratory. The IPES spectrum is shown at the bottom of figure 1. As seen in the figure the spectrum has three peaks as indicated by α, β and γ. The core-absorption spectra also provide information on the conduction-band DOS, including the selection rule of angular momentum on the optical transitions. By comparing IPES spectrum with core-absorption spectra, we can derive the contribution of each orbital components in conduction-band DOS [1,2].

The Ge 2s and 2p, and Se 2p core-absorption spectra were measured on BL-1A of UVSOR facilities using double Beryl monochromator. The core-absorption measurements were performed by the total electron yield mode at room

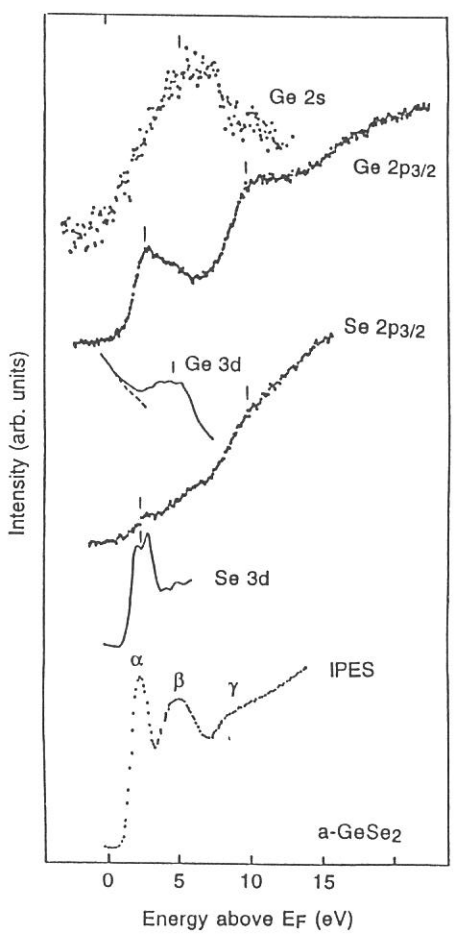

Figure 1. The core-absorption and the inverse-photoemission spectra of a-$GeSe_2$. The Ge 3d and Se 3d core-absorption spectra by Inoue et al. [3] are also shown.

*Present address : Research Institute for Scientific Measurements, Tohoku University, Aoba-ku, Sendai, 980

temperature. The sample film of a-$GeSe_2$ with thickness of 1000Å was evaporated onto a clean Au substrate in a preparation chamber that was taken into UVSOR from our laboratory. The sample was *in situ* transferred into an analyzer chamber under base pressure below 5×10^{-10} Torr.

Large solid circles in Fig. 1 show core-absorption spectra. Solid lines in the figure indicate the Ge 3d and Se 3d spectra measured by Inoue et al. [3]. The energy position of the α peak in the IPES spectrum is nearly equal to those of the first peaks in Ge $2p_{3/2}$ and Se 3d, and the first shoulder in Se $2p_{3/2}$ core spectra. The position of the β peak corresponds to those of the peaks in Ge 2s and Ge 3d, and that of the γ peak agrees with those of the second one in Ge $2p_{3/2}$ and second shoulder in Se $2p_{3/2}$ core spectra. Such characteristic features of the core-absorption spectra and the IPES spectrum suggest that the α, β and γ peaks are mainly composed of the Ge 4s and Se 4p, the Ge 4p and Se 4p, and the Ge and Se 4d and/or 5s orbitals, respectively.

We have also measured the core-absorption spectra of a-GeSe, a-GeTe, a-As_2Te_3, a-As_2Se_3, and discussed the contributions of partial DOS's in their conduction bands.

Reference

[1] S. Hosokawa, K. Nisihara, Y. Hari, M. Taniguchi, O. Matuda and K. Murase, Phys. Rev. B **47** (1993) 15509.

[2] S. Hosokawa, Y. Hari, K. Nishihara, M. Tamura and M.Taniguchi, Proc. 15th Int. Conf. on Amorphous Semiconductors, in press.

[3] K. Inoue, T. Katayama, K. Kawamoto and K. Murase, Phys. Rev. B **35** (1987) 7496.

Soft X-ray Absorption Spectra of $Cd_{1-x}Mn_xTe$ Diluted Magnetic Semiconductors

H. Sato, N. Happo, M. Taniguchi, A. Hiraya[1] and N. Kosugi[1]

Department of Materials Science, Faculty of Science, Hiroshima University, Kagamiyama 1-3, Higashi-Hiroshima 724, Japan
[1]Institute for Molecular Science, Myodaiji, Okazaki 444, Japan

$Cd_{1-x}Mn_xTe$ alloys have attracted a great deal of attention as a new class of semiconductors, since the replacement of Cd with Mn yields novel magneto-optical properties[1]. Such phenomena are derived from a hybridization of the Mn 3d states in the high spin configuration with the sp-band states of the host crystals. We have investigated the electronic structures of $Cd_{1-x}Mn_xTe$ by means of photoemission and inverse-photoemission spectroscopy, so far. In the inverse-photoemission spectra, which give information on the total density of states (DOS) in conduction-band (CB), the unoccupied Mn 3d$\downarrow$ and sp-band states have been observed as a narrow peak at 3.6 eV and a broad structure around 7 eV above the valence-band maximum, respectively[2]. In the present study, we performed the soft x-ray absorption spectroscopy experiments on $Cd_{1-x}Mn_xTe$ to separate *l* components of the unoccupied states by use of dipole-allowed transitions.

The absorption spectra were taken at BL-1A of UVSOR equipped with a double crystal monochromator. A set of β-alumina was used. Clean surfaces for the measurements were prepared by scraping with a diamond file under ultrahigh vacuum below 2×10^{-9} Torr in a preparation chamber. Then, the sample was *in situ* transferred into the analysis chamber with base pressure of 5×10^{-10} Torr. The Cd 3s, 3p, Mn 2s, 2p, Te 3s and 3p absorption spectra were recorded in total electron yield mode and normalized to the monochromator output by use of yield from Au mesh. All measurements were performed at room temperature. Bulk single crystals of CdTe and $Cd_{0.40}Mn_{0.60}Te$ were grown through a Bridgman method. We verified the samples forming homogeneous crystal phase by x-ray diffraction measurement. The Mn concentration was determined by electron-probe micro-analysis.

Because of a poor signal to noise ratio of obtained spectra, it was difficult to compare them with inverse-photoemission spectra and separate *l* components of the CB-DOS. We can, however, roughly remark the following

items on the Mn 2p absorption spectrum. The intense peak at 637 eV in the Mn 2p absorption spectrum of $Cd_{0.40}Mn_{0.60}Te$ in Fig. 1 is mainly ascribed to the dipole-allowed transitions from Mn $2p_{3/2}$ core level to the unoccupied Mn $3d\downarrow$ states. It should be noticed that the Mn $2p_{1/2}$ spectrum is significantly different from the Mn $2p_{3/2}$ one with respect to their intensity and shape, and the crystal field multiplets of the $2p^63d^5 \rightarrow 2p^53d^6$ transitions show up also in the spectra. Detailed analysis is in progress.

[1] *Dilute Magnetic Semiconductors*, Vol. 25 of Semiconductors and Semimetals, edited by J. K. Furdyna and J. Kossut (Academic, New York, 1988).

[2] M. Taniguchi, K. Mimura, H. Sato, J. Harada and Y. Ueda, unpublished.

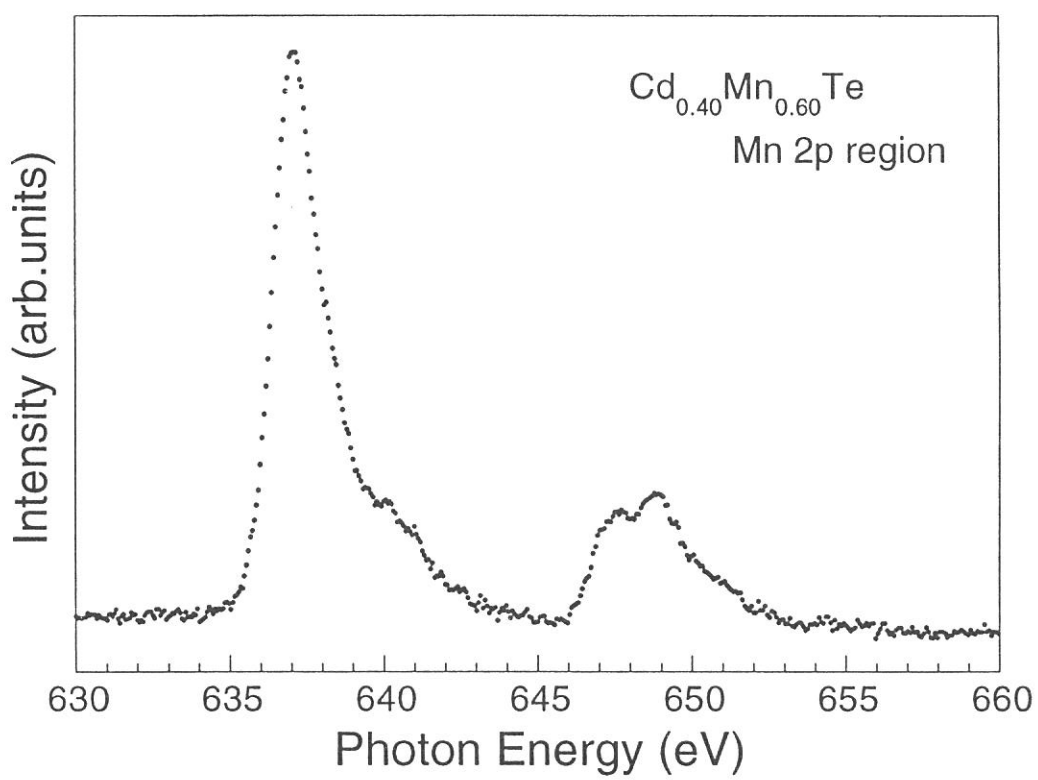

Fig. 1 Mn 2p absorption spectrum of $Cd_{0.40}Mn_{0.60}Te$. The structures around 637 and 648 eV correspond to transitions from Mn $2p_{3/2}$ and $2p_{1/2}$ initial states, respectively.

ORIGIN OF STRUCTURES IN PHOTOCONDUCTIVITY EXCITATION SPECTRA OF SUPERCRITICAL XENON DOPED WITH ANTHRACENE

Norihisa OTODA, Aiko KIMURA and Kazumichi NAKAGAWA

Division of Natural environment and Physics, Faculty of Human Development, Kobe University,Tsurukabuto, Nada-Ku, Kobe 657, Japan

Photoconductivity excitation spectra of nonpolar fluids doped with anthracene have been extensively studied with a interest on origin of structures observed in these spectra[1, 2]. Three groups (Holroyd et. al.[1], Tweeten and Lipsky[2], Nakagawa et. al[3]) have suggested their own interpretations. In this work, we have measured the photoconductivity excitation spectra with smaller increment of xenon density than previous machine time with an attempt to get a final answer.

Experiment were performed at the BL1B beam line of the UVSOR. We used a high pressure photoconductivity cell with electrode gap distance of Ø.2 mm and a MgF_2 front window. Monochromatic light with a band width of Ø.8 nm from a 1 meter Seya-Namioka monochromator was used. Density of xenon was controlled at 3ØØ K from Ø.3x1Ø^{21} cm^{-3} to 8.Øx1Ø^{21} cm^{-3} by changing the pressure.

Figure 1 shows photoconductivity excitation spectra. Peak positions of structures observed in Fig. 1 were plotted in Fig. 2 as a function of xenon density together with peak positions observed in optical absorption spectra measured at previous machine time.

We analyzed the peak shift in terms of a cluster model [4] which successfully reproduced the density dependence of ionization potential Ip,

$$E^i(N) = E^i(0) + \frac{\Delta E^i \, n_m \, N}{N_1 (n_m - 1) + N} \quad ,$$

where, $E^i(N)$ is the peak position of peak i under xenon density N, $E^i(Ø)$ is the peak position of peak i observed in gas phase, ΔE^i is shift due to association of one xenon atom to anthracene, n_m is the maximum association number, N_1 is the xenon density under which density one xenon atom associate to anthracene. In the best fit procedure, we assumed that N_1 and n_m values should be the same with the case of ionization potential; N_1=Ø.8x1Ø^{21} cm^{-3} and n_m=6. Moreover, $E^i(Ø)$ values should be equal with the absorption peaks observed for gas phase anthracene[5]. Thus ΔE^i is the only one parameter to be best fit. Curves B to G in Fig. 2 show a result of the

fitting procedure. The best fit values of ΔE^i are determined to be -Ø.Ø56, -Ø.1, -Ø.Ø97, -Ø.Ø81, -Ø.Ø96, and -Ø.Ø62 eV, for peaks B, C, D, E, F, and G, respectively.

As seen from the figure, observed peak shift seem to be well reproduced via the cluster model except for the curve C. The reason why the only bud fit was obtained for curve C is not clear at the present time.

REFERENCES [1]R.A.Holroyd et. al., J. Phys. Chem. 88(1984)278.
[2]D.W.Tweeten and S.Lipsky, J. Phys.Chem. 93(1989)2683.
[3]K.Nakagawa et. al., Chem.Phys.Lett. 155(1989)278.
[4]K. Nakagawa et. al., UVSOR Activity Report 1991, p.56.
[5]E.E.Koch et. al., Chem. Phys. Lett. 21(1973)5Ø1.

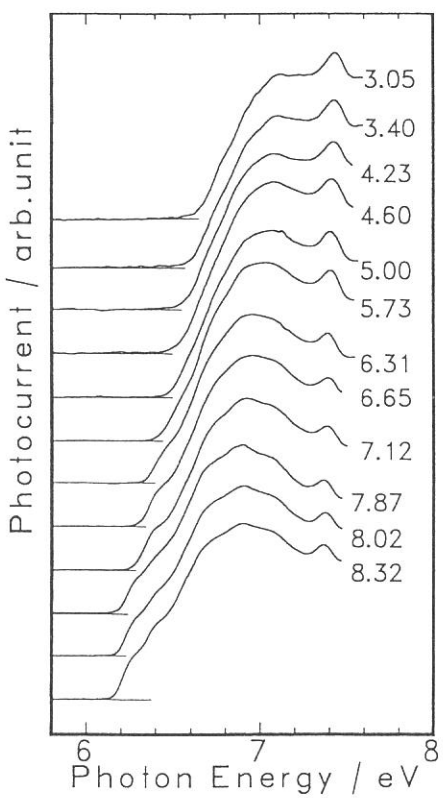

Fig. 1 Photoconductivity excitation spectra of anthracene-doped supercritical xenon fluids. Numbers near the photocurrent curves designate xenon densities in the unit of $1Ø^{21}$ cm^{-3}.

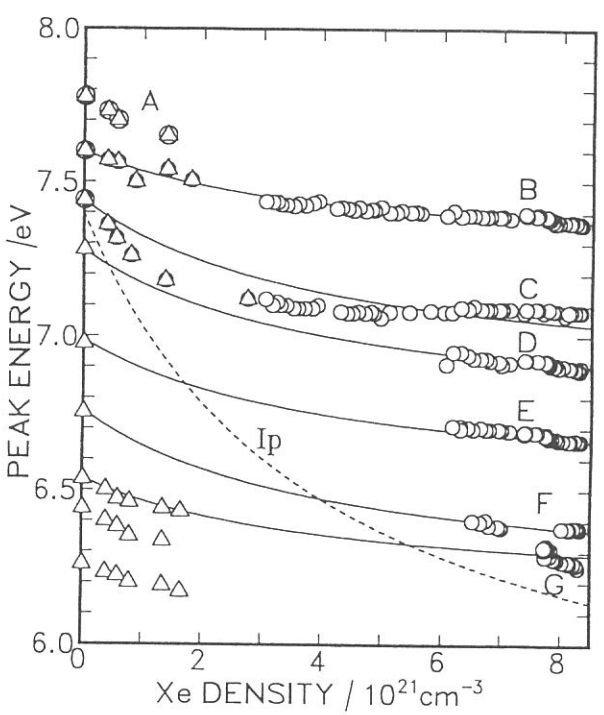

Fig. 2 Peak positions of photocurrent peaks (○) and optical absorption peaks (△) as a function of xenon density.

PHOTOIONIZATION POTENTIAL OF C_{60} DOPED IN LIQUID 2,2-DIMETHYLBUTANE

Iwao SHIMOYAMA, Norihisa OTODA, Aiko KIMURA and Kazumichi NAKAGAWA

Division of Natural environment and Physics, Faculty of Human Development, Kobe University, Tsurukabuto, Nada-Ku, Kobe 657, Japan

It was reported[1] that the magnitude of polarization energy P of C_{60} positive ion in C_{60} solid are smaller than that (typically 1.7 eV[2]) of other polycyclic aromatic hydrocarbons. The value P was estimated by the equation; $I_S=I_g+P$, where I_S (=6.17 eV[1]) is the threshold energy of photoemission of solid C_{60} and I_g (=7.6 eV[3]) is the gas phase ionization threshold energy of C_{60}. In this work, we measured photoionization potential of C_{60} doped in a typical nonpolar liquid, 2,2-dimethylbutane (22DMB), in an attempt to study the nature of polarization of C_{60} ions in nonpolar liquids.

C_{60} sample supplied by Professor Y. Achiba of Tokyo Metropolitan University was used after purification via vacuum evaporation. 22DMB from Aldlich Co. (99%) was purified by degassing at 150 K after passing a column filled with the molecular sieves 4A at 220 K which was activated at 720 K for 24 hours.

Photoconductivity measurements were performed at the BL1B beam line of the UVSOR. Monochromatic light with a band width of 0.8 nm from a 1 meter Seya-Namioka monochromator was introduced between the two electrodes. Intensities of transmitted light and photocurrent were measured and recorded simultaneously. About 17 pA of photocurrent was observed at ~180 nm. Value of photoionization quantum yield η was calculated from absorbed photon number and photocurrent values.

Value of ionization potential I_p was estimated via a semi-empirical threshold law[4], $\eta(h\nu)=B(h\nu-I_p)^{5/2}$, where, $h\nu$ is the incident photon energy, B is a constant. Figure 1 shows a plot of $\eta^{2/5}$ vs. incident photon energy. From the figure, I_p value was estimated to be ~6.53 eV. It has been well established that ionization potential I_p of aromatic hydrocarbons doped in nonpolar liquids is written with the polarization energy P of the cation and the conduction band energy V_0 of the liquid, $I_p=I_g+P+V_0$[4]. Using the experimental values of I_p=6.53 eV together with Ig=7.54 eV and V_0= -0.20 eV, we estimated the P value to be -0.94 eV. The Born formula is

known to be appropriate to reproduce P values for aromatic hydrocarbon cations in nonpolar liquid with the dielectric constant ε,

$$P = -\frac{q^2}{8\pi\varepsilon_0 R}\left(1 - \frac{1}{\varepsilon}\right) ,$$

where, q and R is the charge and radius of cation, respectively. As the ε=1.87 for 22DMB, radius R of C_{60} cation in liquid 22DMB is estimated to be 0.419 nm. This value is smaller than the van der Waals radius 0.55 nm of C_{60} molecules calculated from solid density by 24%. The same tendency is observed for the case of anthracene; cation radius R in nonpolar liquids is ~0.325 nm[5] and the van der Waals radius is ~0.38 nm, the latter is smaller than the former by 15%.

In summary, interaction between C_{60} cation and 22DMB molecule is of nearly the same nature with interaction between aromatic hydrocarbon cations and 22DMB molecules. Thus the small shift in ionization potential from C_{60} gas phase to solid phase is due to weakness of polarization effect between C_{60} cation and C_{60} molecules in solid C_{60}.

REFERENCES [1]N.Sato et. al.,Chem. Phys. Lett.162(1992)433. [2]M.Pope and C.E.Swenberg, "Electronic Precesses in Organic Crystals", Clarendon Press, New York, 1982. [3]D.L.Lichtenberger et. al.,Chem.Phys.Lett. 176 (1991) 203. [4]B.S.Yakovlev and V.Lukin, Adv. in Chem. Phys. 60(1985)99. [5]R.A.Holroyd et.al., J.Chem.Phys. 79(1983)483.

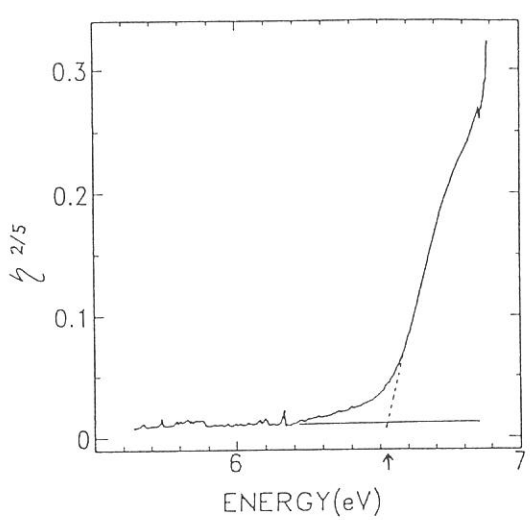

Fig. 1 Photoionization quantum yield η of C_{60} doped in liquid 2,2-dimethylbutane as a function of incident photon energy. In vertical axis, $\eta^{2/5}$ is plotted.

VUV Reflection Spectra of Densified Silica Glass

Naoyuki Kitamura, Kohei Fukumi, Kohei Kadono, Hiroshi Yamashita and Kaichi Suito[A]
Government Industrial Research Institute, Osaka
[A]Faculty of Engineering Science, Osaka University

Amorphous silica(a-SiO_2) much attracts many researchers for understanding structure and properties of amorphous materials. Densification of the a-SiO_2 is one of interesting phenomena to understand the amorphous structure. The structure of dense a-SiO_2 was studied well by the measurements of infrared(IR) absorption[1] and Raman scattering[2] spectra or neutron diffraction[3]. Influence on the electronic structure by densification was, however, little reported. Recently we[4] had suggested that band in the VUV region, which assigned by interband transitions, shift toward lower energy with increasing density. In this report, reflection spectra of dense a-SiO_2 has been measured in the VUV region. Dependence of the band seen in the spectra on density is discussed by relating to the microscopic structural deformation.

A fused silica synthesized directly by hydrogen-oxygen flame hydrolysis was used as a starting material. Densification was carried out with a 6-8 multi-anvil type high pressure apparatus. The density was measured by Archimedes' method. The vacuum ultraviolet(VUV) reflectance was measured at a beam-line BL7B of UVSOR facility. Lithium fluoride single crystal was used for relative calibration of photon energy. The measurement was performed at room temperature in the region 8-12eV with a resolution of about 0.03eV.

The reflection spectra of glasses undensified and densified by 2% and 16% at 300K are shown in Figure 1. A strong reflection band at 10.3eV and a weak band at 11.4eV are observed. Line widths of the both bands broaden with increasing density. The peak positions of the strong and the weak bands shift toward lower energy by about 0.2eV after the 16% densification.

First, the shift of both bands toward lower energy with increasing density is in agreement with the model proposed by Kitamura et al.[4]. The model was derived from an unification of the extended point dipole theory and the harmonic oscillator model. In the model, the centripetal force for the oscillators decreases with increasing density resulting in lower energy shift of their resonance frequencies because of increasing their number in an unit volume. So that a resonance energy at 10.2eV in the model, which corresponds to the strong band, shift toward lower energy. The model also predicts that the lower energy shift of the 10.2eV band is estimated by about 0.05eV after 16% densification. The estimated values is smaller than the value of the shift observed in the VUV reflection spectra. Difference between the estimated and observed values is probably due to a

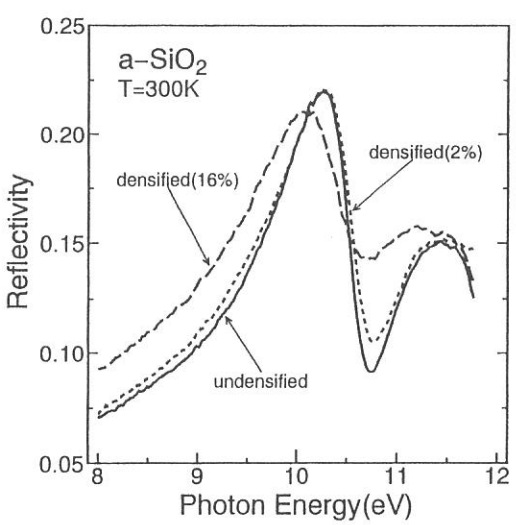

Fig.1 VUV Reflectivity for a-SiO_2 undensified and densified by 2% and 16% at 300K.

change in band gap energy, since a change in electronic structure by densification is not took into account in the model. Narrowing of the mean bond angle between SiO_4 tetrahedra(Si–O–Si) and slight elongation of Si–O bond on densification were suggested from Raman scattering spectra[5]. Xu et al[6]. pointed out no relationship between the Si–O–Si bond angle and the band gap energy on all polymorphic crystalline SiO_2, while the band gap energy widens with a increase of the Si–O bond length. Since the length increases slightly with increasing density, it is deduced that the band gap energy decreases to some extent resulting in the shift of the bands toward lower energy in the VUV region by densification. The narrowing of bond angle corresponds to increasing number of the tetrahedra in an unit volume resulting in increasing number of the harmonic oscillators. It is concluded that the decrease of the centripetal force of the harmonic oscillator and the elongation of Si–O bond length are the origin of the lower energy shift of the two bands with increasing density.

Secondly, the broadening of the strong and weak bands is probably due to an increase of randomness on a certain microscopic structure, because the band width of the a–SiO_2 in the VUV reflection spectra is wider than that of the crystalline SiO_2. In the radial distribution function obtained from the neutron diffraction measurement[3], broadening of a band attributed to the second nearest Si–O length was found with increasing density. The broadening of distribution on the second nearest Si–O length by densification suggests that the rotational arrangement between two SiO4 tetrahedra have diversity as compared with the undensified state. Although the band gap energy did not calculated elsewhere, increasing of the diversity on the rotational arrangement might be the reason of the broadening. Another possible reason of the broadening is a distortion of the SiO_4 tetrahedra. Susman et al.[3] derived broadening of the distribution for the O–Si–O bond angle along with narrowing of the distribution for the Si–O–Si bond angle by MD simulation. Since the O–Si–O bond is in the tetrahedron,the broadening suggests some increase in distortion of the tetrahedra which should correspond to the broadening of the two bands at 10.3eV and 11.4eV.

Acknowledgement

The authors wish to express their appreciation to Nippon Silica Glass Yamaguchi Company for supplying a synthetic a–SiO_2. They are also grateful to Dr. H. Onuki and Dr. K.Awazu of ElectroTechnical Laboratory in Agency of Industrial Science and Technology for helpful discussions on the measurement of the VUV reflectivity for a–SiO_2 by using synchrotron radiation lights.

References

1) J. R. Ferraro, M. H. Manghnani and A. Quattrochi: Phys. Chem. Glasses, 13(1972)116.
2) F. A. Seifert, B. O. Mysen and D. Virgo: Phys. Chem. Glasses, 24(1983)141.
3) S. Susman, K. J. Volin, D. L. Price, M. Grimsditch, J. P. Rino, R. K. Kalia, P. Vashishta, G. Gwanmesia. Y. Wang and R. C. Liebermann: Phys. Rev., B43(1991)1194.
4) N.Kitamura, S.Funo, Y.Toguchi, H.Yamashita and M.Kinoshita: J. Non–Cryst. Solids, 159(1993)241.
5) G. E. Walrafen and M. S. Hokmabadi: "*Structure and Bonding in Non–Crystalline Solids*", ed. by G. E. Walrafen and A. G. Revesz, (Plenum Press, New York, 1986), p.185.
6) Y. Xu and W. Y. Ching: Phys. Rev., B44(1991)11048.

VUV ABSORPTION SPECTRA OF THERMAL-POLED SiO_2 GLASSES WITH OPTICAL SECOND HARMONIC GENERATION ACTIVITY

Jun MATSUOKA, Hideki OKAMOTO, Hiroyuki NASU and Kanichi KAMIYA

Faculty of Engineering, Mie University, Tsu 514

Second harmonic generation (SHG) should not be theoretically observed for solids having macroscopic inversion symmetry such as glass. However, when some inversion asymmetry is introduced to these solids, induced SHG activity will occur. In 1991, Myers *et. al.*[1] reported the SHG activity in electrically polarized SiO_2 glass, and in the next year, Okada *et. al.*[2] observed SHG from corona-polarized SiO_2 glass surface. We also observed SHG from electrically polarized SiO_2 glasses and found that the SHG intensity increases with increasing the concentration of hydroxyl group in the glass[3].

Recently, we found that the SHG activity depends not only on the OH concentration but also on the preparation method of SiO_2 glass. SHG was not observed from SiO_2 glass prepared by vapor axial deposition (VAD) method though it contains relatively high amount of OH group as shown in Fig.1. SHG signal with its intensity depending on the OH concentration was observed only from glasses prepared by sol-gel method and by direct melting of quartz crystal. Furthermore, ESR measurement indicated that SHG intensity does not depend on the concentration of paramagnetic imperfection centers.

So, in this study, measurement of VUV absorption spectra of the SiO_2 glasses prepared by different methods was carried out to investigate the relation between the SHG intensity and the concentration of imperfections which have absorption bands in the VUV region.

Fig.2 shows the absorption spectra of SiO_2 glasses prepared by direct melting and by VAD, in which the former shows the SHG activity but the latter does not. These two spectra are very similar. It is reported[4] that Si-Si homobond in SiO_2 glass shows the absorption band around 7.6 eV, H_2O molecule around 7.5 eV, Si-Si-Si bond around 6.7 eV, silicon E' center (three-ford coordinated silicon radical) around 5.5 eV, silicon lone pair center (two-ford coordinated silicon) around 5.2 eV, and O_3 molecule around 4.8 eV.

However, any of these absorption bands is observed in the spectra of both glasses. Fig.3 shows the absorption spectra of sol-gel synthesized SiO_2 glasses prepared under two different conditions. One has absorption band around 6.9 eV and the other around 7.3 eV, though origin of these bands is not identified yet. Although SiO_2 glasses both prepared by melt-quenching and by sol-gel have SHG activity, their VUV absorption spectra were different to each other.

In addition, no obvious change was observed between the absorption spectra of electrically polarized and unpolarized SiO_2 glasses.

In summary, VUV absorption spectra of both SHG active and inactive silica glasses were measured, but no relation was found between the VUV absorption spectra and SHG activity.

References

1. R. A. Myers, N. Mukherjee and S. R. J. Brueck, Opt. Lett., 16 (1991), 1732
2. A. Okada, K. Ishii, K. Mito and K. Sakaki, Appl. Phys. Let., 60 (1992), 2853
3. H. Nasu, H. Okamoto, A. Mito, J. Matsuoka and K. Kamiya, Jpn. J. Appl. Phys., 32 (1993), L406
4. K. Awazu, *Bunkou-Kenkyuu*, 41 (1992), 81 [in Japanese]

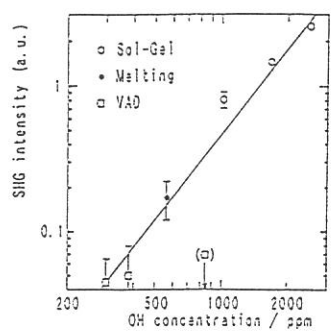

Fig.1 Relation between SHG intensity and OH content of SiO_2 glasses. Data except for that of VAD sample lies on one line.

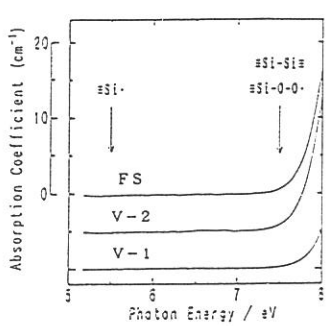

Fig.2 VUV absorption spectra of SiO_2 glasses prepared by direct melting (FS) and by VAD (V-1, V-2) methods.

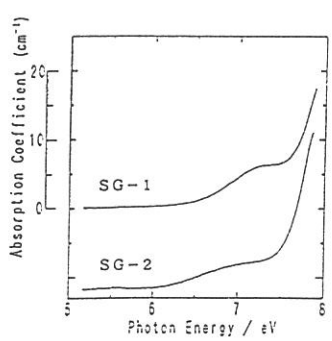

Fig.3 VUV absorption spectra of SiO_2 glasses prepared by sol-gel(SG-1, SG-2) method.

The electron affinity of CVD diamond with surface modification

Nobuhiro Eimori, Akimitsu Hatta, Toshimichi Ito and Akio Hiraki
Department of Electrical Engineering, Osaka University, Suita, Osaka 565

1 Introduction

The successes in diamond synthesis from vapor phase and substantial improvement in its quality raise the possibility of realization of diamond-based semiconductor devices with special characteristics which cannot be attained using silicon devices. Furthermore, a semiconductor diamond film has a possibility for an efficient cold cathode or photocathode due to its negative electron affinity on the (111) surface [1, 2].

In general, the negative electron affinity can be observed either for insulators, such as wide band-gap compounds, or surfaces after suitable treatments, e. g ., Cs-O-treated Si, which is chemically sensitive. Although the large photothreshold (E_{th}=5.5±0.05 eV) of diamond (111) surface precludes its use as a photocathode in the visible and near-ultraviolet light regions, it still has potentially interesting and useful photoemission properties such as high photoyield efficiency in the vacuum ultraviolet region. In case of natural diamond, it is known that the quantum yield (electrons per photon) of the (111) surface increases nearly linearly with photon energies ranging from the photothreshold (5.5 eV) to $h\nu = 9$ eV (20%), and then increases to 40%-70% throughout the energy range of $12 < h\nu < 35$ eV which is ten times larger than that of silicon.

In this study, we investigated the electron affinity of homoepitaxial single crystalline and polycrystalline diamond surfaces grown by a chemical-vapor-deposition (CVD) method Surfaces with H termination or O adsorption were examined. H-terminated surfaces were obtained for CVD diamond exposed to hydrogen plasma after the diamond growth. Some of diamond films were exposed to hydrogen and oxygen plasma for 10 s to obtain the O-adsorbed surface. The resistance of O adsorbed specimen is higher than that of H-terminated specimen.

2 Experimental

Diamond films were synthesized by means of a microwave plasma CVD on diamond (111) and p^+-Si (100) substrates. The process parameters used were as follows: substrate temperature of 900 °C (as monitored by an optical pyrometer), 40 Torr in pressure, 10% CO and 90% H_2 gas, and gas flow rate of 100 sccm. A dilute B_2H_6 gas was used for boron doping in order to prevent the specimens from charging during electron spectroscopic measurements.

Photoyield measurements were carried out using synchrotron radiation from the 750-MeV storage ring of the Institute for Molecular Science. Specimens were biased to -240V so as to collect emitted electrons. A LiF filter was used to eliminate higher-order lights of $h\nu > 11.6$ eV.

3 Results and discussion

Figure 1 shows photoemission yields of (111) single crystalline CVD diamond. These spectra were corrected by a relative beam intensity of incident photons. As seen in the inset of Fig. 1, the photoemission yield (curve a) appears although is weak in intensity just above 5.5 eV (the fundamental band gap) and starts to increase for $h\nu > 6.8$ eV, which corresponds to the onset of the vertical transitions between the valence band and the conduction band. This lineshape reproduces an absorption coefficient curve reported by Roberts and Walker. This fact signifies the existence of a negative electron affinity since the onset of band-to-band transitions is well correlated to the onset of electron emissions.

The H-terminated surface (curve a) can emit more electrons than the O-adsorbed surface (curve b). In the case of the O-adsorbed surface, the onset of photoyield shifts to the higher energy side by $\sim$ 0.3 eV, compared to the H-terminated surface. A possible

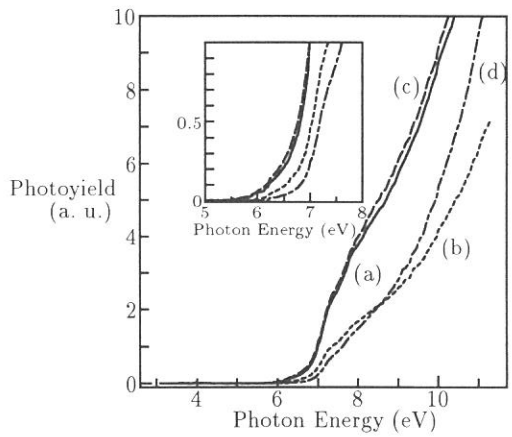

Figure 1: Photoyield of (a) H- and (b) O-adsorbed surfaces of (111) single crystalline CVD diamond and (c) H- and (d)O-adsorbed surface of polycrystalline CVD diamond.

origin of the shift is an increase in the work function after the oxygen plasma treatment. A high electronegativity of oxygen may play the major role on the increase in work function. In the case of silicon, the work function increases for (111) surfaces exposed to oxygen.

Photoemission yield spectra of polycrystalline diamond (curve c, d) are similar to those of the (111) single crystalline diamond (curve a, b) as shown in Fig. 1. This indicates that the photoemission is mainly determined by the (111) surfaces with the lowest work function, as described above.

On the other hand, the photoemission yield from polycrystalline diamond is larger than that from the (111) surface. The crystallainity of (111) and (100) CVD diamond films may influence the photoemission yield. The escape depth for secondary electrons may be determined by distributed defects which can prevent the photo-excited electrons from escaping to vacuum. More defects are present in the (111)-oriented diamond films than in the (100)-oriented one. At lower photon energies, where only the (111) surface contributed to the yield the observed photoyield of polycrystalline diamond containing (111) and (100) surfaces is similar to that of the single crystalline (111) surface. At higher photon energies, on the other hand, the photoyield is stronger than that of the (111) surface. The large yield at the high photon energy is considered to be due to the defference of photoemission area since the surface area of polycrystalline diamond is larger than the (111) single crystalline diamond due to the surface morphology.

4 Summary

We have investigated the electron affinity of the single crystalline and polycrystalline CVD diamond surfaces.

The photoemission yield of H-terminated surface is higher than that of O-adsorbed surface in (111) single crystalline CVD diamond. The electron affinity is negative for the H-terminated (111) diamond while slightly positive for the O-adsorbed one. In the case of polycrystalline CVD diamond, the photoemission yield at low photon energies near the band gap energy is determined mainly by (111) surfaces appearing in the specimen.

References

[1] F. J. Himpsel *et al.*,Phys. Rev. **B20**, 624 (1979).

[2] M. W. Geis *et al.*, IEEE Trans. Electron Devices **38**, 619(1991).

VUV Optical Characteristics in TEOS–SiO_2 Films Prepared by PECVD

Keisuke ISHII, Yoshimichi OHKI and Hiroyuki NISHIKAWA*

Department of Electrical Engineering, Waseda University,
3–4–1 Ohkubo, Shinjuku–ku, Tokyo 169, Japan

*Department of Electrical Engineering,
Tokyo Metropolitan University,
1–1 Minami–Osawa, Hachioji, Tokyo 192–03

Deposition of SiO_2 thin films from TEOS by PECVD is widely utilized for the deposition of interlevel dielectric layer in ultra–large–scale integrated circuit (ULSI) devices, because TEOS–SiO_2 is featured by low deposition temperature and good step–coverage [1]. However, little is known about structural imperfection which might be included in TEOS–SiO_2. Analysis of photoluminescence spectra has been proved to be a powerful tool to study the defect structure in SiO_2 [2]. Therefore, optical absorption and photoluminescence of TEOS–SiO_2 films measured by synchrotron radiations were studied.

The TEOS–SiO_2 films were deposited using an apparatus shown in Fig.1, with the deposition parameters listed in Table 1. Oxygen, used as carrier and oxidation gas, was introduced from the top a glass bell–jar and excited with an RF power of 13.56 MHz through a capacitive coupling. TEOS gas vaporized and transported at 70 °C was led into the 'tail–flame' of the oxygen plasma. The SiO_2 films can be raised to 700 °C.

Figure 2 shows vuv absorption spectra. The OH–related absorption seen as a sharp slope from 7.5 eV to 8.0 eV decreases with an increase in the deposition temperature. These results indicate that a SiO_2 film with a less amount of OH–related impurities is deposited at a higher deposition temperature.

On the other hand, Fig.2 also indicates that an absorption band appears at 7.6 eV in the 600 °C–deposited SiO_2. By the absorption of these 7.6–eV photons, the photoluminescence, of which intensity has a negative dependence on the measurement temperature, is observed around 4.4 eV. Referring to the studies on high–purity silica [3], the absorption at 7.6 eV and photoluminescence at 4.4 eV are considered to be due to the oxygen vacancy (≡Si–Si≡). This indicates that the optimum substrate temperature for the deposition of SiO_2 is around 500 °C, and that OH–groups and oxygen vacancies appear below and above this temperature respectively.

A semilog plot of the decay of 4.4–eV luminescence at 53 K excited by 7.6–eV photons shown in Fig.3 indicates that the luminescence decays very fast (< 3 ns) and nonexponentially. The reason for this nonexponential decay is discussed by analysis to estimate the distribution of decay constant. The solid curve in Fig.3, obtained by assuming a stretched–exponential function: $\beta/\tau\cdot(\tau/t)^{1-\beta}\cdot\exp(-(t/\tau)^{\beta})$ and the least squares method; the distribution of decay constants is considered to correlate with $1/\beta$. This distribution in TEOS–SiO_2 films (β =0.78) is contrast to the nearly single–exponential decay observed for the 4.4–eV luminescence in high–purity silica glass (β = 0.93), although the effective decay constant τ is consistent with the silica glass (2.5–2.8 ns)[4].

Compared with the FT–IR absorption spectra around 1070 cm^{-1} indicating the states of Si–O–Si structure, the 1070 cm^{-1}–band in TEOS–SiO_2 deposited at 600 °C is broader than in thermal silicon dioxide. This means that the TEOS–SiO_2 film deposited at 600 °C has more distorted structure than thermal oxide. Such distorted structure seems to bring about electronic and/or structural perturbation of oxygen vacancies,

resulting in the distribution of the decay constant.

References
[1] NIKKEI MICRODEVICE, Vol.7 (1991) 80 (in Japanese).
[2] H. Nishikawa, Y. Ohki, et al: Transactions of the Materials Research Society of Japan, Vol.8 (1992) 120.
[3] H. Nishikawa, Y. Ohki, et al: Phys.Rev.B, Vol.45, No.2 (1992) 586.
[4] H. Nishikawa, Y. Ohki, et al: (submitted).

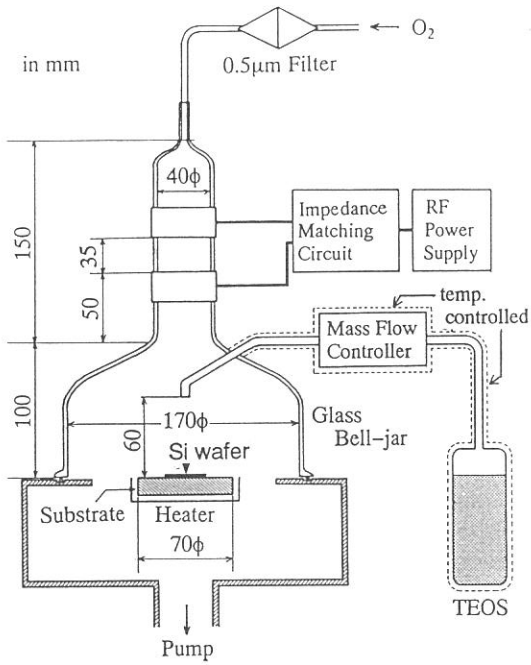

Fig.1. Plasma CVD apparatus for SiO_2 deposition.

Table 1. Deposition Conditions.

RF power	20	W
TEOS flow rate	1	sccm
O_2 flow rate	10	sccm
pressure	0.2	Torr
substrate temp.	300–600	°C
TEOS temp.	70	°C

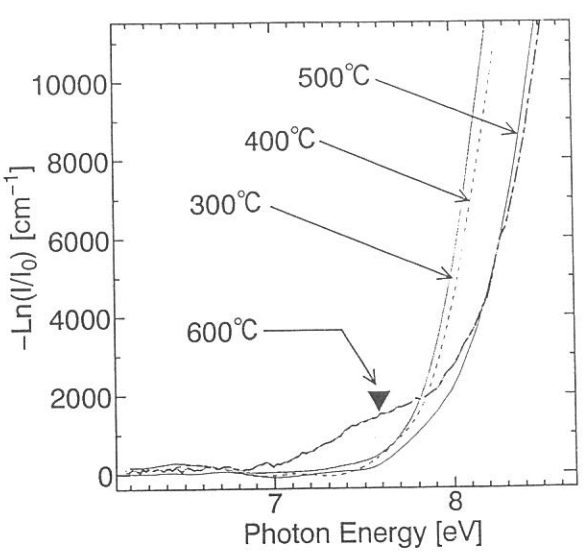

Fig.2. Effect of the deposition temperature on the vuv absorption spectra. (▼ shows the absorption at 7.6 eV.)

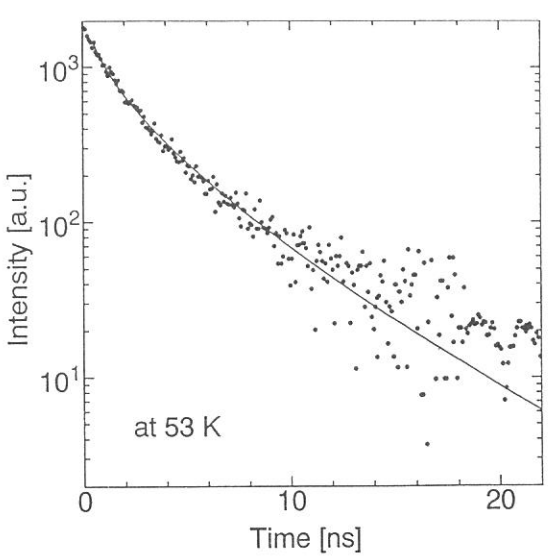

Fig.3. Semi-log plot of the decay of 4.4-eV luminescence band obtained at 53 K for TEOS-SiO_2 deposited at 600 ℃ excited by 7.6-eV photons. The solid curve is drawn by assuming the stretched-exponential function.

Optical Properties of Heavy Metal Fluorides

Hiroshi MIZOGUCHI,[1] Naoyuki UEDA,[2] Hideo HOSONO,[1] and Hiroshi KAWAZOE[2]

[1] Research Laboratory of Engineering materials, Tokyo Institute of Technology, Midori-ku, Yokohama 227

[2] Institute for Molecular Science, Myodaiji, Okazaki 444

In most cases, the energy level of non-bonding F 2p is much shallower than that of occupied outer orbitals of metal ions in solids. However, the energy level of outer s-orbital of heavy metals is comparable to that of 2p in F or O in ionic solids because lower valence state becomes favorable for these heavy metal ions as exemplified that Tl^{+} ($6s^2$) is more stable than Tl^{3+} ($6s^0$). It is of interest to examine the relation between the optical and electric properties and nature of energy band structure for heavy metal fluorides. In this project we focused to elucidate the energy band structure of $TlAlF_4$ using UV SOR BL1B.

Samples used here were prepared on synthetic SiO_2 glass substrate by vacuum evaporation method and the thickness was ~ 500 nm.

Figure 1(a) and (b) shows the reflection spectrum (incident angle; 45 °) and absorption spectrum obtained by K-K transformation from (a), respectively. Three distinct bands centered at 6.0 , 6.7 , and 7.9 eV were observed in the energy region higher than the band gap (5.3 eV). The assignment of these bands is in progress with the aid of molecular orbital calculations.

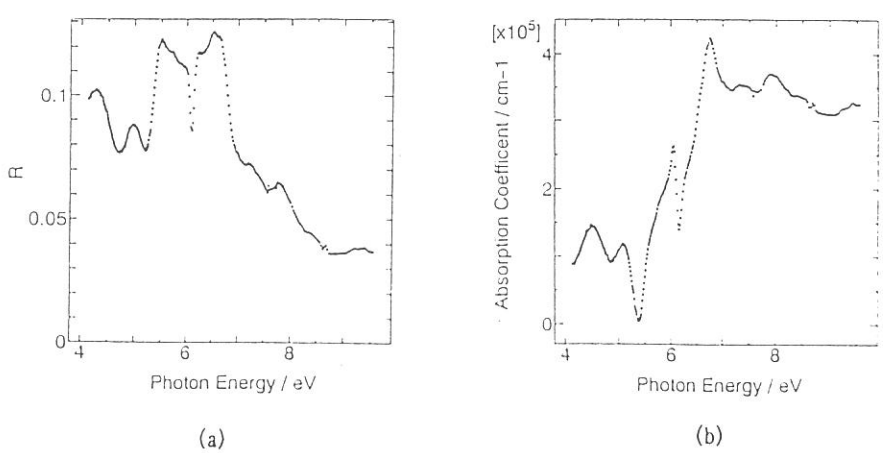

Fig.1 Reflection spectrum (a) and absorption spectrum (b) calculated by K-K transformation

Optical Conductivity of FeSi

S. Kimura[1], H. Ohta[2], E. Kulatov[3], S. V. Halilov[4], T. Nanba[2] and M. Motokawa[2]
[1]*UVSOR, Institute for Molecular Science, Okazaki 444*
[2]*Department of Physics, Kobe University, Kobe 657*
[3]*General Physics Institute, Academy of Sciences of Russia, Moscow, Russia*
[4]*Kurchatov Institute of Atomic Energy, Academician Kurchatov Square, Moscow, Russia*

FeSi is known as a narrow gap semiconductor which shows anomalous magnetic properties. It shows large magnetic susceptibility maximum around 500 K which is difficult to interpret by normal band picture of semiconductor.[1] Moriya interpreted this anomalous magnetic susceptibility qualitatively by temperature induced moment deduced from spin fluctuation theory,[2] and this temperature induced moment was confirmed by neutron measurement.[3] But the origin of the narrow energy gap has been unclear yet. Recently, Fisk *et al.* proposed that the material is one of Kondo insulators,[4] i. e. the energy gap originates from the hybridization between a conduction band and a localized magnetic moment as rare-earth compounds. So there is an interest in the electronic structure including the origin of the energy gap state. We have measured the reflectivity spectrum of the high quality single crystal in the energy range from 50 meV to 32 eV using a beam line 7B and a laboratorial spectrometer system. The crystal structure is *B20* type of distorted NaCl structure. The energy band including a spin-orbit effect and the theoretical optical conductivity (OC) have been calculated by Kulatov. Mattheiss *et al.* also calculated the band structure but using more simple model with a simple cubic and without a spin-orbit effect.[5] These calculated results are similar to each other but the gap energy is different from other one, i. e. the former's energy gap is 0.05 eV and the latter 0.11 eV. Moreover the advantage of Kulatov's calculation is that we can make direct comparison of the OC spectra which are obtained theoretically and experimentally.

The obtained OC spectra at 300 and 6 K after a Kramers-Kronig transformation of reflectivity spectra are shown in Fig. 1. At 300 K, the OC spectrum is like a metal because the intensity below 0.1 eV is almost flat. However, an energy gap of about 0.1 eV opens at 6K because the OC intensity becomes weak below 0.15 eV.

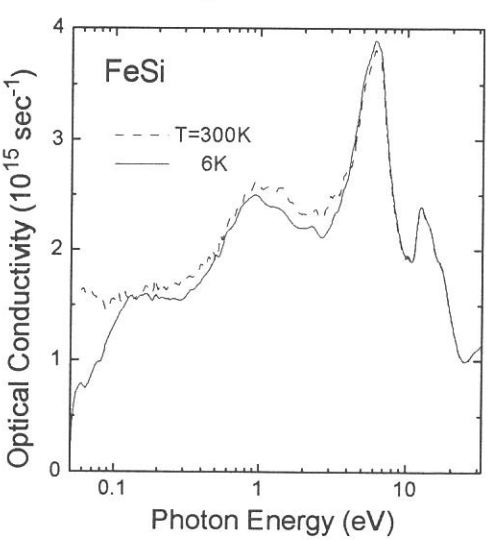

Fig. 1 Optical conductivity of FeSi single crystal in the energy range from 0.05 to 32 eV. The energy gap is seen in the energy position of about 0.1 eV at 6 K.

The result is qualitatively equal to that measured by Schlesinger *et al.*[6] They suggested that the energy gap is due to the creation of a Kondo insulator. But the gap energy is comparable to the thermal energy at 300 K. So the energy gap can be hidden by the thermal excitation at 300 K. In Fact, the calculated joint density of states using the Kulatov's band calculation results show that the energy gap is hidden by the thermal excitation at high temperature. Therefore we think that the temperature dependence of energy gap observed in the spectra can be explained by the thermal excitation in the rigid band without considering the gap formation of a Kondo insulator around 100 K.

Other structures in the OC spectrum are expected by the band calculation. The calculated OC spectrum is shown by a dashed line in the lower part of Fig. 2 and by a solid line which is smoothed by Lorentzian with the band width of 0.4 times the energy position. After smoothing, the measured and calculated OC are very similar to each other expect for the intensity ratio of 1 eV and 2 eV peaks.

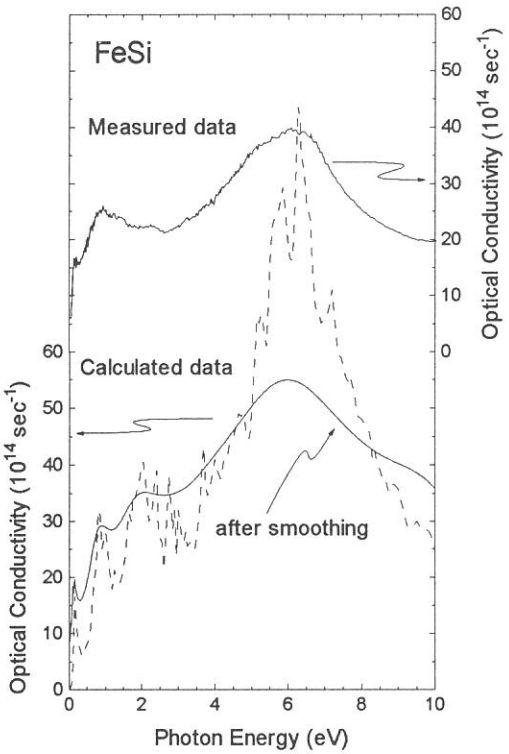

Fig. 2 Measured (upper part) and calculated (lower part) optical conductivity of FeSi. The solid line of calculated data is after smoothing of the dashed data. (See text in detail.)

In conclusion, the results of the optical measurement can be understood fairly well by band calculation, but the connection between the band calculation and the strong correlation in FeSi is still unclear.

The authors are grateful to Dr. A. A. Povzner for supplying the sample of FeSi.

References

[1]V. Jaccarino, G. K. Wertheim, J. H. Wernick, L. R. Walker and S. Arajs, Phys. Rev. **160**, 476 (1967).

[2]T. Takahashi and T. Moriya, J. Phys. Soc. Jpn. **46**, 1451 (1979).

[3]K. Tajima, Y. Endoh, J. E. Fischer and G. Shirane, Phys. Rev. B **38**, 6954 (1988).

[4]G. Aeppli and Z. Fisk, Comments Condens. Matter Phys. **16**, 155 (1992).

[5]L. F. Mattheiss and D. R. Hamann, Phys. Rev. B **47**, 13114 (1993).

[6]Z. Schlesinger, Z. Fisk, Hai-Tao Zhang, M. B. Maple, J. F. DiTusa and G. Aeppli, Phys. Rev. Lett. **71**, 1748 (1993).

VUV Reflectivity Spectra of Rare-Earth Sesquioxides III

Fumitaka ARAI, Shin-ichi KIMURA*, Yasuhiko SATO,
Mikihiko IKEZAWA and Mareo ISHIGAME
Research Institute for Scientific Measurements, Tohoku University,
Aoba-ku, Sendai 980
**Institute for Molecular Science,*
Myodaiji, Okazaki 444

We measured reflectivity spectra to investigate the electronic state of a series of R_2O_3's. We have already reported the VUV reflectivity spectra of seven kinds of R_2O_3 single crystals [1, 2]. In this report, we measured the reflectivity spectra of another three kinds of R_2O_3 single crystals (R= Pr, Sm and Eu) in addition.

From the X-ray diffraction patterns, it is shown that R_2O_3's of La, Pr and Nd have hex type crystal structure (called A-type), Sm and Eu have monoclinic type (B-type), and Er, Tm, Yb, Lu and Y have bcc type (C-type). Measurements of reflectivity spectra were done in the photon energy region between 3 eV and 40 eV at 300K at the beam line BL7B.

The reflectivity spectra of all R_2O_3 materials are similar to other ones which have even a different crystal structure. This means that the origin of the main structure of these spectra is almost equal to one another. We will make a detailed analysis using the optical conductivity spectra (Figure 1), which are derived from the Kramers-Kronig transformation of the reflectivity spectra. There are three structures in common, which are located around 10 eV (here called a), 18 eV (b) and 30 eV (c). In our previous papers, we have explained the origin of the main part of the structure a, b and c, i. e. a is due to the transition from O-2*p* to R-5*d*, b is O-2*p* to R-6*s* and c is R-5*p* to R-5*d*. In addition, the difference of the detailed structures of peak a is due to the difference of the expanse of the R-4*f* states due to the 4*f* multiplet [2].

The peak c has doublet structure in R_2O_3's (R= Er $\sim$ Y). That is explained that R-5*p*3/2 and R-5*p*1/2 states are divided in the C-type crystals. From La to Lu, it is clearly seen that the position of the structure c is gradually shifted to the high energy with the increase of the atomic number (57 - 71). The reason is the screening to the potential energy from the nucleus of the 4*f* electron. Because the 4*f* electron locates at the inner shell, the outer band of the rare-earth site does not affect from the coulomb potential of the atomic nucleus, i. e. the 5*p* state goes to the high binding energy and the 5*d* state does not move as the atomic number increases. Therefore we can observe that the 5*p*-5*d* absorption shows a blue shift with the increase of the atomic number.

The spectra which belong to the A-type crystal structure are not only similar to one another but also those of B-type. This means the above explanation can be applied to other crystal structure groups. In detail, the peak structure at about 10 eV in La_2O_3 is different from that of Pr_2O_3 or Nd_2O_3, that is thought to be an effect of the unoccupied 4*f* states. The origin of the peak structures at 4.1 eV in Pr_2O_3 and 5.2 eV in Nd_2O_3 are unknown up to the present.

In conclusion, it is thought that the information about the fundamental electronic state in the R_2O_3's were obtained. To the next step, we are going to investigate a series of the

Pr oxides, which is said to be in mixed valence state and change the degree of oxidation from Pr_2O_3 (Pr^{3+}) to PrO_2 (Pr^{4+}).

References
[1] S. Kimura, F. Arai, M. Ikezawa, Y. Chiba and M. Ishigame, UVSOR Activity Report 1991, 86 (1992).
[2] F. Arai, S. Kimura, Y. Sato, M. Ikezawa, Y. Chiba and M. Ishigame, UVSOR Activity Report 1992, 41 (1993).

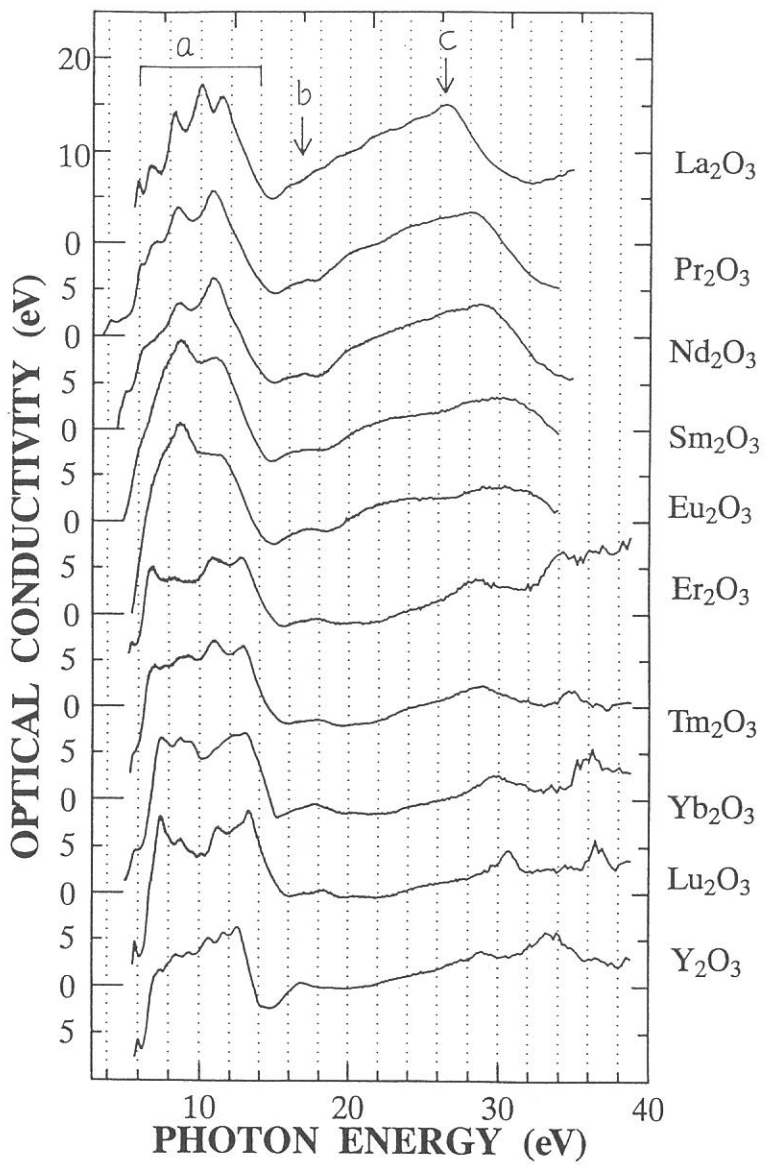

Fig. 1
Optical conductivity spectra of R_2O_3's from the Kramers-Kronig transformation of the reflectivity spectra.

Exciton Absorption Spectra of Thin KCN and RbCN Crystals

Masami INABA and Satoshi HASHIMOTO
Kyoto University of Education, Fushimi-ku, Kyoto 612

Alkali cyanide crystals, when cooled from the pseudocubic disordered phase into the low temperature phase of CN^- elastic order and higher symmetries, break up into a multi-domain structure. The crystals become to be opaque since each domain shows birefringence and multiple scattering of light is occurred.

Much attention has been paid to the excitonic properties of the ionic molecular crystals as well as the mechanism of the phase transition. However, from the lack of a convenient method of sample preparation of opaque materials, little study on the exciton has been carried out except the measurement of the reflection spectra [1].

For the first time, absorption spectra of very thin KCN and RbCN crystals have been measured in UV region at the BL-7B of UVSOR facility. The crystals with thicknesses of 0.1-10 μm were prepared from the melt using capillarity for pulling it into a narrow gap of a cell made by two CaF_2 single-crystal plates. This technique has already been applied to the cases of alkali halides [2] and CuCl.

Figures 1 and 2 show the absorption spectra of KCN and RbCN, respectively. Measurements were done at 300 K(a) and 32 K(b) for the samples with thicknesses of about 1 μm. We can see clear vibrational structures of 0-0, 0-1,$\cdots$ molecular excitons with an interval of about 200 meV in the region of 6.7-8.6 eV. Maximum absorption coefficient in this region is estimated to about 10^5 cm^{-1}. This large value suggests that the excited states of the CN^- ions are singlet, which coincides with the assignment that the exciton states are attributed to an $X^1\Sigma^+ \rightarrow A^1\Pi$ vibronic transition in CN^- ions [1].

In KCN, a complicated structure was observed below 80 K in the region of 8.0-8.5 eV as shown in Fig. 1(b). This structure is due to overlapping of two progressions of Davydov splitting corresponded to two CN^- ions situated in a unit cell of orthorombic symmetry. The ferroelastic ordered phase is formed at 168 K, and a second-order phase transition leading to the

order of the electric dipole of the CN^- occurs at 83 K. Such splitting was not observed in RbCN because of an orientational glassy state of CN^- ions around 32 K. The vibrational structure almost disappeared with increasing temperature in KCN, while little change was observed in RbCN. The onset of a charge transfer exciton band is seemed to appear at higher energies. This onset shifts to low energy side with increase of temperature for both specimens.

A very sharp structure is indicated on the 0-0 exciton band of KCN in Fig. 1(b). This sharp peak shifts to high energy side with increase of temperature and disappears above 80 K. Similar behavior was observed for the angle of incoming light; the peak disappears above several degrees. A large fraction of the crystal axes of the orthorombic domains can be aligned because the thin crystals are under uniaxial stresses acting on the surface of the sample [3,4]. This peak may be related to the "partially ordered multi-domain structure". The similar peak was not found in RbCN, in which the degree of order is lower than that of KCN.

[1] M.A.Bosch and G.Zumofen: Phys.Rev. Lett. 41 (1978) 590.
[2] S.Hashimoto and M.Itoh: Jpn.J.Appl. Phys. 27 (1988) 726.
[3] N.Ohno,et al.: J.Phys.Soc.Jpn. 59 (1990) 361.
[4] D.Durand,et al.: Phys.Rev. B22 (1980) 4005.

Fig.1

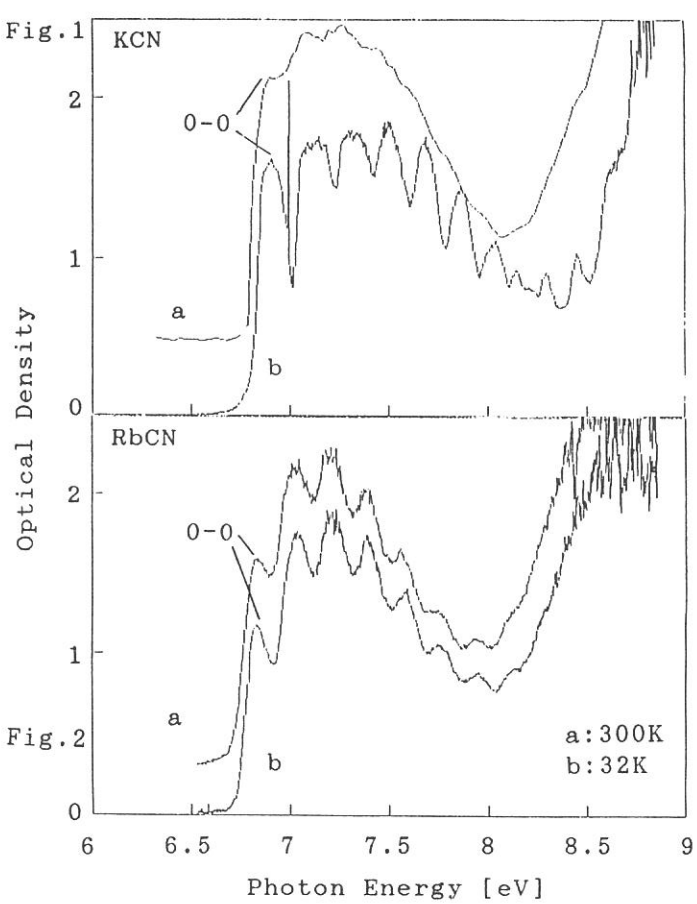

Fig.2

OPTICAL SPECTRA OF TIN(II) IODIDE

Masami FUJITA Kazutoshi FUKUI,[+] Kazunori HAYAKAWA,[+]
Hideyuki NAKAGAWA,[+] Takeshi MIYANAGA[++] and Makoto WATANABE[+++]

Maritime Safety Academy, Wakaba, Kure 737
[+]Department of Electrical and Electronics Engineering, Faculty of Engineering, Fukui University, Bunkyo, Fukui 910
[++]Department of Physics, Faculty of Education, Wakayama University, Sakaedani, Wakayama 640
[+++]Institute for Molecular Science, Myodaiji, Okazaki 444

Tin(II) iodide (SnI_2) is a layered material and the crystal structure of SnI_2 belongs to a monoclinic C_{2h}^3 (C2/m) space group.[1] SnI_2 has the isoelectronic configuration of PbI_2. In contrast to the case of well studied PbI_2, optical properties of SnI_2 have been known very scarcely. Only the optical spectra below 3 eV have been reported for evaporated thin films and single crystals.[2] In the present study, polarized reflection spectra of SnI_2 single crystals were measured.

Single crystals of SnI_2 were grown from vapor phase. The crystals were obtained as brilliant red needles elongated along *b*-axis. Crystals were also grown by the Bridgman method and it was found by the X-ray diffraction measurement that the crystals are cleaved along the (201) plane. Figure 1 shows reflection spectra of SnI_2 grown from vapor phase. Spectra were measured at 13K for polarization parallel ($E//b$) and perpendicular ($E \perp b$) to the *b*-axis. The direct exciton peak is observed at 2.564 eV for $E//b$, while it is observed at 2.572 eV for $E \perp b$. The peak position in single crystal is about 0.09 eV higher than that in evaporated thin film at 86K.[2] The intensity of the exciton peak for $E//b$ is about three times stronger than that for $E \perp b$. The peak position of the exciton band of SnI_2 is close to that of PbI_2. The exciton transition is regarded as the intra-atomic excitation in the cation site ($5s^2 \rightarrow 5s5p$ in Sn^{2+}) as is the case of PbI_2.[3] The polarization dependence of the exciton band would be ascribed to the combined effect of the crystal field splitting and the spin-orbit interaction of the $5p$ level in Sn^{2+} ion.

Doublet peaks are found at 26.17 eV and 27.04 eV as shown in Fig. 2. They are attributed to the core exciton transition from the Sn^{2+} $4d$ core level to the $5p$ level. The dichroism in this region is weak compared to the fundamental absorption region in Fig. 1. This indicates that the anisotropic crystal field effect

is weak and the excitons are highly localized as is the case of Pb^{2+} 5*d* core excitons in orthorhombic lead halides.[4)]

The authors would like to thank professor K. Itoh of Hiroshima University for X-ray diffraction measurement to determine crystal orientation.

References

1) R. A. Howie, W. Moser and I. C. Trevena: Acta Cryst. **B28** (1972)2965.
2) I. S. Gorban, V. F. Gorchev and T. N. Sushkevich: Sov. Phys. Solid State **18**(1976)1220.
3) I. Ch. Schluter and M. Schluter: Phys. Rev. **B9**(1974)1652.
4) M. Fujita, H. Nakagawa, K. Fukui, H. Matsumoto, T. Miyanaga and M. Watanabe: J. Phys. Soc. Jpn. **60**(1991)4393.

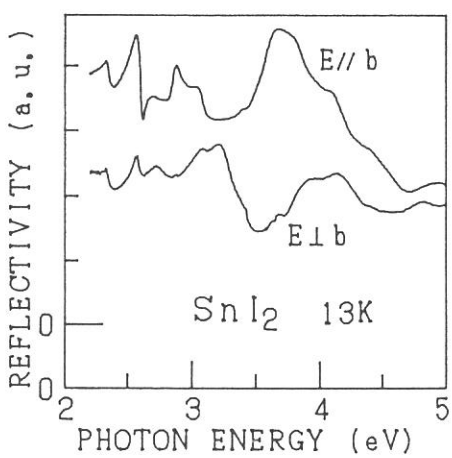

Fig. 1.
Reflection spectra of SnI_2 below 5 eV.

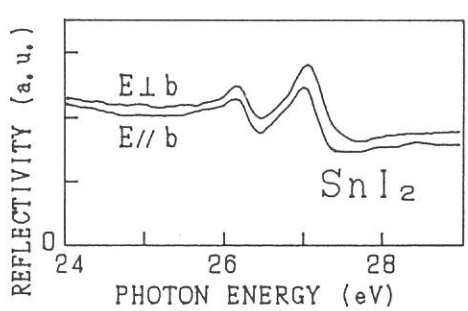

Fig. 2.
Reflection spectra of SnI_2 in the Sn^{2+} 4*d* core exciton region.

OPTICAL PROPERTIES OF GALLIUM IODIDE

N. OHNO, Y. UZAWA and M. ITOH†

Faculty of Engineering, Osaka Electro-Communication University, Neyagawa, Osaka 572
†Faculty of Engineering, Shinshu University, Nagano 380

Gallium halides belong to III-VII compounds. Amongst III-VII materials, thallous halides and indium halides have been extensively studied mainly because of their characteristic optical properties and the polaron nature of electrons and holes of an intermediate coupling strength [1]. Unlike these mono-halides, gallium mono-halides are quite unstable, while tri-iodide GaI_3 is obtained as a stable material although it is quite hygroscopic [2]. It crystallizes in a layered orthorhombic structure. In the present study, optical properties of GaI_3 single crystals are investigated for the first time using a optical flat surface cleaved in a vacuum.

Figure 1 shows the reflection spectrum of a GaI_3 single crystal measured at 15 K. There appear sharp lines at 3.8 eV, 4.1 eV and 4.3 eV probably due to a creation of excitons, and at a higher energy broad structures are also observed.

In Fig. 2 are shown absorption spectra of a GaI_3 single crystal near the absorption edge for various temperatures. At 15 K, the absorption spectrum shows an unstructural band tail starting around 3.1 eV, and the tail shows an apparent red shift with increasing temperature. It is found that a logarithmic plot of the absorption coefficient gives a straight line for all temperatures investigated, indicating that the absorption edge of GaI_3 is well described by the Urbach rule. The best fit to the data obtained gives the steepness constant $\sigma_0 = 0.3$ and the converging energy $E_0 = 3.44$ eV. The small value of the steepness parameter suggests that the exciton-phonon interaction is very strong in GaI_3.

We also measured luminescence spectra of GaI_3 at low temperatures. However, no luminescence was detected near the absorption edge and at a lower energy region. This indicates that excitons in GaI_3 are unstable in a free state in agreement with the small value of the steepness constant.

References

[1] K. Kobayashi, *Excitonic Processes in Solids* (Springer Verlag, 1986), ed. M. Ueta *et al.*, Chap.7.

[2] J.D. Corbett and R.K. McMullan, J. Am. Chem. Soc., **80** (1955) 4217.

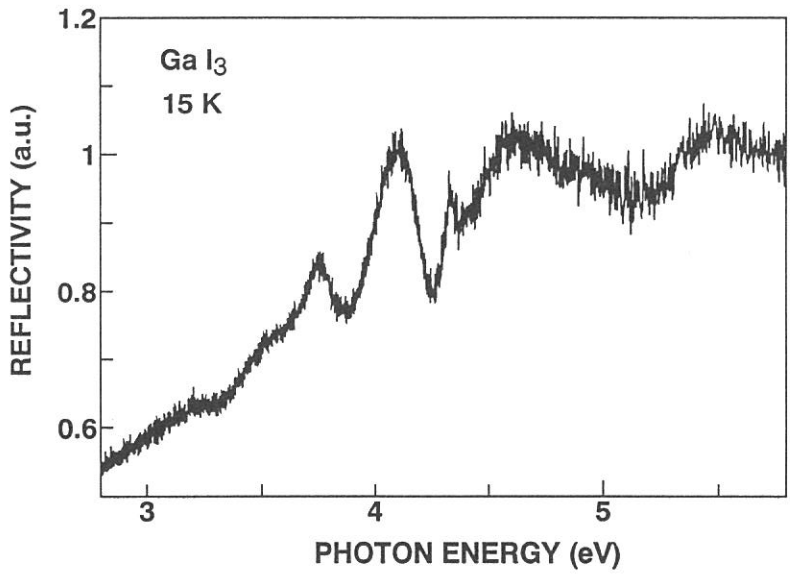

Fig.1 Reflection spectrum of a GaI_3 single crystal at 15 K.

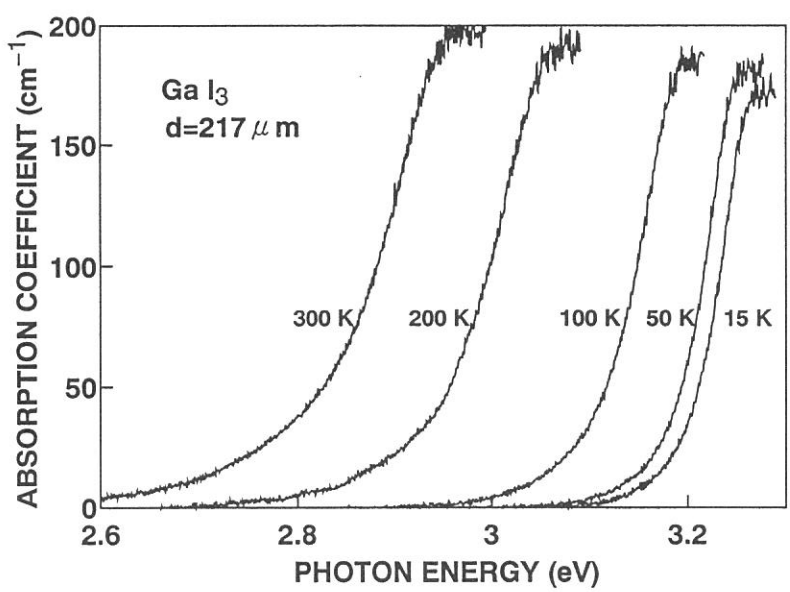

Fig.2 Absorption spectra of a GaI_3 single crystal near the absorption edge for various temperatures.

Reflection Spectra of Thallous Halides in 5d Core Exciton Region

N. OHNO, Y. KIYAMA, M. FUJITA† and K. NAKAMURA††

Faculty of Engineering, Osaka Electro-Communication University, Neyagawa, Osaka 572
†*Maritime Safety Academy, Kure 737*
††*Department of Physics, Okayama University, Okayama 700*

In the optical spectra of heavy-metal halide crystals, there appear sharp lines due to the metal d core-exciton transition in vacuum ultraviolet region. The lines are accompanied with fine structures in many halide crystals, which have not been well understood as yet. In the present study, polarized reflection spectra of cubic TlCl and TlBr and orthorhombic TlI have been measured in the energy region up to 30 eV.

Figure 1 shows the reflection spectrum of TlCl in 2 - 25 eV region at room temperature. The spectral features are consistent with the previous result of Hinson and Stevenson [1]. Two sharp peaks observed in 14 - 17 eV region of the spectrum are due to the Tl^+ $5d$ core-exciton transition.

Figure 2(a) and (b) show reflection spectra of TlCl and TlBr, respectively, in the Tl^+ $5d$ core-exciton region. The peaks 1, 2 and 3 can be ascribed to the allowed transition in Tl^+ ion from the $^1S_0$ ground state to the J=1 excited states of $^3P_1$, $^1P_1$ and $^3D_1$, respectively, as is the case of Pb-halide crystals [2, 3]. The J=3 excited states of $^3F_3$, $^1F_3$ and $^3D_3$, and J=4 excited state of $^3F_4$, which are optically forbidden in a free-ion state, can couple with the J=1 states through a cubic crystal-field interaction. The subpeaks denoted by 0 and 1′ is probably due to such transitions.

In Fig.3 are shown polarized reflection spectra of orthorhombic TlI in the Tl^+ $5d$ core-exciton region at 16 K. The spectra are somewhat dichroic; weak structures denoted by 1′ and 2′ are observed for $\boldsymbol{E}//\boldsymbol{a}$ polarization, but the counterparts are not found for $\boldsymbol{E}//\boldsymbol{c}$. Similar polarization dependences have been reported in the In^+ $4d$ core-exciton spectra of indium halides [4], which have the same crystal structure and similar electronic configurations. Therefore, the observed dichroism in TlI would be explained by an atomic excitation picture including the anisotropic crystal-field effect.

We thank Prof. S. Hashimoto for providing TlCl and TlBr single crystals.

References

[1] D. C. Hinson and J. R. Stevenson: Phys. Rev. **159** (1967) 711.

[2] M. Fujita, H. Nakagawa, K. Fukui, H. Matsumoto, T. Miyanaga and M. Watanabe: J. Phys. Soc. Jpn **60** (1991) 4393.

[3] M. Fujita, H. Nakagawa, A. Kashino, K. Fukui, T. Miyanaga and M. Watanabe: UVSOR Activity Report **1992** (1993) 46.

[4] K. Nakamura, Y. Sasaki, T. Kishigami, M. Watanabe and M. Fujita: *10th Int. Conf. VUV Rad. Phys.*, Paris, Abstract Th137 (1992).

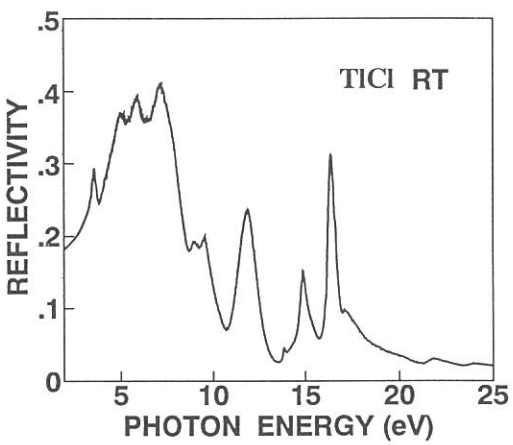

Fig.1. The reflection spectrum of TlCl at room temperature.

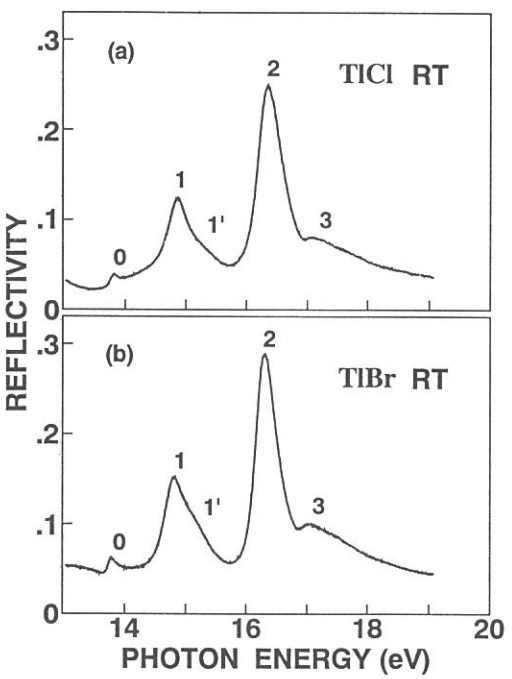

Fig.2. Reflection spectra of (a) TlCl and (b) TlBr in Tl^+ $5d$ core exciton region at room temperature.

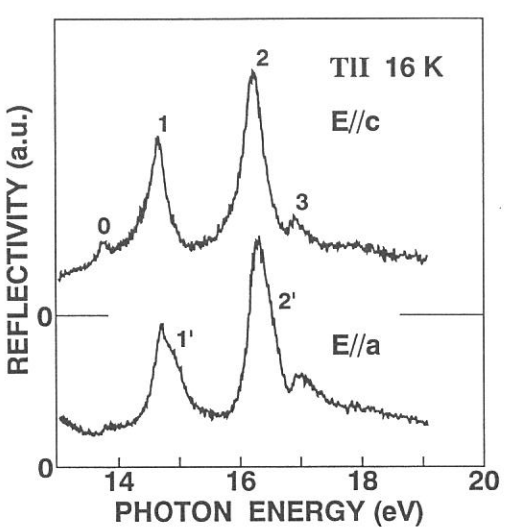

Fig.3. Reflection spectra of orthorhombic TlI in Tl^+ $5d$ core exciton region at 16 K.

Luminescence due to Self-Trapped Excitons in Fluor-phlogopite

M. ITOH,† N. OHNO, Y. UZAWA and Y. KIYAMA

†*Faculty of Engineering, Shinsyu University, Nagano 380*
Faculty of Engineering, Osaka Electro-Communication University, Neyagawa, Osaka 572

Synthetic mica fluor-phlogopite $KMg_3AlSi_3O_{10}F_2$, whose crystalline structure is based on the hexagonal network of linked (Si, Al)O_4 tetrahedra, is a typical example of layered insulators [1]. However, its fundamental optical properties have been little studied, in spite of the wide application in various fields of science and technology. In the present work, we have performed luminescence measurements on mica fluor-phogopite at low temperatures.

Figure 1 shows the luminescence spectrum of fluor-phlogopite measured at 10 K. An intense emission band is observed at 5.4 eV, with a tail toward the low-energy side. This band is stimulated with VUV photons of an energy equal to or larger than that of the lowest exciton absorption band at 8.7 eV, indicating that it is of intrinsic origin. The large Stokes shift (= 3.3 eV) suggests strongly that the 5.4-eV luminescence is emitted after considerable lattice relaxation, i.e., excitons are self-trapped by deforming the lattice around them. The self-trapping of excitons could be caused by the strong exciton-phonon coupling which is a characteristic feature of insulator with large band-gap energy. The present result is the first observation of intrinsic luminescence originating from self-trapped excitons in mica crystals.

Intensity of the 5.4-eV luminescence is almost constant up to 70 K, and is reduced to $\sim 1/10$ at 300 K. The activation energy for thermal quenching is estimated to be 49 meV.

Figure 2 shows the decay profile of the 5.4-eV luminescence measured at 10 K under the single-bunch operation. It appears that the 5.4-eV luminescence exhibits two decay components; a long-lived phosphorescent component with a lifetime of 0.48 μs and a weak fluorescent component with a short lifetime of 1.8 ns. This means that the initial luminescent state would be a pair of the triplet and singlet states separated slightly by the exchange interaction. Such a situation is analogous to that of the self-trapped exciton luminescence in alkali halides, ammonium halides and rare-gas solids [2, 3].

References

[1] L. Bragg and G. F. Claringbull: *Crystal Structures of Minerals* (G. Bell and Sons Ltd., 1965) ch.13.

[2] K. Kan'no, K. Tanaka, H. Kosaka, T. Mukai, Y. Nakai, M. Itoh, T. Miyanaga, K. Fukui and M. Watanabe: Physica Scripta **41** (1990) 120.

[3] N. Ohno, M. Itoh and S. Hashimoto: J. Lumin. **53** (1992) 121.

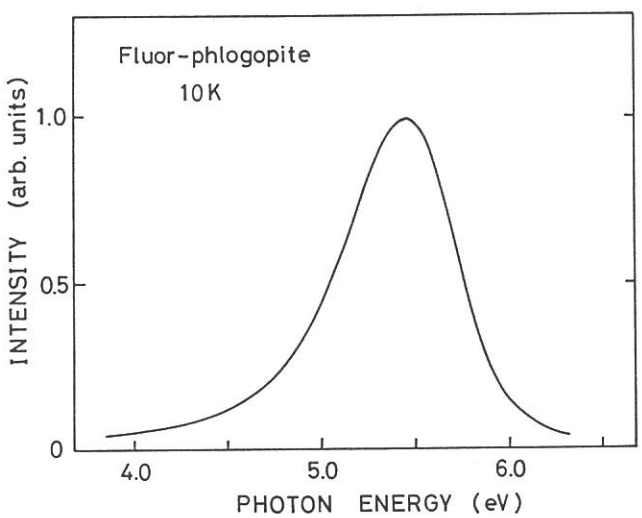

Fig.1. Luminescence spectrum of a single crystal of fluor-phlogopite measured at 10 K under the excitation with UV light at 8.86 eV.

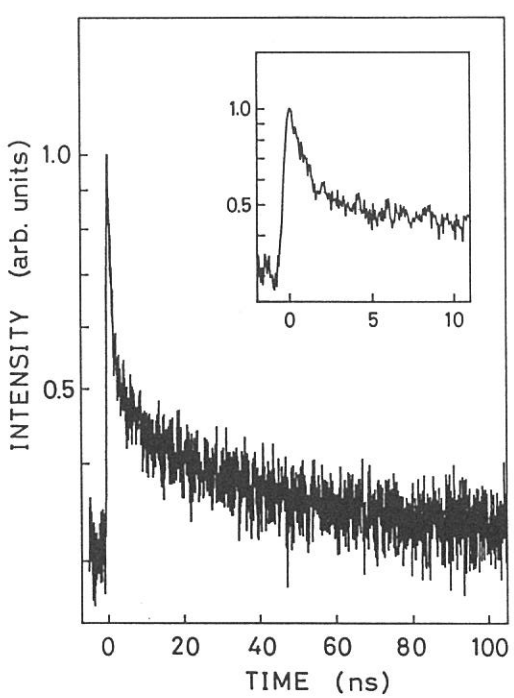

Fig.2. Decay behavior of the 5.46-eV luminescence observed at 10 K under the single-bunch operation at 8.86 eV. The inset shows the fast decay component in an expanded scale.

TIME-RESOLVED MEASUREMENTS OF AUGER-FREE LUMINESCENCE

T. Matsumoto, K. Kan'no, M. Itoh*, H. Hara* and N. Ohno**

Department of Physics, Kyoto University, Kyoto 606
**Faculty of Engineering, Shinshu University, Nagano 380*
***Faculty of Engineering, Osaka Electro-Communication University, Neyagawa 572*

Auger-Free (AF) luminescence in CsF, CsCl, CsBr, RbF and BaF_2 has been studied under excitation with monochromatic light pulses from BL1B equipped with a 1 m Seya-Namioka vacuum monochromator under single bunch operation. Time-resolved spectra were obtained using a system for simultaneously detecting signals through two different time windows.[1]

In fig. 1 are shown time-resolved emission spectra for 5 crystals under excitation into outermost-core band with 21.4 eV light. Solid curves indicate spectra for fast decay components with lifetimes of ~ 1 ns and dotted ones those for slow decay components with lifetimes of hundreds of ns or longer. The solid curves coincide with previously reported spectra for fast decay components under excitation with pulsed electron beam or pulsed X-rays.[2,3] The lifetime of the fast decay component for each crystal was in reasonable agreement with the reported value[4] and was found to have the same value at three emission energies shown by arrows. This indicates that the solid curves are due to AF luminescence in all energy region.

If a hole produced in the core state relaxes to the top of the band before radiative transition, and if the effects of lattice relaxation and deformation of the valence band could be neglected, luminescence band will be located in the range of $Evc - \Delta Ev < h\nu < Evc$, where Evc is the energy difference between the tops of the valence band and the outermost-core band and ΔEv is the valence-band width. The energy range estimated from the results of photoemission[5] is shown by horizontal line for each crystal in the figure. The low energy edges of the observed luminescence are situated at the energies lower than the estimated ones by 0.5 - 1 eV for all cases. Therefore, the effects neglected above are important in the radiative decay process of core holes.

The strong slow decay components appearing in the lower energy side of AF luminescence in CsCl, CsBr and BaF_2 are due to valence holes as they were also observed when excited in the valence-band region. In RbF and BaF_2, however, a weak slow component appears in the higher energy region, as shown by shadow in the figure. Its peak energy is larger than that of the fast component in each crystal. In fig.2 is shown an emission decay curve for BaF_2 observed at 5.63 eV. The lifetime of the slow component is estimated to be longer than 500ns. Its intensity at t=0 is smaller than 0.1% of that of the fast component but its time-integrated intensity is ~ 8% of that of the fast component. In fig.3 are shown time-resolved excitation spectra for both of the components observed at

5.63 eV. The slow component (dotted curve) shows the same excitation spectrum as the fast one (solid curve) and it is not observed under excitation into valence band. This clearly shows that the slow component can also be attributed to the core holes. As the lifetime of AF luminescence is determined by the fastest radiative transition,[2] existence of a forbidden transition would not result in such a slow decay component. Further investigation is necessary to clarify the mechanism to explain this slow decay component.

1) T. Matsumoto, K. Kawata, A. Miyamoto and K. Kan'no: J. Phys. Soc. Jpn. **61** (1992) 1098.
2) J.L. Jansons, V.J. Krumins, Z.A. Rachko and J.A. Valbis: Phys. Stat. Sol. **(b) 144** (1987) 835.
3) P.A. Rodnyi and M.A. Terekhin: Phys. Stat. Sol. **(b) 166** (1991) 283.
4) S. Kubota, J. Ruan, M. Itoh, S. Hashimoto and S. Sakuragi: Nucl. Instr. and Meth. **A289** (1990) 253.
5) J.A. Smith and W. Pong: PR **B12** (1975) 5931, C.S. Inoue and W. Pong: PR **B15** (1977) 2265, W. Pong, C.S. Inoue and S.K. Okada: PR **B18** (1978) 4422.

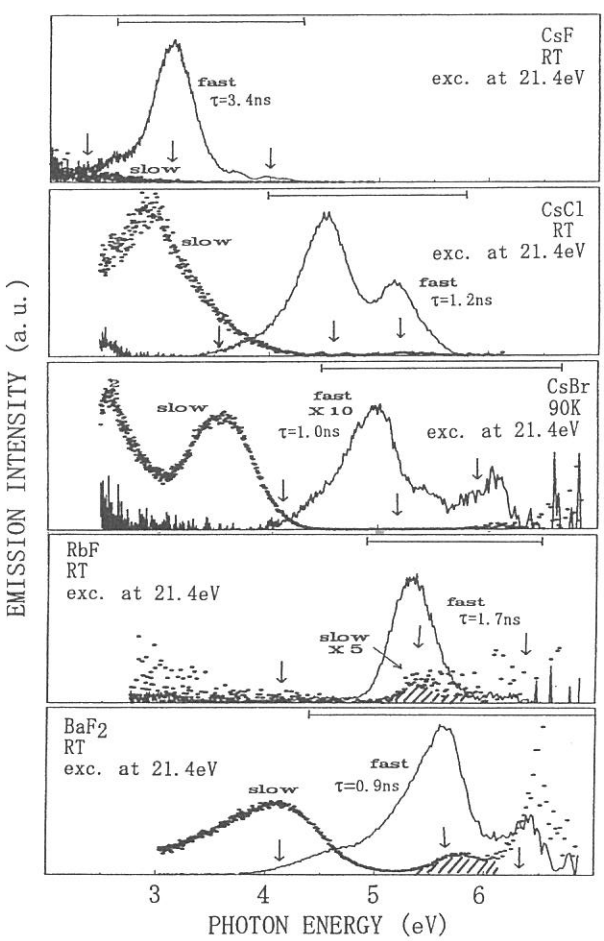

Fig. 1

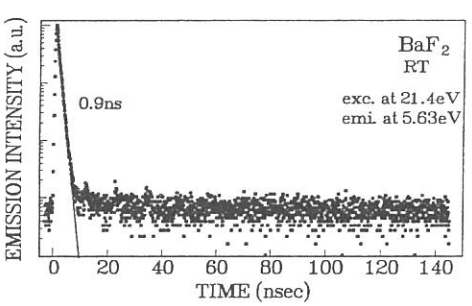

Fig. 2

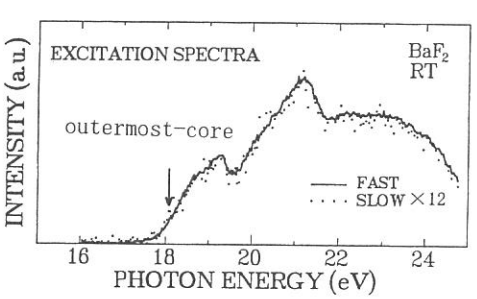

Fig. 3

INTRINSIC LUMINESCENCE FROM SELF-TRAPPED EXCITONS IN BaFBr

Akimasa OHNISHI, Ken-ichi KAN'NO, Yasuo IWABUCHI* and Nobufumi MORI*
Department of Physics, Kyoto University, Kyoto 606, Japan
** Fuji Photo Film Co., Ltd., Miyanodai, Kaisei-machi, Kanagawa 258, Japan*

BaFBr crystal, a layered ionic crystal having the tetragonal structure, is a useful host material for application to photo-stimulated luminescence phosphors[1]. In the present study, recombination luminescence from BaFBr has been investigated under excitation with vacuum ultra-violet at BL1B beam line of UVSOR.

Figure 1(a) shows an emission spectrum observed at 6.5K under excitation at 8.85eV above the band gap energy. Three emission bands are observed at 5.0eV, 3.7eV and 2.4eV. An excitation spectrum for 5.0eV band, shown in the right side of the figure, rises with a threshold at 7.6eV, which corresponds to the absorption band tail of the n=1 exciton due to Br^- valence hole. Positions of halogen doublet are shown by arrows at 7.6eV and 8.1eV. The broken curve shows an absorption spectrum due to O^{2-} impurities contained in the measured sample. It should be remarked that the band exists in position overlapping with the 5.0eV emission band. When excited at 5.06eV corresponding to the peak energy of the O^{2-} absorption band, only the 2.4eV emission band appears (Fig.1(b)).

Figure 2(a) shows emission spectra observed at 14K and 100K under excitation at 7.75eV. In raising temperature, a new emission band is found to appear at 4.1eV with quenching of the 5.0eV and 2.4eV bands. An excitation spectrum for the 4.1eV band, shown in the right side of the figure, exhibits a threshold at 7.6eV as that of the 5.0eV band. In Fig.2(b) is shown the temperature dependence of emission intensities at 5.0eV, 4.1eV and 2.4eV measured by stimulating with 7.75eV light. Solid curves are calculated curves (ΔE=118meV, $\tau_0\nu=2.42\times10^7$). As seen in the figure, the 5.0eV and 2.4eV bands weaken in the same way around 70~100K with growth of the 4.1eV band.

Among several emission bands observed, only two of the 5.0eV band at low temperatures and the 4.1eV band at high temperatures exhibit the clear threshold at 7.6eV for excitation into the lowest exciton absorption due to Br^- valence holes. No other emission bands were observed when excited into the inner valence band originating from F^- p states. This suggests that the free hole created in the F^- p states immediately relaxes into the uppermost valence band to self-trap finally as out-of-plane Br_2^-, being in line with theoretical calculation by Baetzold[2]. Therefore, it is most likely that the 5.0eV and 4.1eV bands both come from STE's with the Br_2^- ion core. As seen from Fig.2(b), the 5.0eV band is observed at temperatures much lower than 120K,

where the Br_2^- is stable[3]. We conclude that the 5.0eV band is intrinsic luminescence from STE's with the out-of-plane Br_2^- core. On the other hand, the 4.1eV band appearing above 80K and still strongly at temperatures much higher than 120K is hardly attributed to the intrinsic luminescence. This band comes probably from perturbed STE's ; [Br_2^- + e] trapped in the vicinity of impurity ions or point defects.

Measurements with a time correlated single photon counting method under single-bunch operation made it sure that both the 5.0eV band at low temperatures and the 4.1eV band at high temperatures are phosphorescence with a lifetime longer than μs. Thus, the 5.0eV band has characteristics of triplet luminescence with a long lifetime, so that it can be regarded as a family of triplet π bands of the STE luminescence in alkali bromides. As for alkali halides, the π emission bands are classified into three types (I, II and III) with respect to the magnitude of Stokes-shift energy[4]. In this connection, it is noteworthy that the Stokes-shift of the 5.0eV band is almost the same to that of the type I π band in NaBr. Based on this point, we suppose that the STE responsible for the 5.0eV band is situated on-center.

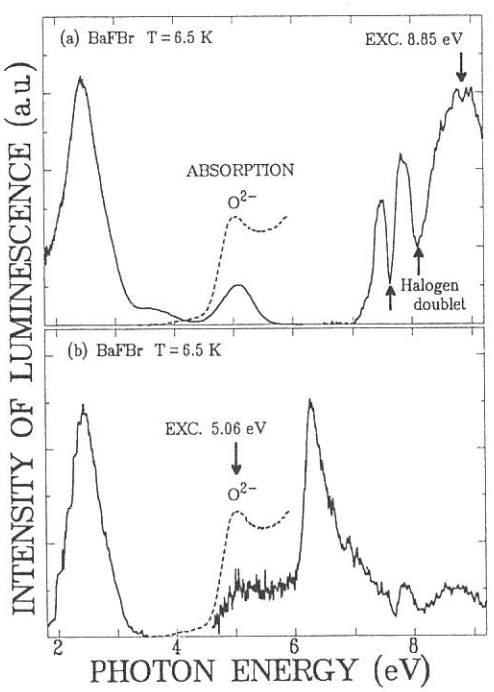

Fig. 1

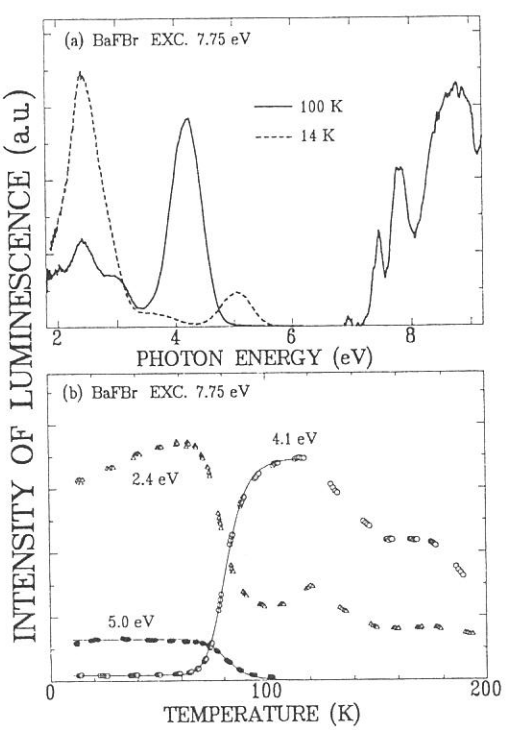

Fig. 2

REFERENCES

1 M. Sonoda, M. Takano, J. Miyahara and H. Kato ; Radiology, 148 (1983) 833
2 R. C. Baetzold ; Phys. Rev. B36 (1987) 9182
3 T. Hangleiter, F. K. Koschnick, J.-M. Spaeth, R. H. D. Nuttall and R. S. Eachus ; J. Phys : Condens. Matter ; 2 (1990) 6837
4 K. Kan'no, K. Tanaka and T. Hayashi ; Rev. Solid State Science 4 (1990) 383

Decay Behavior of UV-luminescence in $CdCl_2$–$CdBr_2$

Hideyuki NAKAGAWA, Mamoru KITAURA, Kazutoshi FUKUI, Takeshi MIYANAGA,+
Masami FUJITA* and Makoto WATANABE◇

Department of Electrical and Electronics Engineering, Faculty of Engineering, Fuki University, Fukui 910
+Department of Physics, Faculty of Education, Wakayama University, Wakayama 640
*Maritime Safety Academy, Kure 737
◇Institute for Molectular Science, Okazaki 444

Cadmium chloride (bromide) crystallizes in a layer–type structure. A cadmium ion is located at the center of an octahedron composed of six halogen ions sitting at the vertices. The top of the valence band consists mainly of halogen 3p (or 4p) orbitals while the bottom of the conduction band has cadmium 5s character. Intrinsic absorption corresponds to the transitions from np (halogen) to 5s (cadmium). Two luminescence bands (UltraViolet and Yellow) are observed with UV–light excitation in the fundamental absorption region. They are associated with radiative decay of self–trapped excitons (STE). The STE–states in $CdCl_2$ and $CdBr_2$ are believed to be the excited states of the $[Cd^{2+}X_6^-]^{4-}$–complex molecular ions (X=Cl or Br), that is, optically created excitons cause formation of the complex ions to localize around them. The lowest excitonic state is the T_{1u} state of which the electron–hole configuration is expressed as $\{a_{1g}(\sigma^a),t_{1u}(\pi^n)\}$ with using the molecular orbitals of $[Cd^{2+}X_6^-]^{4-}$ in O_h symmetry. This state split into E_u and A_{2u} states by the axial field of D_{3d} symmetry. The STE state connected to the UV emission is assigned to the A_{2u} state in D_{3d} symmetry. On the other hand, the Y–emission is related to the Eg state arising from the $\{a_{1g}(\sigma^a),e_g(\sigma^a)\}$ configuration.

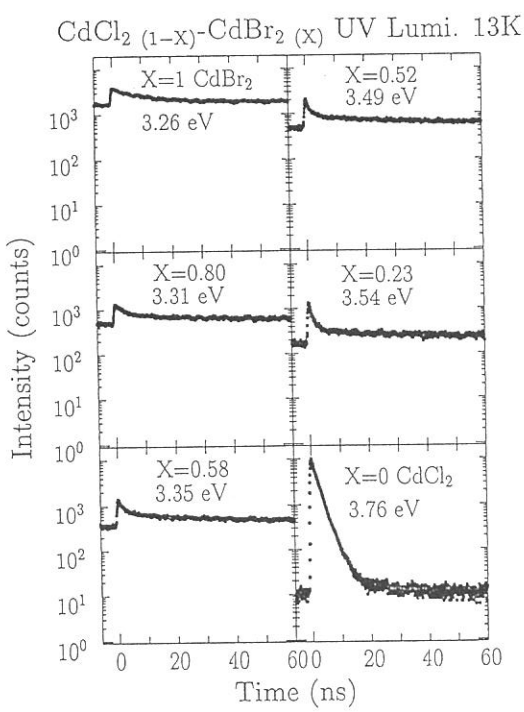

Fig.1

The UV–emission would be directly connected to the STE of the lowest energy exciton. The decay curves of the UV-emission consist of two exponential components, namely, the fast (τ_f=2.0 ns for $CdCl_2$ and 11 ns for $CdBr_2$) and the slow($\tau_s \gg 178$ ns) ones. They are attributed to the radiative decay of the spin singlet and triplet STE's. The existence of the triplet component indicates that some of optically created singlet excitons are switched into the triplet ones through spin-orbit interaction. The decay profiles of the UV–emission much differ between $CdCl_2$ and $CdBr_2$ in the time-integrated intensity ratios of τ_f to τ_s components (97:3 for $CdCl_2$, 6:94 for $CdBr_2$), which reflects the difference between Cl^- and Br^- in the strength of the spin-orbit interaction.

Decay profiles of the UV–emission were investigated on the $CdCl_{2(1-X)}$-$CdBr_{2X}$ mixed crystals, where X denotes the concentration of $CdBr_2$ in the mixture. Excitation was made with single-bunched undulator radiation from UVSOR (36eV, 0.5 ns duration, 178 ns interval).

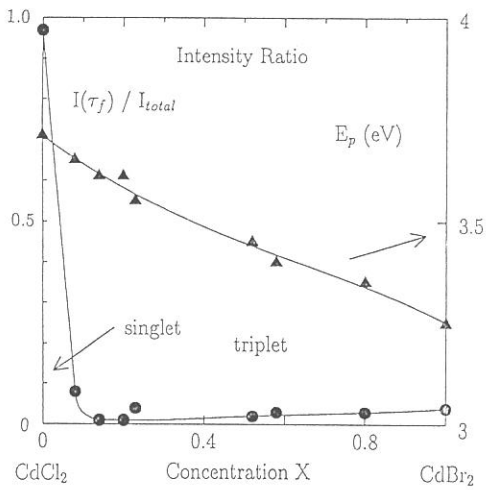

Fig.2

The observed results are shown in Fig.1. As increasing X in the mixed crystal, the decay profile changes rather drastically from the $CdCl_2$– to the $CdBr_2$–type in the region of $X < 0.2$. On the other hand, the UV–emission spectral band shifts rather continuously from 3.76 eV to 3.26 eV and enhances its intensity gradually, when increasing X.

In Fig.2 are shown concentration dependence of the peak position and the time-integrated intensity ratio of the fast (singlet) component to the total intensity of the UV-emission in the $CdCl_{2(1-X)}$-$CdBr_{2X}$ mixed crystals. As increasing X from 0 to 0.1, the intensity ratio of the fast component decreases abruptly from 0.97 to 0.02. Above $X = 0.1$, almost all UV-luminescence comes from the slow (triplet) components. The peak position of the UV-emission band shifts almost linearly with X from thatin $CdCl_2$ to that in $CdBr_2$.

The figure 3 shows the STE-states associated with the UV-emission. The A_{2u} state is the excitonic state having a hole on the a_{2u} molecular orbital derived from the halogen np (n=3 for Cl^- and 4 for Br^-) and an electron on the antibonding a_{1g} orbital derived from the cadmium 5s. This state split into the singlet and the triplet states by exchange interaction as shown in the figure. The singlet state is connected with the lowest excitonic absorption band. In STE, these states correspond to the initial states responsible for the UV-emission. The fast decay component of the UV-emission comes from the singlet state which is populated directly with the optical excitation, while the slow decay component is related to the triplet state which is not to be populated without spin-orbit interaction. The triplet state split into two states with s-o interaction and further split with a Jahn-Teller distortion as shown in the figure. Atributing to these states, the slow decay component is further decomposed into three components ,the temperature dependence of which shows rather complex behavior due to phonon-assisted nonradiative processes among these adjacent three levels.

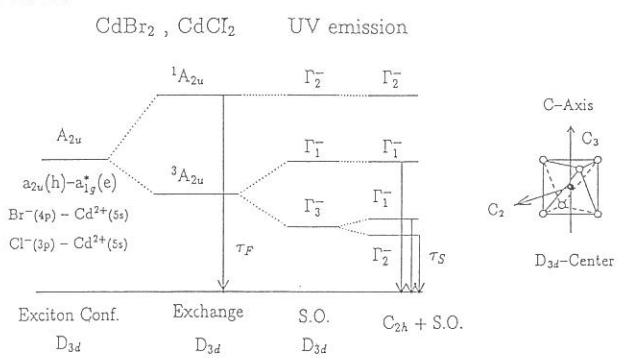

Fig.3

In conclusion, The S-T conversion rate increases surprisingly with increase of X in the region below 0.1 in the mixture, which is explained with larger s-o interaction and smaller electron affinity of Br^- than those of Cl^-.

LUMINESCENCE DECAY OF Pb ION CLUSTERS IN $Pb_{1-x}Cd_xI_2$ SOLID SOLUTIONS

Ping GU, Masayuki WATANABE* and Tetsusuke HAYASHI*
Department of Physics, Kyoto University, Kyoto 606, JAPAN
**Faculty of Integrated Human Studies, Kyoto University, Kyoto 606, JAPAN*

By an admixture of a small amount of PbI_2 into a crystal of CdI_2, Cd ions are substituted with Pb ions randomly in the two dimensional cationic layer of the D_{3d} type crystal. The heavy doping gives rise to a solid solution of $Pb_{1-x}Cd_xI_2$ in which small aggregates or clusters of Pb ions are dispersed in CdI_2 matrix. The lowest energy absorption of the solid solution in the range of x from 0.9 down to 0.5 is associated with an electronic excitation of Pb ion clusters, originating from 6s-6p transition of Pb ions.[1] Optical excitation of the cluster induces a luminescence band near the absorption edge. In order to investigate the character of the excited states in the cluster, we have studied the decay characteristics of the luminescence.

In Fig.1(a) are shown emission and excitation spectra measured on a sample with x=0.7 at 10K. The spectrum denoted by "Total" is the emission measured under steady state excitation at 2.80eV. The broken curve is the excitation spectrum measured at the emission peak. A decay profile of the emission measured at 2.75eV is shown in (b). It consists of a fast and a slow decay components. The inset shows the time response of the fast component measured with short light pulses from the beam line BL1B of UVSOR under single bunch operation. The dotted curve is the response function of the detection system (a microchannel plate photomultiplier equipped with a time-correlated single photon counting system) , and the decay time of ~600ps was derived by a deconvolution analysis. The time resolved emission spectra for the fast and slow components are shown in (a) denoted by F and S. The emission band of the slow component is clearly seen to locate at an energy lower than that of the fast component. It is natural to suppose that the fast and slow components of the emission originate from singlet and triplet manifolds of the excited state of a cluster. The splitting energy between singlet and triplet bands has been found to increase with the decrease in the content of Pb ions, and hence with the decrease in the cluster size. The result can be explained in terms of the change in the strength of an exchange interaction between electrons and holes due to their confinement in the cluster. Details of the discussion will be given elsewhere.[2]

In Fig.2 are shown emission spectra of the fast component (curves) and the decay times (dots) measured at various emission energies for three different excitation energies. The emission band shifts to lower energy with the decrease in the excitation energy. Excitation in the lower energy region corresponds to excitation of clusters with larger size. The decay times, being nearly constant against the emission energy as seen in (b) and (c), would be due to selective excitation of larger clusters, and it must be determined by a radiative decay rate of the excited singlet state of a cluster and the relaxation rate into the triplet state.

On the other hand, for excitation in higher energy region (case (a)), the decay time changes remarkably with the emission energy. This fact indicates that the emission band is composed of that from various clusters with different size. Furthermore, it is to be noted that the value of the decay time in higher emission energies is lower than those in (b) and (c), while it is higher for lower energy emission. The fact suggests that excitation of clusters with larger size is induced by an energy transfer from those with smaller size. The transfer rate is of a similar order of magnitude to the radiative decay rate, which suggests the dipole-dipole transfer process.

References

[1] A. Ishibashi, M. Watanabe and T. Hayashi: J. Phys. Soc. Jpn. **62** (1993) 1767.
[2] T. Hayashi, P. Gu and M. Watanabe: to be published in Solid State Commun.

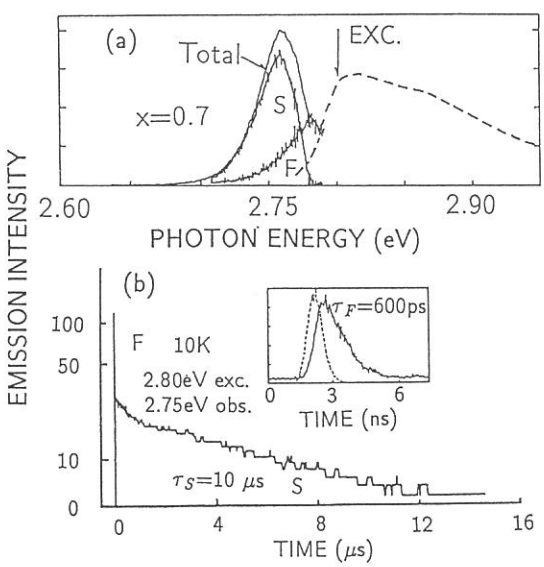

Fig.1 (a):Emission and excitation spectra at 10K in $Pb_{1-x}Cd_xI_2$ with x=0.7. F and S are time-resolved emission spectra of the fast and slow decay components. (b):Decay profile of the emission at 2.75eV. The inset is the time response of the fast component.

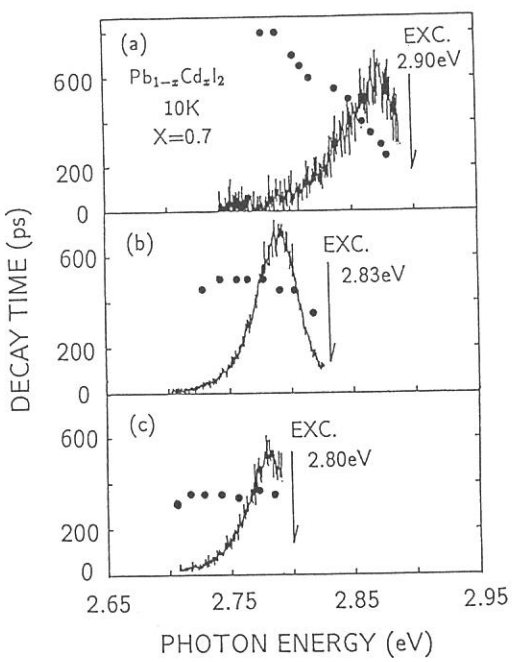

Fig.2 Emission spectra of the fast decay component measured for three excitation energies. Decay times (dots) are plotted as a function of emission energy.

VARIATION OF DECAY CURVES FOR AUGER-FREE LUMINESCENCE FROM BaF_2 AGAINST EXCITING PHOTON ENERGY

Norihisa YAHAGI, Yoshihiko NUNOYA, Zian-zhi RUAN(GEN) and Shinzou KUBOTA
Rikkyo University, Nishi-Ikebukuro 3, Tokyo 171

Non-radiative process of the outermost core holes at the distance of the order of 100 Å from the crystal surface is proposed to interpret the very fast component with decay time from 0.3 ns to 0.6 ns for Auger-free luminescence(AFL) from BaF_2 and CsCl crystals in our previous paper[1]. In order to confirm the non-radiative process near crystal surface, the decay curves of the AFL from BaF_2 were measured for different excitation photon energies from the threshold energy E_{th} of the excitation of the outermost core holes upto 35 eV for the luminescence intensity down to the 1/5000 of the peak intensity.

Figure 1 shows typical decay curves from the cleaved BaF_2 crystal excited under 23 eV and 28 eV photon excitation at normal incident angle. The absorption lengths are 60 Å and 140 Å for 23 eV and 28 eV photons, respectively[2]. The decay curves have a very fast luminescence component of decay time of 0.3 ns and the main luminescence component of 0.83 ± 0.17 ns as reported in[1], together with a slow component of decay time of 4.3 ± 1.0 ns. The faster decrease in the intensity is observed under 23 eV photon excitation compared with that under 28 eV photon excitation. The decay curves after about 3 ns from the peak intensity are nearly independent of excitation photon energy. The intensity of the slow component of 4.3 ns is about 2 % of the total intensity.

Figure 1 also shows the luminescence decay curve from polished crystal with 23 ev photons. It is expected that the polished crystal may have some additional defects at near crystal surface compared with those in a cleaved crystal. Polishing procedure is the same as that for the preparation of a crystal for scintillation counter: first polished with SiC no. 300-1000, then finally polished with aluminum no. 2000-8000. The faster decrease in the intensity is observed for the polished crystal, as compared with that for the cleaved crystal.

The quenching rate $Q(t=3ns) = -\ln[I(t=3ns)/I_0(t=3ns)]$ is introduced in[3]. Here, $I(t)$ and $I_0(t)$ are the measured time dependence and that for the radiative decay free from non-radiative process. In Fig. 2, the measured $Q(t=3ns)$ values are plotted against excitation photon energy together with the absorption coefficient reported in [2]. The large $Q(t=3ns)$ values are observed in the energy region of E_{th} to 26 eV, in which the absorption coefficient is large.The smallest $Q(t=3ns)$ at 28 eV is observed in the energy less than $E_{th} + E_g$. The larger $Q(t=3ns)$ at 32 eV is explained in terms of the non-radiative process induced by interaction of the outermost core hole and the electronic excited state that is produced by the photoelectron being accompanied with the outermost core hole[3].

In conclusion the very fast component of AFL from BaF_2 crystal under vuv photon excitation is explained in terms of the additional non-radiative process of the outermost core holes at near crystal surface.

REFERENCES

1. Y.Nunoya, J.Ruan(Gen) and S.Kubota, Nucl. Instr. and Methods, in press.

2. C.Tarrio, D.E.Husk and S.E.Schnatterly, J.Opt. Soc.Am. B8,1588(1991).

3.M.A.Terekhin, A.N.Vasil'ev, M.Kamada, E.Nakamura and S.Kubota, Progress Report of this volume.

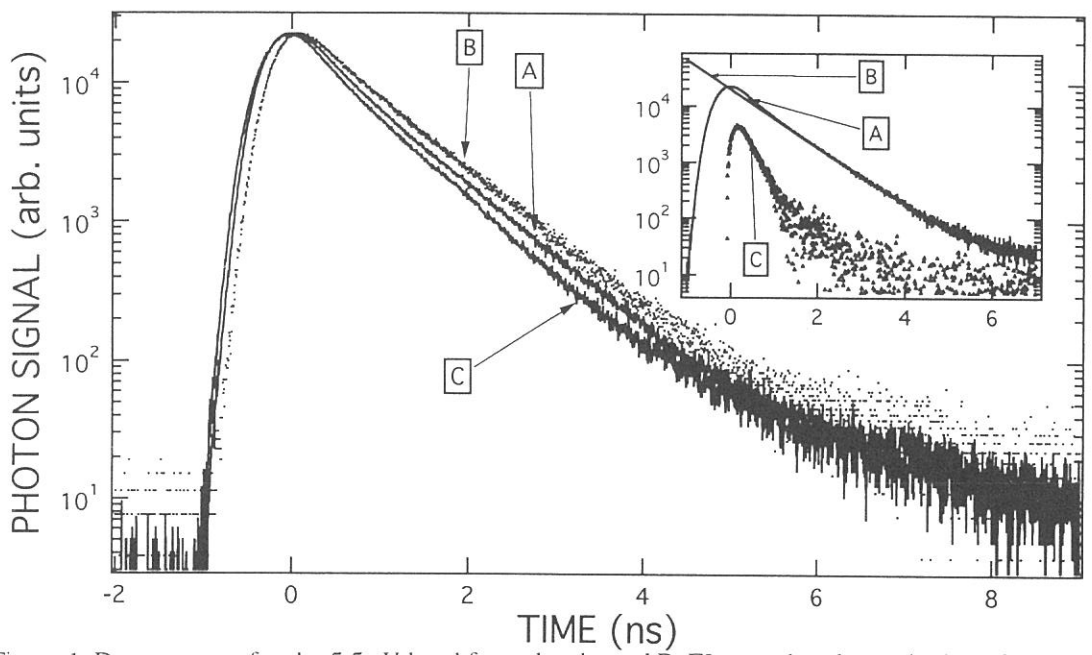

Figure 1. Decay curves for the 5.5 eV band from the cleaved BaF2 crystal under excitation of 23 eV photons(A) and excitation of 28 eV photons(B), and the decay curve from the polished BaF2 crystal under excitation of 23 eV photons(C). Inserted figure shows the decay curve for the 23 eV photon excitation(A), the fitted curve with two decay times of 0.83 ns and 4.3 ns(B). The curve (C) is the very fast luminescence component.

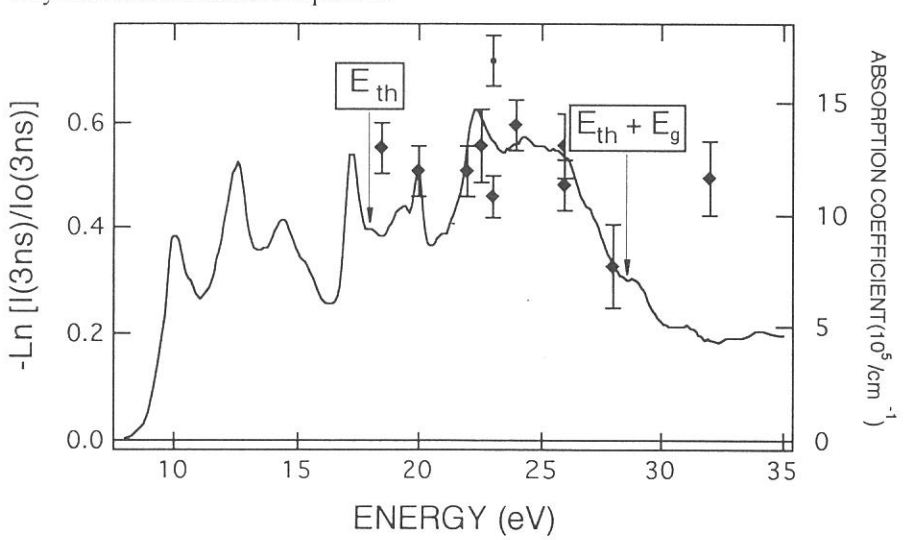

Figure 2. The measured Q(t=3ns) values from the cleaved BaF2 crystal(♦) and from the polished crystal (•) plotted against excitation photon energy together with the absorption coefficient reported in [2].

EXCITATION SPECTRA OF LUMINESCENCE σ-BAND IN KBr THIN CRYSTALLINE LAYERS GROWN ON KCl SUBSTRATE.

Arisato EJIRI, Akira HATANO and Kazumichi NAKAGAWA*

Faculty of Education, University of Ryukyus, 1 Senbaru, Nishihara, Okinawa 903-01.
*Faculty of Human Development, Kobe University, 3-11 Tsurukabuto, Nadaku, Kobe 659

The present authors have first observed the intrinsic luminescence σ-band of KBr crystalline thin layers[1] and suggested that the substrate excitation strongly affects on the observed band in its intensity. In the present studies, excitation spectra of the σ-band in the KBr thin layers grown on KCl single crystal substrates, as well as in KBr and KCl bulk crystals, are observed, and the substrate excitation effect is clearly revealed.

The KBr thin layers were grown on the creaved surface of KCl single crystals in the vacuum of 2×10^{-6}Torr by means of the molecular vapor deposition technique consisting of a slow deposition rate of 1nm/min and of a thermal annealing at 180 C for 15 minutes. Luminescence experiments were performed at BL-1B by the use of a 1m Seya-Namioka monochromator with a slit width of 10Å band path and also the use of a Jobin-Ybon grating monochromator with a slit width of 20Å. Excitation spectra of the σ-band were measured in the photon energy range 6-12 eV at 30K in the vacuum more than 2×10^{-8}Torr. The observed excitation spectra for the σ-band (4.53eV) of the KBr 200Å layer and for that (4.43eV) of the KBr bulk crystal are partially shown in Fig. 1. The later spectrum well coincides with previous literatures[2,3] in its profile. Difference of the former from the later means that the 200Å layer spectrum (the former) includes some KCl-substrate-excitation-effect. In order to estimate the effect, the bulk spectrum multiplied a small factor is subtracted from the layer spectrum.

Remained spectrum is shown in Fig. 2 with an absorption spectrum of KCl at 10K[4] for comparison. It can be said that the profile of the remained spectrum starting to rise at 7.5 eV and gradually increasing in the high energy region indicates the contribution of the electron excited in the substrate to the luminescence σ-band in the layer. A sharp peak existing at 8.2 eV corresponds to the high energy tail of the Γ-exciton in KCl and also to the conduction band edge of KBr.[5] This suggests the presence of some interactions between a discrete exciton level of KCl substrate and a continuum state of the KBr layer at the interface.

References

1) A. Ejiri, A. Hatano and K. Nakagawa; UVSOR Act. Rep. (IMS) 1991, 44.
2) M. Ikezawa and T. Kojima; J. Phys. Soc. Jpn. 27 (1969) 1561.
3) M. Yanagisawa, K. Kondo and H. Kanzaki; J. Phys. Soc. Jpn. 52 (1983) 4937.
4) K. Teegarden and G. Baldini; Phys. Rev. 155 (1967) 896.
5) A. Ejiri, A. Hatano and K. Nakagawa; J. Phys. Soc. Jpn. 63 (1994) 314.

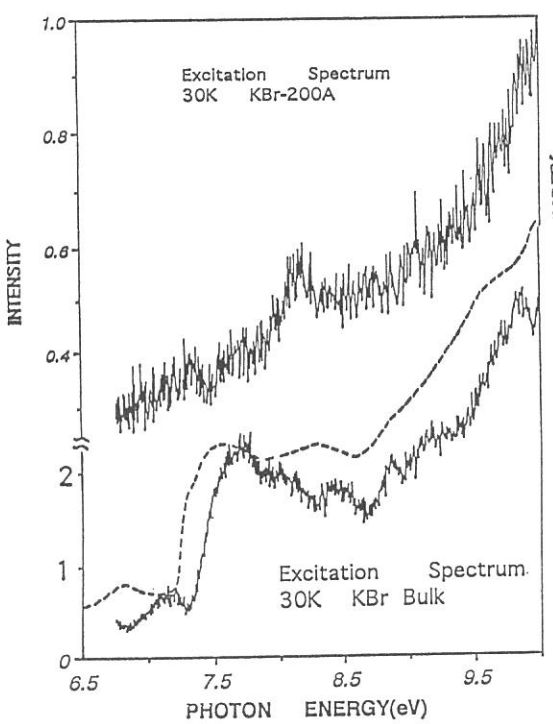

Fig. 1. Excitation Spectra of σ-band in KBr-200Å and in KBr-bulk. Broken line curve is a previous data of KBr-bulk from Ref. 3.

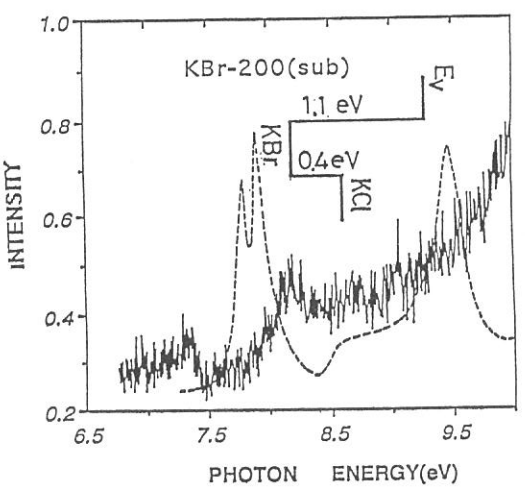

Fig. 2. Remained Spectrum of KBr-200Å and an absorption spectrum of KCl (broken line) from Ref. 4. Vertical lines indicate the vacuum level (E_V) and bottoms of the conduction band in KBr and KCl.

Exciton Absorption Spectrum of CuCl Microcrystal under Pressure

Takao NANBA, Toshiaki TAKAGI and Toshihiro NOTAKE

Department of Physics, Faculty of Science, Kobe University
Rokkodai 1-1, Nada-ku, Kobe 657

The exciton absorption spectrum of CuCl microcrystal under pressure was measured at 100 K. In the bulk state of CuCl, the Z_{12} and Z_3 exciton absorption bands appear at 3.29 and 3.22 eV . They correspond to the electronic transitions from the Γ_8 and Γ_7 valence bands to the Γ_6 conduction band, respectively. The purpose of the present experiment is to make clear the behavior of the exciton state of CuCl in the microcrystalline state in relation with the structural phase transition under pressure. In general the exciton state in the microcrystal state suffers from the quantum size effect according to the decrease in the size of the particle. Such phenomenon at normal pressure has been studied by many groups from the optical study. However, the response of the exciton state in the microcrystal to homogenious high pressure has not been studied yet. The volume compression by the applied pressure decreaes , for example, continuously the size of the particle and leads to the increase of the quantum size effect. In addition, the study of the phase transition in the microcrystal under pressure through the spectral change under pressure is very interesting subject to investigate the role of atoms at surface in the phase transition in the microcrystal. In the microcrystal, the critical pressure for the phase transition might be different from that in the bulk state because of the important role of atoms at surface.

The CuCl fine microcrystal was prepared by a conventional gas evaporation technique . Obtained CuCl microcrystals were mixed with silicon grease which works as a pressure transmitting material. The shape of the microcrystals and the size distribution were observed by an electron microspopic experiment. The shape was found to be almost spherical. The size of CuCl microcrystals which was used in the present experiment was rather large and 1950 A in average. In general, the quantum size effect of the exciton state in the mezoscopic system is considered to occur ,for example, for the case of particle of which size is smaller than about 20 times of a Bohr radius of the exciton. Such critical size of CuCl is considered to be smaller less than about 500 A. In the present experiment , the energy positions of two peaks observed in the microcrystal CuCl at normal pressure coincided well with those of the bulk. This means that the quantum size effect does not occur for the present case in consistent with the result of the electron microspopic observation.

The conventional lever-arm diamond anvil cell was used as the pressure cell up to 8 GPa installed at the BL1B spectroscopic system of the UVSOR.

Obtained absorption spectra of CuCl microcrystals at 100 K from 3 to 4.5 eV energy range are shown in Fig.1. At normal pressure Z_3 band of the exciton state appeared at 3.22 eV and the Z_{12} at 3.28 eV. The peak positions were coincided with those of bulk CuCl because of the large particle size. With pressure the peak showed a blue shift and the intensities decreased rapidly. At pressure between 4.6 and 5.1 GPa, the profile of the absorption spectrum suddenly changed. The observed peak positions of the Z_3 and Z_{12} bands were plotted with pressure in Fig.2. Double vertical broken lines means the pressure region at which the phase transition from a zinc blende structure to a tetragonal

occurs in the bulk state. In the tetragonal structure , the Z_3 band disappered and the Z_{12} band splitted into two peaks. The slopes of the lines which show the energy shift of the Z_3 and Z_{12} peaks with pressure were smaller than those in the bulk state. The precise analysis revealed that such difference in the slope of the curves can be explained if the volume compressibility of the microcrystal becomes smaller by 26 % than that of the bulk state. This means that the material becomes harder in the microcrystal than in the bulk state. Futher analysis is now on progress.

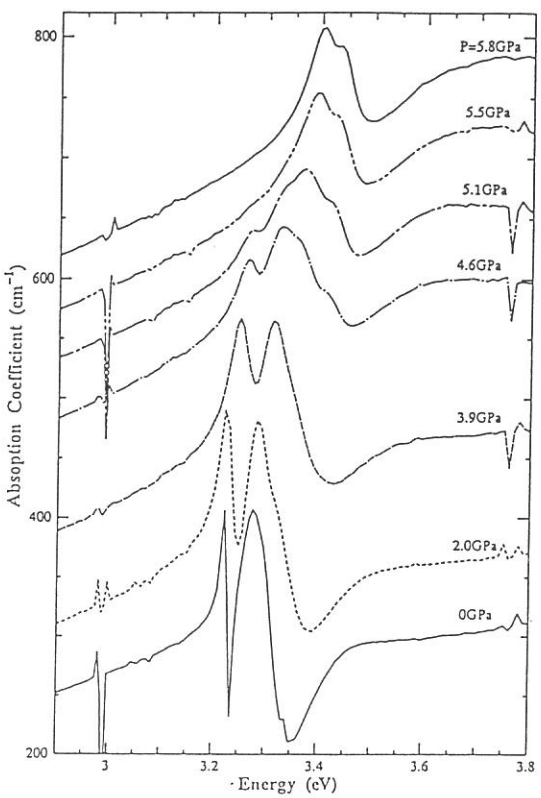

Fig.1
Absorption spectra of CuCl microcrystals with pressure at 100 K.

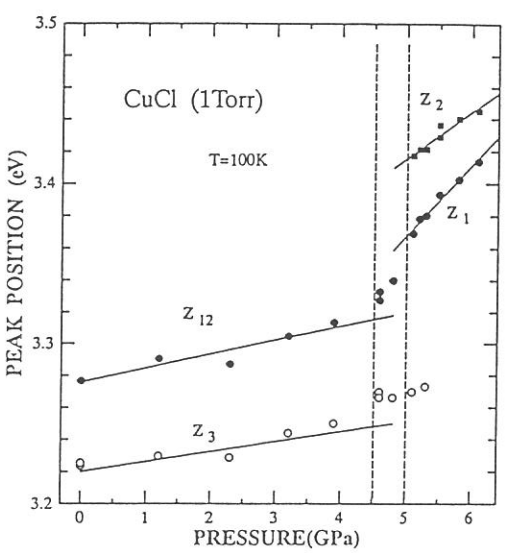

Fig.2
Plotting of the peak positions of Z_3 and Z_{12} bands shown in Fig.1

FLUORESCENCE SPECTROSCOPY OF CRAB MUSCLE FIBERS USING SYNCHROTRON RADIATION FROM UVSOR:EFFECT OF MAGUMESIUM ION

*M. Taniguchi, I. Yoda and N. Watanabe**

*Department of Physics, Faculty of Science, Nagoya University Chikusa-Ku, Nagoya 464-01 (Japan) and *Institute of Applied Physics, University of Tukuba, Tukuba 305 (Japan)*

Intracellular free magnesium concentration plays an significant role in muscle contraction. Effect of magnesium ion on the fluorescence of glycerinated crab muscle fibers in a rigor solution was measured. The time-resolved fluorescence from tyrosyl and tryptophanyl residues of the fibers was studied at the BL7b of UVSOR. The experimental setup for the excitation-emission spectroscopy is almost same as described previously (1). The excitation beam was passed through a 1 m Seya-Namioka monochromator in BL7B beam line and collimated a silica lens to a spot in a fused quartz cell. The fluorescence emission from the sample fibers was collect with fused quartz lenses. The emission viewed at 180^0 to the incident light axis was collected by a quartz lens and passed through a filter(350 nm) from emissions. Fluorescence decay times were measured by using the technique of time-correlated single photon counting under the single bunch. A bundle of glycerinated fiber from crab *Portunus puber* which was prepared by 50 % glycerin and 10 mM buffer (pH 7.2) was used. The rigor solution contained 100 mM KCl, 5 mM EGTA, 10 mM phosphate buffer (pH 7.2) and various concentrations of $MgCl_2$. All fluorescence measurements were done at room temperature. Fig. 1 shows the excitation spectra of the rigor muscle as a function of magnesium concentration. The fiber has two bands peaking at 235, 275 and 295 nm, when emitted at 340 nm. We found that the band around 295 nm was dynamically changed by magnesium ion, as shown in Fig.2. The fluorescence intensities and decay times of the fibers were drastically changed around 3.5 of

p[Mg], indicating two conformers in the excited states.

(1) UVSOR Activity Report 1990 p119.

We are very grateful to Prof. K. Kamada and all staffs of UVSOR for their technical assistance. This study was carried out under the UVSOR Cooperative Research Program.

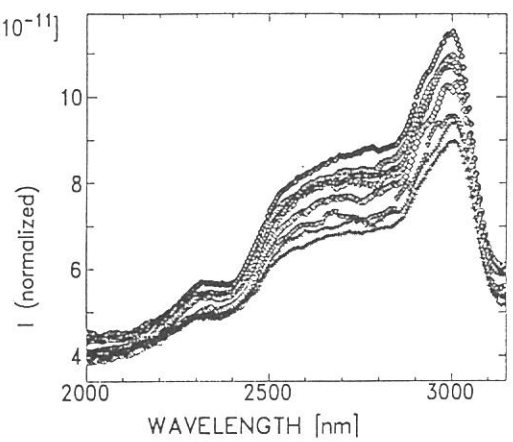

Fig. 1(a) Excitation spectra of glycerinated crab muscles in rigor solutions at various magnesium concentra tions. Emission at 350 nm.

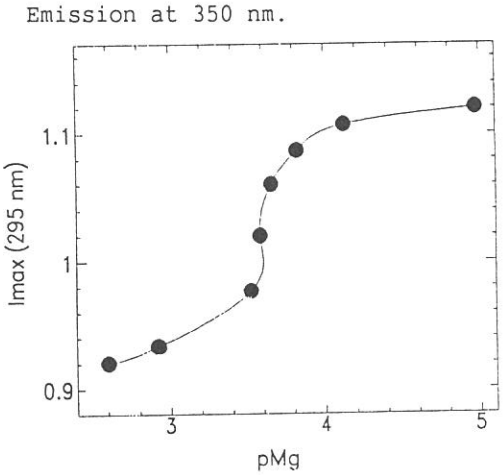

Fig. 2 Intensity maxima of excitation as a function of magnesium ion concentration. Excitation at 280 nm. Emission at 350 nm.

Soft X-Ray Microscope with Zone Plates at UVSOR

N. Watanabe[1)], S. Aoki[1)], Y. Shimanuki[2)], K. Kawasaki[2)], M. Taniguchi[3)], E. Anderson[4)], D. Attwood[4)], D. Kern[5)], S. Shimizu[6)], H. Nagata[6)], and H. Kihara[7)]

1) Institute of Applied Physics, Tsukuba University, Tsukuba
2) Department of Oral Anatomy, Tsurumi University, Yokohama
3) Department of Physics, Nagoya University, Nagoya
4) Lawrence Berkeley Laboratory, Berkeley, CA
5) IBM Research Center, Yorktown Heights, NY
6) Nikon Corp., Nishi-ooi, Shinagawa-ku, Tokyo
7) Physics Laboratory, Department of the Liberal Arts, Kansai Medical University, Osaka

A Soft x-ray imaging microscope with zone plates was set up at UVSOR BL8A and imaging tests were performed at 3.2 nm. This year, a photographic film was used as a detector instead of a microchannel plate (MCP), and the resolution was improved.

The optical system is almost the same with the last type. The system consists of a filter (SiN, thickness: 100 nm and Al, thickness: 39 nm), a condenser zone plate (CZP) (ϕ4.3 mm, outermost zone width: 0.25 μm. The third order radiation was used for illumination.), a pinhole (ϕ10 μm or ϕ30 μm), a specimen, and an objective zone plate (OZP) (ϕ50 μm, outermost zone width: 45 nm). The magnification ratio was 660. Using MCP monitored by an SIT camera, the field of view was searched and focused. Then, sliding the MCP perpendicularly to the optical axis, a soft X-ray image was taken with a photographic film (Fuji Mini copy HR II).

The performance was estimated using a zone plate as a specimen, which has the same characteristics with OZP. Fig.1 show the image of the zone plate. The observable finest zone width in Fig. 1 is 63 nm.

Dry biological specimens, such as diatoms (Fig.2), collagen fibers, and muscle myofibrils (Fig.3) were observed. An environmental chamber using SiN windows (thickness: 0.1 μm) was made and a preliminary test was performed at 2.4 nm. This result is shown in Fig.4.

In the present microscope, the numerical aperture of CZP was much smaller than that of OZP. To adjust both the numerical apertures in order to prevent 0th-order radiation of OZP from reaching the imaging field, an ellipsoidal condenser mirror system was made (Fig.5). This experiment is currently under way.

Acknowledgments

The author are grateful to the help and encouragements by Prof. M. Watanabe, Mr. T. Kinoshita, and other staffs of the Institute for Molecular Scinece. They also express their thanks to all sample suppliers.

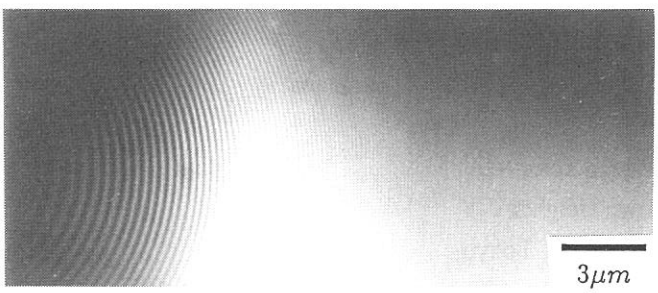

Figure 1. Zone plate image. Minicopy film, 5 min. A 63 nm pattern can be resolved.

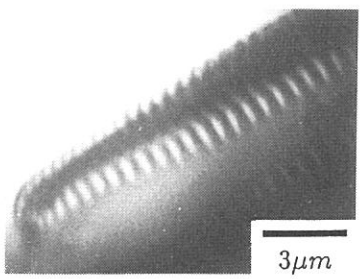

Figure 2. Diatom image. Minicopy film, 10 min.

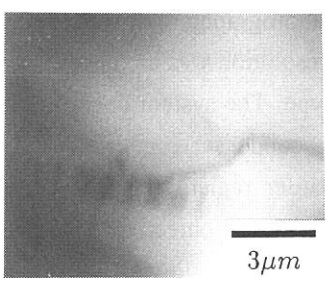

Figure 3. Rabbit myofibril image. Minicopy film, 12 min.

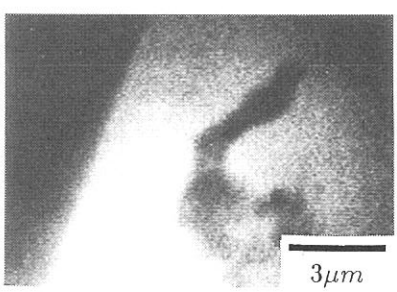

Figure 4. Image using the wet cell. MCP and SIT camera were used as a detector. Accumulation time: 4s.

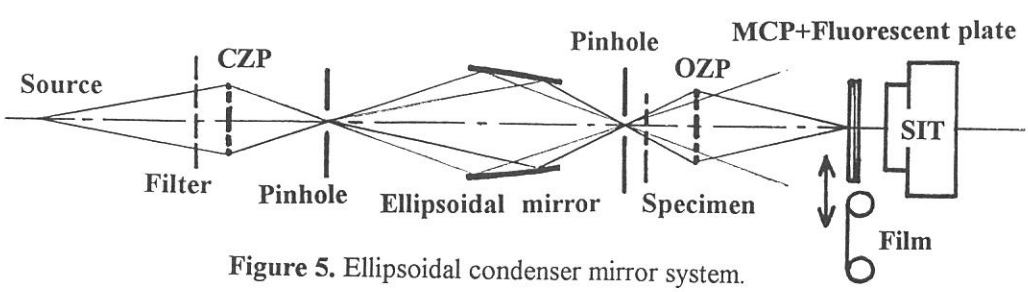

Figure 5. Ellipsoidal condenser mirror system.

Application of synchrotoron radiation to accumulated photon echoes

Hiroshi Itoh[1], Shunsuke Nakanishi[1], Masaya Kawase[2], Hitoshi Fukuda[3], Hiroki Nakatsuka[3] and Masao Kamada[4]

[1]Department of Physics, Kagawa University, Takamatsu 760.
[2]Department of Chemistry, Kagawa University, Takamatsu 760.
[3]Institute of Applied Physics,University of Tsukuba, Tsukuba 305.
[4]UVSOR, Institute for Molecular Science, Okazaki 444.

We have applied synchrotron radiation (SR) as a excitation source to investigate a phase relaxation time T_2 of an organic dye molecule doped in polymer. This is the first observation of incoherent accumulated photon echoes generated by the SR. The accumulated photon echoes are useful method to measure T_2 when the excitation source has the limited power intensity. Because the population grating formed in a sample can be efficiently accumulated by the continuous pumping if there exists a bottleneck state that has relatively longer lifetime, we obtain the large photon echo signal.

The experiment was performed at the BL-8A. The SR beam was filtered by a bandpass filter with the center wavelength of 605 nm and the bandwidth of about 13 nm. The beam was split into two beams, the pump and the probe beam, in a Michelson interferometer and the probe beam was temporally delayed relative to the pump beam. The pump and the probe beam were aligned to collinearly overlap. The pump beam was phase modulated with a piezoelectric transducer at f=6.5 kHz. The pump and the probe beams were focused onto the sulforohdamine 640 (SRh640) doped in polyvinyl alcohol (PVA) at 29 K. The transmitted beams were detected by a PIN photodiode and its output was fed into a lock-in amplifier.

The field autocorrelation curve of the excitation beam was measured to determine the time resolution of our echo experiment. Figure 1 shows the observed interferogram of the SR passed through the bandpass filter mentioned before. From this curve we can obtain the time resolution of about 133 fs. Side humps in the curve are attributed to the squarish transmission characteristics of the bandpass filter. The inset in Fig. 1 shows an enlarged trace of the correlation curve.

Figure 2 shows the accumulated photon echo decay curve on a logarithmic scale, where the delay time τ was scanned from 1.2 ps to 10 ps. The dephasing time T_2 obtained from Fig. 2 is about 4.8 ps. At a fixed delay time, ten data were taken after accumulating a population grating for 60 sec. Then the grating was erased by slowly changing the delay time until the next sampling delay time by taking 60 sec with the two excitation beams on.

In conclusion, we have shown, for the first time, that the SR beam is applicable to the nonlinear optical experiment such as accumulated photon echoes. Our echo

experiments show that it could be possible by the SR beam to time resolve the echo signals with resolution of less that 1 fs in the wide spectral range from VUV to far infrared.

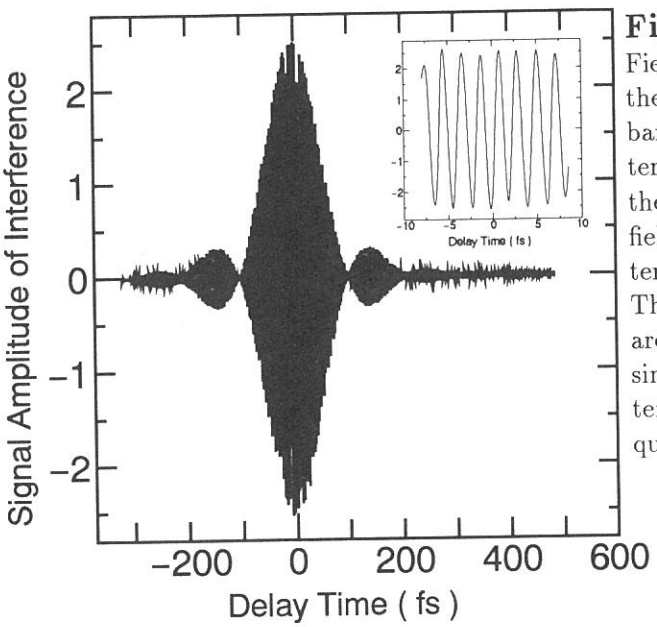

Fig. 1
Field autocorrelation trace of the SR beam filtered with a bandpass filter having the center wavelength of 605 nm and the bandwidth of 13 nm. The field correlation time is determined to be about 133 fs. The inset is an enlarged trace around $\tau = 0$, showing the sinusoidal modulation of interference at the optical frequency.

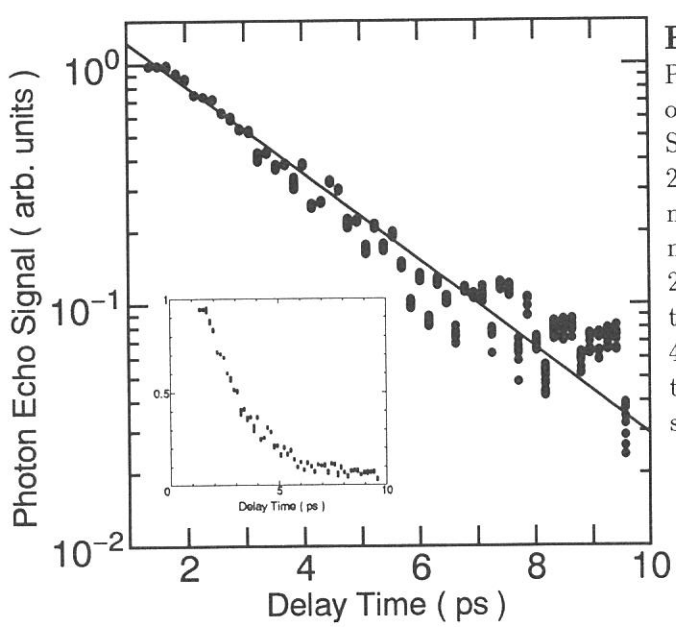

Fig. 2
Photon echo decay curve on a logarithmic scale for SRh640 doped in PVA at 29 K, showing the exponential decay of echo signal with time constant of 2.4 ps which corresponds to the dephasing time of 4.8 ps. The inset shows the same curve on a linear scale.

Imaging Plates as Recording Medium for VUV–XUV Photons

Kou KUROSAWA, Ryoichi SONOUCHI, Wataru SASAKI,
Masahito KATTO*, and Kazuo NAKAMAE*

Department of Electrical Engineering, University of Miyazaki, Miyazaki 889–21
**Department of Electronics, University of Osaka Prefecture, Sakai, Osaka 593*

For recording and storing data of two–dimensional image and spectra in VUV and XUV, AgBr films have been used so far in spite of their disadvantages of narrow dynamic range and low sensitivity. Recently photostimulable phosphor has drawn special attention in medical x–ray diagnostics because of their advantages of high sensitivity, wide dynamic range and easy data acquisition with computers. We have already confirmed that the imaging plates have the sensitivity for nanosecond pulsed ArF (193nm), KrF(248nm), and Ar_2 (126nm) excimer laser outputs as well as for continuous radiation in the x–ray spectral range and further the ability for recording the beam images. The next interesting point for us is to clarify the wavelength range over what imaging plates are usable. In order to make clear this point, we measure the wavelength dependence of the response of an imaging plate, and further confirm the linear response at several wavelengths.

An imaging plate which consists of $BaFBr:Eu^{2+}$ crystallites bound on a plastic sheet was placed in the sample chamber in the BL–1B beam line. The recording was performed by exposing an imaging plate to monochromatized radiation by a given duration. The recorded photon numbers were changed by changing the exposure time. As for stimulation measurements, a He–Ne laser was used. The emission induced by the photo–stimulation (PSL) was detected with a photomultiplier tube through an optical filter for decreasing the He–Ne scattered light intensity.

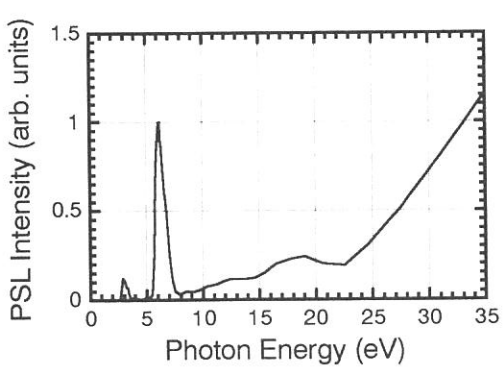

Fig. 1 Wavelength dependence of PSL intensity.

When SR photons were incident on the imaging plate during a constant time of 10s, we measured the PSL intensity. The relative PSL intensity defined as a PSL intensity for a given photon number, was calculated from the measured data and incident SR intensity. In Fig.1 is shown the relative PSL intensity as a function of incident photon energy.

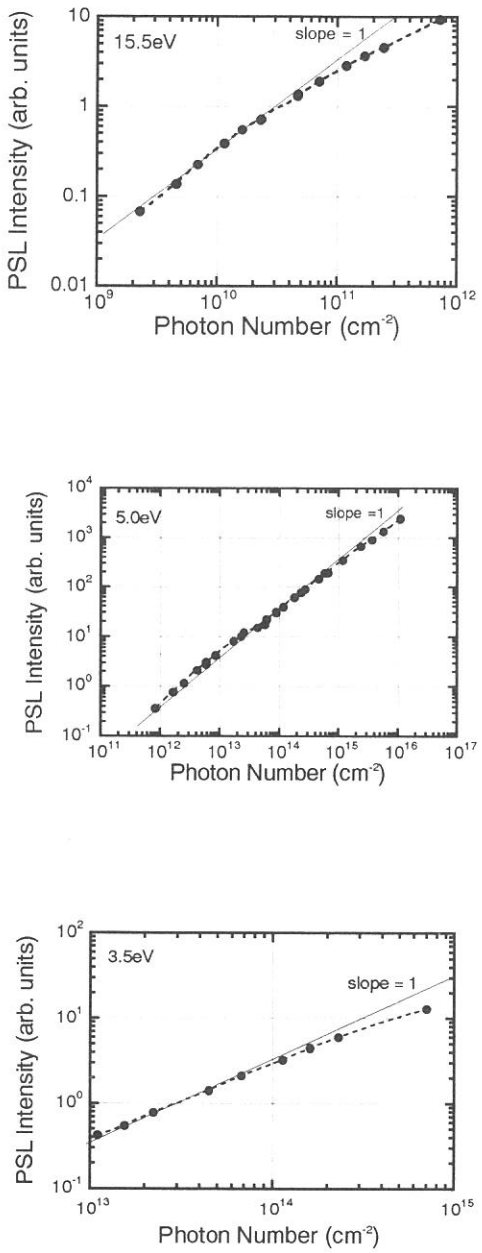

Fig. 2 PSL intensity plotted as functions of photon numbers.

There is such a tendency than the intensity increases exponentially with the incident photon energy except for two peaks around 3 and 6.2eV. The 3eV peak comes from a resonance effect for the excited and ground states of Eu^{2+} ions. The 6.2eV peak is considered to be due to a fact that the PSL intensity is determined by the product of the electronic transition probability and the penetration depth.

In order to confirm the linear response for incident photon numbers when the photon energy was fixed at 15.5, 5.0, and 3.5eV. The results are plotted in Fig. 2. For all photon energy taken here, the PSL intensity increased linearly in proportional to the photon numbers, although a tendency to saturate was observed above photon numbers. It should be noted here that the lower limit of the PSL intensity is determined with the detection system, and thus we can measure much lower photon numbers if we employ photomultiplier tubes with high sensitivity and efficient collection optics.

In summary, we have clarified that imaging plates have an ability to record incident photon numbers in the spectral range much wider than expected based upon the energy diagram, and that two-dimensional images such as laser beam pattern, holograms and spectra can be recorded and stored on the imaging plate in the visible to x-ray spectral range.

References

[1] M.Katto *et al.*, Rev. Sci. Instrum.,**64**(1993)319.
[2] M.Katto *et al.*, submitted to Opt. Engineer.

Diamond Film Mirrors for Vacuum Ultraviolet Excimer Lasers

Kou KUROSAWA, Ryoichi SONOUCHI, Wataru SASAKI,
Masahito KATTO*, and Kazuhito NISHIMURA**

Department of Electrical Engineering, University of Miyazaki, Miyazaki 889-21
**Department of Electronics, University of Osaka Prefecture, Sakai, Osaka 593*
***Osaka Diamond Industrial Co. Ltd., Sakai, Osaka 593*

In order to generate intense, short-wavelength, coherent radiation from rare-gas excimer lasers, one of the most important technical problems to be solved is the development of a cavity mirror with high reflectivity and high damage-resistance. Several materials have been tested as a cavity mirror for electron-beam pumped high-power krypton and argon excimer lasers which operate at 146 and 126nm, respectively. Among several materials so far tested, a SiC mirror provided the highest output energy of 80mJ but sometimes surface damages were observed, so that the SiC mirrors were not suitable for the stable operation. In our case because almost all materials have absorption coefficients as large as $10^5 cm^{-1}$, and because the laser output pulses have at most a $200MW/cm^2$ intensity and 5-10ns duration time, the main cause for the laser radiation damages is considered to be melting or decomposition of the mirror surface layers due to temperature rising by absorption. On the basis of the thermal and optical data, the most promising material becomes crystalline diamond, and the films have become to be grown by thermal decomposition of hydrogen carbides with relatively good quality. In this paper, we fabricate crystalline and amorphous diamond films, measure their reflectivity with the BL-1B beam-line at UVSOR, and test them as the cavity mirror for the krypton excimer laser.

Diamond films were deposited on sintered S_3N_4 ceramics by thermal decomposition of a CH_3+H_2 mixture. The thickness was around 15μm. The diamond crystals we re grown with the average dimension of 5μm under a suitable condition, and under a condition the films were amorphous. The surfaces finished by a diamond lapping method had 1nm-rms roughness.Reflection spectra were recorded over the wavelengths of 50-600nm at an incidence angle of 10 degree. The measured reflectance spectra are shown in Figs. 1 and 2. The reflectivity of the crystalline and amorphous films are not different from each other, and that at 146nm is 25%, which is very close to the reference one of 30%.

We have tested the two kinds of diamond mirrors as a cavity mirror of an electron beam pumped krypton excimer laser. In combination with a MgF_2 output coupler, we obtained the output energy of 70mJ for the crystalline diamond film mirror and that of 62mJ for the amorphous diamond film mirror. There is not significant difference in the output energy, but in the surface feature. For the case of the amor-

phous film mirror, the surface damage was observed when the output energy exceeded the value of 13mJ which corresponded to the fluence on the mirror surface of 160mJ/cm^2. On the contrary, the crystalline surface was not suffered from the damage for 70mJ which corresponded to the surface fluence of 875mJ/cm^2.

The diamond films can be deposited on substrates having any curvature. The radiation damage threshold of this kind of diamond mirrors was found to be higher than 4J/cm^2 based on the thermal failure considerations. The diamond mirrors are expected to be useful also as a grazing incidence mirror and as a substrate for multilayered coatings for intense extreme ultraviolet and x-ray radiations.

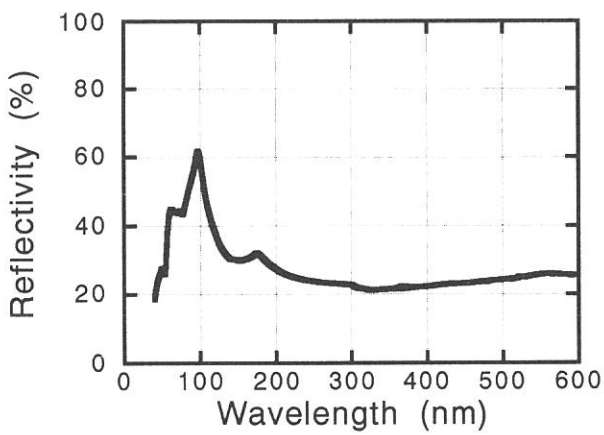

Fig. 1 Reflectivity curve of a crystalline diamond mirror.

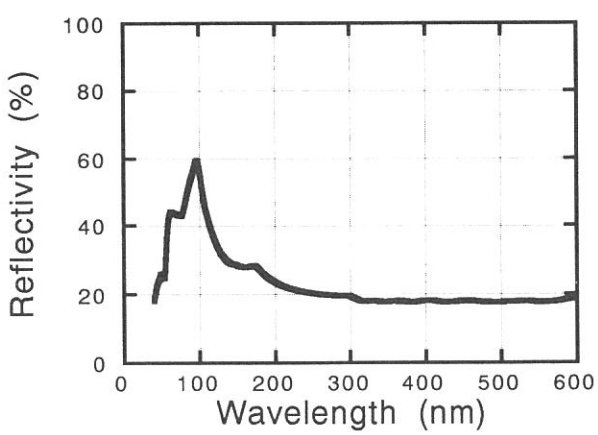

Fig. 2 Reflectivity curve of an amorphous diamond mirror.

References

[1] Kou Kurosawa *et.al.*, Rev. Sci. Instrum., **61**(1990)728.

[2] Kou Kurosawa *et al.*, IEEE J. Quantum Electron., **QE-27**(1991)71.

REFLECTANCE SPECTRA OF GaAs-AlAs-GaAs HETEROSTRUCTURES IN THE Al-2p ABSORPTION REGION

Koichi INOUE, Chen WU, Kazuhiro SHIBA, and Hisao NAKASHIMA

The Institute of Scientific and Industrial Research, Osaka University,
8-1 Mihogaoka, Ibaraki, Osaka 567

Many investigations have been made about valence excitons in semiconductor heterostructures, for example superlattices and quantum wells of AlAs-GaAs system. Core-excitons in the heterostructures, however, have not been well understood, owing to the experimental difficulties.

Intense core-excitonic structures of AlAs in the Al-2p core-excitation region have been firstly observed by M.K.Kelly et al. in partial-yield-photoemission spectra.[1] To obtain clean AlAs surfaces, they deposited a thin Al overlayer on a freshly cleaved GaAs substrate and subsequently activated the Al-Ga exchange reaction.

In the study of core-excitons, heterostructures have advantages and disadvantages. Since in heterostructures, the layer of interest is usually protected by some overlayers. As for AlAs whose surface is unstable in the atmosphere, the technique adopted by M.K.Kelly et al. is not necessary if the sample is covered with a stable GaAs layer. On the other hand, it becomes difficult to obtain signals from the layer through the overlayers.

In this report, we examined the possibility of detections of the Al-2p core-excitons in a GaAs(100Å)-AlAs(300Å)-GaAs heterostructure in the reflectance spectra. Samples were fabricated on a GaAs (100) substrate using the molecular-beam-epitaxy. Since the thickness of AlAs layer is probably thicker than the core-exciton radius, the Al-2p core-excitons in this layer will be almost the same with bulk core-excitons. Reflectance spectra were taken using the plane grating monochromator and the calibration chamber at BL5B.

Figure 1 shows the p-polarized reflectance spectra of the GaAs-AlAs-GaAs heterostructure in the Al-2p absorption region. The doublet structure due to Al-2p core-excitons is clearly observed in spite of the GaAs overlayer. For example in the spectra of 40 degrees of incidence, the topmost peak reflectance at about 76.5 eV is nearly twice as large

as the bottom reflectance at about 75.5 eV. Depending on the incidence angle indicated on the right side in the figure, the spectral shape is dramatically changed. Obviously, it is due to the interference effect in the GaAs overlayer. The reflectance spectra will be consistent with the previous result[1], though we can not compare them directly owing to the interference effect. Since the absorption coefficient of GaAs in this region has been known,[2] it will be possible to remove the interference effect numerically, and in the next stage of study, core-excitons in thinner AlAs layers will be interesting.

References

1. M.K.Kelly, D.W.Niles, P.Perfetti, E.Colavita, A.Savoia, G.Margaritondo and M.Henzler, *Phys. Rev.* **B32**, 5525 (1985).
2. For example, *Handbook of Optical Constants of Solids,* edited by E.D.Palik, (Academic Press, London, 1985).

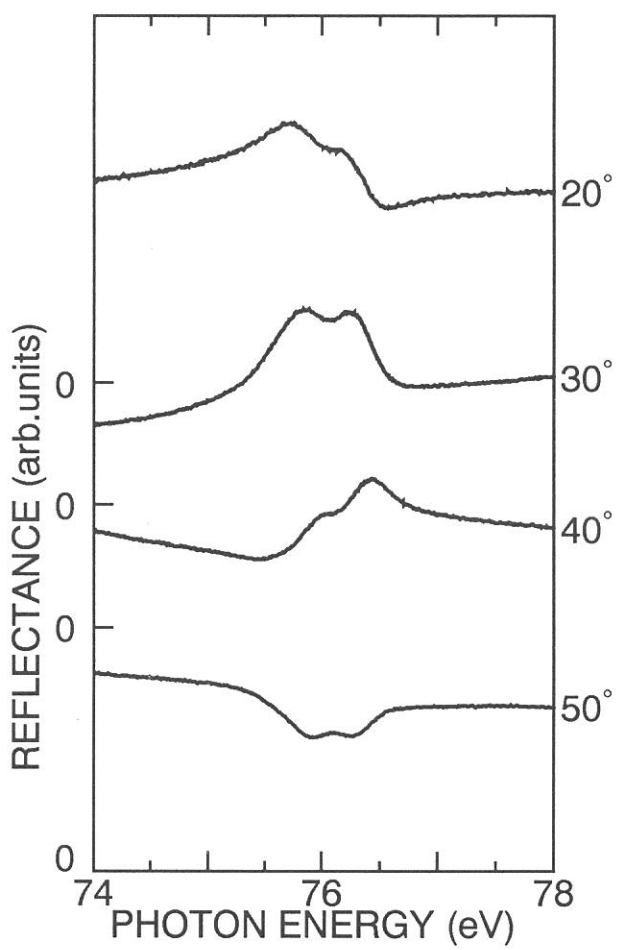

Fig.1. Reflectance spectra of the GaAs-AlAs-GaAs heterostructure in the Al-2p absorption region. The spectra were taken in the p-polarization. Incidence angles are indicated on the right side.

PHOTOINDUCED EFFECTS IN AMORPHOUS CHALCOGENIDE FILMS BY THE USE OF UVSOR

Koji HAYASHI, Daisaku KATO*, Shigeki TAKEDA*,
Koich SHIMAKAWA*, and Akira YOSHIDA+

Institute for Molecular Science, Okazaki 444
**Department of Electronics and Computer Engineering, Gifu University, Gifu 501-11*
+Toyohashi University of Technology, Toyohasi 441

Amorphous chalcogenide semiconductors show a variety of photoinduced effects[1]. The most prominent photoinduced effects in these material is the so-called photodarkening arising from the shift of the absorption edge. This darkened state can be removed by annealing at the glass-transition temperature. However, the details of the mechanism are still unknown. In this work, we investigate what kind of photoinduced effects in amorphous chalcogenides occurs by exciting inner core electron with the irradiation of the vacuum ultra-violet light.

Thin films of amorphous chalcogenide were prepared onto Corning 7059 substrates by the conventional evaporation technique. After evaporation, samples were annealed at near the glass-transition temperature for two hours in a vacuum with a pressure of 1×10^{-6} Torr. The experiments were performed at BL3A1 beam line of the UVSOR facility in Okazaki. The samples were irradiated with the vacuum ultra-violet light that is filtered through a Al film from undulator line and have 45 eV photon energy. The appropriate filter can efficiently cut the higher harmonic components of the undulator light.

Figure 1 shows the optical absorption spectra before and after irradiation. After irradiation, the optical absorption edge shifts to a lower energy side. This change is similar to the photodarkening with irradiation of bandgap light and is returned to the original state by annealing near the glass-transition temperature.

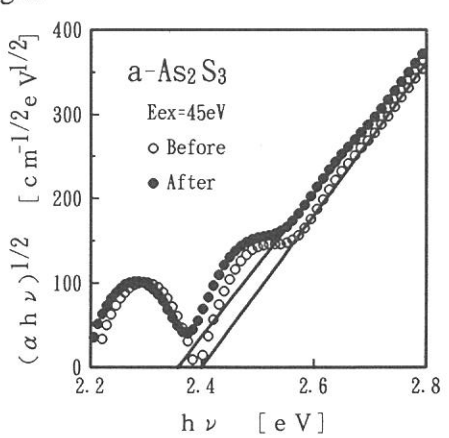

Figure 1 Optical absorption spectra of a-As_2S_3 film before (open circles) and after (closed circles) irradiation.

REFERENCE

1. Ke. Tanaka, Rev. of Solid State Sci., **4**(1990)641.

Ablation of Polymer by Simultaneous Irradiation of Oxygen Plasma and SOR Photon

Shinzo Morita, Chunlin Shao and Shuzo Hattori*
Nagoya university, CCRAST Nagoya 464-01, Japan
* Nagoya Industrial Science Research Institute,Nagoya 464,Japan.

A new process for resist stripping was proposed, which is performed by cooperative ablation with ring discharge plasma of oxygen and SOR X-ray photons.

For cooperative irradiation of the disk plasma and the SR photons on Si substrate coated by a resist, a discharge reaction chamber with a ring-shaped cathode was installed conveniently on the window of BL8A beam line chamber of UVSOR at Institute for Molecular Science, Okazaki National Research Institute.

The sample holder equipped with a water cooling system and a thermocouple can be moved along the horizontal direction in the reaction chamber to change the distance between the sample and the edge of active disk plasma in order to investigate effect of distance on the etching results.

The disk plasma was excited by a ring-shaped cathode of 8 cm diameter placed at the distance of 5 m away from the SOR source point, and operated in the soft vacuum electron-beam mode.

The Si substrate was set on the sample holder, in a downstream plasma, and the upstream plasma was operated at oxygen pressure of 0.02-0.27 Torr and a discharge power of 70-140 W.

The base pressure of the reaction chamber, which is pumped by a 330 l/s turbomolecular pump, was 1.0*10^-8 Torr. Then Oxygen gas of 99.999% purity was introduced into the discharge chamber through a mass flow controller. The Oxygen gas pressure in the reaction chamber was ranged from 0.02 to 0.27 Torr, and was controlled both by a gas flow rate in the gas inlet line and by a choke valve between the reaction chamber and the turbomolecular pump.

When the pressure in the reaction chamber was controlled at 0.3 Torr, the pressure in the differential pumping chamber was 2.0*10^-4 Torr which was limited value to maintain the ultra high vacuum of SOR beam line .

The pressure in reaction chamber was monitored by a pirani gauge and an ionization gauge.

The photon beam was introduced into a reaction chamber

through the disk plasma area and irradiated vertically on a sample surface.

The temperature of samples was maintained to be 27 C during the etching process.

In this experiment, the oxygen gas was introduced into the upstream of plasma, and the sample was set in a field-free downstream region.

In order to measure the ashing speed of resist, a silicon wafer coated with OFPR-800 resist (1.27 micrometer)was placed at a different distance from the disk plasma electrode of a 8.3 cm-diam ring cathode. The discharge was operated at an oxygen gas pressure Of 0.06 Torr and discharge power of 45W.

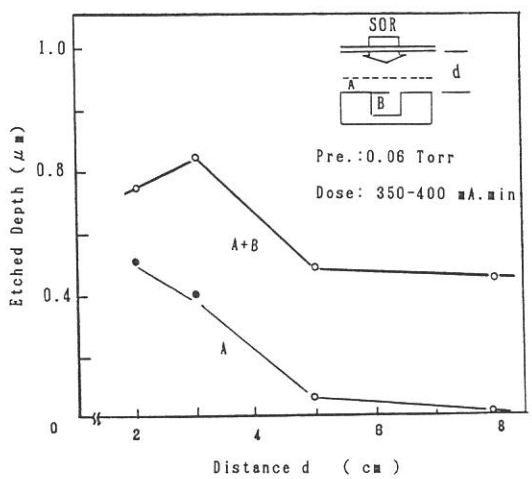

Fig.1, Relation between the etched depth and the distance.

Dependance of the etched depth on the distance, the DC discharge voltage, and the discharge time was investigated. The results are showed in Fig.1, Fig.2 and Fig.3.

It is clear that, the resist can not be etched perfectly until to surfasce of silicon by the SOR and oxygen radical,and ablation of resist can be enhanced at the some experimental conditions of high discharge voltage.

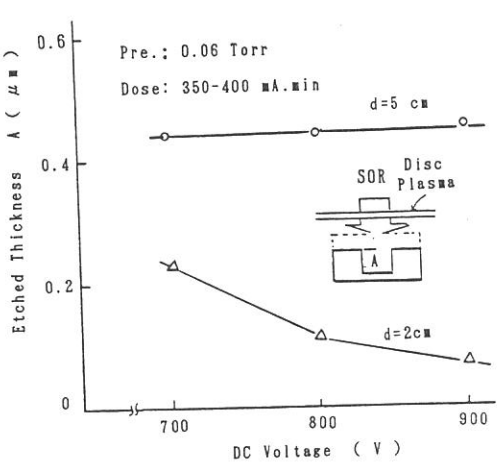

Fig.2, Dependance of the etched thickness A on the DC discharge voltage.

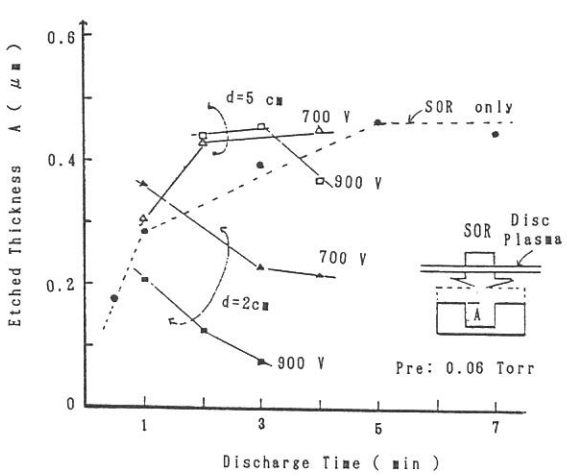

Fig.3 Relation between the etched thickness A and the discharge time.

Synchrotron radiation (SR) assisted deposition of carbon film employing methyl alcohol

Masanobu IKEDA, Muneto INAYOSHI*, Masaru HORI, Mineo HIRAMATSU*, Masahito NAWATA*, Toshio GOTO and Atsunari HIRAYA**

Department of Quantum Engineering , School of Engineering, Nagoya University, Furo-cho, Chikusa-ku, Nagoya 464-01
**Department of Electrical and Electronic Engineering, Faculty of Science and Technology 1-501, Shiogamaguchi, Tenpaku-ku, Nagoya 468*
***Institute for Molecular Science, Myodaiji, Okazaki 444*

Diamond has many excellent properties in mechanical, electrical and optical fields and has many applications for industrial materials. SR is one of the most effective excitation source in the vacuum ultra-violet (VUV) region where hydrocarbon gases have large absorption bands.[1] Considering that SR has been applied for the lithography process, SR is expected to be valuable for the fine pattern deposition of the thin film because it provides a high spatial resolution. Therefore, we consider that SR assisted deposition process is necessary for the formation of fine pattern of diamond thin film.

In the present work, we prepared a new chemical vapor deposition (CVD) system as shown in figure. 1 for the aim on the synthesis of a diamond thin film, where a film was deposited by the simultaneous irradiation of SR and CO_2 laser beams employing the methyl alcohol as the source gas. In this system, the base pressure was evacuated to 10^{-6} Pa, the SR and CO_2 laser beams were introduced perpendicular and at 60° to the substrate, respectively.

The experiments were carried out at BL8A of UVSOR. Ni (formed on SiO_2 by a vacuum evaporation technique) and Si (n-type (100) single crystal) were used as the substrates and the substrate was heated by the irradiation of continuous wave CO_2 laser (wave length 10.6 μm). Methyl alcohol was used as the source gas because it was generally applied to synthesize a diamond film using a plasma CVD[2] and also has the absorption bands for the wavelength of SR and CO_2 laser. Therefore, it is expected that the Methyl alcohol gas is dissociated effectively by SR and CO_2 laser irradiations. During the irradiation of SR beam to the substrate, the methyl alcohol pressure in the reaction chamber was maintained at 14.7 Pa. The dosage of SR to the substrate and the substrate temperature were varied from 23,000 to 80,000 mA.min and from 27 °C to 200 °C, respectively.

It was observed that the film was deposited only at the area of SR irradiation on the substrate. Figure 2 showed the dependence of deposition rate on substrate temperature. It was indicated that the deposition rate was decreased with an increase in substrate temperature.

The deposited films were characterized by Fourier transform infrared (FT-IR) absorption spectroscopy. Figures 3 and 4 showed the FT-IR absorption spectra of the films deposited on the Ni and Si substrate, respectively. The absorption peaks near 3500cm^{-1} and 2900cm^{-1} attributed to OH and CH bonds, respectively in the film deposited on the Ni substrate were not observed even at the room temperature. On the other hand, these bonds in the film deposited on the Si substrate were observed clearly. They decreased and the peak near 1000 cm^{-1} attributed to C-C bond on the Si and Ni substrate increased with an increase in substrate temperature From these results, it was assumed that the dissociated reaction of the methyl alcohol on the Si substrate by SR was quite different from that on the Ni surface.

Reference
(1) W. W. Duly : Laser Processing and Analysis of Materials (PLENUM PRESS, NEW YORK AND LONDON)
(2) M. Kadono, T. Inoue, A. Miyanaga, S. Yamazaki : Jpn. J. Appl. Phys.32 (1993) 3231

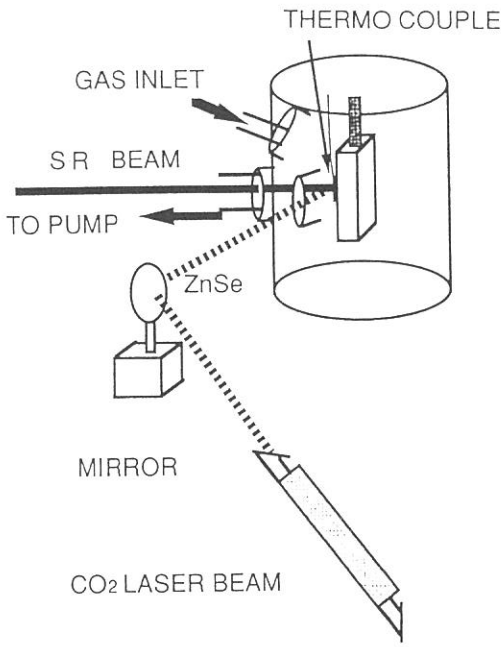

Figure 1. Schematic of SR-CVD system

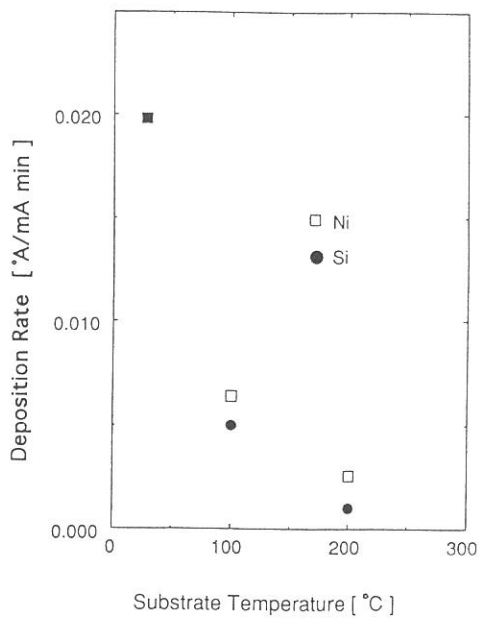

Figure 2. Dependence of Deposition rate on substrate temperature

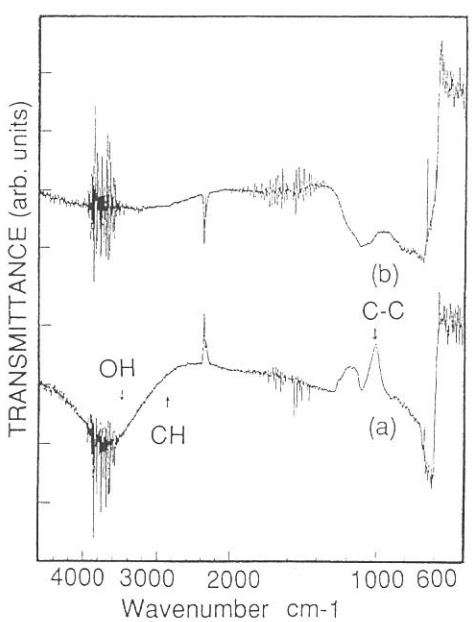

Figure 3. FT-IR absorptionspectra of film deposited on Ni substrate at (a)100 ℃ and (b)200 °C

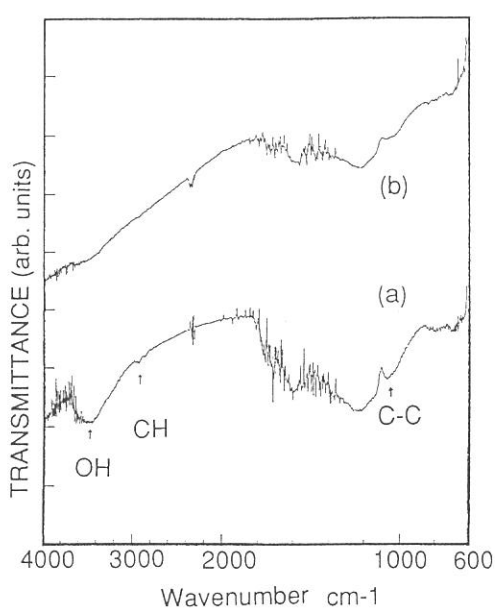

Figure 4. FT-IR aborption spectra of film deposited on Si substrate at (a) 27 °C and (b) 100 °C

LOW TEMPERATURE GROWTH OF ZnO FILMS BY PHOTO-ENHANCED CHEMICAL VAPOR DEPOSITION USING UNDULATOR RADIATION

Hideyuki OKABE and Akira YOSHIDA

Department of Electrical and Electronic Engineering, Toyohashi University of Technology, Tempaku, Toyohashi, 441, Japan

Recently, ZnO films have gained attention as transparent electrodes in many kinds of optoelectronic devices. ZnO films are preferable, because of low cost and high chemical stability, compared with SnO_2, In_2O_3 and ITO films.

In this study, we have deposited ZnO films on Si substrates using undulator radiation photo-CVD at room temperature for the first time and investigated the films with XPS.

We used growth and analysis system consisting of three chambers; preparation, growth and analyzer chambers. The schematic arrangement of the three chambers is shown in Fig. 1. The chambers were evacuated to around 10^{-6}, 10^{-8} and 10^{-9} [Torr], respectively. Films were grown in the growth chamber. DEZn and O_2 were used as source gases, and introduced through the variable leak valves. The O_2/DEZn ratio was changed from 10 to 2000. As a light source we used UR through no window from UVSOR facility. The spectrum of the UR with gap length of 60[mm] has a peak at 36.0[eV]. Si substrates were set in the evacuated growth chamber, and the source gases were introduced. After the deposition, in-situ XPS mesurements were performed in the analyzer chamber. The composition of the films was determined from XPS spectra. Increasing the O_2/DEZn ratio, we observed the increase of oxygen component on the film.

Fig. 2 shows the spectra in XPS mesurements. The peak in the spectra comes from O 1s peak. It is asymmetrical and decomposed into two peaks, as shown in Fig. 2. Dotted lines in Fig. 2 show two decomposed gaussian O 1s peaks: one from Zn-O bond and the other from hydroxide bond. In Fig. 2, the peak in low energy side is from Zn-O bond, and from hydroxide bond in high energy side. Increasing the O_2/DEZn ratio, we observed the increase of Zn-O bond.

From these results, we obtained the dependence of oxygen composition in ZnO films as a function of the O_2/DEZn ratio, as shown in Fig. 3. We also tried the deposition of ZnO films from O_2 and DEZn sources using an ArF excimer laser. A similar dependence is obtained with respect to the oxygen composition in the films. However, the former behavior

(UR enhanced CVD) is sharply dependent on the introduced gas ratio, suggesting a different deposition process between the two processes: ArF excimer laser-induced and UR-enhanced processes. The ZnO film with oxygen content of 43.6[%] is obtained at the O_2/DEZn ratio of 2000.

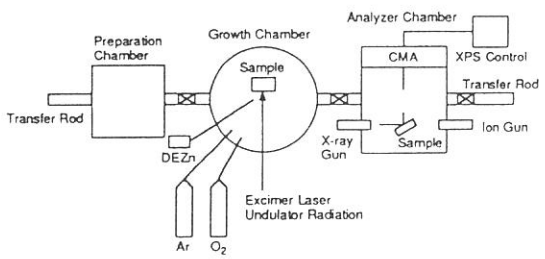

Fig. 1. Experiment System

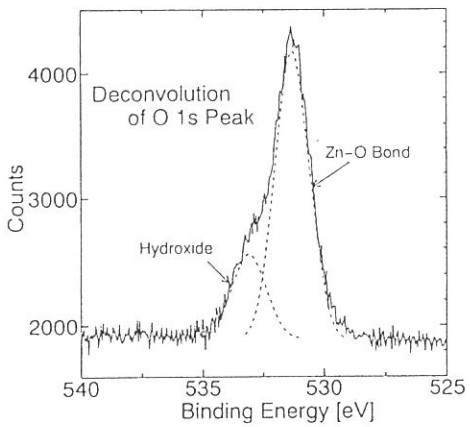

Fig. 2. Deconvolution of O 1s Peak

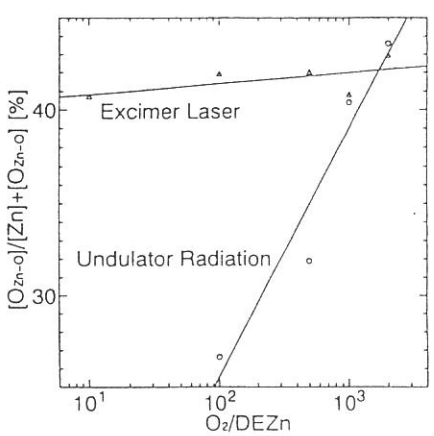

Fig. 3. O content in the films vs The O_2/DEZn ratio

APPENDIX

ORGANIZATION

Staff

Director			
	Kyuya	YAKUSHI	Professor
Scientific Staff			
Light Source			
	Goro	ISOYAMA	Associate Professor
	Hiroyuki	HAMA	Research Associate
Beam Line			
	Makoto	WATANABE	Associate Professor(- September 1993)
			Adjunct Professor from Tohoku
			Univ.(October 1993- March 1994)
	Masao	KAMADA	Associate Professor
	Atsunari	HIRAYA	Research Associate
	Shin-ichiro	TANAKA	Research Associate
	Shin-ichi	KIMURA	Reaserch Associate (October 1993-)
	Shigeo	OHARA	IMS Fellow (-November 1993)
Technical Staff			
	Kusuo	SAKAI	Section Chief Engineer
	Osamu	MATSUDO	Unit Chief Engineer
	Toshio	KINOSHITA	Engineer
	Masami	HASUMOTO	Engineer
	Jun-ichi	YAMAZAKI	Engineer
	Eiken	NAKAMURA	Engineer
Secretary			
	Hisayo	HAGIWARA	

Guest Scientist

	Kazumichi	NAKAGAWA	Adjunct Associate Professor
			from Kobe Univ. (April 1993-)

Graduate Student

Sayumi	HIROSE	

Representententative of Beam Lines (January 1994)

BL1A	Nobuhiro	KOSUGI	Dept. Vacuum UV Photoscience
BL2A	Nobuhiro	KOSUGI	Dept. Vacuum UV Photoscience
	Kosuke	SHOBATAKE	Adjunct Professor from

			Nagoya Univ. (April 1994-)
BL2B2	Koichiro	MITSUKE	Dept. Vacuum UV Photoscience
BL3B	Koichiro	MITSUKE	Dept. Vacuum UV Photoscience
BL4A	Tsuneo	URISU	Dept. Vacuum UV Photoscience
BL4B	Tsuneo	URISU	Dept. Vacuum UV Photoscience
BL6A2	Masao	KAMADA	UVSOR
BL6B	Kyuya	YAKUSHI	Dept. Molecular Assemblies
BL8B2	Kyuya	YAKUSHI	Dept. Molecular Assemblies
	Nobuhiro	KOSUGI	Dept. Vacuum UV Photoscience
Others	Masao	KAMADA	UVSOR

Steering Committee (April 1992 - March 1994)

Kyuya	YAKUSHI	IMS Chairman
Masahiro	KOTANI	Gakushuin Univ.
Kaizo	NAKAMURA	Okayama Univ.
Yukinori	SATO	Tohoku Univ.
Noriaki	ITOH	Nagoya Univ.
Akito	KAKIZAKI	Tokyo Univ.
Toshio	KASUGA	KEK
Tadashi	MATUSHITA	KEK
Kazumichi	NAKAGAWA	Kobe Univ., IMS
Yusei	MARUYAMA	IMS
Keitaro	YOSHIHARA	IMS
Norio	MORITA	IMS
Koichiro	MITSUKE	IMS
Makoto	WATANABE	IMS and Tohoku Univ.
Goro	ISOYAMA	IMS
Masao	KAMADA	IMS

JOINT STUDIES (fiscal year 1993)

Special Project	:2
Cooperative Research	:37
Cooperative Research (invited)	:9
Use of Facility	:123
Use of Facility (Private Company)	:2
User's Meeting	:1
Workshop on Beam Dynamics and Free Electron Laser	:1
User's Time	:42 (weeks)

LIST OF PUBLICATIONS (1993)

1) "Single–, Double–, and Triple–Photoionization Cross Sections of Carbonyl Sulfide (OCS) and Ionic Fragmentation of OCS^{+}, OCS^{2+}, and OCS^{3+}"

   T. Masuoka and H. Doi

   Phys. Rev. A **47** (1993) 278.

2) "Luminescence of High–Temperature Single–Crystal Superconductors Cleaved in Ultrahigh Vacuum"

   V. G. Stankevitch, N. Yu. Svechnikov, K. V. Kaznacheev, M. Kamada, S. Tanaka, S. Hirose, R. Kink, G. A. Emel'chenko, S. G. Karabachev, T. Wolf, H. Berger and F. Levy

   Phys. Rev. B **47** (1993) 1024.

3) "Ionic Fragmentation Processes following Si:2p Core Level Photoexcitation and Photoionization of 1,1,1–Trimethyltrichlorodisilane"

   S. Nagaoka, J. Ohshita, M. Ishikawa, T. Masuoka and I. Koyano

   J. Phys. Chem. **97** (1993) 1488.

4) "Gain Measurement of a Free Electron Laser with an Optical Klystron on the UVSOR Storage Ring"

   S. Takano, H. Hama and G. Isoyama

   Jpn. J. Appl. Phys. **32** (1993) 1285.

5) "Test of Holographic SiC Gratings for High–Power Synchrotron Radiation"

   E. Ishiguro, H. Maezawa, M. Sakurai, M. Yanagihara, M. Watanabe, M. Koeda, T. Nagano, K. Sano, Y. Akune and K. Tanino

   SPIE **1739** High Heat Flux Engineering (1992) 592.

6) "Mechanisms of Synchrotron Radiation–Excited Etching Reactions of Semiconductor Materials"

   H. Ohashi, A. Yoshida, K. Tabayashi and K. Shobatake

   Applied Surface Science **69** (1993) 20.

7) "Solid–state Effects on Nonradiative Decay of $4d^9 4f^1$ States in Barium Halides"

   M. Kamada, K. Ichikawa and O. Aita

   Phys. Rev. B **47** (1993) 3511.

8) "Laser Beam Profiler in the Vacuum Ultraviolet Spectral Range using Photostimulable Phosphor"
M. Katto, R. Matsumoto, K. Kurosawa, W. Sasaki, Y. Takigawa and M. Okuda
Rev. Sci. Instrum. **64** (1993) 319.

9) "Photoelectron Spectra of Acetone and Acetone Dimer"
K. Furuya, S. Katsumata and K. Kimura
Journal of Electron Spectroscopy and Related Phenomena **62** (1993) 237.

10) "Control of the Bunch Length on an Electron Storage Ring"
H. Hama, S. Takano and G. Isoyama
Nucl. Instrum. Meth. Phys. A **329** (1993) 29.

11) "Dissociation Dynamics of Doubly-and Triply-charged Molecules Studied by the Triple Photoelectron-photoion-photoion Coincidence Method"
T. Masuoka
J. Chem. Phys. **98** (1993) 6989.

12) "Desorpion, Dissociation and Orientation of Oxygen Admolecules on a Reconstructed Platinum(110)(1×2) Surface Studied by Thermal Desorption and Near-edge X-ray-Absorption Fine-Structure"
Y. Ohno, T. Matsushima, S. Tanaka and M. Kamada
Jpn. J. Appl. Phys. **32** (1993) Suppl. 32-2, 383.

13) "Polarized Cu L Absorption Spectra of $Bi_2Sr_2Ca_{1-x}Y_xCu_2O_8(x=0.0,0.6)$"
S. Nakai, K. Matsuda, A. Kamata, K. Sano, K. Noguchi, H. Ishii, I. Shiozaki and H. Arai
Jpn. J. Appl. Phys. **32** (1993) Suppl. 32-2, 602.

14) "Time-Resolved Luminescence Study of Relaxed Excitons in KBr:I and KCl:Br"
T. Matsumoto, K. Ichinose and K. Kan'no
J. Phys. Soc. Jpn. **62** (1993) 1860.

15) "Lasing of a Free Electron Laser in the Visible on the UVSOR Storage Ring"
S. Takano, H. Hama and G. Isoyama
Nucl. Instrum. Meth. Phys. A **331** (1993) 20.

16) "Positive Ion-negative Ion Coincidence Spectroscopy of O_2 and H_2 using Synchrotron Radiation"
K. Mitsuke, H. Yoshida, H. Hattori
Z. Phys. D **27** (1993) 267.

17) "Negative-ion Mass Spectrometric Study of Ion-pair Formation in the Vacuum Ultraviolet. VII-$SO_2 \rightarrow O^- + SO^+, O^- + S^+ + O$"

K. Mitsuke, S. Suzuki, T. Imamura, I. Koyano

Organic Mass Spectrometry **28** (1993) 335.pp

18) "Photodissociation of BrCN in the Vacuum Ultraviolet Region"

K. Kanda, S. Katsumata, T. Nagata, Y. Ozaki, T. Kondow, K. Kuchitsu, A. Hiraya and K. Shobatake

Chem. Phys. **175** (1993) 399.

19) "Single-and Double-Photoionization Cross Sections of Nitric Oxide (NO) and Ionic Fragmentation of NO^+ and NO^{2+}"

T. Masuoka

Phys. Rev. A **48** (1993) 1955.

20) "Dissociation of Doubly Charged $CH_2=CD_2$ and $CH_2=CF_2$ in the Region of Valence Shell Photoexcitation"

T. Ibuki, T. Imamura, I. Koyano, T. Masuoka and C. E. Brion

J. Chem. Phys. **98** (1993) 2908.

21) "X-ray Excited Luminescence Yield Spectra of NaBr and NaBr:Cu Single Crystals"

T. Murata, K. Harada, S. Emura, M. Nomura, K. R. Bauchspiess, H. Maeda, A. Hiraya and M. Watanabe

Jpn. J. Appl. Phys. **32** (1993) Suppl. 32-2, 217.

22) "Core Electron Absorption Spectra of Polyester Films"

I. Ouchi, I. Nakai, M. Kamada and S. Tanaka

Reports on Progress in Polymer Physics in Japan **36** (1993) 413.

23) "Control System Capable of Gracefully Degraded Operation for the 750 MeV Synchrotron Radiation Source"

N. Kanaya, H. Hama, J. Yamazaki, O. Matsudo, G. Isoyama

T-NS **40** (1993) 1286.

24) "Ion-Pair Formation from Saturated Hydrocarbons Through Photoexcitation of an Inner-Valence Electron"

K. Mitsuke, H. Hattori and H. Yoshida

J. Chem. Phys. **99** (1993) 6642.

25) "Luminescence Decay Behavior of the On-Center Self-Trapped Excitons in Alkali Halides"
T. Matsumoto, T. Kawata, A. Miyamoto and K. Kan'no
Proceedings of ICDIM Nordkirchev (1992) 327.

26) "X-ray Absorption Near Edge Structure (XANES) Studies of Diluted Magnetic Semiconductors (DMS) $Zn_{1-x}Y_xS$ (Y=Mn, Fe, Co) Systems"
W. F. Pong, R. A. Mayanovic, K. T. Wu, P. K. Tseng, B. A. Bunker,
A. Hiraya and M. Watanabe
Jpn. J. Appl. Phys. **32** (1993) Suppl. 32-2, 722.

27) "Optical Study of Electronic Structure and Nonmetal-Metal Transition of Gd_2S_3"
S. Kimura, F. Arai, T. Suzuki and M. Ikezawa
J. Phys. Soc. Jpn. **62** (1993) 4331.

28) "Energy Gap State of Gd_2S_3"
S. Kimura, T. Suzuki, M. Ikezawa and T. Kasuya
Phys. B 186-188 (1993) 387.

29) "Molecular Orientation in Thin Films of Bis(1,2,5-thiadiazolo)-*p*-Quinobis(1,3-dithiole) on Graphite Studied by Angle-resolved Photoelectron Spectroscopy"
S. Hasegawa, S. Tanaka, Y. Yamashita, H. Inokuchi, H. Fujimoto, K. Kamiya,
K. Seki and N. Ueno
Phys. Rev. B **48** (1993) 2596.

30) "Infrared Lattice Vibration Spectra at Low Temperature in β-ZnP_2"
M. Sugisaki, M. Eguchi, O. Arimoto, K. Nakamura and M. Watanabe
J. Phys. Soc. Jpn. **62** (1993) 4533.

31) "Double RF System for Suppression of Longitudinal Coupled Bunch Instability on UVSOR Storage Ring"
K. Tamura, T. Kasuga, M. Tobiyama, H. Hama, G. Isoyama and T. Kinoshita
Jpn. J. Appl. Phys. **33** (1994) **L**59-**L**62.

32) "Angel-resolved Photoemission from Langmuir-Blodgett films of Copper tetrakes(b-buthoxycarbonyl)phthalocyanine with Synchrotron Radiation"
N. Ueno, K. Kamiya, K. Ogawa, H. Yonehara, M. Takahashi, H. Nakahara,
K. Seki, K. Sugita, K. Fukuda and H. Inokuchi
Thin Solid Films **210/211** (1992) 678.

33) "Local Distortion of AsO_4 and PO_4 Molecules in KDP-Family Crystals"
Y. Noda, H. Maeda, H. Terauchi, H. Kasatani, K. Ogura, K. Kamon, T. Umeki, Y. Yoneda, S. Murakami and Y. Kuroiwa
Jpn. J. Appl. Phys. **32** (1993) Suppl. 32-2, 740.

34) "Structures and Catalytic Behavior of Some Niobium Oxides"
S. Hasegawa, H. Aritani and M. Kudo
Catalysis Today **16** (1993) 371.

35) "Fluorescence Excitation Spectra and Quantum Yield in Vacuum Ultraviolet Photodissociation of CF_3CN"
D-C. Che, T. Kasai, H. Ohoyama, K. Kuwata, M. Kono, K. Tabayashi and K. Shobatake
Chem. Lett. (1994) 133.

36) "Single-, Double-, and Triple-photonization Cross Sections of Carbon Monoxide (CO) and Ionic Fragmentation of CO^+, CO^{2+}, and CO^{3+}"
T. Masuoka and E. Nakamura
Phys. Rev. A **48** (1993) 4379.

37) "Photoemission and NEXAFS Studies of Organic Molecular and Polymeric Materials"
K. Seki
Vacuum Ultraviolet Radiation Phys. (1993) 385.

38) "Auger-Free Luminescence from Large Gap Insulators"
S. Kubota
Vacuum Ultraviolet Radiation Phys. (1993) 511.

39) "Mechanism of the Photolysis of Iron Pentacarbonyl Adsorbed on a Pt Suface"
S. Sato and Y. Ukisu
Surf. Sci. **283** (1993) 137.

40) "Infrared Reflection Absorption Spectroscopy, X-ray Photoelectron Spectroscopy and Temperature-programmed Desorption Study on the Adsorption and Decomposition of Fe(CO)5 over Silver Surfaces"
S. Sato, Y. Ukisu, H. Ogawa and Y. Takasu
J. Chem. Soc. Faraday Trans. **89** (1993) 4387.

41) "Study on VUV Photochemical Reactions over Solid Surfaces"
S. Sato
New Functionality Materials, Vol. C Synthetic process and Control of Functionality Materials. Ed. by T. Tsuruta, M. Doyama and M. Seno (Elsevier, 1993) 201.

42) "Soft X-ray Microscope with Zone Plates at UVSOR"
N. Watanabe, Y. Shimanuki, M. Taniguchi and H. Kihara
Proc. SPIE 1741 (1992) 85.

43) "Observation of Biological Materials by X-ray Photoelectron-Conversion Microscopy"
N. Watanabe, T. matsumura, Y. Inagaki, K. Kinoshita, Y. Shimanuki, K. Furuya, T. Taguchi, M. Taniguchi and H. Kihara
J. Microscopy **170** (1992) 141.

44) "Soft X-ray Microscopy with Zone Plates at UVSOR I: Its Performance"
N. Watanabe, Y. Shimanuki, M. Taniguchi and H. Kihara
Jpn. J. Appl. Phys. **32**(10) (1993) 4791.

45) "Time Response of Photon-Stimulated Desorption of Excited-State Sodium Atoms from Sodium Halides"
S. Hirose and M. Kamada
Phys. Rev. B **48** (1993) 17641.

46) "Spectral Characteristic of Metallic State of Polyacetylene"
J. Tanaka, C. Tanaka, T. Miyamae, K. kamiya, M. Shimizu, M. Oku, K. Seki, J. Tsukamoto, S. Hasegawa and H. Inokuchi
Syn. Metals 55-57 (1993) 121.

47) "Electronic Structure of Bis [1,2,5] Thiadiazolo-*p*-quinobis (1,3-dithiole) (BTQBT) Studied by Ultraviolet Photoemission Spectroscopy"
H. Fujimoto, K. Kamiya, S. Tanaka, T. Mori, Y. Yamashita, H. Inokuchi and K. Seki
Chem. Phys. **165** (1992) 135.

48) "Photoemission and Inverse Photoemission of Alkali-doped C_{60}"
T. Takahashi, T. Morikawa, H. Katayama-Yoshida, S. Hasegawa and H. Inokuchi
J. Phys. Chem. Solids **53** (1992) 1699.

49) "Collapse of Mott-hubbard Framework by Hole Doping in $Bi_2Sr_2CaCu_2O_8$"
T. Takahashi, S. Suzuki, T. Kusunoki and H. Katayama-Yoshida
Vacuum Ultraviolet Radiation Phys. (1992) 330.

50) "Pseudo-Gap and Electronic Structure Near the Fermi Level in Doped C_{60}"
T. Takahashi
Comments Cond. Mat. Phys. **16** (1992) 113.

51) "Photoemission Study of Superconductive and Non-superconductive Alkali-doped C_{60} and C_{70}"
T. Takahashi
Materials Science and Engineering **B19** (1993) 117.

52) "Precursor to Paramagnetic Centers Induced in Gamma-irradiated Doped Silica Glasses"
K. Awazu, H. Kawazoe, K. Harada, K. Kido and S. Inoue
J. Appl. Phys. **73** (1993)1644.

53) "Chemical Reactions of Ge-related Species in SiO_2:GeO_2 optical Fibers"
K. Awazu, H. Hosono and H. Kawazoe
SPIE **2044** (1993) 78.

54) "Photoelectron Spectra of a Higher Fullerene Compound C_{82} and Its Potassium Complex"
S. Hino, K. Matsumoto, S. Hasegawa, K. Iwasaki, K. Yakushi, T. Morikawa, T. Takahashi, K. Seki, K. Kikuchi, S. Suzuki, I. Ikemoto and Y. Achiba
Synthetic Metals **55-57** (1993) 3191.

55) "Electronic Structure of Doped C_{60}: Strog Correlation or Lattice Distortion?"
T. Takahashi, T. Morikawa, H. Katayama-Yoshida, S. Hasegawa, H. Inokuchi, K. Seki, S. Hino, K. Kikuchi, S. Suzuki, K. Ikemoto and Y. Achiba
Physca B **186-188** (1993) 1068.

56) "Ultraviolet Photoelectron Spectre of C_{82} and K_xC_{82}"
S. Hino, K. Matsumoto, S. Hasegawa, K. Iwasaki, K. Yakushi, T. Morikawa, T. Takahashi, K. Seki, K. Kikuchi, S. Suzuki, I. Ikemoto and Y. Achiba
Phys. Rev. B **48** (1993) 8418.

57) "Pseudo-gap at the Fermi Level in K3C60 Observed by Photoemission adninverse Photoemission"

T. Takahashi, S. Suzuki, T. Morikawa, H. Katayama-Yashida, S. Hasegawa, H. Inokuchi, K. Seki, K. Kikuchi, S. Suzuki, K. Ikemoto and Y. Achiba

Phys. Rev. Lett. **68** (1992) 1232.

58) "Mono- and Multilayers of Novel Molecular Complex of Thiphene Derivative with Long-chain TCNQ"

H. Nakahara, A. Nagasawa, A. Ishii, J. Nakayama, M. Hoshino, K. Fukuda, K. Kamiya, C. Nakano, U. Nagashima, K. Seki and H. Inokuchi

Mol. Cryst. Liq. Crust. **227** (1993) 13.

59) "Angle-resolved Photoemission Spectroscopy of Ultrathin Films of H2-ph Thalocyanine on MoS2 Surfaces"

N. Ueno, K. Suzuki, S. hasegawa, K. Kamiya, K. Seki and H. Inokuchi

J. Chem. Phys. **99** (1993) 7169.

60) "Mechanism of Photostimulated Luminescence Process in BaFBr:Eu^{2+}Phosphors"

Y. Iwabuchi, N. Mori, K. Takahashi, T. Matsuda and S. Shionoya

Jpn. J. Appl. Phys. **33** (1994) 178.

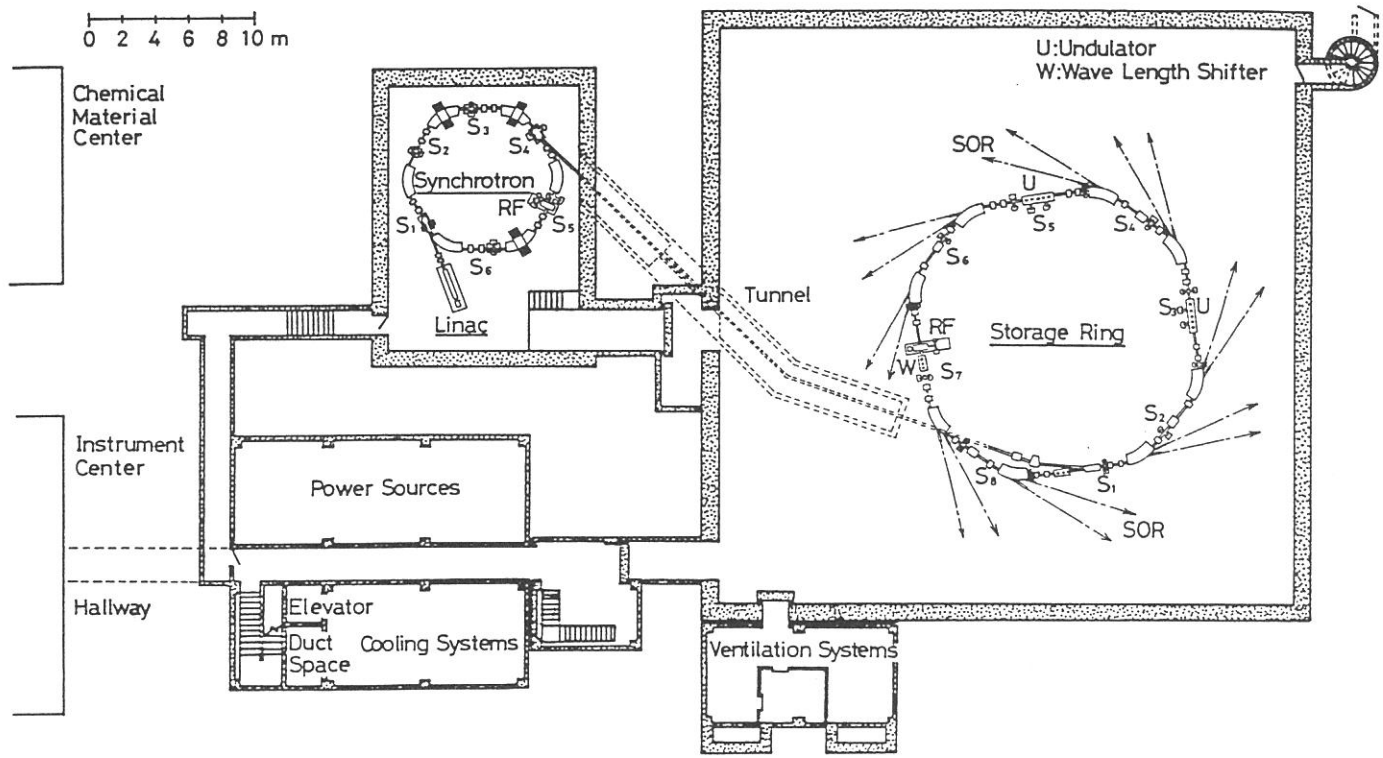

Ground plan of the basement of the UVSOR Facility

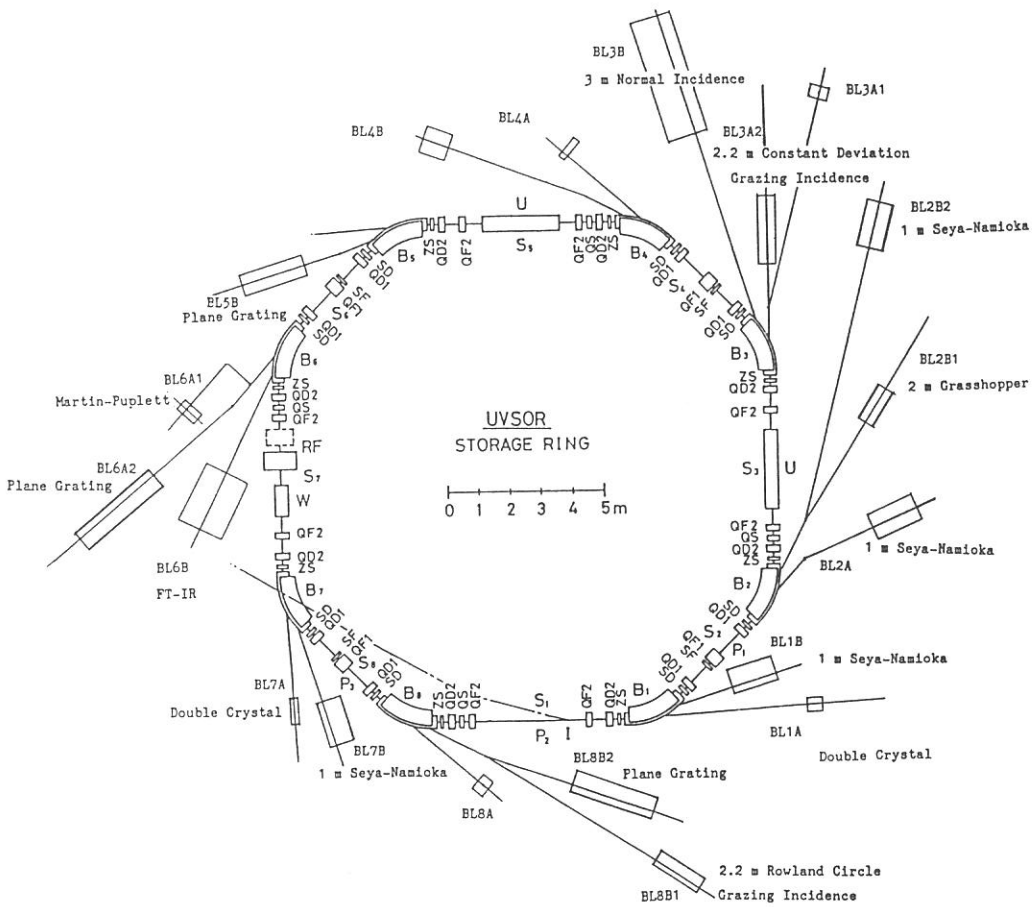

The UVSOR storage ring and the beam lines.

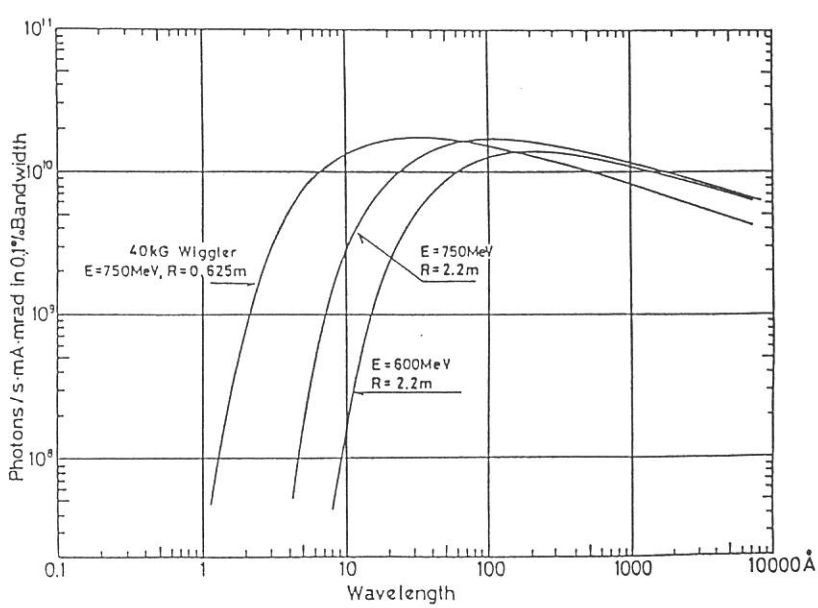

Intensity distribution of the UVSOR radiation.

Tabel 1. Main Parameters of UVSOR Storage Accelator Complex

Linac		
Energy	15	Mev
Frequency	2.856	GHz
Synchrotron		
Energy	600	MeV
Current	32	mA
Circumference	26.6	m
Surperperiodicity	6	
Bending Radius	1.8	m
Harmonic Number	8	
RF Frequency	90.115	MHz
Repetition Ratio	2.6	Hz
Storage Ring		
Energy	750	MHz
Critical Energy of SR	425	eV
Beam Current (Nominal)		
Multi-bunch mode	200	mA
Single-bunch mode	60 - 70	mA
Beam Lifetime	180	min. (at I = 200 mA)
Circumference	53.2	m
Superperiodicity	4	
Bending Radius	2.2	m
Betatron Wave Numbers		
Horizontal	3.19	
Vertical	2.22	
Momentum Compaction Factor	0.032	
Radio Frequency	90.115	MHz
RF Voltage	50	kV
Natural Emittance		
Horizontal	1.15×10^{-7}	πm rad
Vertical	1.15×10^{-8}	πm rad*
Beam Sizes		
Horizontal	0.39	mm
Vertical	0.27	mm*
Bunch Length	170	psec

*10% coupling is assumed.

Table 2. Beam Lines at UVSOR

Beam Line	Monochromator, Spectrometer	Wavelength Region		Acceptance Angle(mrad)			Experiment
					Horiz.	Vert.	
BL1A	Double Crystal	15 - 8 Å			4	1	Solid
BL1B	1m Seya-Namioka	6500 - 300 Å			60	6	Gas &Solid
BL2A	1m Seya-Namioka	4000 - 300 Å			40	6	Gas
BL2B1	2m Grasshopper	600 - 15 Å			10	1.7	Gas & Solid
BL2B2	1m Seya-Namioka	2000 - 300 Å			20	6	Gas
BL3A1	None (Filter, Mirror)			(U)	0.3	0.3	Gas & Solid
BL3A2	2.2m Constant Deviation	1000 - 100 Å			10	4	Gas & Solid
	Grazing Incidence			(U)	0.3	0.3	
BL4A	None				6	6	Irradiation
BL4B	None				8.3	6	Irradiation
BL3B	3m Normal Incidence	4000 - 300 Å			20	6	Gas
BL5B	Plane Grating	2000 - 20 Å			10	2.2	Calibration
BL6A1	Martin-Pupplet	5 mm - 50 μm			80	60	Solid
BL6A2	Plane Grating	6500 - 80 Å			10	6	Solid
BL6B	FT-IR	200 - 1.7 μm			70	25	Solid
BL7A	Double Crystal	15 - 8 Å			2	0.3	Solid
		15 - 2 Å		(W)	1	0.15	Solid
BL7B	1 m Seya-Namioka	6500 - 300 Å			40	8	Gas & Solid
BL8A	None (Filter)				25	8	Irradiation, User's Instrm.
BL8B1	15m-Constant Deviation Grazing Incidence	400 - 20 Å			10	1.5	Gas & Solid
BL8B2	Plane Grating	6500 - 80 Å			10	6	Solid

U: with an undulator, W: with a wiggler

LOCATION

Ultraviolet Synchrotron Orbital Radiation (UVSOR) Facility, Institute for Molecular Science (IMS) is located at Okazaki. Okazaki (population 300,000) is 260 km southwest of Tokyo, and can be reached by train in about 3 hours from Tokyo via New Tokaido Line (Shinkansen) and Meitetsu Line.

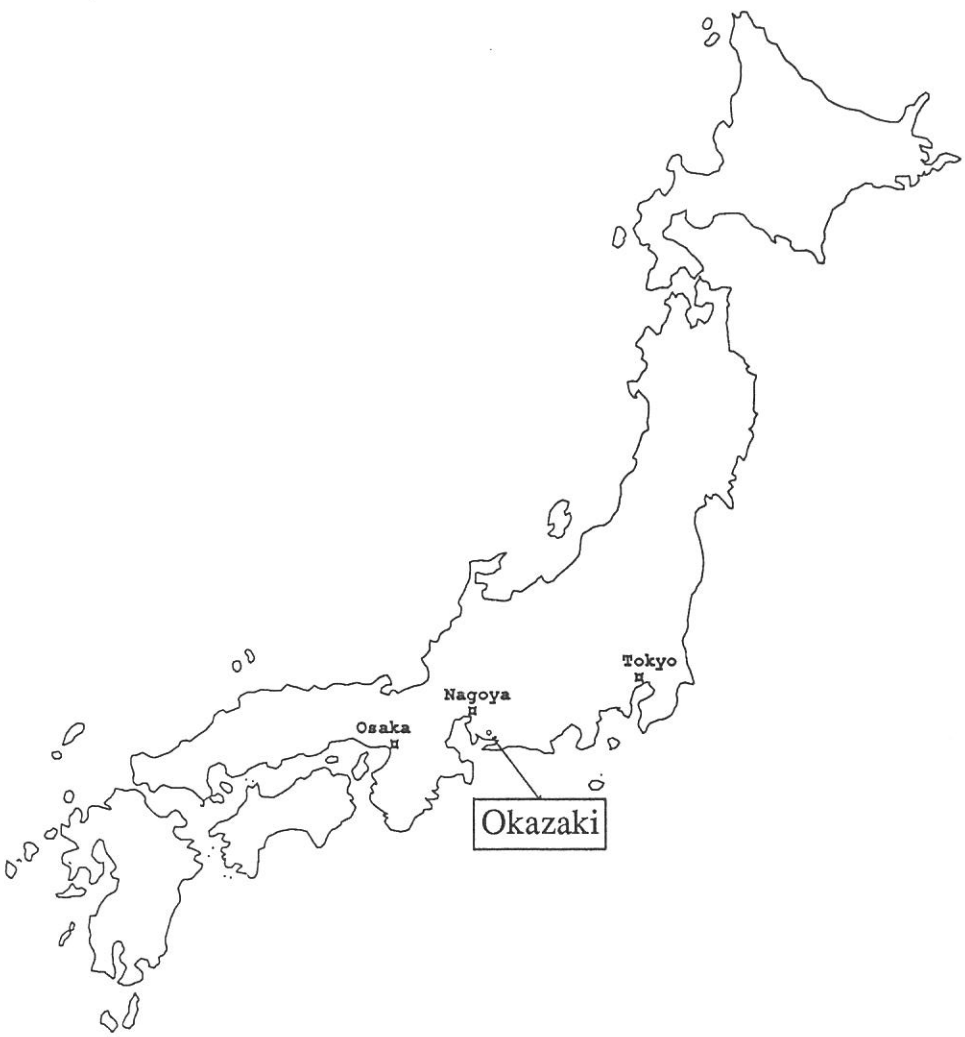

Address
UVSOR Facility, Institute for Molecular Science
Myodaiji, Okazaki 444, JAPAN

Telephone 0564-55-7402 (Secretary, UVSOR)
0564-52-6101 (UVSOR)
Fax 0564-54-7079 (UVSOR)
Telex 4537475 KOKKEN J (IMS)

Editors: S. Tanaka and M. Kamada